The effects of motion and heterogeneity on stochastic population dynamics

A thesis submitted to the University of Manchester
for the degree of Doctor of Philosophy
in the Faculty of Science and Engineering

2019

Francisco Herrerías Azcué

School of Physics and Astronomy

Contents

Word count 54263

List of Figures

The University of Manchester

The effects of motion and heterogeneity on stochastic population dynamics

Francisco Herrerías Azcué

Doctor of Philosophy

10th May 2019

Abstract

Noise has come to be accepted as a quintessential part of social and biological processes. It has transcended the misconception of being an obstacle, which hinders our understanding of 'true mechanisms' hiding behind the randomness, and is now recognised as the cause of many important phenomena. Different sources of noise exist, and their combined effect is not trivial to understand. In this thesis, we contribute by studying models which combine *intrinsic* and *extrinsic* noise. We consider systems with discrete interacting components; as a consequence, they are subject to *intrinsic* noise. At the same time, we explore how two sources of *extrinsic* noise modify the time evolution of these models: motion, and agent-to-agent heterogeneity.

We investigate motion of individuals in a two dimensional setting. Members of the population take positions in space and are moved by an external flow. The position of agents defines an interaction graph, so the population is structured. The interaction network is modified as the flow advects individuals in space. We choose an evolutionary dynamics setting, and study how the changing population structure alters the probability with which a mutant invades a population of wild-type individuals. We find that seemingly subtle changes in the mechanics of evolution, which implement birth and death events, can lead to significant changes in the mutant's chances of success. Therefore, we propose these differences can be used to identify the underlying mechanism in a given experimental setting. Furthermore, we debate that the commonly used term to describe the invasion process in unstructured populations, 'well-mixed', is a misnomer, which must be used with care.

To study agent-to-agent heterogeneity we use models of epidemics and opinion dynamics. For the latter we explore how the achievement, maintenance or alternation of consensus are affected by the presence of more than two co-evolving opinions, with potentially different conviction strengths. In the model of disease spread, we study how heterogeneity in the susceptibility and infectiousness of individuals influences the frequency and amplitude of outbreaks. In both models heterogeneity is represented by an arbitrary number of compartments that describe the 'type' of the agents. To be able to simplify the mathematical description of these systems, we approach them by aggregating these compartments into bigger groups. In both cases, we find that this marginalised description provides a good approximation of the model dynamics. We are able to characterise the recurrence and severity of outbreaks using the aggregated components; similarly, we provide an analytical description of the simplified opinion dynamics, which is an approximation when conviction strengths differ, and exact when they are homogeneous.

Declaration

No portion of the work referred to in the thesis has been submitted in support of an application for another degree or qualification of this or any other university or other institute of learning.

Copyright Statement

i. The author of this thesis (including any appendices and/or schedules to this thesis) owns certain copyright or related rights in it (the "Copyright") and s/he has given The University of Manchester certain rights to use such Copyright, including for administrative purposes.

ii. Copies of this thesis, either in full or in extracts and whether in hard or electronic copy, may be made **only** in accordance with the Copyright, Designs and Patents Act 1988 (as amended) and regulations issued under it or, where appropriate, in accordance with licensing agreements which the University has from time to time. This page must form part of any such copies made.

iii. The ownership of certain Copyright, patents, designs, trade marks and other intellectual property (the "Intellectual Property") and any reproductions of copyright works in the thesis, for example graphs and tables ("Reproductions"), which may be described in this thesis, may not be owned by the author and may be owned by third parties. Such Intellectual Property and Reproductions cannot and must not be made available for use without the prior written permission of the owner(s) of the relevant Intellectual Property and/or Reproductions.

iv. Further information on the conditions under which disclosure, publication and commercialisation of this thesis, the Copyright and any Intellectual Property and/or Reproductions described in it may take place is available in the University IP Policy (see http://documents.manchester.ac.uk/DocuInfo.aspx?DocID=487), in any relevant Thesis restriction declarations deposited in the University Library, The University Library's regulations (see http://www.manchester.ac.uk/library/aboutus/regulations) and in The University's Policy on Presentation of Theses.

Acknowledgements

I believe that a PhD is only possible because there is a wide community supporting the person that ends up baring the title. Among the people behind this particular PhD there are some to which I am particularly grateful.

It is not hard to see why Ivonne, my wife, should come at the top of this list. Her unwavering support since I chose to study abroad has inspired me to continue. Marian, my daughter, although only in the picture for the last year or so, was a refreshing sight every time I got home and, despite taking up good chunks of my time, brought me more energy and joy than she could ever possible take. The constant (albeit digital) presence of my parents, brothers and sister were also instrumental to my sanity and well-being. I cannot thank you all enough for caring for me as you do.

My mental health was looked after by the above, but my academic and intellectual progress would not have been possible without Tobias, my supervisor. I am truly thankful for being introduced to this fascinating part of physics, for the many advices and instructive talks, the fruitful work together and the heated discussions; they all helped in making me grow both as a person and as a scientist. I'd also like to thank Niels Walet, for being always willing to help with technical problems and also for inadvertently opening my eyes to better coding, optimization and use of cluster computing facilities.

Almost as important in my understanding of our field were Peter, Joe, Laura, Ernesto, Danna and Annie, as well as Rory, Pierre and Henry. The office would've been a much less productive place without each of you in it, the many questions to which everyone contributed in answering, the off-topic office-wide conversations that lightened the day and helped ease the way of thoughts, the nickname votes, Spanish lessons and lunch breaks.

I should mention Chloe, Oli, Araceli, Daniel, Ernesto and Eric as well, whose friendship in Manchester definitely contributed in my ability to carry out my research.

Finally, I must thank CONACyT for the financial support to study my degree at the University of Manchester, and all the staff here that makes research possible.

Chapter 1

Introduction

All of the work presented in this thesis has the common goal of modelling social or biological processes. We consider systems composed of discrete entities, such as molecules, cells, or animals, which interact with one another. The discrete and probabilistic nature of these interactions gives rise to 'noisy' dynamics. For instance, the encounters between predators and their prey are inherently random. Similarly, changes in the concentration of the proteins that regulate gene transcription, the exchange of opinions in social networks, mutations in cellular division, the spread of diseases, and the evolution of language, for example, all happen in a non-deterministic fashion.

The mathematical tool with which these 'noisy' dynamics are described has come to be known as 'stochastic processes', and has been a lively area of research since the end of the 19th century. At that time, the interest focused on understanding the behaviour and properties of gases and the random movement of pollen particles floating on water [1, 2]. Since then, however, stochastic processes have found widely varying applications, from finance to medicine, telecommunications and many others [3–7].

Describing these processes in full is often impossible due to their complexity. To study them, therefore, we conceive of a simple representation of the system which approximately reproduces the real-world dynamics, which we call *models*.

In this introduction, we outline the general principles that guide our choice of model components, starting with the importance of including noise in the description of these systems. Then, a brief overview of the technical tools needed for their mathematical analysis is given. Finally, we introduce the specific models studied in the following chapters, and make some comments on the structure and format of this thesis.

1.1 The simpler the better

Statistical physics was born from the need to describe phenomena that are so complex that a detailed and exact description of the entire system becomes impossible. To be able to study them one must take a step back and, instead of being interested in the microscopic detail of the behaviour of each molecule, describe the system as a whole and characterize it through its macroscopic properties. After all, it is the latter that we experience in day-to-day life; while standing in a room, we do not worry about how many molecules bounce on our bodies or how fast, but we do feel the temperature around us. The approach is successful when macroscopic quantities, such as temperature, can be described using a *simple* microscopic model, like the Maxwell-Boltzmann distribution.

One of the main tasks in statistical physics is to decide which elements are essential in the description of a complex system. It is not always easy to see, however, which macroscopic quantities are important and which are not. Similarly, it can be difficult to choose microscopic components that can explain the phenomena we want to describe, and to discard those which are less relevant. A good model needs to contain sufficient detail to reproduce the desired dynamics, but at the same time be simple enough to be mathematically tractable.

The dynamics of social and biological processes in which this thesis focus are particularly complex. In order for a model to be simple, then, certain assumptions and simplifications must be made. These assumptions are not always to the detriment of a theory; in fact, they can be quite the opposite. In many cases, the simpler the model the more insight is gained about the basic principles behind the process.

The success of this approach speaks for itself. Mechanistic models as the above have allowed the scientific comunity to gain insight into the nature of financial markets [8], the spread of diseases [9], and even biological evolution [10]. These are not merely theoretical achievements; such models have proved crucial in the design and planning of, for example, vaccination policies [11–14], public transport and traffic networks [15, 16], or crime prevention and patrolling programs [17, 18].

1.2 The key ingredient: noise

When the system is composed of very large populations, the noise of stochastic processes is typically so small that a deterministic description is all that is required. Models in biology were only considered deterministically for many decades, and useful insights have been obtained from them. The predator-prey Lotka-Volterra equations [19], for example, have proved useful in modelling ecological systems, but in many cases they fall short. For instance, they are unable to capture extinctions; particularly when populations are small, predators can drive their prey to non-existence, even when the deterministic model would lead one to believe that a stable equilibrium is attainable [20, 21].

This thesis focuses on studying dynamics that arise due to the presence of noise. Therefore, it is intentionally included in all our models and analysis. Noise is commonly classified in two categories [22]:

Intrinsic noise reflects the stochastic dynamics that arise from the discrete nature of the elements that make up the system. It is considered inalienable to the dynamics, as it is introduced in the very definition of the process. Examples include the death and birth of individuals, mutation, imitation, infenction and recovery. Intrinsic noise has been shown to be useful in understanding many important phenomena, such as sustained oscillations due to stochastic amplification [23–25], noise-induced transitions [26–29], and extinction or evolution [10, 20, 30].

Extrinsic noise is, broadly, 'the rest' of the noise. It is often characterised as an external or additional characteristic of the system. An example of this is a change in the environment that controls the parameters of the model; when modelling bacteria, for instance, applying antibiotics or changing the concentration of nutrients can modify the reproduction and death rates of the model. The difference in the results between 'identical' experiments with variation in these external parameters is characterized as extrinsic noise.

In the models studied in this thesis we explore the interplay between these two types of noise. Extrinsic noise comes from many sources, but this work shall be restricted to only two: agent-to-agent heterogeneity, and motion. While we will treat these as *extrinsic*, the line that divides what is inherently part of the dynamics and what is an

added component is naturally not as sharp as the categories above suggest. Part of the aim of the work presented in the following chapters is to determine whether treating these two characteristics as secondary is justifiable, or if they must be considered more carefully.

Both motion and heterogeneity are ubiquitous in nature. At the same time, however, how either of them influence stochastic dynamics is not well understood.

Heterogeneity. Broadly, two types of heterogeneity have received attention in the literature. One of them is *parametric heterogeneity*; it describes variation accross experiments in model parameters which are universal to all agents in the system (see Fig. 1.1 (a)). This type of heterogeneity has been the focus of many studies (e.g. refs. [31–36]), particularly in models of gene transcription. It allows one to explore models where environments have different parameters, but where the environment is the same for all the members of the population in each experiment.

Global changes in the model parameters are relevant for some particular applications, but in many biological systems parameter variation is more localized. For example, individual variations in factors such as host susceptibility and virus reproduction have been observed [37]. For the modelling of epidemics, therefore, it is essential to determine how this heterogeneity across individuals affects the dynamics. In other contexts, we may consider that some individuals seek more actively to convince others of their opinions, or that resistance to antibiotics varies among different strains of bacteria.

These examples are cases of a second type of heterogeneity, often referred to as *agent-to-agent heterogeneity*. This describes variation at the level of individuals [see Fig. 1.1 (b)]. Some studies do exist exploring heterogeneity in this form [38, 39], but the overwhelming majority of research on the subject have been conducted in a deterministic setting.

It may not be immediately obvious why agent-to-agent heterogeneity is considered 'external' to the system. To understand why this is the case, let us consider modelling the spread of a disease in a population conformed by discrete entities. In order to do this, one must take into account that two individuals have to meet in order for the pathogen to spread. Therefore, the random encounters are considered intrinsic to the model. One can assume, however, that all individuals get sick, spread the disease and

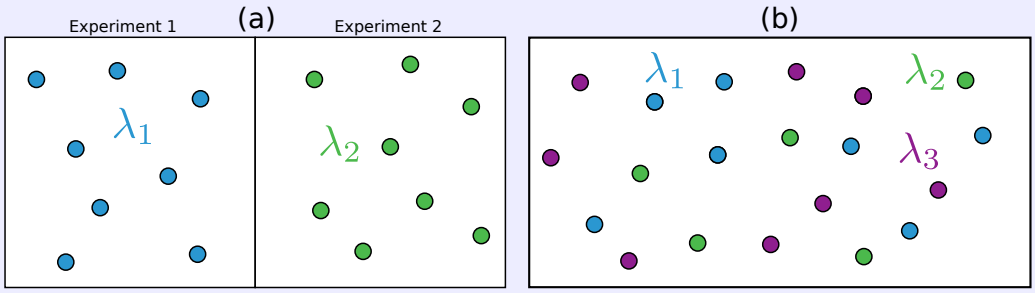

Figure 1.1: Two types of heterogeneity. Parametric heterogeneity is shown in panel (a); the environment that controls the model parameters changes from one experiment to the next, but all agents observe the same environment. Agent-to-agent heterogeneity is shown in panel (b); individuals have varying characteristics in a single experiment.

recover with similar probabilities to one another. In other words, that the population is homogeneous. Heterogeneity, then, is considered an *added* component to the basic model, and so it is regarded as extrinsic.

Other examples of added heterogeneity in models include the stochastic Kuramoto model in the context of coupled oscillators [40–42]; this introduces noise on the order parameter of the synchronization of different oscillators, which leads to metastable states of full-synchronicity of the ensamble. Similarly, populations with a continuous distribution of a trait, such as particle sizes, are studied as polydisperse systems [43–45]; this effectively introduces an infinite number of species, and leads to particular states of order and mixing, known as phase equilibria. In the context of ecology, Random Matrix Theory has also been successfully used [46–49], where the interaction rates of different species in a food network are drawn from random distributions; the stability of the system to extinction of one or more species is then studied.

Motion In social and biological processes individuals are, more often than not, in motion. For example, our social circles are dynamic, plankton swims and is moved by flows, animals migrate in search of mates, and commercial flights transport pathogens across the world. Just as with heterogeneity, it is not always immediately obvious why motion should be considered external to a system. Let us use an individual-based model of evolution to exemplify why this is the case. For such a model one must take into account that individuals attempting to reproduce need to interact with others, both in competition for resources and because of the necessity of finding a mate.

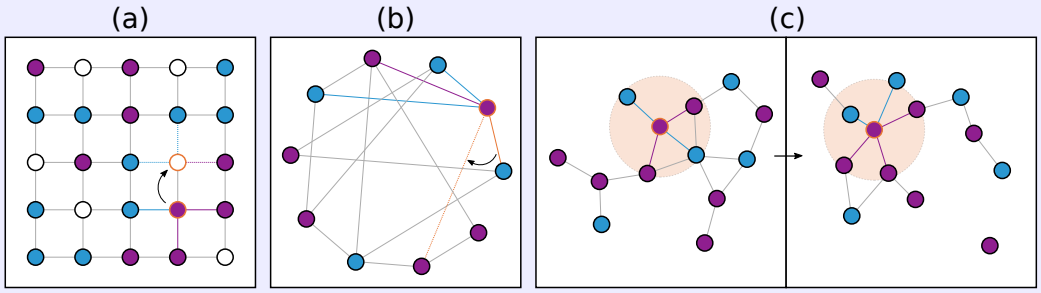

Figure 1.2: Examples of options for the implementation of motion. Migration is shown in panel (a); an individual moves to a neighbouring site, therefore changing the interaction network. An adaptive network is shown in panel (b); one end of a link is moved to a different individual. Movement in space is shown in panels (c); individuals take positions in space, and their interaction radius determines which individuals are connected to each other. They then move in space, and the interaction network is updated accordingly.

These interactions are then considered intrinsic to the model. The choice of which individuals interact, however, can be assumed to be random. In other words, one can assume that the population is unstructured. For movement to be considered there has to be an underlying population structure, i.e., an interaction network that specifies which individuals can interact with one another. This structure, and the possibility of individuals to dynamically generate an interaction network through movement, are considered an addition to the process; they are therefore thought of as extrinsic.

In models, motion can be implemented in several ways. A common way in which it is included is in the form of 'migration' of individuals to neighbouring sites in the network [50–52]. In these models the interaction network is static; individuals hop from one node to another and in this way modify the events possible in the model dynamics (see Fig. 1.2 (a)). An alternative that has also been considered is the use of adaptive networks [53–56]. In this case it is not the individuals that move, but rather the links connecting them that change (see Fig. 1.2 (b)).

The above models of motion can provide significant insight; however, they fall short of describing the complexities and implications of individuals' motion. Notably, they neglect the finite interaction radius of agents. For example, the evolution of language is constrained by the range with which the words can be spoken. Similarly, predators can only look so far for their prey, and bacteria can only sense the concentration of nutrients in their close surroundings.

In the study of motion, networks generated by the positions in space of the agents of the model have, until recent years, received little attention [57–60]. In this context, individuals are linked to each other if they are within the given interaction radius. Motion changes the spatial location of the individuals, which in turn modifies the interaction network (see Fig. 1.2 (c)).

This thesis addresses the above highlighted issues in the present state of the art. We examine the implementation and implications of models with agent-to-agent heterogeneity in two chapters, and two more chapters are dedicated to investigating the consequences of motion in populations with finite interaction radius. The key set of tools and techniques required to perform these studies are outlined in the next section.

1.3 Technical introduction

In this section we provide a brief overview of the mathematical tools we use throughout this thesis. First, we look into the exact description of the stochastic processes and the methods with which they can be directly studied. Then, we explore how and why approximations to this exact description can be obtained. Finally, we outline the terminology used for the description of interaction networks. Whenever more specific mathematical tools are used, their description is given within each chapter.

1.3.1 Master equations

In this thesis we study individual-based models. That is, we study systems which are composed of discrete entities, and whose states are determined by the composition of the population and its interaction network. We assume for all our models that the dynamics are Markovian [61, 62]; i.e., we approximate the systems as being completely free of memory, such that the state into which they will evolve depends only on the present state.

The systems described above can be mathematically described by a 'master equation' [21, 63, 64]. A master equation describes the time evolution of the probabilities with which each discrete state of the system occurs.

For a system with states described by $\underline{n}$, the *forward master equation* is given by

$$\frac{\partial}{\partial t}P(\underline{n},t|\underline{n}_0) = \sum_{\underline{n}'} T_{\underline{n}'\to\underline{n}} P(\underline{n}',t|\underline{n}_0) - \sum_{\underline{n}'} T_{\underline{n}\to\underline{n}'} P(\underline{n},t|\underline{n}_0), \tag{1.1}$$

where $P(\underline{n},t|\underline{n}_0)$ describes the probability that the system is in state $\underline{n}$ at time t, given that it started at $\underline{n}_0$ at $t=0$. The sums are, respectively, contributions to the *inflow* and *outflow* of probability from and to the other states $\underline{n}'$. The *forward* master equation is written in form of sums over the possible 'destinations' of the system. Its elements describe where the system can go.

Alternatively, the same system can be represented using the *backward master equation*, given by

$$\frac{\partial}{\partial t}P(\underline{n},t|\underline{n}_0) = \sum_{\underline{n}'} T_{\underline{n}_0\to\underline{n}'} \left[P(\underline{n},t|\underline{n}') - P(\underline{n},t|\underline{n}_0)\right]. \tag{1.2}$$

In the backward master equation P increases if by moving from state $\underline{n}_0$ into state $\underline{n}'$ the system is more likely to reach $\underline{n}$ from there, than if it had stayed in state $\underline{n}$. The *backward* master equation is written in form of sums over the possible 'origins' of the system. Its elements describe where the system can start from.

Both equations above describe the same dynamics, but are generally used with different objectives in mind. The backward equation is most useful to determine, for example, fixation probabilities or first-passage times. We will use this form in Chapters 2, 3, and 5. The forward master equation, on the other hand, is used when one intends to study a stationary probability distribution, or a system that equilibrates around a fixed state. We will use this form in Chapters 4 and 5.

Exact solutions

Ideally, the solution to the master equation would be obtained directly. For many systems this is not possible; only the simplest models are amenable to exact analytical solution [21, 63, 64]. In these simple cases one can find the solution by inspection of a recursion equation of the state space [21, 65].

As an example, let us consider a two-species birth-death process with fixed population size N. The state space is defined by the number of individuals i of one of the two species; the other species is composed of $N-i$ individuals. Let $T_i^{\pm}$ describe the probability with which the system transitions from state i to state $i\pm 1$. Furthermore,

let the states $i = 0$ and $i = N$ be absorbing, so that $T_0^{\pm} = 0$, $T_N^{\pm} = 0$. That is, once these states are reached, the dynamics stop; if $i = N$, we say that the species has reached fixation. Two questions are then commonly asked, namely, how likely this is to happen, and how long it takes. We illustrate the answer to these questions below.

Fixation probability. We denote with ϕ_i the probability that the system will reach fixation if it is currently in state i. The recursive equation that describes this process is then[1]

$$\phi_i = \phi_{i-1} T_i^- + \left(1 - T_i^+ + T_i^-\right) \phi_i + \phi_{i+1} T_i^+, \tag{1.3}$$

and given that the boundary states are absorbing, one has $\phi_0 = 0$ and $\phi_N = 1$. Using these conditions one can solve the above equation for ϕ_{i+1}, for example, and write a few terms explicitly to determine a pattern, thereby obtaining a closed form solution. For the current example we find [66]

$$\phi_i = \frac{1 + \sum_{j=1}^{i-1} \prod_{k=1}^{j} \frac{T_k^-}{T_k^+}}{1 + \sum_{j=1}^{N-1} \prod_{k=1}^{j} \frac{T_k^-}{T_k^+}}. \tag{1.4}$$

This equation is the exact solution of the master equation; it involves no approximations.

Time to fixation. In a similar way, we could ask how many evolutionary steps are needed (in average) to reach fixation. Using t_i to denote the number of events necessary to go from a state with $i > 0$ mutants to a fixed state $i = N$ or $i = 0$, we can write for the master equation

$$t_i = 1 + t_{i-1} T_i^- + t_{i+1} T_i^+ + \left(1 - T_i^+ + T_i^-\right) t_i, \tag{1.5}$$

which after rewriting in terms of $\theta_i = t_i - t_{i-1}$ (the average transition time from the state $i - 1$ to i) and rearranging leads to the recursive equation

$$\theta_{i+1} = \frac{\theta_i T_i^- - 1}{T_i^+}. \tag{1.6}$$

Using $t_0 = t_N = 0$, and therefore $\theta_1 = t_1$, we can obtain a closed form solution for θ_i. Since the sum of this transition times amounts to the time to fixation, we also obtain the solution for t_i, which is given by [67]

$$t_i = -\sum_{j=i+1}^{N} \theta_j = \sum_{j=i}^{N-1} \left(-t_1 \prod_{k=1}^{j} \frac{T_j^-}{T_j^+} + \sum_{k=1}^{j} \frac{1}{T_k^+} \prod_{m=k+1}^{j} \frac{T_m^-}{T_m^+} \right). \tag{1.7}$$

[1] Note that the terms on the right hand side constitute a sum over the possible 'origins' of the system; it is in the form of a backward master equation.

This equation again does not involve approximations, and is therefore an exact solution of the master equation.

Stationary distribution. Another common question when studying Markov processes is what the stationary distribution is; that is, if the system is permitted to evolve for a long time, what state is it likely to be found in? For the example above the answer is simple: it is fixed in of the two species. If, however, random mutations are added to the model, for example, transition between the two species without the need of an interaction partner are possible; the absorbing states are thus eliminated and the above question then becomes more meaningful.

To address this problem, the forward form of the master equation is used. The stationary distribution $\underline{P} = \{P_i\}$ is found by setting the left hand side of Eq. (1.1) to zero. For the current example, we then obtain

$$P_i \left(T_i^- + T_i^+\right) = P_{i+1} T_{i+1}^- + P_{i-1} T_{i-1}^+. \tag{1.8}$$

As with the fixation probability and time, this can be re-arranged into a recursive equation, which leads to the identification of the exact solution. Taking into account that $P_{-1} = 0$, $T_0^- = 0$, $T_N^+ = 0$, $P_{N+1} = 0$ and $\sum P_i = 1$, we obtain

$$P_i = \left(1 + \sum_{i=1}^{N} \prod_{j=1}^{i} \frac{T_{j-1}^+}{T_j^-}\right)^{-1} \prod_{j=1}^{i} \frac{T_{j-1}^+}{T_j^-}. \tag{1.9}$$

Importantly, T_0^+ and T_N^- are non-zero due to the random mutations.

As in the other two cases, this solution is exact and valid for any population size.

Many systems result in recursive equations that cannot be closed, and this type of approach is not possible. However, the systems studied in Chapters 2 and 5 are such that they allow for these simple representations, and so we will use an approach similar to the one described above.

1.3.2 Approximating the master equation

Under certain assumptions one can approximate the master equation using existing mathematical methods. This can lead to analytical solutions, which facilitate insight into the process at hand. Furthermore, even if the resulting expressions need to be numerically solved, this tends to be less computationally intensive than directly solving

the master equation; the stochastic differential equations that one can obtain from these approximations can be approached using, for example, the Euler–Maruyama method [68].

The approximations rely on the assumption that although the population is composed of discrete individuals, there are many of them. Changes in the composition of the population occur through single individuals, i.e., the size of a *jump* in the state of the system is ± 1; in contrast, the number of bacteria in a Petri dish, for example, is overwhelming. The *proportion* of individuals $x_i = \mathrm{n}_i/N$ in each state can then be treated as a continuous quantity[2].

The assumption of large system sizes may be completely reasonable; when describing epidemics, for example, one deals with cities or even countries, which imply large populations. One must be careful, however, when attempting to extrapolate results and use them on a local level.

Kramers–Moyal expansion

In the spirit of approximating population densities as a continuum, the Kramers–Moyal expansion [21, 63, 64] is perhaps the most natural approach. It consists of a truncated Taylor expansion of the master equation in powers of the inverse system size. In what follows, we restrict the analysis to systems in which the transition between states $T_{\underline{\mathrm{n}}'\to\underline{\mathrm{n}}}$ correspond to a decrease in n_j and increase n_i; we therefore use T_{ij} to denote the transition rates. Writing the master equation as a function of the proportion of individuals we then have

$$\frac{\partial}{\partial t}P\left(\underline{x},t\right) = \left[\sum_i \sum_j \left(\mathbb{E}_i^- \mathbb{E}_j^+ - 1\right) T_{ij}\right] P\left(\underline{x},t\right), \tag{1.10}$$

where we defined the step operators $\mathbb{E}_i^{\pm}$ by their action $\mathbb{E}_i^{\pm} P\left(x_1,...,x_i,...,x_n,t\right) = P\left(x_1,...,x_i \pm \frac{1}{N},...,x_n,t\right)$. Therefore, $\mathbb{E}_i^- \mathbb{E}_j^+ P\left(\underline{x},t\right)$ describes a state with one less individual of strategy i and one extra individual of strategy j compared to $P\left(\underline{x},t\right)$.

The approximation proceeds by assuming that $N \gg 1$, and so these operators can be expanded in powers of $\frac{1}{N}$,

$$\mathbb{E}_i^{\pm} = 1 \pm \frac{1}{N}\partial_{x_i} + \frac{1}{2}\frac{1}{N^2}\partial_{x_i}^2 \pm \frac{1}{3!}\frac{1}{N^3}\partial_{x_i}^3 + ... \tag{1.11}$$

[2] In biological settings, the proportions of a population are often called *frequencies*; these should not be mistaken for temporal frequencies.

Introducing the above expansion into Eq. (1.10) leads to

$$\frac{\partial}{\partial t}P\left(\underline{x},t\right)\approx\left\{\sum_{i}\sum_{j}\left[\frac{1}{N}\left(\partial_{x_j}-\partial_{x_i}\right)+\frac{1}{2}\frac{1}{N^2}\left(\partial_{x_i}-\partial_{x_j}\right)^2+\mathcal{O}\left(\frac{1}{N^3}\right)\right]T_{ij}\right\}P\left(\underline{x},t\right). \tag{1.12}$$

If the series is truncated to leading order one obtains a Liouville equation, which leads to the mean-field equations,

$$\dot{\underline{x}}=\underline{f}\left(\underline{x},t\right), \tag{1.13}$$

where $\underline{f}\propto\lim_{N\to\infty}T^{\pm}(\underline{\mathrm{n}})/N$, and describes the deterministic drift of the system.

In the sub-leading order, a Fokker-Planck equation is obtained

$$\frac{\partial}{\partial t}P\left(\underline{x},t\right)=-\sum_{i=1}^{N}\frac{\partial}{\partial x_i}\left[f_i\left(\underline{x}\right)P\left(\underline{x},t\right)\right]+\frac{1}{2}\sum_{i=1}^{N}\sum_{j=1}^{N}\frac{\partial^2}{\partial x_i x_j}\left[B_{ij}\left(\underline{x}\right)P\left(\underline{x},t\right)\right], \tag{1.14}$$

where $f_i\left(x\right)$ is again the drift term, and B_{ij} is known as the diffusion matrix; with $f_i\left(x\right)=0$ and constant B_{ij}, the above equation describes a diffusive system. It is B_{ij} which interests us, as it describes the noise of the process. In general, the Kramers–Moyal expansion produces a Fokker-Planck equation with multiplicative noise; that is, the noise can be a function of $\underline{x}$.

Eq. (1.14) can be of use directly if, for example, one is interested in the stationary probability distribution of the system. As in the case for the exact solution, this is obtained by setting the left hand side of the equation to zero. For a one dimensional system, like the one used as an example to obtain Eq. (1.9), this results in

$$0=-2fP_{st}+\frac{\partial}{\partial x}\left[BP_{st}\right], \tag{1.15}$$

which is satisfied by $P_{st}=\exp\left[\int_x\frac{2f-\partial_x[B]}{B}\right]$, where the integral is not necessarily trivial. As opposed to Eq. (1.9), this solution is only valid for large system sizes.

Van Kampen expansion

An alternative, related approximation, is known as the van Kampen system-size expansion [21, 63, 64]. The method consists on approximating the dynamics by making an ansatz of the form

$$\underline{x}=\underline{f}\left(\underline{x},t\right)+\frac{1}{\sqrt{N}}\underline{\xi}(t). \tag{1.16}$$

where $\underline{\xi}$ is independent of $\underline{x}$. The ansatz considers noise in the dynamics by including a noise term (ξ) with an appropriate scaling of the population size ($N^{-1/2}$). This ensures that the variance of the stochastic variable is finite, but not vanishing. The approximation is also known as the linear noise approximation.

One proceeds to write the master equation in terms of the new coordinates ξ_i. Writing $\partial\xi_i/\partial t = -\sqrt{N}\dot{x}_i$, we have

$$N\frac{\partial}{\partial t}P\left(\underline{x},t\right) = \frac{\partial}{\partial t}\Pi\left(\underline{\xi},t\right) - \sqrt{N}\sum_i \dot{x}_i\frac{\partial}{\partial \xi_i}\Pi\left(\underline{\xi},t\right), \tag{1.17}$$

where we used Π to make the change of variable more explicit. Using Eq. (1.10) as a start point, we first realise that the action of the step operators on the new variables is $\mathbb{E}_i^{\pm}\Pi\left(\xi_1,...,\xi_i,...,\xi_n,t\right) = \Pi\left(\xi_1,...,\xi_i \pm \frac{1}{\sqrt{N}},...,\xi_n,t\right)$. Expanding this in powers of $N^{1/2}$ leads to

$$\mathbb{E}_i^{\pm} = 1 \pm \frac{1}{\sqrt{N}}\partial_{\xi_i} + \frac{1}{2}\frac{1}{N}\partial_{\xi_i}^2 \pm \frac{1}{3!}\frac{1}{N^{3/2}}\partial_{\xi_i}^3 + ... \tag{1.18}$$

Introducing the above equations into Eq. (1.10) we find

$$\begin{aligned}\frac{1}{N}\frac{\partial}{\partial t}\Pi\left(\underline{\xi},t\right) - \frac{1}{\sqrt{N}}\sum_i \dot{x}_i\frac{\partial}{\partial \xi_i}\Pi\left(\underline{\xi},t\right) \approx \\ \left\{\sum_i\sum_j\left[\frac{1}{\sqrt{N}}\left(\partial_{x_j}-\partial_{x_i}\right) + \frac{1}{2}\frac{1}{N}\left(\partial_{x_i}-\partial_{x_j}\right)^2 + \mathcal{O}\left(\frac{1}{N^{3/2}}\right)\right]T_{ij}\right\}\Pi\left(\underline{\xi},t\right).\end{aligned} \tag{1.19}$$

As in the Kramers–Moyal expansion, collecting the leading-order terms one can extract the mean-field equations, and collecting the subleading-order terms results in a Fokker-Planck equation. However, the van Kampen expansion results in Fokker-Planck equations that contain additive noise only.

In many cases this linear-noise approximation is sufficient to describe the dynamics and, if the original model contains additive noise only, both expansions result in the same equations. In some ocasions, however, this is not the case, and details are lost by doing the van Kampen expansion [21, 69].

Langevin equations

It is useful to remark the fact that the Fokker-Planck equation corresponds to a set of stochastic differential equations, known as Langevin equations; these are of the form

$$\dot{\underline{x}}\left(t\right) = \underline{f}(\underline{x},t) + \underline{\eta}(t) \tag{1.20}$$

where the correlation of the noise terms η_i is given by

$$\langle \eta_i(t)\eta_j(t')\rangle = B_{ij}\delta\left(t-t'\right). \tag{1.21}$$

The Langevin equations encapsulate a continuous stochastic process which approximates the original dynamics, described by the master equation. These permit the analytical study of the noise terms. In the system studied in Chapter 4, for example, the intrinsic noise produces stochastic quasi-cycles around the fixed point. Using the Langevin equations, one can obtain analytical expressions that help us to determine the periodicity and amplitude of these cycles.

Numerical solutions

If analytically solving the master equations is not possible, numerical solutions can be obtained emplying Euler forward or other Runge–Kutta methods [70, 71]. However, for large system sizes these methods can be computationally intensive, and also entail approximations due to the implementation of the algorithms [71].

Another option is to explore the dynamics of the model through Monte Carlo methods. The Gillespie algorithm and similar approaches [72–75] efficiently generate individual trajectories of stochastic processes. The statistics of these trajectories can help in understanding the model. However, one needs a large ensemble of realizations in order to obtain useful information. Even if generating an individual trajectory is very efficient, running thousands or millions of them makes the process very time consuming.

Nonetheless, these methods involve no approximations to the dynamics and can be particularly illuminating; visualization of single trajectories can provide some physical intuition about the evolution of the system. Therefore, we will use them to test our analytical results.

1.3.3 Networks

To be able to represent motion the use of interaction networks is necessary. In this section we introduce the terminology relevant for this thesis, and illustrate it in Fig. 1.3.

Network/Graph. We will use these two words interchangeably. They are constituted of nodes, and links that connect pairs of nodes.

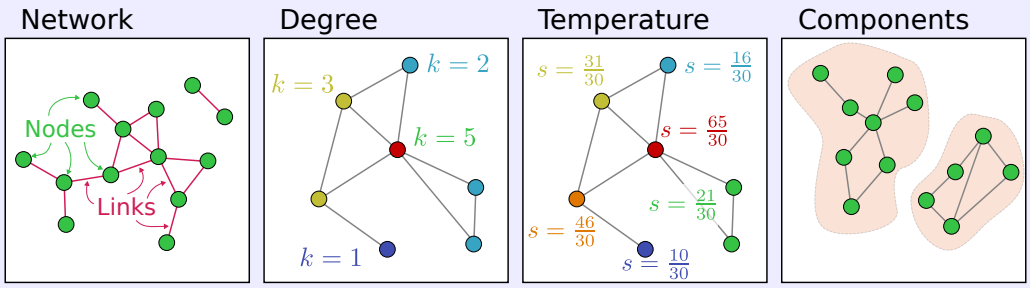

Figure 1.3: A network and its elements. The terminology used to describe networks is exemplified.

Node. Individuals in our models are represented in a network by nodes. We assume they are point-like; as such, there is no spatial restriction for their positions. In all diagrams, we represent nodes as circles. Two nodes are said to be **neighbours** if there is a link connecting them.

Link. The purpose of graphs in this thesis is to describe which pairs of individuals can interact. This is graphically represented by lines connecting pairs of nodes, termed links. Throughout this thesis links are considered *undirected*; interactions can occur between a connected pair of nodes, regardless of their order. For the sake of simplicity, we also assume equal weights throughout; that is, events are equally likely to occur in all links.

Degree. The degree k of a node describes the number of immediate neighbours of an individual, i.e., how many links it has.

Temperature. The temperature s of a node is a measure of how potentially 'active' it is. Since we only consider undirected, unweighted graphs, it can be defined as the sum of the inverse degree of its immediate neighbours, i.e., $s = \sum_i 1/k_i$, where i enumerates the node's neighbours, and k_i is the degree of neighbour i.

Component. If there is at least one 'path' to connect every pair of nodes in a group, the group of nodes and the links between them are collectively called a component. This is sometimes emphasised by referring to them as *connected* components. A graph may be composed of one or more components.

1.3.4 Time scales of motion and mixing

In chapters 2 and 3 we will study populations stirred by flows, and how the speed of the motion affects the evolution of the system. Two separate time scales interact in this case: the rate of 'interaction' between individuals, and their 'speed' of movement. Each of these time scales are not completely meaningful by themselves; rather, the ratio of the two is the relevant quantity.

In-line with the literature we will describe this by the so-called **Damköhler** number Da [76–78]; in the context of our model, the Damköhler number describes the ratio of the time scales of the flow and the evolutionary process. The flows we use to stir the population in space are periodic (up to a random phase), and so we use this period to specify the time scale of the flow. The time interval between evolutionary events sets the reaction rate, so we use a generation (N events, where N is the population size) as an indicator of the time scale of the evolutionary process. The Damköhler number is then given by

$$\mathrm{Da} = \frac{T}{N\Delta t}. \tag{1.22}$$

Large values of Da indicate that the flow is slow compared to evolution. With everything else fixed, decreasing values of Da are equivalent to increasing the displacement of individuals in space between evolutionary events.

The focus of this thesis is on flows that mimic chaotic motion; the correlation of the position of two particles then decreases with time (see Fig. 2.2). This amounts to effectively mixing the population. For very small Da, enough time elapses between evolutionary events to completely re-shuffle the positions of the whole population. We characterise this by a **mixing time** τ, which depends on the interaction radius of individuals and the parameters of the flow (see Sec. 2.2.3).

The time scale τ describes the time needed to completely de-correlate the interaction network of the population. That is, after flowing for τ units of time, the neighbours of an individual are effectively sampled uniformly from the whole population, regardless of who it was neighbours with before. For a fixed Da, increasing the interaction radius of the individuals results on an increased mixing time τ. Alternatively, for fixed interaction radii the mixing time increases as Da is also increased.

The relevance of this mixing time scale will become more evident in Chapter 2, where

'well-stirred' populations are studied, and the effect of mixing is explicitly explored.

1.4 Structure and format

This thesis follows the 'journal format' of the University of Manchester. The contents of Chapters 2–5 are therefore in the form of papers. The articles in Chapters 2 and 4 have been reviewed and published by Nature Scientific Reports [79, 80]. The contents of Chapters 3 and 5 have been submitted to PLOS Computational Biology and Physical Review E, respectively. Both are also publicly available on arXiv [81, 82].

The contents of each chapter are as close to their published/pre-print versions as possible. However, they have been typeset to be in line with the format of the rest of the thesis. This simplifies pagination, and will hopefully improve the reading experience.

The papers are not presented in order of publication, but rather are arranged to provide a logical progression across the material. Two of them address motion as a source of extrinsic noise, while the other two focus on heterogeneity. We here briefly summarize the contents in each of the following chapters.

Chapter 2: Stirring does not make populations well mixed [79]. Individual-based models commonly assume that any individual can interact with any other at all times because this greatly simplifies the mathematical description of models [21, 63]. In evolutionary dynamics, this set-up is commonly known as 'well-mixed populations' [83–85]. In more realistic models, however, the assumption of all-to-all interaction is relaxed by the use of an interaction graph. If the interaction network connects all nodes with every other node, it is said to be 'complete'; this is the formal way of recovering the all-to-all interaction. If the network is *not* complete, however, but is generated by connecting nodes if they are within a given interaction radius, then one could naturally ask how the movement of individuals changes the dynamics of the system. One could wonder, for example, if the term 'well-mixed' used to describe complete interaction graphs can actually be related to the movement of the population.

In this chapter we use this question as motivation, but we are also able to draw more general conclusions. We use a simple evolutionary dynamics description of an

invasion process; a single mutant, with a different 'fitness' from the resident population, competes to reproduce (and not die), eventually either going extinct or reaching fixation. At the same time, the population is moved by a flow. We assume that the flow is very fast compared to the time between reproduction/death events, so that the system can be considered 'well-mixed'. The interaction graph for each evolutionary event is then assumed to be generated by individuals taking random positions in space. Using this, we obtain a mathematical description of the model in closed form. From our analytical result, we extract an 'effective' fitness, which simplifies the equations describing the model to the ones that would be obtained if the interaction graph was complete. However, this effective fitness contains information about the particular type of evolutionary process in use, which is lost when the analysis is done assuming a complete-interaction graph.

Chapter 3: Motion, fixation probability and the choice of an evolutionary process [81]. This chapter provides a logical continuation of the ideas of the previous chapter. The same model is used, but the focus here is directly on the role of the speed of the motion and how it may change the outcome of the evolutionary process. We thereby abandon the assumption of very fast flows, but as a consequence our possibility of giving a formal mathematical description of the process is hindered.

We therefore resort to exploring the model dynamics by means of Monte Carlo simulations. Roughly, three flow-speed regimes can be identified. In the fast-flow limit, the results obtained in the previous chapter are recovered. We compare the results in the slow-flow limit with what is known from previous studies of evolutionary dynamics on static networks. We find that the outcome of the invasion process in this regime is strongly affected by the order of birth and death events. In order to understand the results obtained at intermediate speeds, we further the results of ref. [86]; we justify our argument both numerically and through an example set of graphs.

Chapter 4: The effects of heterogeneity on stochastic cycles in epidemics [80]. This chapter marks a change of direction. While we still explore how extrinsic noise interacts with intrinsically noisy systems, we now focus on individual-to-individual heterogeneity, rather than motion. The field of epidemics provides an interesting framework for this. Host heterogeneity has been reported [37], and the dynamics of

infection and recovery are, as we have mentioned, intrinsically noisy.

In this article we use the well-known Susceptible-Infected-Recovered model [87], or SIR for short. The original model takes its name from the fact that a population is divided into those three categories; each individual transitions from one stage to the next sequentially. Individuals may also die at any point, in which case they are replaced by a new susceptible individual. Models like this are known to give rise to so-called 'stochastic quasi-cycles' [88]; the system equilibrates around a certain distribution of the population in the three groups, and oscillates around this fixed point.

We introduce heterogeneity to the model by subdividing both the susceptible and infected groups into sub-groups; each of these sub-groups gets infected or spreads the disease at different rates. In reality, however, only the macroscopic groups are observable; One can count the number of infected individuals, but measuring the susceptibility or infectiousness of every individual in the population is impossible. Therefore, we build our mathematical description around the aggregate of the sub-groups, i.e., the total number of susceptible or infected individuals. We perform a van Kampen system-size expansion to make the model dynamics analytically tractable, and characterize stochastic quasi-cycles around the fixed point. We then use these analytic results to explore which statistical properties of the original sub-groups are most important for the description of the aggregate dynamics. For example, we ask whether the frequency or amplitude of the cycles can be approximately described with the mean susceptibility or infectiousness of individuals, or whether they depend on the dynamic state of the system. In this way, we evaluate the importance of heterogeneity as an ingredient in models of phenomena with stochastic quasi-cycles.

Chapter 5: Consensus and diversity in multi-state noisy voter models [82]. In this chapter we build upon the so called 'noisy voter model' [89]. In its original formulation, the noisy voter model consists of a population in which individuals can be of two types, which represent opinions, political alignments or spins, for example. Members of the population interact in a pairwise manner; in each interaction one individual imitates the type of the other. Additionally, random changes of the type of an individual can occur, hence the term 'noisy'. These systems are characterised by multiplicative noise, which gives rise to a so-called 'noise-driven transition'; as the

population size is increased, the system moves from a bimodal to a unimodal stationary distribution.

In our extension to this model we allow for multiple types; This allows multiple opinions to compete at the same time, or multiple species to co-evolve. The characteristic noise-driven transition observed in the two-state model are still seen in the multi-state system. In order to be able to study this expanded model we construct an effective system that reproduces the system dynamics from the point of view of a single type; the members of all the other types are considered as a 'the other' group. We then consider two cases. First, we assume that the imitation and mutation rates of all types are equal. The effective model constructed from this *homogeneous* case is simple enough to be solved exactly, and analytical expressions to characterize the transition can be obtained. In the other case we consider a *heterogeneous* model, where the different types have different imitation or mutation rates. To address this we approximate the model by taking a weighted average of the characteristics that make the different types heterogeneous, so that 'the others' can be considered as a single type. We show that this approximation is sufficient to describe the overall behaviour of the system to good accuracy. Most importantly, it enables us to get insight into the effect of heterogeneity in this multi-state expansion of the noisy voter model.

The strategy used in this chapter is consistent with the one used in the previous chapter; we describe a heterogeneous model through its aggregated sub-groups. However, it differs in a few key aspects. For instance, the model we use in this chapter allows us to use exact methods for the solution of the master equation, which was not possible for the epidemics model. We also focus on a different aspect of the dynamics; in this case, we look at noise-induced transitions [27, 69]. Furthermore, since we need not rely on a system-size expansion, we are able to study populations of just a handful of individuals. For small population sizes, intrinsic noise can completely dominate the dynamics; as a consequence, the system may not tend to a stable fixed point. We continue, however, in our aim to determine how important individual-to-individual heterogeneity may be for stochastic population dynamics.

Chapter 6, Conclusions. Finally, here we provide a summary of the salient features of Chapters 2, 3, 4, and 5. It is important to remark that because these are

in the format of journal articles, each of them has its own conclusions. To prevent repetition, in this final chapter we do not exhaustively list the findings of each of them. Rather, we remark on the most relevant ones, and concentrate on the opportunities for further work, for which the research presented here paves the way.

Bibliography

[1] Boltzmann, Ludwig (1877), 'Über die Beziehung zwischen dem zweiten Hauptsatz der mechanischen Wärmetheorie und der Wahrscheinlichkeitsrechnung respektive den Sätzen über das Wärmegleichgewicht', *Sitzungsberichte der Kaiserlichen Akademie der Wissenschaften in Wien, Mathematisch-Naturwissenschaftliche Classe. Abt. II* **76**:373–435.

[2] Einstein, A (1905), 'Über die von der molekularkinetischen Theorie der Wärme geforderte Bewegung von in ruhenden Flüssigkeiten suspendierten Teilchen', *Annalen der Physik* **322** (8):549–560, DOI: 10.1002/andp.19053220806.

[3] Paul, Wolfgang and Jörg Baschnagel (2013), *Stochastic Processes: From Physics to Finance*, Springer International Publishing.

[4] Laing, Carlo and Gabriel J. Lord (2010), *Stochastic Methods in Neuroscience*, Oxford University Press, Oxford, UK.

[5] Baccelli, Francois and Bartlomiej Blaszczyszyn (2010), *Stochastic Geometry and Wireless Networks*, Foundations and trends in networking, Now Publishers Inc, Hanover, Masachusets.

[6] Lande, Russell, Steinar Engen and Bernt-Erik Sæther (2003), *Stochastic Population Dynamics in Ecology and Conservation*, Oxford series in ecology and evolution, Oxford University Press, Oxford, UK.

[7] Bressloff, Paul C. (2014), *Stochastic Processes in Cell Biology*, Interdisciplinary Applied Mathematics, Springer International Publishing.

[8] Bouchaud, Jean-Philippe and Marc Potters (2003), *Theory of Financial Risk and Derivative Pricing*, Cambridge University Press, Cambridge, UK.

[9] Driessche, Fred Brauer, Pauline van den Driessche and Jianhong Wu (2008), *Mathematical Epidemiology*, ed. by Fred Brauer, Pauline van den Driessche and Jianhong Wu, vol. 1945, Lecture Notes in Mathematics, Springer Berlin Heidelberg, Berlin, Heidelberg, DOI: 10.1007/978-3-540-78911-6.

[10] Nowak, Martin A. (2006a), *Evolutionary Dynamics*, Harvard University Press, Cambridge, Massachusetts.

[11] Keeling, Matthew J. and Pejman Rohani (2008), *Modeling Infectious Diseases in Humans and Animals*, Princeton University Press, Princeton, NJ.

[12] Colizza, Vittoria et al. (2006), 'The modeling of global epidemics: Stochastic dynamics and predictability', *Bulletin of Mathematical Biology* **68** (8):1893–1921, DOI: 10.1007/s11538-006-9077-9.

[13] Cairns, Andrew J. G. (1989), 'Epidemics in heterogeneous populations: Aspects of optimal vaccination policies', *Mathematical Medicine and Biology* **6** (3):137–159, DOI: 10.1093/imammb/6.3.137.

[14] Anderson, Roy M. and Robert M. May (1985), 'Age-related changes in the rate of disease transmission: implications for the design of vaccination programmes', *Journal of Hygiene* **94** (03):365–436, DOI: 10.1017/S002217240006160X.

[15] Fu, Liping and L.R. Rilett (1998), 'Expected shortest paths in dynamic and stochastic traffic networks', *Transportation Research Part B: Methodological* **32** (7):499–516, DOI: 10.1016/S0191-2615(98)00016-2.

[16] Yu, X.-H. and W.W. Recker (2006), 'Stochastic adaptive control model for traffic signal systems', *Transportation Research Part C: Emerging Technologies* **14** (4):263–282, DOI: 10.1016/j.trc.2006.08.002.

[17] Rosenshine, Matthew (1970), 'Contributions to a Theory of Patrol Scheduling', *Journal of the Operational Research Society* **21** (1):99–106, DOI: 10.1057/jors.1970.21.

[18] Eck, John E. and Lin Liu (2008), 'Contrasting simulated and empirical experiments in crime prevention', *Journal of Experimental Criminology* **4** (3):195–213, DOI: 10.1007/s11292-008-9059-z.

[19] Murray, James D. (2002), *Mathematical biology*, 3rd ed., vol. 17, Interdisciplinary Applied Mathematics, Springer-Verlag, Berlin Heidelberg, DOI: 10.1007/b98868.

[20] Maynard Smith, John (1982), *Evolution and the Theory of Games*, Cambridge University Press, Cambridge, UK.

[21] Gardiner, Crispin W. (2003), *Handbook of stochastic methods*, 3rd ed., Springer, Berlin Heidelberg.

[22] Wang, Ruiqi (2013), 'Noise, Intrinsic and Extrinsic', *Encyclopedia of Systems Biology*, ed. by Werner Dubitzky et al., Springer New York, New York, NY, p. 1527, DOI: 10.1007/978-1-4419-9863-7_353.

[23] Black, Andrew J. et al. (2009), 'Stochastic fluctuations in the susceptible-infective-recovered model with distributed infectious periods', *Physical Review E* **80** (2):021922, DOI: 10.1103/PhysRevE.80.021922.

[24] Rozhnova, Ganna, Ana Nunes and Alan J. McKane (2011), 'Stochastic oscillations in models of epidemics on a network of cities', *Physical Review E* **84** (5):051919, DOI: 10.1103/PhysRevE.84.051919.

[25] Samoilov, Michael, Sergey Plyasunov and Adam P. Arkin (2005), 'Stochastic amplification and signaling in enzymatic futile cycles through noise-induced bistability with oscillations', *Proceedings of the National Academy of Sciences* **102** (7):2310–2315, DOI: 10.1073/pnas.0406841102.

[26] Horsthemke, W. and R. Lefever (1984), *Noise-Induced Transitions: Theory and Applications in Physics, Chemistry, and Biology*, vol. 15, Springer Series in Synergetics, Springer-Verlag, Berlin Heidelberg, DOI: 10.1007/3-540-36852-3.

[27] Biancalani, Tommaso, Tim Rogers and Alan J. McKane (2012), 'Noise-induced metastability in biochemical networks', *Physical Review E* **86** (1):010106, DOI: 10.1103/PhysRevE.86.010106.

[28] Carro, Adrián, Raúl Toral and Maxi San Miguel (2016), 'The noisy voter model on complex networks', *Scientific Reports* **6** (1):24775, DOI: 10.1038/srep24775.

[29] Acharyya, Muktish (1999), 'Nonequilibrium phase transition in the kinetic Ising model: Existence of a tricritical point and stochastic resonance', *Physical Review E* **59** (1):218–221, DOI: 10.1103/PhysRevE.59.218.

[30] Ovaskainen, Otso and Baruch Meerson (2010), 'Stochastic models of population extinction', *Trends in Ecology & Evolution* **25** (11):643–652, DOI: 10.1016/j.tree.2010.07.009.

[31] Singh, Abhyudai and Mohammad Soltani (2013), 'Quantifying intrinsic and extrinsic variability in stochastic gene expression models', *PLoS ONE* **8** (12):e84301, DOI: 10.1371/journal.pone.0084301.

[32] Scott, Matthew, Brian Ingalls and Mads Kærn (2006), 'Estimations of intrinsic and extrinsic noise in models of nonlinear genetic networks', *Chaos: An Interdisciplinary Journal of Nonlinear Science* **16** (2):026107, DOI: 10.1063/1.2211787.

[33] Li, Yongkai, Ming Yi and Xiufen Zou (2015), 'The linear interplay of intrinsic and extrinsic noises ensures a high accuracy of cell fate selection in budding yeast', *Scientific Reports* **4** (1):5764, DOI: 10.1038/srep05764.

[34] Lenive, Oleg, Paul D. W. Kirk and Michael P. H. Stumpf (2016), 'Inferring extrinsic noise from single-cell gene expression data using approximate Bayesian computation', *BMC Systems Biology* **10** (1):81, DOI: 10.1186/s12918-016-0324-x.

[35] Bayati, Basil S. (2016), 'Deterministic analysis of extrinsic and intrinsic noise in an epidemiological model', *Physical Review E* **93** (5):052124, DOI: 10.1103/PhysRevE.93.052124.

[36] Toni, Tina and Bruce Tidor (2013), 'Combined model of intrinsic and extrinsic variability for computational network design with application to synthetic biology', *PLoS Computational Biology* **9** (3):e1002960, DOI: 10.1371/journal.pcbi.1002960.

[37] Heldt, Frank S. et al. (2015), 'Single-cell analysis and stochastic modelling unveil large cell-to-cell variability in influenza A virus infection', *Nature Communications* **6**:8938, DOI: 10.1038/ncomms9938.

[38] Lafuerza, Luis F. and Raúl Toral (2013), 'On the effect of heterogeneity in stochastic interacting-particle systems', *Scientific Reports* **3** (1):1189, DOI: 10.1038/srep01189.

[39] Masuda, Naoki, Nicolas Gibert and Sidney Redner (2010), 'Heterogeneous voter models', *Physical Review E* **82** (1):1–4, DOI: 10.1103/PhysRevE.82.010103.

[40] Bag, Bidhan Chandra, K. G. Petrosyan and Chin-Kun Hu (2007), 'Influence of noise on the synchronization of the stochastic Kuramoto model', *Physical Review E* **76** (5):056210, DOI: 10.1103/PhysRevE.76.056210.

[41] DeVille, Lee (2012), 'Transitions amongst synchronous solutions in the stochastic Kuramoto model', *Nonlinearity* **25** (5):1473–1494, DOI: 10.1088/0951-7715/25/5/1473.

[42] Sonnenschein, Bernard and Lutz Schimansky-Geier (2013), 'Approximate solution to the stochastic Kuramoto model', *Physical Review E* **88** (5):052111, DOI: 10.1103/PhysRevE.88.052111.

[43] Sollich, Peter, Patrick B. Warren and Michael E. Cates (2001), 'Moment free energies for polydisperse systems', *Advances in Chemical Physics*, vol. 116, John Wiley & Sons, New York, NY, p. 265–336.

[44] Sollich, Peter (2002), 'Predicting phase equilibria in polydisperse systems', *Journal of Physics: Condensed Matter* **14**:R79–R117, DOI: 10.1088/0953-8984/14/3/201.

[45] Varga, Szabolcs, Amparo Galindo and George Jackson (2003), 'New types of phase behaviour in binary mixtures of hard rod-like particles', *Molecular Physics* **101** (6):817–825, DOI: 10.1080/0026897021000037654.

[46] May, Robert M. (1972), 'Will a Large Complex System be Stable?', *Nature* **238** (5364):413–414, DOI: 10.1038/238413a0.

[47] Jansen, Vincent A. A. and Giorgos D. Kokkoris (2003), 'Complexity and stability revisited', *Ecology Letters* **6** (6):498–502, DOI: 10.1046/j.1461-0248.2003.00464.x.

[48] Allesina, Stefano and Si Tang (2012), 'Stability criteria for complex ecosystems', *Nature* **483** (7388):205–208, DOI: 10.1038/nature10832.

[49] Gibbs, Theo et al. (2018), 'Effect of population abundances on the stability of large random ecosystems', *Physical Review E* **98** (2):022410, DOI: 10.1103/PhysRevE.98.022410.

[50] Houchmandzadeh, Bahram and Marcel Vallade (2011), 'The fixation probability of a beneficial mutation in a geographically structured population', *New Journal of Physics* **13** (7):073020, DOI: 10.1088/1367-2630/13/7/073020.

[51] Thalhauser, Craig J. et al. (2010), 'Selection in spatial stochastic models of cancer: Migration as a key modulator of fitness', *Biology Direct* **5** (1):21, DOI: 10.1186/1745-6150-5-21.

[52] Krieger, Madison S., Alex McAvoy and Martin A. Nowak (2017), 'Effects of motion in structured populations', *Journal of The Royal Society Interface* **14** (135):20170509, DOI: 10.1098/rsif.2017.0509.

[53] Zimmermann, Martín G. and Víctor M. Eguíluz (2005), 'Cooperation, social networks, and the emergence of leadership in a prisoner's dilemma with adaptive local interactions', *Physical Review E* **72** (5):056118, DOI: 10.1103/PhysRevE.72.056118.

[54] Ehrhardt, George C. M. A., Matteo Marsili and Fernando Vega-Redondo (2006), 'Phenomenological models of socioeconomic network dynamics', *Physical Review E* **74** (3):036106, DOI: 10.1103/PhysRevE.74.036106.

[55] Pacheco, Jorge M., Arne Traulsen and Martin A. Nowak (2006), 'Coevolution of Strategy and Structure in Complex Networks with Dynamical Linking', *Physical Review Letters* **97** (25):258103, DOI: 10.1103/PhysRevLett.97.258103.

[56] Gross, Thilo and Bernd Blasius (2008), 'Adaptive coevolutionary networks: A review', *Journal of the Royal Society Interface* **5** (20):259–271, DOI: 10.1098/rsif.2007.1229.

[57] Perlekar, Prasad et al. (2011), 'Particle algorithms for population dynamics in flows', *Journal of Physics: Conference Series* **333** (1):012013, DOI: 10.1088/1742-6596/333/1/012013.

[58] Pigolotti, Simone and Roberto Benzi (2014), 'Selective Advantage of Diffusing Faster', *Physical Review Letters* **112** (18):188102, DOI: 10.1103/PhysRevLett.112.188102.

[59] Plummer, Abigail et al. (2019), 'Fixation probabilities in weakly compressible fluid flows', *Proceedings of the National Academy of Sciences* **116** (2):373–378, DOI: 10.1073/pnas.1812829116.

[60] Minors, Kevin, Tim Rogers and Christian A. Yates (2018), 'Noise-driven bias in the non-local voter model', *EPL (Europhysics Letters)* **122** (1):10004, DOI: 10.1209/0295-5075/122/10004.

[61] Rogers, L. C. G. and David Williams (2000), *Diffusions, Markov Processes, and Martingales: Volume 1, Foundations*, Cambridge Mathematical Library, Cambridge University Press, Cambridge, UK.

[62] Norris, James R. (1998), *Markov Chains*, Cambridge University Press, Cambridge, UK.

[63] Kampen, Nico G. van (1992), *Stochastic processes in physics and chemistry*, 3rd ed., Elsevier, Amsterdam.

[64] Risken, Hannes (1996), *The Fokker-Planck Equation*, 2nd ed., Springer-Verlag, Berlin Heidelberg, DOI: 10.1007/978-3-642-61544-3.

[65] Nowak, Martin A. (2006b), 'Five rules for the evolution of cooperation', *Science* **314** (5805):1560–1563, DOI: 10.1126/science.1133755.

[66] Altrock, Philipp M. and Arne Traulsen (2009), 'Fixation times in evolutionary games under weak selection', *New Journal of Physics* **11**:013012, DOI: 10.1088/1367-2630/11/1/013012.

[67] Traulsen, Arne and Christoph Hauert (2009), 'Stochastic evolutionary game dynamics', *Reviews of nonlinear dynamics and complexity*, ed. by Heinz Georg Schuster, vol. II, Wiley-VCH, Weinheim, p. 25–61, DOI: 10.1002/9783527628001.

[68] Kloeden, Peter E. and Eckhard Platen (1992), *Numerical Solution of Stochastic Differential Equations*, Springer Berlin Heidelberg, Berlin, Heidelberg, DOI: 10.1007/978-3-662-12616-5.

[69] Biancalani, Tommaso, Louise Dyson and Alan J. McKane (2014), 'Noise-Induced Bistable States and Their Mean Switching Time in Foraging Colonies', *Physical Review Letters* **112** (3):038101, DOI: 10.1103/PhysRevLett.112.038101.

[70] Atkinson, Kendall E. (1989), *An introduction to numerical analysis*, 2nd ed., Wiley, New York.

[71] Arfken, George B., Hans J. Weber and Frank E. Harris (2012), *Mathematical Methods for Physics and Engineering: A Comprehensive Guide*, 7th ed., Elsevier Academic Press, Oxford, UK.

[72] Gillespie, Daniel T. (1977), 'Exact stochastic simulation of coupled chemical reactions', *The Journal of Physical Chemistry* **81** (25):2340–2361, DOI: 10.1021/j100540a008.

[73] — (2000), 'The chemical Langevin equation', *Journal of Chemical Physics* **113** (1):297–306, DOI: 10.1063/1.481811.

[74] Gibson, Michael A. and Jehoshua Bruck (2000), 'Efficient Exact Stochastic Simulation of Chemical Systems with Many Species and Many Channels', *The Journal of Physical Chemistry A* **104** (9):1876–1889, DOI: 10.1021/jp993732q.

[75] Vestergaard, Christian L. and Mathieu Génois (2015), 'Temporal Gillespie Algorithm: Fast Simulation of Contagion Processes on Time-Varying Networks', *PLOS Computational Biology* **11** (10):e1004579, DOI: 10.1371/journal.pcbi.1004579.

[76] Sandulescu, Mathias et al. (2007), 'Plankton blooms in vortices: the role of biological and hydrodynamic timescales', *Nonlinear Processes in Geophysics* **14** (4):443–454, DOI: 10.5194/npg-14-443-2007.

[77] Neufeld, Zoltán, Peter H. Haynes and Tamás Tél (2002), 'Chaotic mixing induced transitions in reaction–diffusion systems', *Chaos: An Interdisciplinary Journal of Nonlinear Science* **12** (2):426–438, DOI: 10.1063/1.1476949.

[78] Young, William R., Anthony J. Roberts and Gordan R. Stuhne (2001), 'Reproductive pair correlations and the clustering of organisms', *Nature* **412** (6844):328–331, DOI: 10.1038/35085561.

[79] Herrerías-Azcué, Francisco, Vicente Pérez-Muñuzuri and Tobias Galla (2018), 'Stirring does not make populations well mixed', *Scientific Reports* **8** (1):4068, DOI: 10.1038/s41598-018-22062-w.

[80] Herrerías-Azcué, Francisco and Tobias Galla (2017), 'The effects of heterogeneity on stochastic cycles in epidemics', *Scientific Reports* **7** (1):13008, DOI: 10.1038/s41598-017-12606-x.

[81] Herrerías-Azcué, Francisco, Vicente Pérez-Muñuzuri and Tobias Galla (2019), 'Motion, fixation probability and the choice of an evolutionary process', *arXiv preprint*, arXiv: 1901.03596.

[82] Herrerías-Azcué, Francisco and Tobias Galla (2019), 'Consensus and diversity in multi-state noisy voter models', *arXiv preprint*, arXiv: 1903.09198.

[83] Ohtsuki, Hisashi et al. (2006), 'A simple rule for the evolution of cooperation on graphs and social networks', *Nature* **441** (7092):502–505, DOI: 10.1038/nature04605.

[84] Tarnita, Corina E. et al. (2009), 'Evolutionary dynamics in set structured populations', *Proceedings of the National Academy of Sciences* **106** (21):8601–8604, DOI: 10.1073/pnas.0903019106.

[85] Santos, Francisco C., Jorge M. Pacheco and Tom Lenaerts (2006), 'Evolutionary dynamics of social dilemmas in structured heterogeneous populations', *Proceedings of the National Academy of Sciences* **103** (9):3490–3494, DOI: 10.1073/pnas.0508201103.

[86] Antal, Tibor, Sidney Redner and Vishal Sood (2006), 'Evolutionary Dynamics on Degree-Heterogeneous Graphs', *Physical Review Letters* **96** (18):188104, DOI: 10.1103/PhysRevLett.96.188104.

[87] Kermack, William O. and Anderson G. McKendrick (1927), 'A contribution to the mathematical theory of epidemics', *Proceedings of the Royal Society A: Mathematical, Physical and Engineering Sciences* **115** (772):700–721, DOI: 10.1098/rspa.1927.0118.

[88] Alonso, David, Alan J. McKane and Mercedes Pascual (2007), 'Stochastic amplification in epidemics', *Journal of The Royal Society Interface* **4** (14):575–582, DOI: 10.1098/rsif.2006.0192.

[89] Granovsky, Boris L. and Neal Madras (1995), 'The noisy voter model', *Stochastic Processes and their Applications* **55** (1):23–43, DOI: 10.1016/0304-4149(94)00035-R.

Chapter 2

Stirring does not make populations well mixed

Preface

The contents of this chapter constitute a manuscript published by Scientific Reports[1]. The manuscript was authored by Francisco Herrerías-Azcué[2], Vicente Pérez-Muñuzuri[3] and Tobias Galla[2].

F.H.A.'s contributions include the inception of the project, performing all calculations and analysis, coding simulations, producing the data for all figures, finalising all figures, and writing all sections of the paper alongside V.P.M. and T.G.

[1]F. Herrerías-Azcué, V. Pérez-Muñuzuri, and T. Galla, (2018), "Stirring does not make populations well mixed", *Scientific Reports* **8**(1):4068. doi:10.1038/s41598-018-22062-w.

[2]Theoretical Physics, School of Physics and Astronomy, The University of Manchester, Manchester, M13 9PL, United Kingdom.

[3]Group of Nonlinear Physics, Faculty of Physics, University of Santiago de Compostela, E-15782, Santiago de Compostela, Spain.

Abstract

In evolutionary dynamics, the notion of a 'well-mixed' population is usually associated with all-to-all interactions at all times. This assumption simplifies the mathematics of evolutionary processes, and makes analytical solutions possible. At the same time the term 'well-mixed' suggests that this situation can be achieved by physically stirring the population. Using simulations of populations in chaotic flows, we show that in most cases this is not true: conventional well-mixed theories do not predict fixation probabilities correctly, regardless of how fast or thorough the stirring is. We propose a new analytical description in the fast-flow limit. This approach is valid for processes with global and local selection, and accurately predicts the suppression of selection as competition becomes more local. It provides a modelling tool for biological or social systems with individuals in motion.

2.1 Introduction

Population dynamics describes the changes of the composition of a group of individuals over time. Broadly speaking, there are two modelling approaches. One involves well-mixed populations, implying an all-to-all interaction. This is contrasted with structured populations, or populations on networks. Mathematically, the interaction network of well-mixed populations is often assumed to be a 'complete graph' (see e.g. [1–4]), i.e., a network in which interaction links exist between any two individuals at all times. In the context of epidemics, for example, an infection event can affect any of the susceptible individuals in the population; in evolutionary dynamics, it indicates that competition occurs between all members of the population. This effectively means that there is no spatial structure at all, or at least that interaction is sufficiently long-range that spatial structure is not relevant for the evolutionary process.

Assume we place a population of discrete individuals in a container and stir the system. In an experimental situation this could be a bacterial population in a stirred-tank reactor for example, or swimmers who move on their own accord [5–8]. One would naturally think that a well-mixed system can be obtained in this way, provided the stirring is sufficiently thorough, and that one waits long enough. We use computer

simulations and analytical theory to study this scenario. We take a finite population and immerse it in different chaotic flows to mimic stirring. We focus on the situation in which a single mutant invades this population, and ask when the theory for well-mixed populations quantitatively predicts its chances of success. In the language of population genetics, we study the probability of fixation [9].

Work has been done studying the fixation probability on fixed random graphs [1, 10] or adaptive networks [11, 12], where links are rewired to benefit individuals. Our model is different, in that the changes of the interaction network are solely induced by the flow, and cannot be controlled by the individuals at the nodes of the graph. This is closer to what is studied in [13]. In the present paper, however, we focus on frequency-independent selection, so our results cannot directly be compared to those of [13].

Our simulations and analysis show that the predictions of the conventional theory for well-mixed populations do not always capture the outcome of evolutionary processes in stirred environments. Its validity seems not to be primarily a question of the nature or speed of the stirring; instead, it is determined by the interaction range and the type of evolutionary process. As a consequence we think the term 'well-mixed', which at least suggests external stirring, needs to be used with care.

We present an analytical approach to describe stirred populations, in which we abandon the assumption that the interaction graph is complete at all times. Instead, we rely on a broader definition: a population is well mixed if every pair of individuals interacts with the same probability [14–16]. This does not imply, however, that competition occurs among all individuals at all times. At any one time particles take positions in space and compete within an interaction radius. Any given individual therefore competes only against a subset of individuals in the population. If the population is stirred at sufficiently high rates, and if the flow is such that it 'mixes' all parts of the system, the positions of the particles are random at each evolutionary step. The possible interaction partners of a given individual are then effectively sampled uniformly from the entire population, and any two individuals are equally likely to interact. This process can be described analytically, and fixation probabilities can be obtained. In contrast to the conventional theory for well-mixed populations, this method accurately reproduces simulation results for stirred systems.

We show that the conventional theory is only valid for processes in which selection is global, i.e., it occurs between *all* individuals in the population. The method presented here, on the other hand, is also valid for local selection, or a combination of the two. Since the details of the evolutionary dynamics in real-world systems are rarely known with certainty, this flexibility makes our approach relevant for the modelling of experiments where the interacting individuals are in motion.

2.2 Results and methods

2.2.1 Mathematical definition of well-mixed populations

It is fair to say that there is a consensus on what constitutes a well-mixed population in mathematical models of evolutionary dynamics. In order to illustrate this, we focus on stochastic dynamics in finite populations, and use a discrete-time process with frequency-independent fitness. In the first instance we choose a so-called death-birth update; this is sufficient to present our results. Other mechanics of evolution (for example birth-death processes) are considered in Sections 2.4 and 2.5.

The population consists of N individuals; we assume that its size is constant over time. Each individual can either be a mutant or a wildtype. The state of the population at any point in time is characterised by the number of mutants, m; the number of wildtypes is $N - m$. In a traditional well-mixed approach the actual positions of the individuals in space are irrelevant, as everyone can interact with everyone else at all times. There is then nothing else to know about the state of the population. In the Moran model, evolution occurs through combined death-birth events. In each event, one individual is picked at random, regardless of its type, and is removed from the population. One of the remaining individuals is then selected for reproduction and generates an offspring. Selection is based on fitness, and the offspring is of the same species as its parent. We assume frequency-independent selection, and set the fitness of wildtype individuals to one. The invading mutant has fitness r, which can be smaller than one (for disadvantageous mutations) or greater than one (for advantageous mutations). For $r = 1$ the process is neutral.

The dynamics proceed through a sequence of death-birth events until the mutants have either gone extinct ($m = 0$), or reached fixation ($m = N$). When either has

occurred the dynamics stop, as there is only one type of individual left in the population. We focus on the probability, ϕ, for a single invading mutant to reach fixation. Using the theory of Markov processes, an explicit mathematical expression can be found for the fixation probability (see e.g. [9, 17–19]). The fixation probability depends on the fitness of the mutant species, r, and the population size, N. For the death-birth process one has [3, 20]

$$\phi = c\,\frac{1-r^{-1}}{1-r^{-cN}}, \tag{2.1}$$

where $c = (N-1)/N$ for the process described above. We will refer to this as the prediction of the conventional theory for well-mixed populations. If asked how to calculate fixation probabilities in well-mixed populations, most evolutionary theorists would likely point to results such as the one in Eq. (2.1). The details of the mathematical expression may vary for different processes (for example $c = 1$ if self-replacement is included, or if the selection is global), but they are all derived from the assumption of an all-to-all interaction at all times.

Can this be achieved by stirring?

Despite the consensus on what constitutes a well-mixed population (mathematically), it is in practice difficult to determine if a particular biological or social system is well mixed. The term is used in the literature without much specificity. Common verbal characterisations include the requirement that 'all pairs of individuals interact with the same probability' (see e.g. [14–16, 21]), but how precisely this is to be interpreted is often not said. For example, do all individuals have to be able to interact with each other at all times? Or it is sufficient if all pairs interact with equal frequency over time? In most cases no detailed explanation is offered how the complete interaction graph leading to Eq. (2.1) would arise. The term attributed to this formalism—evolutionary dynamics in 'well-mixed' populations—at the very least suggests that this all-to-all interaction can be achieved through some type of external stirring or agitation. It is this assumption that we challenge in this paper.

2.2.2 Models of stirred populations

In order to model the effects of external stirring we assume that the population is subject to a continuous-time flow, moving the individuals around in space [22–30]. For example, one may imagine a population of bacteria in an aqueous environment, which is being shaken or stirred mechanically [5–8]. We focus on two-dimensional systems; this is sufficient to develop the main points we would like to make.

Each evolutionary death-birth event of the Moran process is executed as follows. First, one individual in the population is chosen at random for removal; each individual with equal probability $1/N$. Then, its 'neighbours' (individuals within interaction range R) compete to reproduce and fill the vacancy. This competition is decided by fitness: assuming that n wildtypes and m mutants compete, the probability that the reproducing individual is a wildtype is $n/(n+mr)$, and the probability that a mutant reproduces is $mr/(n+mr)$. The offspring is created with the same type as the parent, and is placed at the position of the individual that has been removed.

It remains to say how often evolutionary events take place relative to the timescale of the flow. In-line with the literature we will describe this by the so-called Damköhler number, Da (see e.g. [30–33]); in the context of our model, the Damköhler number characterises the ratio of the time scales of the flow and the evolutionary process. In our simulations, one evolutionary event occurs every $1/(N\mathrm{Da})$ time units. If Da is very large, the flow is slow compared to evolution. The extreme case $\mathrm{Da} \to \infty$ describes the 'no-flow' limit; on the timescale of the evolutionary dynamics, the positions of the individuals are then static. A very small Damköhler number ($\mathrm{Da} \ll 1$) indicates that the flow is fast compared to evolution. If the conventional theory for well-mixed populations is to apply to populations in a flow, then one would expect it to be in this limit.

We performed simulations of the evolutionary process in different chaotic flows. The velocity fields we use have a periodic time dependency. The time units are expressed in units of the period of the flows, which we set to unity throughout. As an initial example, we focus on the so-called periodic parallel-shear flow [34, 35] in two dimensions. In this flow, particles move horizontally during the first half of the period, subject to shear. In the second half, the motion is in vertical direction, again subject to shear. A random phase, drawn every half period, leads to chaotic motion [34, 35]. We will

discuss further flows below. Details of the flows, including the numerical methods we used to simulate them, are described in Section 2.6.

Results of the simulations for the parallel shear flow are shown in the main panel of Fig. 2.1. The thick purple line is the prediction of the conventional theory for well-mixed systems. The markers represent simulation results for different Damköhler numbers. For fixed mutant fitness, the data suggests that the fixation probability approaches a limiting value as Da is decreased (the flow made faster). However, this limiting value is not the one predicted by Eq. (2.1). This indicates that the conventional well-mixed theory is not applicable, even for fast chaotic flows. As seen in Fig. 2.1 the approach to fast-flow limit can be non-trivial. A more detailed study shows that the nature of this approach depends on the exact nature of the evolutionary process and on the initial conditions, among other things. The current paper focuses on the fast-flow limit itself, but not on the details of how exactly this limit is approached. We next return

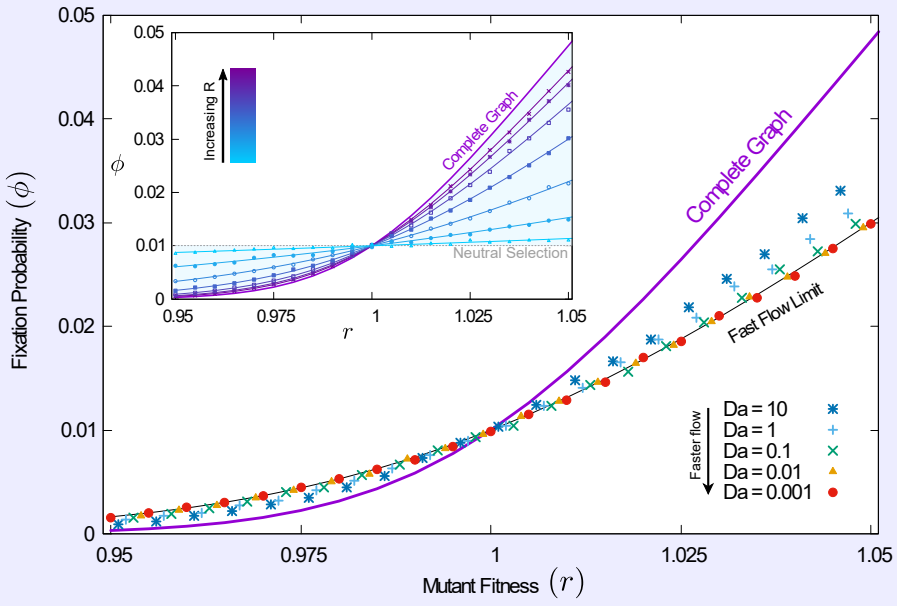

Figure 2.1: Fixation probability of a single mutant in a population stirred by a chaotic flow. The conventional theory for well-mixed systems [Eq. (2.1)] is shown as a thick purple line. Markers represent simulation results. In the main panel, these are shown for different Damköhler numbers. Reducing Da increases the flow speed relative to the evolutionary process. The thin continuous lines represent results from the analytical approach for fast flows [Eq. (2.2)]. The inset shows simulations for different interaction radii. Smaller interaction ranges makes selection increasingly more local, and the fixation probability approaches that of neutral selection, $1/N$, shown for reference (dashed gray line). (Population size $N = 100$; $R = 0.1$ in main panel; Da $= 0.1$ in the inset; interaction radius varies from $R = 0.025$ to $R = 0.175$ in inset. See Section 2.6 for a description of the (parallel-shear) flow.)

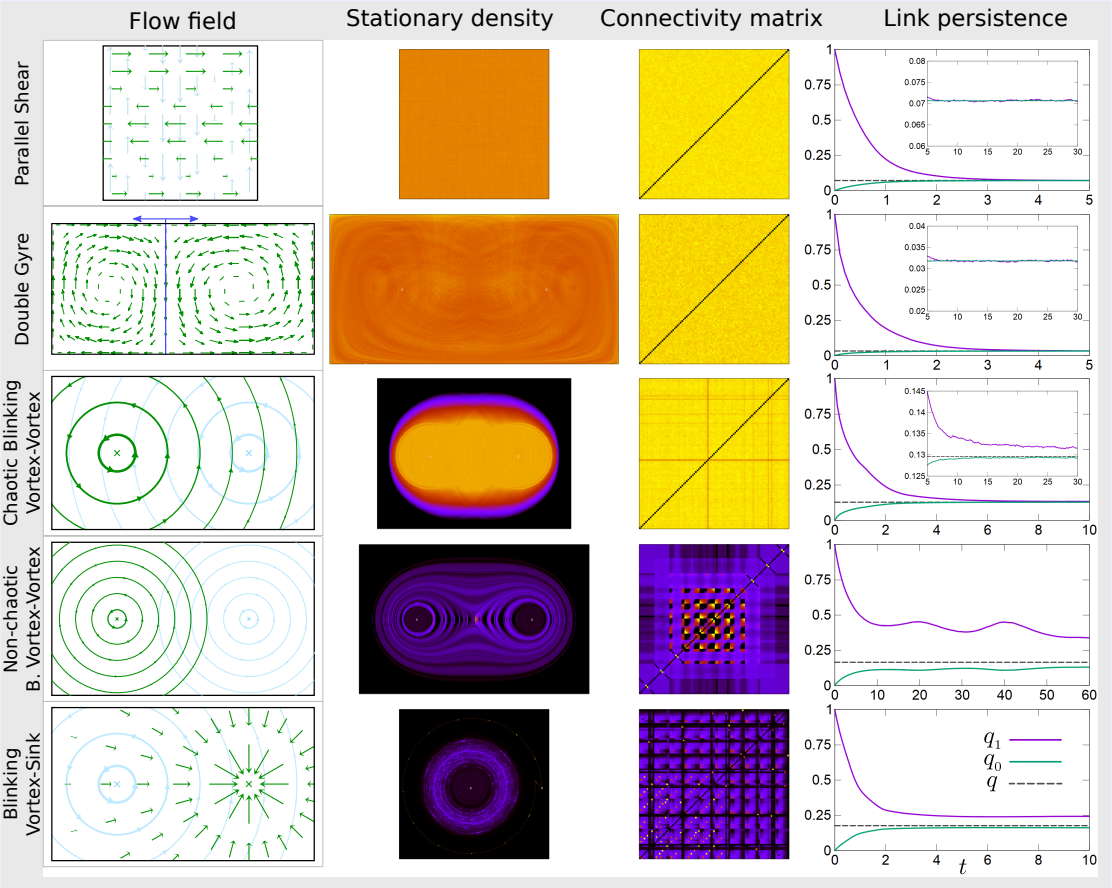

Figure 2.2: Mixing properties of different planar flows. The first column shows a graphical representation of the flow field for a selection of two-dimensional flows (see Section 2.6). Velocity fields are periodic (modulo a random phase), and we use a period of one throughout. Green and blue arrows represent this periodic switching. The second column shows the stationary density of particles in space, as measured from simulations. The fraction of time each pair of particles spend within interaction radius from each other is shown as a connectivity matrix in the third column. Results are from simulations. The fourth column shows the measured link persistence, $q_1(t)$, as well as $q_0(t)$ and the asymptotic connectivity q (see text). Convergence of q_1 and q_0 to a common value q indicates that the flow mixes the system.

to the commonly used verbal description of well-mixed populations, and determine whether any pair of individuals interact with the same probability. Labelling particles and tracking them as the flow proceeds we determine, for each pair, the proportion of time they are within interaction range from each other. This yields a symmetric connectivity matrix, shown in Fig. 2.2. Results indicate that, averaged over time, the parallel-shear flow meets the verbal criterion of good mixing; each individual is equally likely to interact with any other. Now, consider the sequence of times at which a specific individual participates in evolutionary events, i.e., it is chosen to compete or

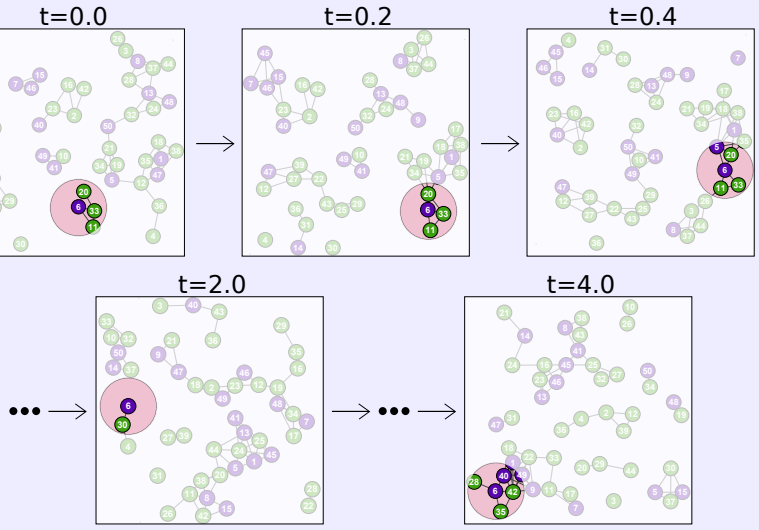

Figure 2.3: Sets of neighbours of an individual at different moments in time. The illustration shows the position of a group of particles as they are moved by the flow. We highlight the time-dependent set of neighbours of one particle. The sets of neighbours remain correlated in the frames shown in the upper row. In the lower row, however, the sets of neighbours are uncorrelated from frame to frame.

to be replaced. In order for a system to be 'well-mixed' it is reasonable to require that the sets of neighbours at the time of an event are uncorrelated from those at earlier events. If this is not the case, the system has not been 'mixed' between the two events. We illustrate this in Fig. 2.3. The top row shows snapshots taken at short intervals, and demonstrates that the sets of neighbours of a particle remain correlated from one frame to the next. If evolutionary steps were to happen on these timescales the system cannot be said to be well mixed. If, on the other hand, evolutionary events occur with lower frequency, the neighbours of a particle at the time of an event are uncorrelated to those at earlier events. This is illustrated in the lower row. To characterise this in more detail, we have measured the probability, $q_1(t)$, that two particles who were within interaction radius at time t_0 are also connected at time $t_0 + t$. In the stationary state, this is independent of t_0. We refer to this quantity as the link persistence. We also measured the probability that two particles who are not connected at an earlier time are connected t units of time later, and denote this quantity by $q_0(t)$. Results are shown in Fig. 2.2.

We write q for probability that two randomly selected individuals are within interaction radius of each other, and refer to this as the connectivity. If a flow mixes

the population well we expect that, eventually, the neighbours of a particle become independent of its earlier neighbours. Then $q_0(t)$ and $q_1(t)$ both tend to q for large enough t. Simulations indicate that this is the case for the parallel-shear flow (see Fig. 2.2). This again confirms that the flow is mixing.

The timescale t_x on which this regime is reached can be obtained from the simulation data shown in Fig. 2.2. It is the point in time when q_0 and q_1 have converged to their common asymptotic value, q. For the parallel-shear flow, as a broad order-of-magnitude estimate, we use $t_x \approx 5$. Mixing thus occurs after approximately five periods with our choice of parameters (see Section 2.6). The stationary particle density is uniform for this flow and, therefore, the stationary value of q can readily be calculated. We expect $q = \pi R^2/A$, where A is the total area of the two-dimensional system and R the interaction radius. In the parallel-shear flow example shown in Fig. 2.2 we have $A = 1$ and $R = 0.15$, consistent with the stationary value of $q \approx 0.07$ observed in the figure.

2.2.3 Analytical description

If the typical time elapsing between evolutionary events involving a fixed particle is larger than t_x, we can assume that the neighbours of the particle are uncorrelated to those in earlier events. This is not dissimilar to the approach of annealed random networks [36, 37]. However, in our case, the interaction network is a random geometric graph [38]. Based on the assumption of uncorrelated neighbourhoods an analytical description can be constructed. In any evolutionary event, one particle is chosen at random for removal. The neighbours of this particle are obtained by randomly sampling the entire population; each particle is in the neighbourhood of the focal individual with probability q. Those neighbours then compete to fill the vacancy. This allows us to derive rates with which mutants replace wildtype individuals or vice-versa. From these rates we then compute the probability for a single mutant to reach fixation; for completeness we also compute times to fixation. Details of these calculations can be found in Section 2.5.5. For r close to one (weak selection) we find

$$\phi = \frac{1 - \widetilde{r}^{-1}}{1 - \widetilde{r}^{-N}}, \tag{2.2}$$

with $\widetilde{r} = r + \langle 1/k \rangle_c (1 - r)$, and where $\langle 1/k \rangle_c$ is the mean inverse degree among individuals who have at least one neighbour. This object depends on the connectivity

q, which in turn depends on the interaction radius R. The weak-selection limit of the result for the complete graph [Eq. (2.1)] is recovered for $q = 1$. If the interaction radius is small, and hence the interaction graph sparse ($q \to 0$), one finds $\langle 1/k \rangle_c \approx 1$, and $\widetilde{r} = 1$, i.e., neutral selection. The finite connectivity of the dynamic interaction graph acts as a suppressor of selection.

The prediction of Eq. (2.2) is shown in the main panel of Fig. 2.1 (solid black line), and agrees with simulations for small Damköhler numbers (fast flows). In the inset of the figure, we show the probability of fixation for different choices of the interaction radius R for fast flows. In all cases, Eq. (2.2) is seen to describe simulations well. The data demonstrates that, depending on the interaction radius, the fixation probability can take any value between the result for neutral selection and the one predicted by the conventional well-mixed theory.

It is important to ask how fast the flow must be for Eq. (2.2) to be valid. Our approach requires that each individual experiences a newly sampled set of neighbours at each event, uncorrelated from its interaction partners at earlier events. Broadly speaking, our approach applies when the typical time τ between events involving a particular individual is larger than the mixing time t_x. The probability that any particular individual is involved in a given evolutionary event can be estimated as $1/N + (1 - 1/N)q$. This means that any individual typically participates in an event every $\tau = [\mathrm{Da}(1 + q(N - 1))]^{-1}$ units of time. In the example of the parallel-shear flow $q \approx 0.07$. For a system with $N = 100$ individuals, $\tau > t_x$ when $\mathrm{Da} \lesssim 0.025$. If this condition is met we expect Eq. (2.2) to apply. This is consistent with the data in Fig. 2.1.

2.2.4 Robustness and applicability to different flow fields

In order to test our approach further we have simulated a range of different flows, as illustrated in Fig. 2.2 and detailed further in Section 2.6. Similar to the parallel-shear flow, the double-gyre flow mixes the system at sufficiently small Damköhler numbers (uniform entries in the connectivity matrix; $q_0, q_1 \to q$). The chaotic blinking-vortex flow is approximately mixing. The non-chaotic blinking-vortex flow and the vortex-sink flow are not mixing, as can be seen in Fig. 2.2. The connectivity matrix resulting from these flows indicates clusters of particles which travel the system together; the set of

neighbours of any one particle can remain correlated indefinitely.

Results for the different flows are shown in Fig. 2.4. Different data points correspond to different choices of the interaction radius, resulting in different connectivities q. The conventional well-mixed theory is represented by the point $q = 1$; our approach interpolates between this value and the one for neutral selection in the dilute limit $q \to 0$. The data in the figure demonstrates that Eq. (2.2) describes the fixation probability accurately for the flows that are mixing. Even for the non-chaotic blinking-vortex and vortex-sink flows it provides a good approximation.

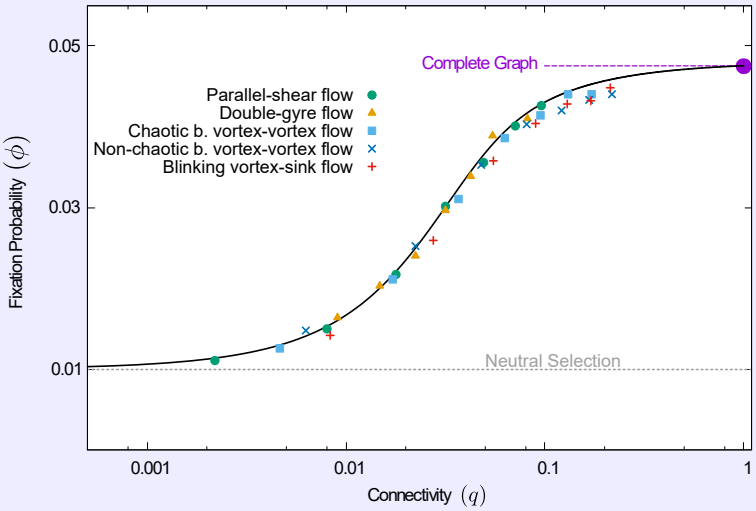

Figure 2.4: Fixation probability as a function of connectivity. Varying the interaction radius interpolates between neutral selection and the theory based on complete graphs. The fast-flow theory applies throughout, provided the flow mixes the particles well. The markers represent simulation results for different flows and different interaction radii, resulting in different connectivities, q. Predictions of the fast-flow theory [Eq. (2.2)] are shown as the solid black line. The conventional well-mixed theory [complete graph, Eq. (2.1)] is indicated by the filled circle at $q = 1$. The dashed gray line is for guidance only, and shows the result for neutral selection, $\phi = 1/N$. (Mutant fitness $r = 1.05$, population size $N = 100$).

2.2.5 Dependence on the size of the population

We show the fixation probability for different population sizes in Fig. 2.5. In the left panel we keep the connectivity q fixed; the average number of neighbours of each individual is then $\langle k \rangle = (N-1)q$. Interestingly, this produces non-monotonic behaviour as a function of N, with minimal fixation probability at a certain population size. For small populations, the sampled neighbourhoods are so small that there is

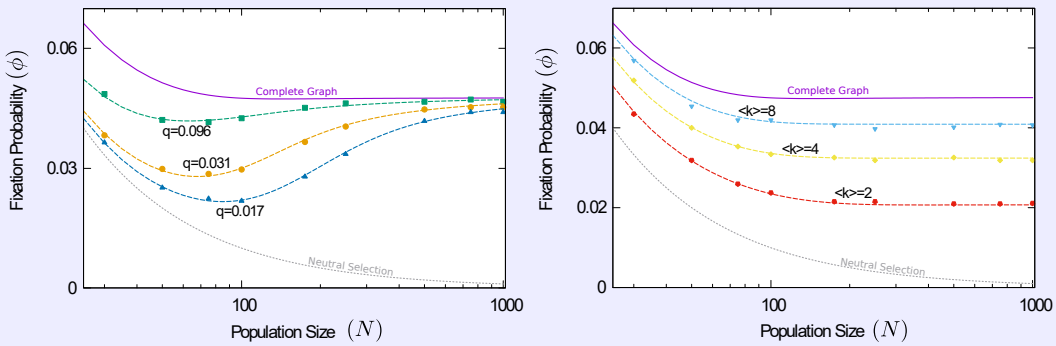

Figure 2.5: Fixation probability as a function of population size. On the left-hand panel, the interaction radius R is fixed as the population size is varied. This results in fixed connectivities, q, but the average number of neighbours of each particle increases with N. On the right-hand panel, the average number of neighbours, $\langle k \rangle$, was fixed by reducing the interaction radius as the population size increases. Markers are simulations for the parallel-shear flow. The conventional theory is shown as the thick purple line. Dashed coloured lines are the predictions of the fast-flow approach. The dashed gray line shows the result for neutral selection. ($r = 1.05$, $\mathrm{Da} = 0.01$ in both panels.)

virtually no competition. The outcome of evolutionary events is dominated by the random composition of the set of neighbours of the removed individual, rather than by fitness. Effectively this results in neutral selection. In this regime, fixation of a single mutant becomes more difficult as N increases, and the fixation probability ϕ is a decreasing function of N. For larger populations, neighbourhoods become large enough to provide a statistically more representative sample of the entire population. Selection becomes increasingly relevant, and the fixation probability of an advantageous mutation increases. In the limit of very large populations, the neighbourhoods are a statistically accurate sample of the entire population. Therefore, the traditional well-mixed theory, based on complete graphs, is recovered. We note that $\langle 1/k \rangle_c$ tends to zero in this limit, so that $\tilde{r} = r$; the predictions of Eqs. (2.1) and (2.2) then agree. In the right panel of Fig. 2.5 the average number of neighbours, $\langle k \rangle$, is kept fixed instead. Interactions are then always within local neighbourhoods, and the conventional complete-graph theory does not apply, even in large populations.

2.3 Discussion

In the existing literature, well-mixed populations are almost always associated with complete interaction graphs. Every member of the population is connected to every

other member at all times. Competition and selection in an evolutionary event then take place among all individuals. The term 'well-mixed' suggests that these conditions can be achieved by stirring spatial systems. As we have shown, this is often not the case. Quantitative differences between the predictions of the conventional theory and simulations of stirred populations can be observed, even when the stirring is fast and when all pairs of individuals are equally likely to interact. We have presented an alternative approach, based on the assumption that any individual, at any one time, interacts with a randomly selected subset of the population. We have demonstrated that our analytical description accurately predicts simulation results, including situations where the conventional theory does not.

So far we have only discussed one type of evolutionary dynamics: a death-birth process. In the model we have described, no competition takes place when the individual for removal is determined. The reproducing individual is selected from the neighbours of the removed and proportional to fitness. This is known as 'local selection' and the process is referred to as a local death-birth process [3, 20, 39]. We write **dB** where the sequence of letters indicates that the death event occurs first and then the birth event, and where the capital letter indicates that selection takes place when the reproducing individual is chosen. Other variants are possible; for example, death-birth processes in which selection only acts when the individual for removal is chosen. This is known as a global death-birth process (**Db**). In very much the same way there are global and local birth-death processes (**Bd**, **bD**) [20, 40]. Similarly selection can act at both the death and birth stages (death-birth process with dual selection (**DB**) or birth-death process with dual selection **BD**). We have tested the applicability of the conventional theory and of our approach to all six different types of processes (see Section 2.5.4). We find that the conventional theory for well-mixed systems is accurate for processes in which selection only acts globally; a description based on a complete interaction graph is then appropriate. The conventional theory becomes invalid, however, when selection acts locally. As summarised in Fig. 2.6, the fast-flow approach we have developed applies in all cases. If the interaction range is limited, individuals do not compete against the entire population at any one time. Our analysis shows that this limited connectivity suppresses selection. Therefore, the conventional theory for well-mixed systems overestimates the fixation probability of advantageous mutants. Our results

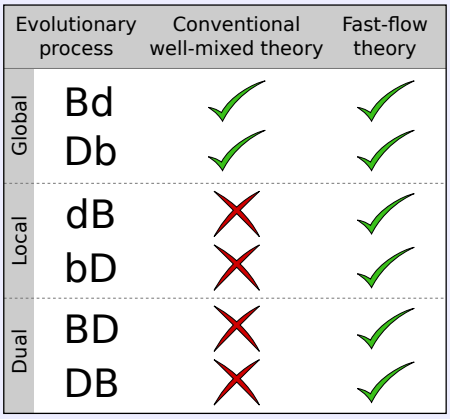

Figure 2.6: Applicability of the conventional well-mixed theory and the fast-flow theory. Evolutionary processes (see text and Section 2.5.4) and indication whether the predictions of the conventional theory for well-mixed systems and of our fast-flow approach agree with simulations. Capital letters in the acronyms for the different processes indicate the presence of selection in the birth or death step. In **Bd** and **Db** competition is in the first step and therefore global. The conventional theory for well-mixed systems applies. In **bD** and **dB** competition is in the second step and therefore selection is local. In **BD** and **DB** competition takes place in both steps (dual selection). In the latter four cases the conventional theory fails. The fast-flow theory predicts simulation results in all six cases.

also suggest that a disadvantageous mutant is more likely to reach fixation when it has a small interaction radius. Similar results have recently been reported by Krieger et al. [29] for structured populations with mobile individuals.

The exact mechanics of evolution and the interaction range of individuals in biological or social systems are often difficult to determine. Mathematical modelling approaches frequently rely on well-mixed populations, due to the fact that these have analytical solutions. In some systems interaction may indeed occur over long distances, for example through signalling, chemical trails or the production of public goods [41–44]. Established approaches based on complete interaction graphs are then appropriate. Most systems, however, have a limited interaction range [21, 45], and as consequence conventional well-mixed theories may not apply.

There is considerable theoretical work on the effects of local interactions in static structured populations [2, 14, 21, 45, 46]. Expressions for the fixation probability of invading mutants are known. However, populations in many social or biological systems are moving and the interaction network is dynamic. The fast-flow approach provides a tool that should prove useful for the modelling of situations in which individuals are in motion.

2.4 Appendix A: Evolutionary processes

Two types of processes are widely used in the literature to model evolutionary dynamics: *birth-death* processes and *death-birth* processes. A birth-death process in a spatial system or network occurs in two steps: first, an individual is chosen for reproduction from the entire population; then, one of its neighbours is chosen, and is replaced by an offspring of the first individual. In the second type of process, death-birth, the individual chosen in step one is removed from the population, and one of its neighbours is chosen to produce an offspring in the 'vacant' place. For clarity we stress again that two particles in the spatial system are considered to be 'neighbours' if their distance is less than the interaction radius.

Each of these steps may or may not include an element of selection. Selection indicates that the choice of individual is based on fitness. Throughout our paper, we focus only on frequency-independent selection, i.e., the fitness of each type of individual only depends on the species it belongs to (mutant or wildtype), but not on the composition of its neighbourhood. In the literature, the most widely used update processes only include selection in the reproduction step. In principle, however, each individual can carry two types of fitness [20]. One is reproductive fitness; when competition occurs in the reproduction stage, it determines the probability that an individual is picked. If selection occurs during the choice of an individual for removal, we think of the resilience (against removal) as a 'death fitness'. It plays the same role as the reproduction fitness, but in the removal stage. Individuals with a higher 'death fitness' are less likely to be chosen for removal. Without loss of generality, we set both fitnesses of the wildtype to one. We write r for the mutant's reproductive fitness, and $1/d$ for its death fitness. The quantity d then describes a propensity to die.

Six possible processes can then be considered. The first three are birth-death processes. Selection can occur only in the birth step (**Bd**), only in the removal step (**bD**), or in both (**BD**). Similarly, for death-birth processes one has **Db**, **dB** and **DB**. Capital letters indicate that the step involves selection, and lower case letters indicate the absence of selection.

It is important to stress that the first individual in each birth-death or death-birth event is chosen from the *entire* population. If selection occurs at this step, this selection

is *global*. The second individual is chosen among the neighbours of the first. Therefore, if selection occurs in this phase, it is *local* selection.

The most general birth-death process involves selection in both steps (**BD**, $r \neq 1$, $d \neq 1$). If $d = 1$, the birth-death process is of the type **Bd**. Selection takes place when individuals are chosen from the entire population, and it is hence global selection. For this reason, the process is also referred to as a global birth-death process. A dynamics of the type **bD** is a local birth-death process process ($r = 1$). The nomenclature for global and local death-birth processes is similar (**Db** denotes the global death-birth process, and **dB** the local death-birth process, respectively).

2.5 Appendix B: The limit of fast flows

2.5.1 Setup and notation

A focal individual is chosen in step one of a birth-death or death-birth process. Interaction then occurs with one of its neighbours (particles within its interaction radius R). In the limit of fast flow, we assume that this neighbourhood is sampled from the entire population at random (excluding the focal individual). Each individual is in the neighbourhood with probability q, and it is not a neighbour with probability $1 - q$.

The connectivity q will depend on the interaction radius. The parallel-shear flow, for example, generates a uniform stationary density of particles. Therefore, any randomly chosen individual will be a neighbour of the focal individual with probability $q = \pi R^2/A$, where A is the total area of the system. This assumes $0 < R < (A\pi)^{-1/2}$ and periodic boundary conditions. For $R \geq (A\pi)^{-1/2}$ the network is fully connected ($q = 1$).

With these assumptions the degree distribution is binomial; the probability that the focal individual has exactly k neighbours is

$$P_k = \binom{N-1}{k} q^k \left(1-q\right)^{N-1-k}. \tag{2.3}$$

Assume now that there are m mutants in the population and $N - m$ wildtypes. If the focal individual is a mutant, the probability that there are l mutants among its k neighbours is

$$P^{(m)}(l|k) = \binom{k}{l} \left(\frac{m-1}{N-1}\right)^l \left(1 - \frac{m-1}{N-1}\right)^{k-l}. \tag{2.4}$$

Instead, if the focal individual is a wildtype the probability that l of its k neighbours are mutants is

$$P^{(w)}(l|k) = \binom{k}{l} \left(\frac{m}{N-1}\right)^l \left(1 - \frac{m}{N-1}\right)^{k-l}. \tag{2.5}$$

We next consider the situation in which k individuals compete (for example to replace a removed individual). Assuming that l of the k individuals are mutants (with fitness r) and $k-l$ are wildtypes (with fitness one) we write $g_{kl}(r)$ for the probability that a mutant is selected. We have

$$g_{kl}(r) = \frac{lr}{(k-l)+lr}. \tag{2.6}$$

The quantity $1 - g_{kl}(r)$ is the probability that a wildtype is selected in this situation. If selection acts during the removal step, the probability that the individual chosen for removal is a mutant is $g_{kl}(d)$.

It is also useful to define

$$\begin{aligned} H^{(m)}(r) &= \sum_{k=1}^{N-1} \sum_{l=0}^{k} P_k \, P^{(m)}(l|k)[1 - g_{kl}(r)], \\ H^{(w)}(r) &= \sum_{k=1}^{N-1} \sum_{l=0}^{k} P_k \, P^{(w)}(l|k) g_{kl}(r), \end{aligned} \tag{2.7}$$

where the double sums run over all neighbourhood compositions of the focal individual. The quantity $H^{(m)}$ describes the probability with which a wildtype is selected among the neighbours of a mutant focal individual, and $H^{(w)}$ the probability that a mutant is selected from the neighbourhood of a wildtype.

In each death-birth or birth-death event, the number of mutants in the population may increase by one ($m \to m+1$), decrease by one ($m \to m-1$), or remain unchanged. We write T_m^+ for the probability that m increases by one, and T_m^- for the probability that m decreases by one. For birth-death processes we have

$$\begin{aligned} T_m^+ &= \frac{mr}{mr+N-m} \times H^{(m)}(d), \\ T_m^- &= \frac{N-m}{mr+N-m} \times H^{(w)}(d), \end{aligned} \tag{2.8}$$

where the fraction on the right-hand side in the expression for T_m^+ is the probability that the individual selected for birth is a mutant, or that it is a wildtype in the expression for T_m^-.

For death-birth processes we have

$$\begin{aligned} T_m^+ &= \frac{N-m}{md+N-m} \times H^{(w)}(r), \\ T_m^- &= \frac{md}{md+N-m} \times H^{(m)}(r). \end{aligned} \tag{2.9}$$

2.5.2 Fixation probability

For any one-step process, the probability of fixation of a single mutant in a population of size N can be written as [19]

$$\phi = \frac{1}{1+\sum_{j=1}^{N-1}\prod_{m=1}^{j}\gamma_m}, \tag{2.10}$$

where $\gamma_m = T_m^-/T_m^+$, sometimes known as the evolutionary drift.

For the **BD** and **DB** processes we have, respectively,

$$\begin{aligned} \gamma_m^{BD}(r,d) &= \frac{N-m}{mr}\frac{H^{(w)}(d)}{H^{(m)}(d)}, \\ \gamma_m^{DB}(r,d) &= \frac{md}{N-m}\frac{H^{(m)}(r)}{H^{(w)}(r)}. \end{aligned} \tag{2.11}$$

We note that $\gamma_m^{BD}(r,d) = \left[\gamma_m^{DB}(d,r)\right]^{-1}$.

Substituting Eqs. (2.11) into Eq. (2.10) yields the fixation probability for the two types of processes:

$$\phi_{BD}(r,d) = \frac{1}{1+\sum_{j=1}^{N-1}\prod_{m=1}^{j}\frac{N-m}{mr}\frac{H^{(w)}(d)}{H^{(m)}(d)}} \tag{2.12}$$

$$\phi_{DB}(d,r) = \frac{1}{1+\sum_{j=1}^{N-1}\prod_{m=1}^{j}\frac{md}{N-m}\frac{H^{(m)}(r)}{H^{(w)}(r)}} \tag{2.13}$$

These closed-form expressions can readily be evaluated numerically.

For the global processes, there is no selection in the second step of evolutionary events, and so the expressions for $H^{(m)}$ and $H^{(w)}$ simplify considerably. If followed through, Eqs. (2.12) and (2.13) can be reduced to

$$\begin{aligned} \phi_{BD}(r,d=1) &= \phi_{Bd} \equiv \frac{1-r^{-1}}{1-r^{-N}}, \\ \phi_{DB}(r=1,d) &= \phi_{Db} \equiv \frac{1-d}{1-d^N}, \end{aligned} \tag{2.14}$$

which are the well-known results for the complete graph [19]. It is important to note that these equations are for processes in which selection acts in the first stage of the birth-death or death-birth events. This means that selection acts globally, and that *all* N individuals in the population are in competition. The **dB** process used in the main text is slightly different. In that model, selection does not act in the first stage of each event, it acts in the second. Therefore, unless self-replacement is allowed, selection is made among $N-1$ individuals even if the interaction graph is complete (the entire population, except the individual chosen in the first stage). This leads to a slightly different expression, see e.g. Eq. (2.1), even though both processes have selection only in the birth stage. As the system size increases, however, the difference between **dB** and **Bd** on a complete graph becomes small, and so the result in Eq. (2.1) tends to that in the first equation of (2.14).

The predictions for the local birth-death and death-birth processes (**bD** and **dB**) do not reduce to expressions as simple as those in Eqs. (2.14). This is perhaps to be expected from previous studies of local processes on static networks, which have shown that the traditional well-mixed theory is only valid for a very narrow set of graphs [46].

2.5.3 Approximation in the limit of weak selection

We now proceed to simplify the expressions in Eqs. (2.12) and (2.13). We will focus on the case of the **DB** process, but similar expressions can be obtained for **BD** upon replacing d by r. We begin by simplifying the expressions for $H^{(m)}$ and $H^{(w)}$ in Eqs. (2.7),

$$\begin{aligned} H^{(m)}(d) &= \sum_{k=1}^{N-1} P_k \sum_{l=0}^{k} \binom{k}{l} \left(\frac{m-1}{N-1}\right)^l \left(1-\frac{m-1}{N-1}\right)^{k-l} \left(\frac{k-l}{ld+k-l}\right), \\ H^{(w)}(d) &= \sum_{k=1}^{N-1} P_k \sum_{l=0}^{k} \binom{k}{l} \left(\frac{m}{N-1}\right)^l \left(1-\frac{m}{N-1}\right)^{k-l} \left(\frac{ld}{ld+k-l}\right). \end{aligned} \quad (2.15)$$

Since $\frac{k-l}{ld+k-l} = 1 - \frac{ld}{ld+k-l}$, we only need to compute objects of the type $\sum_{l=0}^{k} \binom{k}{l} x^l (1-x)^{k-l} \left(\frac{ld}{ld+k-l}\right)$. We expand in powers of $1-d$, and keeping only terms to first order we obtain (after re-arranging terms)

$$\begin{aligned} \frac{ld}{ld+k-l} &= 1 + \left(\frac{l}{k}-1\right) \sum_{i=0}^{\infty} \left(\frac{l}{k}(1-d)\right)^i \\ &= \frac{l}{k}d + \left(\frac{l}{k}\right)^2 (1-d) + \mathcal{O}\left((1-d)^2\right). \end{aligned} \quad (2.16)$$

Using this approximation we find

$$\begin{aligned}
&\sum_{l=0}^{k}\binom{k}{l}x^l\left(1-x\right)^{k-l}\left(\frac{ld}{ld+k-l}\right)\\
&\qquad=\sum_{l=0}^{k}\binom{k}{l}x^l\left(1-x\right)^{k-l}\left[d\frac{l}{k}+\left(\frac{l}{k}\right)^2(1-d)\right]+\mathcal{O}\left((1-d)^2\right)\\
&\qquad=d\;x+(1-d)\left(\frac{x}{k}+\frac{x^2\left(k-1\right)}{k}\right)+\mathcal{O}\left((1-d)^2\right)\\
&\qquad=d\;x+(1-d)\,x^2+\frac{(1-d)\left(x-x^2\right)}{k}+\mathcal{O}\left((1-d)^2\right). \qquad (2.17)
\end{aligned}$$

The expressions in Eqs. (2.15) can therefore be approximated as

$$\begin{aligned}
H^{(m)}(d)&\approx\sum_{k=1}^{N-1}P_k\left[1-d\left(\frac{m-1}{N-1}\right)-(1-d)\left(\frac{m-1}{N-1}\right)^2\right.\\
&\qquad\left.-\frac{1}{k}(1-d)\left(\left(\frac{m-1}{N-1}\right)-\left(\frac{m-1}{N-1}\right)^2\right)+\ldots\right]\\
&=\left(\frac{N-m}{N-1}\right)\left[\left(\sum_{k=1}^{N-1}P_k\right)+(1-d)\left(\frac{m-1}{N-1}\right)\left(\sum_{k=1}^{N-1}P_k\frac{k-1}{k}\right)\right]+\mathcal{O}\left((1-d)^2\right)\\
&=\left(\frac{N-m}{N-1}\right)q_c\left[1+(1-d)\left(\frac{m-1}{N-1}\right)\left(1-\left\langle\frac{1}{k}\right\rangle_c\right)\right]+\mathcal{O}\left((1-d)^2\right),\\
H^{(w)}(d)&\approx\sum_{k=1}^{N-1}P_k\left[d\left(\frac{m}{N-1}\right)+(1-d)\left(\frac{m}{N-1}\right)^2+\frac{(1-d)\left(\left(\frac{m}{N-1}\right)-\left(\frac{m}{N-1}\right)^2\right)}{k}+\ldots\right]\\
&=\left(\frac{m}{N-1}\right)\left[\left(\sum_{k=1}^{N-1}P_k\right)-(1-d)\left(\frac{N-m-1}{N-1}\right)\left(\sum_{k=1}^{N-1}P_k\frac{k-1}{k}\right)\right]+\mathcal{O}\left((1-d)^2\right)\\
&=\left(\frac{m}{N-1}\right)q_c\left[1+(1-d)\left(\frac{N-m-1}{N-1}\right)\left(1-\left\langle\frac{1}{k}\right\rangle_c\right)\right]+\mathcal{O}\left((1-d)^2\right). \qquad (2.18)
\end{aligned}$$

In these expressions we have written

$$q_c\equiv\sum_{k=1}^{N-1}P_k=1-P_0 \qquad (2.19)$$

for the probability that a randomly chosen individual has at least one neighbour, and

$$\left\langle\frac{1}{k}\right\rangle_c\equiv\frac{1}{q_c}\sum_{k=1}^{N-1}\frac{P_k}{k}. \qquad (2.20)$$

This expression describes the average inverse degree of all nodes with at least one neighbour.

Substituting Eqs. (2.18) into Eqs. (2.11), and again expanding in powers of $d-1$ and $r-1$, respectively, yields

$$\begin{aligned}
\gamma^{BD}(r,d)&=\frac{1}{r}\left[1-(1-d)\left(1-\langle 1/k\rangle_c\right)\right]+\mathcal{O}\left((1-d)^2\right),\\
\gamma^{DB}(d,r)&=d\left[\frac{1}{1-(1-r)\left(1-\langle 1/k\rangle_c\right)}\right]+\mathcal{O}\left((1-r)^2\right). \qquad (2.21)
\end{aligned}$$

In contrast with Eqs. (2.11), the first-order expressions on the right-hand side are now independent of m. It is therefore straightforward to evaluate the general expression for the fixation probability of a single mutant [Eq. (2.10)]. For the **BD** process this leads to

$$\begin{aligned}\phi_{BD}(r,d) &= \frac{1}{1+\sum_{j=1}^{N-1}\prod_{m=1}^{j}\frac{1}{r}\left[1-(1-d)\left(1-\langle 1/k\rangle_c\right)\right]} \\ &= \frac{1-\left(\frac{d+\langle 1/k\rangle_c(1-d)}{r}\right)}{1-\left(\frac{d+\langle 1/k\rangle_c(1-d)}{r}\right)^N},\end{aligned} \tag{2.22}$$

where we have neglected contributions of order $(1-d)^2$ and higher.

In the case of the global process (**Bd**, $d=1$), this reduces to Eq. (2.14). For the local process (**bD**) we have $r=1$, and so Eq. (2.22) reduces to

$$\phi_{BD}(r=1,d) = \phi_{bD} = \frac{1-\widetilde{d}}{1-\widetilde{d}^N}, \tag{2.23}$$

with

$$\widetilde{d} = d + \langle 1/k\rangle_c (1-d). \tag{2.24}$$

Similarly, for the **DB** process we have (disregarding corrections of order $(1-r)^2$ and higher)

$$\begin{aligned}\phi_{DB}(d,r) &= \frac{1}{1+\sum_{j=1}^{N-1}\prod_{m=1}^{j} d\left(\frac{1}{1-(1-r)\left(1-\langle 1/k\rangle_c\right)}\right)} \\ &= \frac{1-\left(\frac{d}{r+\langle 1/k\rangle_c(1-r)}\right)}{1-\left(\frac{d}{r+\langle 1/k\rangle_c(1-r)}\right)^N}.\end{aligned} \tag{2.25}$$

Setting $r=1$ recovers the result for the global death-birth process (**Db**) in Eq. (2.14). For the local process (**dB**) we have $d=1$, and so Eq. (2.25) reduces to

$$\phi_{DB}(1,r) = \phi_{dB} = \frac{1-\widetilde{r}^{-1}}{1-\widetilde{r}^{-N}}, \tag{2.26}$$

with

$$\widetilde{r} = r + \langle 1/k\rangle_c (1-r). \tag{2.27}$$

This corresponds to the local death-birth process (**dB**), and is the focus of the main text [see Eq. (2.2)].

To test the accuracy of the weak-selection approximation leading to Eq. (2.26) we compare its predictions against that of the full expression of Eq. (2.13) in Fig. 2.7. In the left-most pane, we plot the fixation probability as a function of the connectivity for different mutant fitnesses. Since the approximation requires weak-selection, deviations are expected when r is significantly different from one. In the other two panels, we show the fixation probability as a function of the population size (see also Fig. 2.5), keeping the connectivity q constant (central panel), or fixing the average number of neighbours $\langle k \rangle$ instead (panel on the right). As can be seen in the figure, the approximation remains valid for any system size.

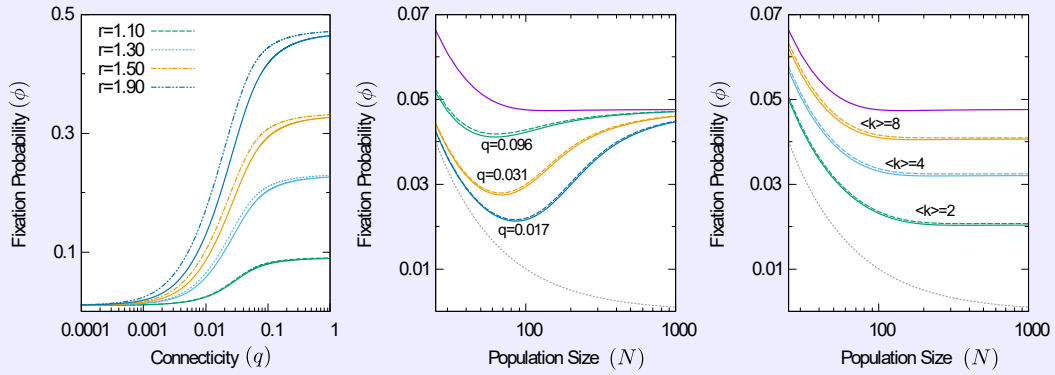

Figure 2.7: Test of the weak-selection approximation. The left panel shows the fixation probability as a function of the connectivity q for different mutant fitnesses. The central and right panel show the fixation probability of a mutant with fitness $r = 1.05$ as a function of the population size (q fixed in central panel, average degree $\langle k \rangle$ fixed on the right). Continuous lines show the equations prior to the approximation [Eq. (2.13)], and dashed lines show the equations after the approximation [Eq. (2.26)]. As can be seen, the approximation is valid for all system sizes, but is sensitive at large fitnesses.

2.5.4 Validity of well-mixed and fast-flow theories for the different evolutionary processes

In this section we comment on the applicability of the conventional well-mixed theory and that of our approach to the six types of birth-death and death-birth processes briefly discussed in the main text. Two individuals directly participate in each evolutionary event. The first is chosen from the entire population, and the second from the neighbours of the first individual. Two particles are 'neighbours' when the distance between them is at most R (the interaction radius). The ordering (birth-death versus death-birth)

indicates whether the individual that is chosen first is removed from the population (death-birth) or whether it reproduces (birth-death). Capital letters in the acronyms indicate whether selection takes place in each of the two steps, i.e., in **BD** and **DB** processes, both steps involve selection, in **Db** and **Bd** only the first step (global selection), and in **dB** and **bD** only the second step (local selection).

Global processes: Db and Bd

The global processes are obtained by setting $r = 1$ in a general death-birth process (resulting in **Db**), or setting $d = 1$ in a general birth-death process (resulting in **Bd**). Our approach for the fast-flow limit then reduces to the conventional well-mixed theory, and the predictions for the fixation probability of a single mutant are those in Eqs. (2.14). These agree well with simulations, as shown in Fig. 2.8 (compare crosses and dark purple line). For simplicity we use $d = 1/r$; in this case the two equations in Eqs. (2.14) are identical.

Local processes: dB and bD

The local processes are obtained by setting $d = 1$ in a general death-birth process (resulting in **dB**), or setting $r = 1$ in a general birth-death process (resulting in **bD**). For weak selection, the predictions from our theoretical approach for the fixation probability of a single mutant is then given by Eq. (2.23) for **bD**, and Eq. (2.26) for **dB**. These are different from the predictions of the conventional theory for well-mixed systems, Eqs. (2.14). The simulation data (empty squares and circles) in Fig. 2.8 agree with the predictions of Eqs. (2.23, 2.26), shown as a dashed blue line (for $d = 1/r$ the predictions of these two equations are indistinguishable on the scale of the graph). The conventional theory (dark purple line) deviates from the simulation data.

Selection in both steps: DB and BD

In the **DB** and **BD** processes selection takes place in both steps. The predictions of our approach are those of Eqs. (2.22) and (2.25) and are shown as a dashed red line in Fig. 2.8 (for $d = 1/r$ the predictions of the two equations are again indistinguishable on the scale of the figre). They agree with the simulation results (solid triangles and pentagons). The predictions of the complete-graph theory for the processes with dual selection is also shown for comparison (light purple line).

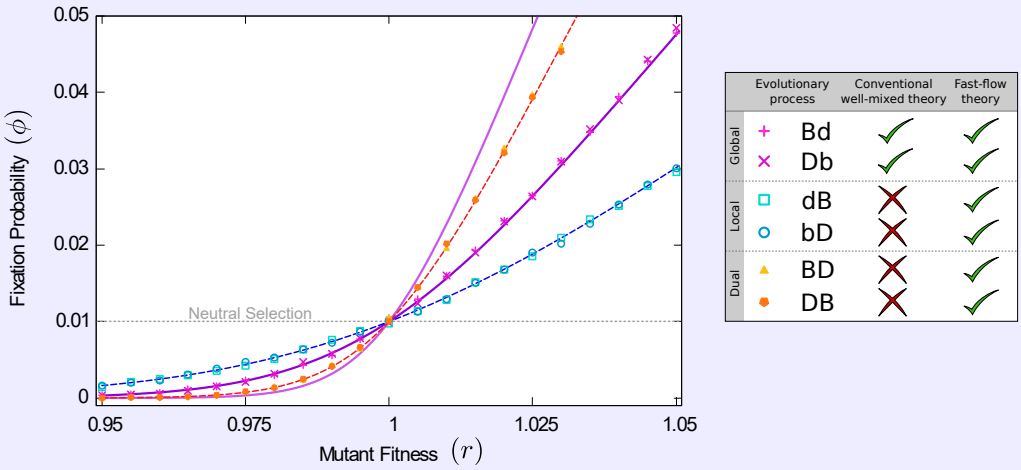

Figure 2.8: Fixation probability as a function of fitness for the different update processes. Continuous thick lines show the conventional well-mixed theory for processes with dual selection (light purple) or selection in only one step (dark purple). Dashed lines show the fast-flow theory for dual selection (red), or local selection (blue). We use $d = 1/r$. The theoretical predictions for **BD** and **DB** are then indistinguishable on the scale of the figure, and similarly for the pairs **Bd-Db**, and **bD-dB** respectively. Simulation results are for the parallel-shear flow, with $\mathrm{Da} = 0.01$, $R = 0.1$ and $N = 100$.

2.5.5 Times to fixation

Another quantity of interest is the time it takes for a single mutant to reach fixation. This is known as the conditional time to fixation, and is described in general by [47]

$$\tau = \sum_{j=1}^{N-1} \sum_{i=1}^{j} \frac{\phi_i}{T_i^+} \prod_{m=i+1}^{j} \gamma_m, \tag{2.28}$$

where ϕ_i is the probability of fixation from state i, in turn given by

$$\phi_i = \frac{1 + \sum_{k=1}^{i-1} \prod_{l=1}^{k} \gamma_l}{1 + \sum_{k=1}^{N-1} \prod_{l=1}^{k} \gamma_l}. \tag{2.29}$$

Using γ_m as defined in Eqs. (2.11), the expression in Eq. (2.28) can be written explicitly as

$$\begin{aligned}
\tau_{BD} &= \sum_{j=1}^{N-1} \sum_{i=1}^{j} \frac{1 + \sum_{k=1}^{i-1} \prod_{l=1}^{k} \frac{N-l}{lr} \frac{H^{(w)}(d)}{H^{(m)}(d)}}{1 + \sum_{k=1}^{N-1} \prod_{l=1}^{k} \frac{N-l}{lr} \frac{H^{(w)}(d)}{H^{(m)}(d)}} \frac{\prod_{m=i+1}^{j} \frac{N-m}{mr} \frac{H^{(w)}(d)}{H^{(m)}(d)}}{\frac{ir}{ir+N-i} \times H^{(m)}(d)}, \\
\tau_{DB} &= \sum_{j=1}^{N-1} \sum_{i=1}^{j} \frac{1 + \sum_{k=1}^{i-1} \prod_{l=1}^{k} \frac{ld}{N-l} \frac{H^{(m)}(r)}{H^{(w)}(r)}}{1 + \sum_{k=1}^{N-1} \prod_{l=1}^{k} \frac{ld}{N-l} \frac{H^{(m)}(r)}{H^{(w)}(r)}} \frac{\prod_{m=i+1}^{j} \frac{md}{N-m} \frac{H^{(m)}(r)}{H^{(w)}(r)}}{\frac{N-i}{id+N-i} \times H^{(w)}(r)},
\end{aligned} \tag{2.30}$$

with $H^{(m)}$ and $H^{(w)}$ defined as in Eqs. (2.7). These equations can be readily evaluated numerically.

As with the fixation probabilities, we note that these expressions greatly simplify for the global processes. Since competition takes place among the whole population, the evolutionary drifts are simply given by $\gamma_m^{Bd}(r,1) = 1/r$ and $\gamma_m^{Db}(1,r) = d$, which results in conditional times to fixation of

$$\begin{aligned} \tau_{Bd} &= \frac{(N-1)}{q_c r\left(1-r^{-N}\right)} \sum_{j=1}^{N-1} \sum_{i=1}^{j} \frac{(ir+N-i)\left(r^{i-j}-r^{-j}\right)}{i\,(N-i)}, \\ \tau_{Db} &= \frac{(N-1)}{q_c\left(1-d^{N}\right)} \sum_{j=1}^{N-1} \sum_{i=1}^{j} \frac{(id+N-i)\left(d^{j-i}-d^{j}\right)}{i\,(N-i)}, \end{aligned} \tag{2.31}$$

with q_c as defined in Eq. (2.19). A similar simplification is not possible for the local processes, but we can make use of the weak selection approximation obtained for the fixation probabilities.

Inserting Eqs. (2.18) and (2.21) into Eqs. (2.30) leads to

$$\begin{aligned} \tau_{BD} &= \frac{(N-1)}{q_c r\left[1-\left(\frac{\tilde{d}}{r}\right)^{N}\right]} \sum_{j=1}^{N-1} \sum_{i=1}^{j} \frac{(ir+N-i)\left[\left(\frac{\tilde{d}}{r}\right)^{j-i}-\left(\frac{\tilde{d}}{r}\right)^{j}\right]}{i\,(N-i)\left[1+\frac{\left(1-\tilde{d}\right)(i-1)}{N-1}\right]}, \\ \tau_{DB} &= \frac{(N-1)}{q_c\left[1-\left(\frac{d}{\tilde{r}}\right)^{N}\right]} \sum_{j=1}^{N-1} \sum_{i=1}^{j} \frac{(id+N-i)\left[\left(\frac{d}{\tilde{r}}\right)^{j-i}-\left(\frac{d}{\tilde{r}}\right)^{j}\right]}{i\,(N-i)\left[1+\frac{(1-\tilde{r})(N-i-1)}{N-1}\right]}, \end{aligned} \tag{2.32}$$

where we used the same notation of $\tilde{r}$ and $\tilde{d}$ as in Eqs. (2.27,2.24). It is straightforward to see that the equations for the global processes are recovered by setting $d = 1$ (therefore $\tilde{d} = 1$) for the BD process, and $r = 1$ (therefore $\tilde{r} = 1$) for the DB process.

The predictions of Eqs. (2.30) and (2.32) are compared with simulation results in Fig. 2.9. The conditional fixation times before the approximation are shown as thick continuous lines. Note that since we set $d = r^{-1}$, birth-death and death-birth processes are indistinguishable in the scale of the graph. The dashed lines represent the weak selection approximation. Note that $\tilde{d} = \tilde{r}^{-1} + \mathcal{O}[(r-1)^2]$, and that the last term of the denominator is different for birth-death and death-birth processes. Therefore, the two update choices do not completely overlap for local and dual selection. For the global processes the approximation recovers Eqs. (2.30), as expected.

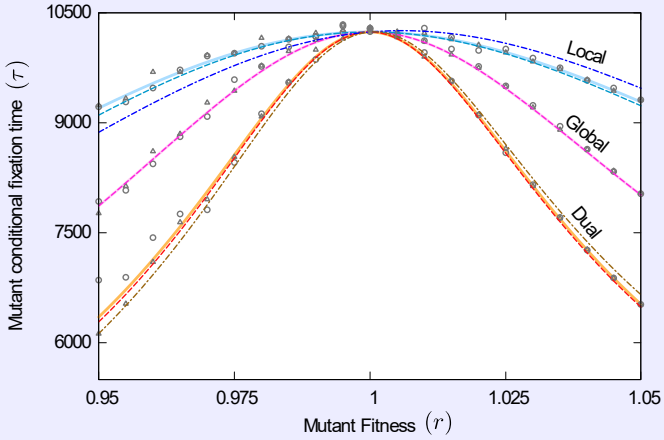

Figure 2.9: Fixation time as a function of fitness for the different update processes. Thick continuous lines represent the fixation times prior to the approximation [Eqs. (2.30)]. We use $d = 1/r$ and so db and bd processes overlap. Dashed lines show the weak selection approximation for birth-death processes, and dash-dotted lines for the death-birth processes [Eqs. (2.32)]. The traditional complete-graph approach overlaps with the global processes. Simulation results are plotted with circles for birth-death processes, and triangles for death-birth processes, and were obtained using the parallel-shear flow, with Da $= 0.01$, $R = 0.1$ and $N = 100$.

2.6 Appendix C: Description of the flows

To test our analytic predictions we have used a selection of different flows, as summarised in Fig. 2.2. These are all planar flows and, as a consequence, an explicit time dependence is necessary to allow for chaotic motion. Each flow is defined by a flow field, $v_x(x, y, t)$ and $v_y(x, y, t)$. We treat the individuals in the population as Lagrangian particles; their motion is governed by $\dot{x} = v_x(x, y, t)$, $\dot{y} = v_y(x, y, t)$. We write $\mathbf{v} = (v_x, v_y)$

All flows we have used are periodic $\mathbf{v}(x, y, t + T) = \mathbf{v}(x, y, t)$, where T is the period (we use $T = 1$ throughout). The only exception is the parallel-shear flow, which additionally involves a phase, randomly chosen at the beginning of each half period. Details of the flows can be found in the literature [34, 35, 48–50]. We briefly describe their main features below.

2.6.1 Parallel-Shear

In this flow, particles move in the domain $0 \leq x, y \leq 1$, with periodic boundary conditions.

For the first half of the period ($nT \leq t < nT + T/2$), the particles move horizontally,

with a velocity which depends on their vertical position. Specifically

$$\begin{aligned} v_x(x,y,t) &= V_{\max} \sin\left(2\pi y_t + \phi\right), \\ v_y(x,y,t) &= 0. \end{aligned} \tag{2.33}$$

The constant pre-factor $V_{\max}$ sets the overall magnitude of the flow. We use $V_{\max} = 1.4$. The phase ϕ is drawn randomly from the interval $[0, 2\pi)$ at the beginning of each half period.

During the second half of each period $[nT + T/2 \leq t < (n+1)T]$, the particles move vertically, with a velocity that depends on their horizontal position,

$$\begin{aligned} v_x(x,y,t) &= 0, \\ v_y(x,y,t) &= V_{\max} \sin\left(2\pi x_t + \phi\right). \end{aligned} \tag{2.34}$$

Within each half period the velocity of each particle is constant. In the first half of each period numerical integration can therefore be carried out using

$$x(t + \Delta t) = x(t) + \Delta t\, V_{\max} \sin\left[2\pi y_t + \phi\right], \tag{2.35}$$

and in a similar way for the second half of each period.

The time step Δt does not need to be kept small, so long as the end of the half-period is not reached. In practice it is convenient to first schedule the times at which evolutionary events occur (they occur at fixed intervals, calculated based on the Damköhler number). At any one time, the time step Δt can then be chosen as the remaining time until the next evolutionary event or the end of the next half-period (whichever is shorter). This generates a very efficient numerical integration scheme.

2.6.2 Double-Gyre

The spatial domain is now given by $0 \leq x \leq 2$ and $0 \leq y \leq 1$. No particular boundary conditions apply, as particles cannot leave the domain.

A *clock-wise* rotating gyre is centred on $(0.5, 0.5)$, and a *counter-clock-wise* rotating gyre on $(1.5, 0.5)$. Each gyre rotates the particles in a spiral motion. In the absence of further external driving there is no flow of particles across the line $x = 1$. However, if the transport barrier between the two gyres is driven back and forth, particles can move between the two spirals.

The flow field is given by

$$\begin{aligned} v_x(x,y,t) &= \pi M \sin\left[\pi a(t)x^2 + \pi b(t)x\right] \cos(\pi y)\,, \\ v_y(x,y,t) &= \pi M \left[2a(t)x + b(t)\right] \cos\left[\pi a(t)x^2 + \pi b(t)x\right] \sin(\pi y)\,, \end{aligned} \tag{2.36}$$

where

$$\begin{aligned} a(t) &= u_0 \sin\frac{2\pi t}{T}, \\ b(t) &= 1 - 2u_0 \sin\frac{2\pi t}{T}. \end{aligned} \tag{2.37}$$

The parameter M sets the amplitude of the flow around the gyres, and u_0 controls the movement of the barrier between the two gyres. We use $M = 1.4$ and $u_0 = 0.4$.

We simulate the flow using an Euler scheme, with time step $\Delta t = 0.001$.

2.6.3 Blinking Vortex-Vortex

The blinking vortex-vortex flow describes motion around two vortices which are 'active' during alternating times. For the first half of the period the particles rotate around a vortex located at $x_c = -b$, and for the second half of the period the centre of rotation takes the position $x_c = b$. In the simulations we use $b = 0.25$.

We first describe the motion of particles around a vortex with fixed centre at $(x_c, 0)$. In this case the equations of motion are[35]

$$\begin{aligned} v_x(x,y) &= -\frac{\Gamma y}{\tilde{x} + y^2} \\ v_y(x,y) &= \frac{\Gamma \tilde{x}}{\tilde{x}^2 + y^2}, \end{aligned} \tag{2.38}$$

where $\tilde{x}(t) = x(t) - x_c$. This motion keeps the distance from the centre of the vortex constant ($r^2 \equiv \tilde{x}^2 + y^2 = \text{const}$), and results in an angular velocity $\omega = \Gamma/r^2$ which is constant for each particle, but which depends on the distance from the vortex centre. The tangential component of the velocity $\mathbf{v}$ is proportional to $1/r$. The constant Γ sets the scale of the flow velocity.

During each half-period (i.e., during rotations about a fixed vortex) the radial distance from the vortex centre remains constant. The motion is implemented conveniently through application of a rotation matrix,

$$\begin{pmatrix} \tilde{x}(t+\Delta t) \\ y(t+\Delta t) \end{pmatrix} = \begin{pmatrix} \cos(\Delta\theta) & -\sin(\Delta\theta) \\ \sin(\Delta\theta) & \cos(\Delta\theta) \end{pmatrix} \begin{pmatrix} \tilde{x}(t) \\ y(t) \end{pmatrix}, \tag{2.39}$$

where

$$\Delta\theta = \frac{\Gamma}{\tilde{x}^2(t) + y^2(t)}\Delta t, \tag{2.40}$$

is the rotation angle in time the interval Δt. As in the parallel-shear flow, there is no requirement to use a small time step Δt; it can be chosen as the time until the end of the next half-period or the time until the next evolutionary event (whichever comes sooner).

Depending on the choice of parameters and the initial conditions, the blinking vortex-vortex flow can either be chaotic or non-chaotic:

Chaotic For $\Gamma \gtrsim \Gamma_c = 0.14$ the flow is chaotic[34]. The simulations for the chaotic case shown in the main text correspond to $\Gamma \approx 0.2$.

Non-Chaotic If Γ is below the critical value, the flow is not chaotic. Instead domains separated by transport barriers are obtained[35]. The flow can then not be expected to be well mixing. Simulations shown in the main text correspond to $\Gamma \approx 0.01$.

Initially we place all particles in the region $-0.24 \leq x, y \leq 0.24$. The domain in which the particles move is in principle not bounded. However, at long times all particles in our simulations are found within a fixed bounded area.

2.6.4 Blinking Vortex-Sink

This flow is very similar to the blinking vortex-vortex flow, but one of the vortices is replaced by a sink. When the sink is active particles are attracted towards its centre, and there is no angular motion. Specifically, in polar coordinates this is of the form

$$\begin{aligned} \dot{\theta} &= 0, \\ \dot{r} &= \frac{m}{2\pi r}, \end{aligned} \tag{2.41}$$

where r is the distance from the sink. This translates into $\frac{d}{dt}r^2 = m/\pi$.

The position of the particles is updated in the same way as in the blinking vortex-vortex flow for the first half of the period. When the sink is active (second half of each period), the numerical scheme involves resizing the radial distance from the sink by a

factor λ. We write $\tilde{x}(t) = x(t) - x_s$, where x_s is the location of the sink. We then have

$$\begin{aligned} \tilde{x}(t + \Delta t) &= \lambda \tilde{x}(t) \\ y(t + \Delta t) &= \lambda y(t). \end{aligned} \tag{2.42}$$

The scale factor is

$$\lambda = \sqrt{1 - \frac{\Delta t\, m}{\pi\left(\tilde{x}^2(t) + y^2(t)\right)}}, \tag{2.43}$$

if $\Delta t\ m \leq \pi\left[\tilde{x}^2(t) + y^2(t)\right]$, and $\lambda = 0$ otherwise. The time step does not necessarily need to be small; it can be chosen in the same way as in the parallel-shear and blinking vortex-vortex flows.

The parameter m is the 'pull' strength of the sink. If m is very large, every node will be inevitably pulled to the sink during the half period in which the sink is active. The entire population will then be concentrated at $(x_s, 0)$. For sufficiently small m, more interesting dynamics are obtained. In our simulations we use $m = 0.03$ and $x_s = 0.25$.

As in the Blinking Vortex-Vortex flow, the domain in which the particles move is not bounded. However, we find that the stationary density is restricted to a finite area.

Bibliography

[1] Ohtsuki, Hisashi et al. (2006), 'A simple rule for the evolution of cooperation on graphs and social networks', *Nature* **441** (7092):502–505, DOI: 10.1038/nature04605.

[2] Nowak, Martin A., Corina E. Tarnita and Tibor Antal (2010), 'Evolutionary dynamics in structured populations', *Philosophical Transactions of the Royal Society B: Biological Sciences* **365** (1537):19–30, DOI: 10.1098/rstb.2009.0215.

[3] Hindersin, Laura and Arne Traulsen (2015), 'Most undirected random graphs are amplifiers of selection for Birth-death dynamics, but suppressors of selection for death-Birth dynamics', *PLOS Computational Biology* **11** (11):e1004437, DOI: 10.1371/journal.pcbi.1004437.

[4] Santos, Francisco C., Jorge M. Pacheco and Tom Lenaerts (2006), 'Evolutionary dynamics of social dilemmas in structured heterogeneous populations', *Proceedings of the National Academy of Sciences* **103** (9):3490–3494, DOI: 10.1073/pnas.0508201103.

[5] Lapin, Alexei, Joachim Schmid and Matthias Reuss (2006), 'Modeling the dynamics of E. coli populations in the three-dimensional turbulent field of a stirred-tank bioreactor - A structured-segregated approach', *Chemical Engineering Science* **61** (14):4783–4797, DOI: 10.1016/j.ces.2006.03.003.

[6] Sokolov, Andrey et al. (2007), 'Concentration Dependence of the Collective Dynamics of Swimming Bacteria', *Physical Review Letters* **98** (15):158102, DOI: 10.1103/PhysRevLett.98.158102.

[7] Venail, Patrick A. et al. (2008), 'Diversity and productivity peak at intermediate dispersal rate in evolving metacommunities', *Nature* **452** (7184):210–214, DOI: 10.1038/nature06554.

[8] Leinweber, Anne, Fredrik R. Inglis and Rolf Kümmerli (2017), 'Cheating fosters species co-existence in well-mixed bacterial communities', *International Society for Microbial Ecology* **11** (5):1179–1188, DOI: 10.1038/ismej.2016.195.

[9] Ewens, Warren J. (2004), *Mathematical Population Genetics 1: Theoretical Introduction*, Springer, New York, NY.

[10] Ohtsuki, Hisashi and Martin A. Nowak (2006), 'The replicator equation on graphs', *Journal of Theoretical Biology* **243** (1):86–97, DOI: 10.1016/j.jtbi.2006.06.004.

[11] Tarnita, Corina E. et al. (2009), 'Evolutionary dynamics in set structured populations', *Proceedings of the National Academy of Sciences* **106** (21):8601–8604, DOI: 10.1073/pnas.0903019106.

[12] Pacheco, Jorge M. et al. (2008), 'Repeated games and direct reciprocity under active linking', *Journal of Theoretical Biology* **250** (4):723–731, DOI: 10.1016/j.jtbi.2007.10.040.

[13] Kun, Ádám and István Scheuring (2009), 'Evolution of cooperation on dynamical graphs', *Biosystems* **96** (1):65–68, DOI: 10.1016/j.biosystems.2008.11.009.

[14] Lieberman, Erez, Christoph Hauert and Martin A. Nowak (2005), 'Evolutionary dynamics on graphs', *Nature* **433** (7023):312–316, DOI: 10.1038/nature03204.

[15] Nowak, Martin A. (2006a), 'Five rules for the evolution of cooperation', *Science* **314** (5805):1560–1563, DOI: 10.1126/science.1133755.

[16] Hauert, Christoph et al. (2007), 'Via freedom to coercion: the emergence of costly punishment.', *Science* **316** (2007):1905–1907, DOI: 10.1126/science.1141588.

[17] Gardiner, Crispin W. (2003), *Handbook of stochastic methods*, 3rd ed., Springer, Berlin Heidelberg.

[18] Nowak, Martin A. (2006b), *Evolutionary Dynamics*, Harvard University Press, Cambridge, Massachusetts.

[19] Traulsen, Arne and Christoph Hauert (2009), 'Stochastic evolutionary game dynamics', *Reviews of nonlinear dynamics and complexity*, ed. by Heinz Georg Schuster, vol. II, Wiley-VCH, Weinheim, p. 25–61, DOI: 10.1002/9783527628001.

[20] Kaveh, Kamran, Natalia L. Komarova and Mohammad Kohandel (2015), 'The duality of spatial death-birth and birth-death processes and limitations of the isothermal theorem', *Royal Society Open Science* **2** (4):140465–140465, DOI: 10.1098/rsos.140465.

[21] Durrett, Richard and Simon Levin (1994), 'The Importance of Being Discrete (and Spatial)', *Theoretical Population Biology* **46** (3):363–394, DOI: 10.1006/tpbi.1994.1032.

[22] Scheuring, István et al. (2003), 'Competing populations in flows with chaotic mixing', *Theoretical Population Biology* **63** (2):77–90, DOI: 10.1016/S0040-5809(02)00035-7.

[23] Pigolotti, Simone et al. (2012), 'Population Genetics in Compressible Flows', *Physical Review Letters* **108** (12):128102, DOI: 10.1103/PhysRevLett.108.128102.

[24] Grošelj, Daniel, Frank Jenko and Erwin Frey (2015), 'How turbulence regulates biodiversity in systems with cyclic competition', *Physical Review E* **91** (3):033009, DOI: 10.1103/PhysRevE.91.033009.

[25] Benzi, Roberto et al. (2012), 'Population dynamics in compressible flows', *The European Physical Journal Special Topics* **204** (1):57–73, DOI: 10.1140/epjst/e2012-01552-0.

[26] Károlyi, György et al. (2000), 'Chaotic flow: The physics of species coexistence', *Proceedings of the National Academy of Sciences* **97** (25):13661–13665, DOI: 10.1073/pnas.240242797.

[27] Károlyi, György, Zoltán Neufeld and István Scheuring (2005), 'Rock-scissors-paper game in a chaotic flow: The effect of dispersion on the cyclic competition of microorganisms', *Journal of Theoretical Biology* **236** (1):12–20, DOI: 10.1016/j.jtbi.2005.02.012.

[28] Cowen, Robert K. (2000), 'Connectivity of Marine Populations: Open or Closed?', *Science* **287** (5454):857–859, DOI: 10.1126/science.287.5454.857.

[29] Krieger, Madison S., Alex McAvoy and Martin A. Nowak (2017), 'Effects of motion in structured populations', *Journal of The Royal Society Interface* **14** (135):20170509, DOI: 10.1098/rsif.2017.0509.

[30] Young, William R., Anthony J. Roberts and Gordan R. Stuhne (2001), 'Reproductive pair correlations and the clustering of organisms', *Nature* **412** (6844):328–331, DOI: 10.1038/35085561.

[31] Sandulescu, Mathias et al. (2007), 'Plankton blooms in vortices: the role of biological and hydrodynamic timescales', *Nonlinear Processes in Geophysics* **14** (4):443–454, DOI: 10.5194/npg-14-443-2007.

[32] Neufeld, Zoltán, Peter H. Haynes and Tamás Tél (2002), 'Chaotic mixing induced transitions in reaction–diffusion systems', *Chaos: An Interdisciplinary Journal of Nonlinear Science* **12** (2):426–438, DOI: 10.1063/1.1476949.

[33] Galla, Tobias and Vicente Pérez-Muñuzuri (2017), 'Time scales and species coexistence in chaotic flows', *EPL (Europhysics Letters)* **117** (6):68001, DOI: 10.1209/0295-5075/117/68001.

[34] Ottino, Julio M. (1989), *The kinematics of mixing: stretching, chaos, and transport*, Cambridge University Press, Cambridge, UK.

[35] Neufeld, Zoltán and Emilio Hernández-García (2010), *Chemical and biological processes in fluid flows: a dynamical systems approach*, Imperial College Press, London, UK.

[36] Boguñá, Marián, Claudio Castellano and Romualdo Pastor-Satorras (2009), 'Langevin approach for the dynamics of the contact process on annealed scale-free networks', *Physical Review E* **79** (3):036110, DOI: 10.1103/PhysRevE.79.036110.

[37] Derrida, Bernard and Yves Pomeau (1986), 'Random Networks of Automata: A Simple Annealed Approximation', *Europhysics Letters (EPL)* **1** (2):45–49, DOI: 10.1209/0295-5075/1/2/001.

[38] Penrose, Mathew (2003), *Random Geometric Graphs*, 1st ed., Oxford University Press, Oxford, UK, p. 348.

[39] Fu, Feng et al. (2009), 'Evolutionary dynamics on graphs: Efficient method for weak selection', *Physical Review E* **79** (4):046707, DOI: 10.1103/PhysRevE.79.046707.

[40] Zukewich, Joshua et al. (2013), 'Consolidating Birth-Death and Death-Birth Processes in Structured Populations', *PLoS ONE* **8** (1):e54639, DOI: 10.1371/journal.pone.0054639.

[41] Koppel, Johan van de et al. (2015), 'Long-Distance Interactions Regulate the Structure and Resilience of Coastal Ecosystems', *Annual Review of Marine Science* **7** (1):139–158, DOI: 10.1146/annurev-marine-010814-015805.

[42] Rauch, Erik M. and Yaneer Bar-Yam (2006), 'Long-range interactions and evolutionary stability in a predator-prey system', *Physical Review E* **73** (2):020903, DOI: 10.1103/PhysRevE.73.020903.

[43] Menon, Rajita and Kirill S. Korolev (2015), 'Public Good Diffusion Limits Microbial Mutualism', *Physical Review Letters* **114** (16):168102, DOI: 10.1103/PhysRevLett.114.168102.

[44] West, Stuart A. et al. (2007), 'The Social Lives of Microbes', *Annual Review of Ecology, Evolution, and Systematics* **38** (1):53–77, DOI: 10.1146/annurev.ecolsys.38.091206.095740.

[45] Tilman, David and Peter M. Kareiva (1997), *Spatial Ecology: The Role of Space in Population Dynamics and Interspecific Interactions*, Princeton University Press, Princeton, NJ.

[46] Pattni, Karan et al. (2015), 'Evolutionary graph theory revisited: when is an evolutionary process equivalent to the Moran process?', *Proceedings of the Royal Society A: Mathematical, Physical and Engineering Science* **471** (2182):20150334, DOI: 10.1098/rspa.2015.0334.

[47] Altrock, Philipp M. and Arne Traulsen (2009), 'Fixation times in evolutionary games under weak selection', *New Journal of Physics* **11**:013012, DOI: 10.1088/1367-2630/11/1/013012.

[48] Kundu, Pijush K. and Ira M. Kohen (1990), *Fluid Mechanics*, 2nd ed., Academic Press, San Diego, California.

[49] Acheson, David J. (1990), *Elementary Fluid Dynamics*, Clarendon Press, Oxford, UK.

[50] Young, Donald F. et al. (2010), *A brief introduction to fluid mechanics*, 5th ed., John Wiley & Sons, Jefferson City.

Chapter 3

Motion, fixation probability and the choice of an evolutionary process

Preface

The contents of this chapter constitute a manuscript currently under review, and also available in ArXiv[1]. The manuscript was authored by Francisco Herrerías-Azcué[2], Vicente Pérez-Muñuzuri[3] and Tobias Galla[2].

F.H.A.'s contributions include the inception of the project, performing all calculations and analysis, coding simulations, producing the data for all figures, finalising all figures, and writing all sections of the paper alongside V.P.M. and T.G.

[1]F. Herrerías-Azcué, V. Pérez-Muñuzuri, and T. Galla, (2019), "Motion, fixation probability and the choice of an evolutionary process", *arXiv preprint*:1901.03596.

[2]Theoretical Physics, School of Physics and Astronomy, The University of Manchester, Manchester, M13 9PL, United Kingdom.

[3]Group of Nonlinear Physics, Faculty of Physics, University of Santiago de Compostela, E-15782, Santiago de Compostela, Spain.

Abstract

Different evolutionary models are known to make disparate predictions for the success of an invading mutant in some situations. For example, some evolutionary mechanics lead to amplification of selection in structured populations, while others suppress it. Here, we use computer simulations to study evolutionary populations moved by flows, and show how the speed of this motion impacts the fixation probability of an invading mutant. Flows of different speeds interpolate between evolutionary dynamics on fixed heterogeneous graphs and in well-stirred populations. We find that the motion has an active role in amplifying or suppressing selection, accomplished by fragmenting and reconnecting the interaction graph. While increasing flow speeds suppress selection for most evolutionary models, we identify characteristic responses to flow for the different update rules we test. We suggest these responses as a potential aid for choosing the most suitable update rule for a given biological system.

3.1 Introduction

Over the years, different models have been proposed to describe evolutionary dynamics; they all describe how populations composed of members of different species change with time. These changes occur through death and birth events, and typically involve competition between individuals [1–3]. The models differ in the order in which these events are implemented and how competition takes place. For example, one distinguishes between 'birth-death' and 'death-birth' processes, or between global and local selection [3–5]. Even though these seem to be relatively minor details, under certain circumstances they can lead to rather disparate outcomes [4–6]. Choosing the right evolutionary model for a given biological system is therefore of great importance, but it is not a simple task.

There appears to be some tendency in the literature to simply choose one model and not argue in detail whether, for example, a birth-death or a death-birth process is better suited for the particular application at hand. While one could argue that most of these models are so stylised that the subtle differences between them are

unimportant, significant differences in their predicted outcomes make it desirable to be able to distinguish between the options. This would enable one to make a more informed choice, and to identify the model which best captures the known behaviour of a given biological system.

In this paper we propose that such a possibility may exist if the members of the population are advected by an external flow. Specifically, we focus on the stochastic dynamics of a population initially composed only of wildtype individuals and a single invading mutant. The mutant will either be eliminated or its offspring will take over the population. We are interested in the latter outcome, and study the rate of successful fixation. We show that the response of the fixation probability to the flow speed can be very different for each evolutionary process. We speculate that this may be used to discriminate between different stylised models. In some experimental settings flow can be controlled externally, or situations without flow can be compared to those with fast flows. Differences in fixation probabilities have been found in static versus stirred populations of *Escherichia coli* for example [7–9]. If such data is available, systematically studying the behaviour of different computational models of evolution in flowing populations can help to select the update mechanism which best captures the features of the biological system at hand.

The simplest approach to modelling stochastic evolution dispenses entirely with the notion of space and population structure, and assumes that the only relevant factors are the frequencies with which the different types of individuals are found in the population [1–3]. Each individual in such an unstructured population can interact with all other individuals at all times. To further simplify matters, birth and death events are usually coupled, so that one is immediately followed by the other; this facilitates the mathematical analysis, as it keeps the size of the population constant [1–3].

If individuals are distributed in space, and have a limited range of interaction, the population becomes structured. Not every individual can interact with every other individual at all times. It is then helpful to consider the interaction graph of the population [10–29]. Nodes of these networks represent individuals, and links between nodes stand for potential interactions. Birth and death events take place between neighbouring nodes, that is, pairs of individuals connected by a link. The case of an unstructured population is recovered if links exist between any two individuals at all

times; the interaction graph is then said to be complete.

Population structure has the potential to change the dynamics of evolutionary processes [10–29]. For example, species that would be selected against in an unstructured population are found to organise in clusters on networks, and in this way they can coexist with fitter types, or even eradicate the resident species. The time it takes for a species to reach fixation can be reduced or increased on networks. Evolution on simple graphs has been characterised mathematically (see for instance [28–33] and references therein), but on more complicated networks the dynamics become much harder to describe analytically.

Further complication arises if the members of the populations are in motion. The interaction graph then becomes dynamic, making mathematical approaches more difficult. At the same time motion is a ubiquitous feature of biological systems, for example due to self-propulsion of microswimmers by means of flagella [34], or advection of bacteria in a fluid environment [35].

Common ways of implementing motion in computer models include migration; in such models individuals move to neighbouring sites on the interaction graph [36–42]. Alternatively, adaptive networks have been considered; in these the link connecting two individuals is re-wired to a different individual, usually with preference for links between individuals of similar types [43–47]. For further examples see also ref. [17] and references therein. In this work, instead, we focus on populations that are not self-propelled, and use the type of motion one could expect in dynamic gaseous or aqueous environments. Specifically, the motion is due to a flow of the medium in which the population resides. The movement is not constrained by the current interaction network, and the interaction graph itself is dynamic. Evolutionary systems with this type of motion have been studied comparatively little; existing work includes refs. [42, 48–55]. In ref. [56] we investigated stirred populations, and presented analytical solutions for the limit of very fast flows. Naively, one would expect that the success of a mutant under fast stirring is the same as the one on a complete graph, a situation also referred to as 'well mixed' [13–15]. However, the results of ref. [56] showed that the fixation probability of an invading mutant approaches a different limiting value for very fast flows.

In this paper we investigate in more detail the effect of the flow speed on the

fixation probability of invading mutants. In particular we also focus on intermediate and slow flows. We find that the way in which the flow affects the success of mutants depends on the choice of the evolutionary update rules. We identify three main contributing factors: how well connected the initial mutant is with the rest of the population, the opportunities mutants have to organise in clustered groups, and how long individuals remain connected for as the flow moves them in space. These factors are influenced by the speed of the flow and, depending on the evolutionary update rule, they can either amplify or suppress selection relative to unstructured populations. This suggests the response of the fixation probability to flow speed as an indicator of the underlying evolutionary process. We think this can be a useful aid for choosing the most appropriate evolutionary model for given biological applications.

3.2 Methods

We use the same setup as ref. [56], and consider a population of fixed size N composed of individuals of two species (wildtype and mutant). Unless specified otherwise, we use $N = 100$. Individuals take positions in space within the two-dimensional domain $0 \leq x, y < 1$ with periodic boundary conditions. Particles are subject to a continuous-time flow, moving them around in space, and to evolutionary dynamics, which change the frequencies of the two species in the population.

The motion of the particles is simulated through the so-called parallel shear flow [57, 58]; we discuss the validity of our results for different flow fields in Sec. 3.4. The velocity field of this flow is periodic in time, except for a random phase described below. During the first half of each period particles are moved vertically; the speed of each individual depends on the horizontal component of their position. During the second half of the period individuals move horizontally, with speeds dependent on their vertical positions. We write $v_x(x, y, t)$ and $v_y(x, y, t)$ for the velocity components of a particle at position (x, y) at time t. Specifically, we use

$$v_y(x, y, t) = 0, \quad v_x(x, y, t) = V_{\max} \sin\left[2\pi y + \psi\right], \quad \text{for } t \in [nT, nT + T/2),$$
$$v_x(x, y, t) = 0, \quad v_y(x, y, t) = V_{\max} \sin\left[2\pi x + \psi\right], \quad \text{for } t \in [nT + T/2, (n+1)T),$$

with $n = 0, 1, 2, \ldots$. The constant $V_{\max}$ sets the amplitude of the flow, and T the period. The phase ψ is drawn randomly from the interval $[0, 2\pi)$ at the beginning of each

half-period. Due to this random phase, the flow mimics chaotic motion; the trajectories of individuals who are initially close to each other diverge over time. At long times, the distribution of individuals moved by this flow is uniform in space [57, 58].

The evolutionary process is implemented through coupled birth and death events. The order in which reproduction and removal take place is important, and so we will distinguish between birth-death and death-birth processes. The evolutionary dynamics occur on an undirected interaction graph, dynamically generated by the flow. Specifically, we will say that one individual is a neighbour of another if they are within a distance R of each other.

Individuals are in continuous motion, but evolutionary events occur at discrete times, $t = \Delta t,\ 2\Delta t, ...$ in our model. Simulations are then implemented as follows:

1. At $t = 0$, a population of N particles is placed into the spatial domain at designated initial positions. These define an initial interaction graph. Of these individuals, $N - 1$ are wildtype and one is a mutant. The mutant is chosen uniformly at random from the population.
2. The individuals are moved by the flow for a time interval Δt, leading to a new interaction graph.
3. An individual is chosen from the entire population. In the case of a birth-death process, it is designated to reproduce; for death-birth processes it is designated to die.
4. One of the neighbours of this individual is chosen to be replaced (birth-death) or to reproduce (death-birth).
5. The individual chosen for death adopts the species (wildtype or mutant) of the reproducing individual.
6. Repeat from step 2.

In each evolutionary step two individuals are chosen. They can either be *picked* at random or *selected* proportional to fitness. For the latter case we focus on frequency-independent selection; we set the wildtype fitness to one, and write r for the fitness of the mutant species. Consider for example a group of n_w wildtype individuals and n_m mutants. A mutant would be selected to reproduce from this group with probability $rn_m/(rn_m + n_w)$, or a wildtype with probability $n_w/(rn_m + n_w)$. If selection is for death we proceed similarly, but with r replaced by $1/r$. In this way, mutants are less

likely to die than wildypes if $r > 1$. For $r < 1$ the mutant species is selected against. The simulation results shown in this paper focus on advantageous mutants; we set $r = 1.05$ throughout.

Selection proportional to fitness can take place either in step 3 of the above algorithm (when an individual is chosen from the entire population) or in step 4 (when it is chosen from the neighbours of an individual). We refer to these cases as *global* and *local* selection, respectively. Since we distinguish between birth-death and death-birth processes, four combinations are possible: global birth-death (**Bd**), global death-birth (**Db**), local birth-death (**bD**) and local death-birth (**dB**). The capital letter in these acronyms indicates that selection dependent on fitness occurs in the respective step. In principle, one could also consider processes in which individuals are chosen proportional to fitness in both steps of the algorithm (**BD**, **DB**) [4, 5]. In order to be able to disentangle the effects that the flow has on fixation probabilities due to local or global selection, we limit the discussion in the main text to scenarios in which selection acts either globally or locally, but not both. The **BD** and **DB** processes are discussed in Sec. 3.7.

We illustrate the different evolutionary processes in Fig. 3.1. The upper two rows correspond to processes in which competition takes place among the entire population (*global selection*). In the lower two rows the first node is picked irrespective of fitness, and competition takes place only among the neighbours of this node (*local selection*). A step-by-step description of each of the processes can be found in the figure caption.

One important characteristic of the flow is the typical timescale over which the set of neighbours of a given individual is renewed. More precisely, the set of neighbours of a given individual at time t, and at a later time $t + \tau$, will be uncorrelated provided τ is sufficiently large (see ref. [56], and Sec. 3.5). This renewal time is in turn determined by the parameters $V_{\max}$, T and R; following refs. [59, 60], we use $V_{\max} = 1.4$ and $T = 1$ throughout, and choose an interaction radius of $R = 0.11$.

This choice of parameters leads to an estimate for the network renewal time of $\tau \approx 6.4$ (see Sec. 3.5 for details). That is, the set of neighbours of one individual at one time is uncorrelated from its set of neighbours approximately six and a half flow periods earlier. It remains to specify how frequent evolutionary events are, i.e. to define the time step Δt in the simulation described above. We treat this as a model

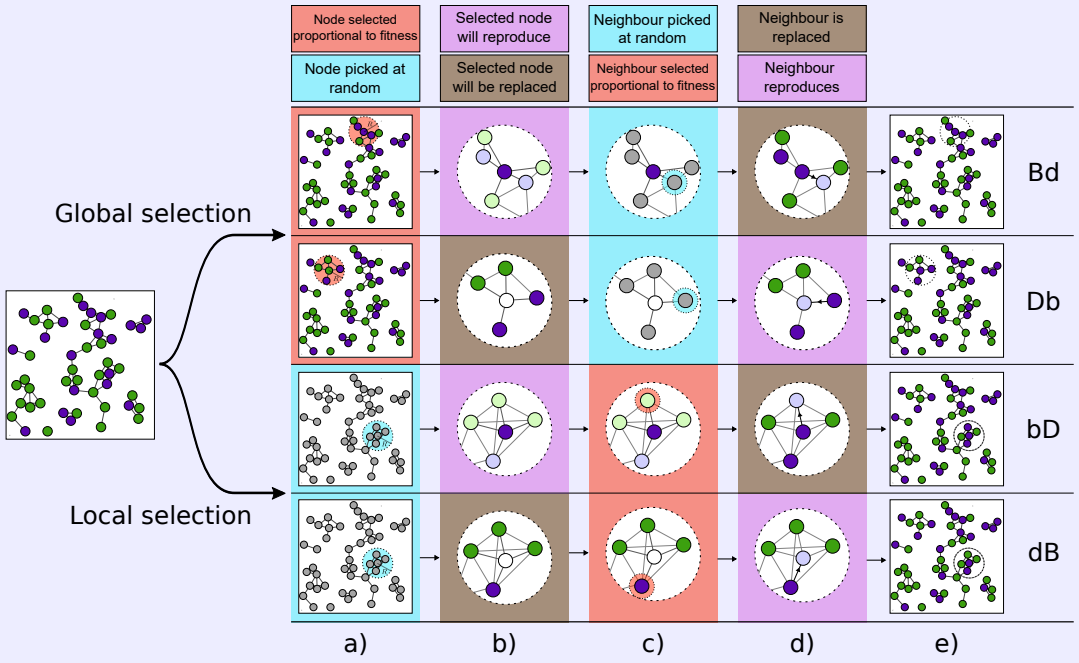

Figure 3.1: Illustration of the update rules. Each row represents one of the different evolutionary update mechanisms. The columns indicate the different steps of each evolutionary event. In column a) an individual is chosen from the whole population; it can be *'selected'* through competition by fitness (red shading), or *'picked'* at random, irrespective of its species (blue shading). This node is destined to either reproduce (pink shading), or to be replaced (brown shading), as shown in column b). Column c) indicates that one neighbour of this node is either *selected* (red), or *picked* (blue). This second node is destined to reproduce (pink), or to be replaced (brown), shown in column d). Column e) shows the result of the evolutionary event; the node chosen to reproduce places an offspring in place of the node chosen to die. Each row is composed of one box of each colour; the sequence of the colours distinguishes the different processes. From top to bottom, the rows correspond to: (i) global birth-death process (**Bd**): an individual is *selected* from the whole population to reproduce, and one of its neighbours is *picked* to be replaced by the first individual's offspring; (ii) global death-birth process (**Db**): an individual is *selected* to die from the whole population, and one of its neighbours is *picked* to place an offspring in its place; (iii) local birth-death process (**bD**): an individual is *picked* from the whole population to reproduce, and one of its neighbours is *selected* to die; (iv) local death-birth process (**dB**): an individual is *picked* from the whole population to die, and one of its neighbours is *selected* to reproduce.

parameter, and use $S = N\Delta t/T$ to quantify the number of generations elapsed in one flow period. Thus, S indicates the speed of the flow relative to that of evolution. For small S, individuals move relatively little between evolutionary events ('slow flow'). Large values of S describe fast flows. From here on, we will refer to S as the *speed* of the flow, and investigate the outcome of evolution for different choices of this parameter. The flow speed S is understood throughout as relative to the rate of evolutionary

events. We note that the inverse of S is related to the Damköhler number in fluid dynamics [61–63].

3.3 Results

3.3.1 Effects of the flow speed on the fixation probability

We first address the case in which the initial coordinates of each individual are drawn from a uniform distribution on the domain $0 \leq x, y < 1$. The initial interaction graph is then a random geometric graph (RGG) [64].

For any non-zero flow rate ($S > 0$) any member of the population can eventually interact with any other individual, even if they were not connected on the initial interaction graph. This is due to the mixing properties of the flow, and means that no individual can indefinitely remain isolated from the rest of the population. As a consequence, the final outcome of the evolutionary process is either fixation or extinction of the mutant.

The fixation probability, ϕ, for a beneficial mutation is depicted in Fig. 3.2 as a function of the flow speed, S. We show simulation results for the four different evolutionary processes **bD**, **dB**, **Bd**, and **Db**. Each data point is obtained from an ensemble of realisations. For comparison, we also show the fixation probability on a complete graph, ϕ_{CG}. By definition, ϕ_{CG} is independent of the flow speed, as all individuals interact with all others at all times. On complete graphs the fixation probability for global and local selection processes differ by a small amount [5].

Several interesting features can be observed in Fig. 3.2: For slow flows, the order of reproduction and removal is found to have a strong effect on the fixation probability, and it is less relevant whether selection takes place in the first or the second step of each evolutionary event. For the local and global death-birth processes (**dB**, **Db**) the fixation probability is lower than on a complete graph, as shown by the green and blue lines in Fig. 3.2. Conversely, both **Bd** and **bD** show a higher fixation probability than on complete graphs (red and purple lines).

In the limit of fast flows, however, the outcome of evolution is mostly determined by whether selection is global or local, and not by the order of the reproduction and removal events (birth-death vs. death-birth). Specifically, when selection acts locally

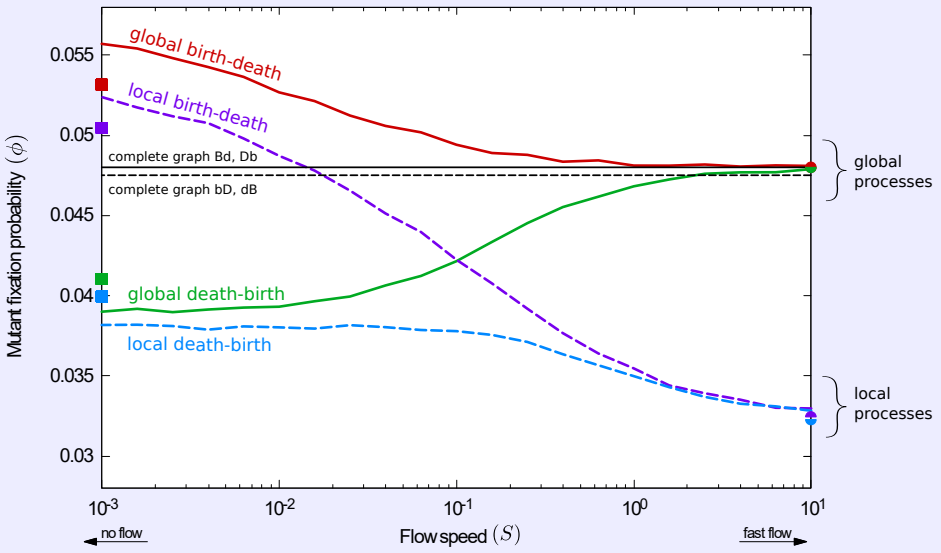

Figure 3.2: Fixation probability as a function of the flow speed for unrestricted random initial positions (random geometric graphs, RGGs). For the global death-birth process, increasing the flow speed increases the fixation probability. The reverse is found for the remaining three processes. Circle markers show fixation probabilities in the fast-flow limit; square markers are results for fixed connected random geometric graphs (CRGGs); see text for further details. The fixation probabilities on a complete graph are shown for reference.

the fixation probability of the mutant is lower than on a complete graph (purple and blue lines). In contrast, when selection is global the fixation probability is the same as on a complete graph (red and green lines).

These observations indicate unique responses of the fixation probability to the flow speed for the different processes. For the **Db** process (continuous green line in Fig. 3.2) the mutant's probability of success increases with the speed of the flow. For the **Bd** process (continuous red line), the fixation probability decreases with increased flow speed, but is always greater than or equal to the one on a complete graph, $\phi \geq \phi_{CG}$. In contrast, the fixation probability for a **dB** process (dashed blue line) is always smaller than ϕ_{CG}. Finally, for the **bD** process (dashed purple line) the fixation probability is higher than on a complete graph when the flow is very slow, but decreases at higher flow speeds and eventually becomes lower than on the complete graph. The **bD** process is the only case in which we observe a transition from amplification to suppression of selection (relative to the complete graph) as the flow speed is increased.

In order to gain some insight into these observations, we first describe the dynamics

in the limit of fast flows, summarising the results of ref. [56]. Then we discuss the no-flow limit, and subsequently the transition between the two extremes, at intermediate flow speeds.

Fast-flow limit: evolution of well-stirred populations

When the flow is sufficiently fast the probability that any two particles are neighbours at the time of an evolutionary event is the same, irrespective of whether they were neighbours at the previous event or not [56]. In global processes selection takes place when the first individual is chosen, i.e., competition acts amongst the whole population. Then, a second individual is picked at random from the neighbours of this first individual. Since any individual is equally likely to be neighbours of the individual selected in the initial step, the second, random pick, is equivalent to a random pick from the entire population. Therefore, in the limit of fast flows the fixation probability of global processes coincides with the one on complete graphs, as observed in Fig. 3.2.

For local processes, on the other hand, in each evolutionary event the first individual is chosen at random from the entire population, irrespective of fitness. Competition then takes place between the neighbours of this individual. Although all members of the population are equally likely to be part of this neighbourhood, at any one time the group of neighbours is a random subset of the population. This subset may not reflect the composition of the population as a whole, which can be shown to lead to suppression of selection [56]. We briefly illustrate this for the case of a very small interaction radius; the majority of individuals then have at most one neighbour at any given time. Since this neighbour is the only contestant in local selection, fitness is irrelevant. Therefore, as the interaction radius becomes small the fixation probability of the mutant approaches the limit of neutral selection. When the interaction radius is large, however, it is more likely that the group of neighbours is large as well, and that population-wide frequencies are accurately represented. Therefore, the suppression effect relative to the complete graph is reduced. If the interaction range is so large that all individuals are connected with all other individuals at all times, a complete interaction graph is recovered.

Analytical results can be obtained for all four processes in the limit of very fast flows [56]. Predictions from this theoretical approach are shown as filled circles on the

right edge of Fig. 3.2.

No-flow limit: evolution on static heterogeneous graphs

On the left-hand side of Fig. 3.2 the flow is so slow that the evolutionary dynamics effectively take place on fixed graphs. Evolutionary processes on static graphs have been widely discussed in the literature (see e.g. [15, 23, 29] and references therein). The focus is often on characterizing specific graphs or graph structures, which either amplify or suppress selection [65–67]. Notably, the authors of ref. [6] report that most undirected graphs amplify selection for birth-death processes, but suppress selection for death-birth processes. However, these findings are only given for relatively small networks, and only for processes in which selection acts in the reproduction step (**Bd** and **dB**).

In order to obtain a more complete picture, we measured in simulations the fixation probability of a single mutant on networks of different sizes, averaged over different static heterogeneous graphs. Each graph is generated by placing individuals at random in the spatial domain (see Sec. 3.2), resulting in a random geometric interaction graph. It is possible that a graph generated in this way consists of several disconnected components. In the absence of flow, the mutant then cannot reach fixation. We therefore restrict simulations to graphs with a single connected component and henceforth use the term *connected* random geometric graphs (CRGGs). We present results for the different evolutionary processes as a function of the size of the graph in Fig. 3.3.

The data shows that the average fixation probability of a single mutant on CRGGs is higher than on the complete graph for birth-death processes, $\phi \geq \phi_{CG}$. For death-birth processes, on the other hand, $\phi \leq \phi_{CG}$. This is in line with the results reported in ref. [6] for small graphs. The data in Fig. 3.3 confirms that the amplification of selection (for birth-death processes) or suppression (for death-birth processes) is present regardless of the size of the network, if an average over many graphs is taken. The rightmost data points in Fig. 3.3 correspond to a population of the same size as the one in Fig. 3.2.

Intuition regarding the amplification or suppression of selection on static networks can be gained by studying the connectivity of the initial mutant (see refs. [20, 68–71]). For death-birth processes, these studies find that the success of an advantageous mutant increases with its degree; for birth-death processes, its success decreases with

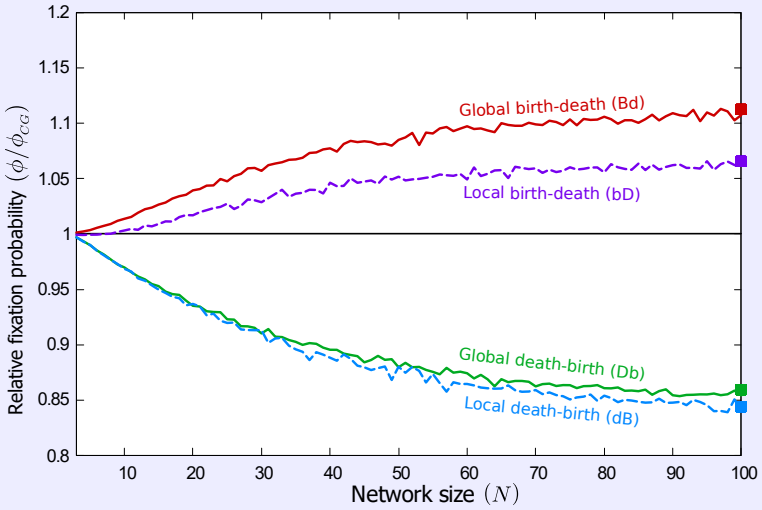

Figure 3.3: Fixed heterogeneous graphs amplify selection for birth-death processes and suppress it for death-birth processes. The figure shows the fixation probability of an invading mutant (ϕ), averaged over static CRGGs. Data is shown relative to the corresponding fixation probability on a complete graph (ϕ_{CG}). Regardless of the population size, selection is amplified for **Bd** and **bD** processes, and suppressed for **Db** and **dB** processes.

connectivity. This can be understood in the following way: In each evolutionary event two individuals are chosen, the first from the entire population, and the second as a neighbour of the first. The degree of an individual does not affect its chances of being chosen in the first step, irrespective of whether selection acts in this step or not. However, the probability of being neighbours with the initial individual is higher for well connected individuals than for individuals with a low degree. Under birth-death processes, higher connectivity of the mutant therefore results in a higher chance of being replaced. For death-birth processes it results in a higher chance of reproduction.

In the literature these predictions have been tested for **Bd** and **dB** processes [20, 68–71]. In the lower panel of Fig. 3.4 we verify that the argument extends to all four evolutionary update rules defined above. We show, for CRGGs, the fixation probability of a mutant, ϕ_k, as a function of its degree, k. For the global and local death-birth processes (**Db**, **dB**) the mutant's success is lower than on a complete graph when the mutant is sparsely connected, but larger if it is highly connected; the reverse is found for global and local birth-death processes (**Bd**, **bD**). These observations are consistent with the above reasoning.

In our model, the initial mutant is chosen uniformly at random from the members

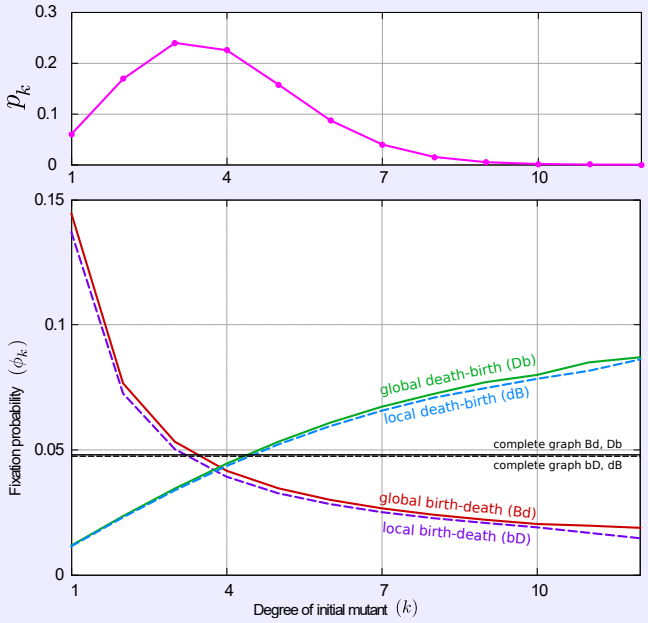

Figure 3.4: Significance of the degree of the initial mutant. The upper panel shows the degree distribution, p_k, of the ensemble of connected random geometric graphs (CRGGs), obtained by placing $N = 100$ individuals into the spatial domain $0 \leq x, y \leq 1$ with uniform distribution, and using an interaction radius $R = 0.11$ and periodic boundary conditions. The lower panel shows the fixation probability obtained from simulating the evolutionary process on these graphs, as a function of the degree of the initial mutant. For the two death-birth processes the mutant's success is below the one on a complete graph if its degree is low, and above ϕ_{CG} at high connectivity. The reverse is found for the two birth-death processes. Data points have been connected as a visual guide.

of the population. The probability that it has degree k is thus determined by the degree distribution of CRGGs. We write p_k for the probability of a random node to have degree k in such a graph, and show the degree distribution for networks of size $N = 100$ in the upper panel of Fig. 3.4 for illustration. The overall probability of fixation of a single mutant is then $\phi = \sum_k p_k \phi_k$. Fixation probabilities obtained in this way are shown as square markers in Fig. 3.2 and 3.3. The results reproduce the amplification and suppression of selection (for birth-death or death-birth processes, respectively) in the limit of slow flows. We attribute quantitative differences between the markers and lines in Fig. 3.2 to effects of the non-zero flow and to the difference in initial conditions; the data shown as lines is obtained from simulations of slowly flowing populations in which the initial graph may consist of more than one component. In Sec. 3.3.2 we will discuss the difference due to initial positions in more detail.

Transition between fast-flow and no-flow limits

As seen above, the outcome of evolution in rapidly stirred populations is very different to that on static interaction graphs. With fast flows, local competition leads to suppression of selection; on the other hand, the success of a mutant is the same as on a complete graph if selection is global. When there is no flow, the order of the birth and death events in the evolutionary process is crucial. In this case, selection is amplified for birth-death processes and suppressed for death-birth processes. At intermediate flow speeds, a crossover between these two regimes is seen. We will now discuss this transition in more detail.

On fixed heterogeneous graphs, the degree of the initial mutant determines whether its chances of success are greater or smaller than on a complete graph. In the presence of flow the interaction network constantly changes, and the number of neighbours of any one individual thus varies over time. Classifying a member of the population as highly or poorly connected is then at best possible over limited time windows. If the flow is slow relative to evolution, many evolutionary events occur in such a time window, and the evolutionary dynamics can conclude before the degrees of nodes undergo significant changes. Therefore the amplification or suppression effect due to the degree of the mutant can still be observed. For faster flows, however, the interaction network changes so quickly that there is no clearly defined notion of a degree of an individual on the time scale of evolution. The amplification or suppression effect set by the initial heterogeneous network is then washed out.

At very fast flow speeds, the set of neighbours of the individual chosen in the first step of an evolutionary update effectively becomes a group sampled at random from the entire population. Therefore, suppression of selection sets in for local processes. The fixation probability of global processes, on the other hand, approaches the one on a complete graph, as described previously.

The main effects leading to the transition between the no-flow and the fast-flow limits are thus the increasing variability (over time) of the degree of individuals, and the random sampling of the group of individuals taking part in evolutionary events. As a result of these two mechanisms, in Fig. 3.2 we see a smooth transition between the two limits. The different responses of the fixation probability to the speed are a consequence of the limiting behaviours for very slow and very fast flows.

Although it is not immediately transparent from the results in Fig. 3.2, the flow has further effects on the evolutionary process. For example, it removes the influence of the initial positions of the individuals in space. Another important feature, particularly at intermediate flow speeds, is that the evolutionary process takes place on slowly changing heterogeneous graphs. The dynamic network constantly splits into disconnected components, which later merge and form new components. This fragmentation promotes the formation of 'clusters' — groups of nodes which are of the same species. This gives rise to further amplification or suppression effects, depending on the details of the evolutionary mechanics. In the following section, we explore these effects further.

3.3.2 Effects of the initial positions of individuals

Our model describes a population in constant motion. It is then natural to assume that the positions of the individuals at the time the initial mutation occurs is drawn from the stationary distribution of the flow. For the periodic parallel shear flow this is the uniform distribution, used as an initial condition in the previous section. However, exploring different starting positions allows us to gain further insight into the effect of the flow on fixation probabilities.

Connected random geometric graphs (CRGGs)

The data shown as lines in Fig. 3.2 was obtained from simulations with random initial positions (RGGs) and non-vanishing flows. For this setup the interaction graph may not be connected, but fixation or extinction will still occur, provided there is non-zero flow. In order to explore the no-flow limit, in Figs. 3.3 and 3.4 we focused on static heterogeneous graphs instead; studying fixation in the strict absence of flow only makes sense when the interaction graph consists of one single connected component, and so we restricted the discussion to connected random geometric graphs (CRGGs). As a result, comparison with the data in Fig. 3.2 is difficult; in particular, we note the quantitative differences between the square markers, obtained from static connected graphs, and the limiting values of the data shown as lines in Fig. 3.2, obtained from slowly moving populations started from RGGs.

For comparison, we show data obtained from mobile populations, but started on

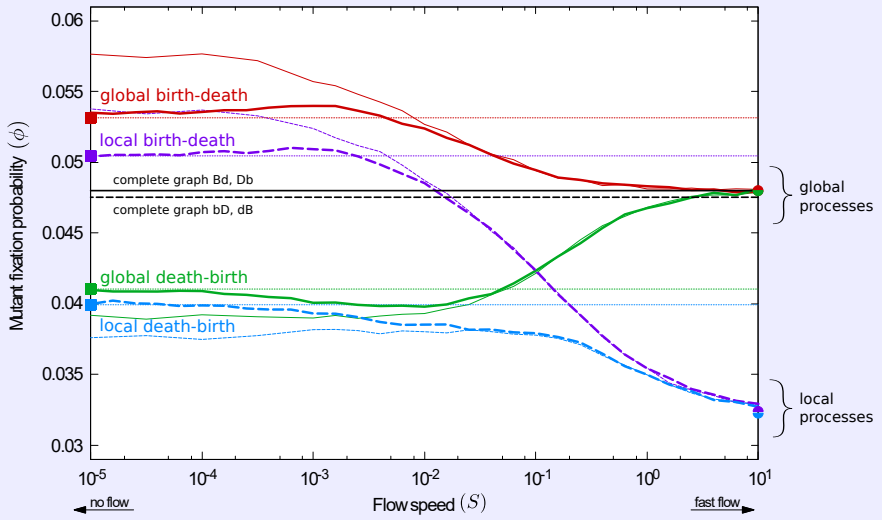

Figure 3.5: Comparison of fixation probability for simulations started from unrestricted and connected random geometric graphs (RGGs and CRGGs, respectively). The fixation probability as a function of the flow speed is shown as thick lines for simulations started on connected graphs; thin lines are for unrestricted initial positions (some of this data is also shown in Fig. 3.2). Square markers indicate the fixation probabilities on *static* CRGGs; see text for details. The fixation probability on complete graphs is shown for reference. A minimum of ϕ is found for the **Db** process; maxima are discernible for **Bd** and **bD** when the dynamics are started from connected graphs. The effect of amplification/suppression of selection at slow flow speeds is more pronounced for simulations initialized from RGGs than from CRGGs.

CRGGs, in Fig. 3.5. The limiting values of the fixation probabilities for very slow flows (end of the tick lines on the left-hand side of the figure) now agree quantitatively with those obtained from static CRGGs (square markers).

The simulation data from Fig. 3.2, from simulations with unrestricted random initial positions, is also shown in Fig. 3.5 (thin lines). If the flow is sufficiently fast, initial conditions are immaterial. On the contrary, for slow flows the fixation probability, ϕ, for simulations started from unrestricted random graphs is different from that for connected initial conditions. For birth-death processes, ϕ is greater for the unrestricted case than for the connected one. The opposite is observed for death-birth processes. This indicates that the initial condition can have a significant effect on the outcome when then flow is slow.

As briefly mentioned before, the fragmented nature of the unrestricted setup can isolate groups of nodes from the rest of the population. As the evolutionary dynamics proceed, this promotes the formation of clusters, i.e. parts of the graph in which all

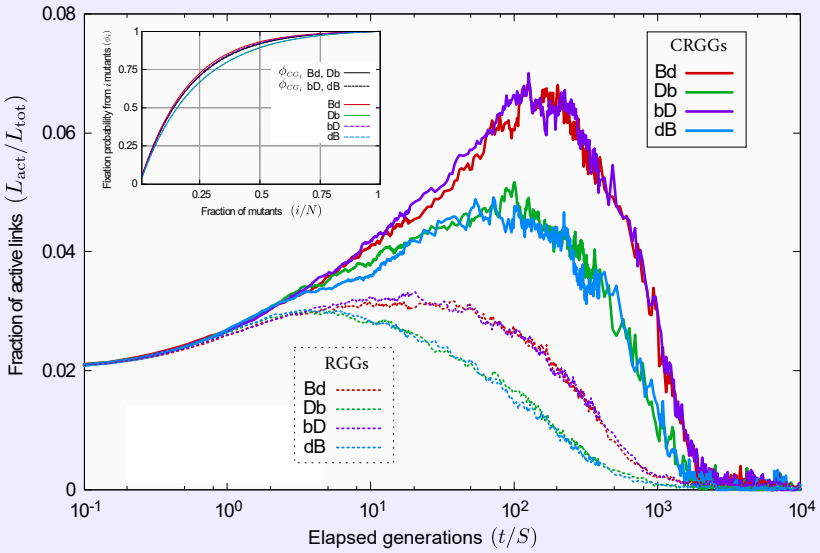

Figure 3.6: Fragmented initialization promotes the formation of clusters. The main panel shows the average proportion of active links as the evolutionary dynamics proceed. Thick lines correspond to simulations started from connected graphs (CRGGs); thin dotted lines to simulations initialized from unrestricted random positions (RGGs). The fraction of active links is lower for RGGs, regardless of the evolutionary process. **Inset:** Fixation probability of the mutant species, once there are i mutants in the population. When mutants are a minority, a small increase in their frequency greatly increases their fixation probability. Conversely, reducing their numbers when they are a majority has only minor effects on their chances of success. Simulations in the inset are initialized from CRGGs.

individuals are of the same species. The degree of clustering can be quantified through the fraction of active links in the network, that is, the proportion of links between mutants and wildtypes among all links in the graph, $L_{\text{act}}/L_{\text{tot}}$. A small fraction of active links is an indicator of clustering. We show measurements of the fraction of active links in Fig. 3.6 for both unrestricted and restricted random initial conditions (thin dotted lines and thick continuous lines, respectively). The data indicates that the fraction of active links is significantly larger when simulations are initialised on CRGGs than when started on RGGs.

The amplification or suppression of selection (for birth-death and death-birth processes, respectively) can then be supported by a similar argument to the one presented for the degree of the initial mutant. A smaller number of active links has the same effect as poor connectivity of the initial mutant; it does not affect the probability that the individual chosen in the first step of the evolutionary process is a mutant or a wildtype, but it reduces the probability that the individual chosen in the second step

is of the opposite species (see also Sec. 3.6).

In the early stages of the evolutionary process mutants are a minority, and are therefore less likely to be chosen in the initial step. A large number of active links then increases the chances that the neighbour of the initial individual is a mutant. Under birth-death processes this means that mutants are more likely to die; for death-birth processes they have more opportunities to reproduce. Therefore, a connected initial configuration (CRGGs), leading to a larger fraction of active links than arbitrary RGGs, reduces the fixation probability of a mutant under birth-death processes, and increases it for death-birth processes. This is in line with the results on the left-hand side of Fig. 3.5; the fixation probabilities for RGGs (dotted lines) are higher than their counterparts on CRGGs for birth-death processes (red and purple lines), but lower for death-birth processes (green and blue lines).

This argument is only valid when mutants are less abundant than wildtypes. The effect is reversed at later stages of the evolutionary process (if mutants become a majority). However, the results presented in Fig. 3.5 suggest that there is a net advantage for the mutant in having fewer active links, for birth-death processes, or in having increased inter-species connectivity, for death-birth mechanics. The inset in Fig. 3.6 helps to understand this further. It shows the conditional fixation probability of the mutant species, given that a state with i mutants has been reached. The shape of the curves indicates that increasing the number of mutants in the population has stronger repercussions on the fixation probability when mutants are a minority ($i/N \leq 0.5$) than when they are the majority ($i/N \geq 0.5$). For death-birth processes, the selective effect due to increased active links drives the population composition to states with approximately equal frequencies of the two species. However, the mutants have more to gain (in terms of fixation probability) when their numbers are small than what they may lose when they are abundant. For birth-death processes, on the other hand, a large number active links acts in the opposite way; it hinders the spread of the mutant species when they are a minority and encourages it once they are abundant. Since more is lost in the early invasion than what can be gained at later stages, the overall fixation probability is lower than when there are fewer active links. The net effect of fragmentation (i.e., a reduced number of active links) is therefore amplification of selection for birth-death processes, and suppression for death-birth update rules.

The amplification/suppression effect caused by the fragmented nature of the network can also be noticed at intermediate flow speeds. In this regime, the flow is sufficiently fast to disrupt the initial network structure before the evolutionary process reaches its conclusion (fixation or extinction of the mutant); disconnected components then develop. At the same time the flow is also slow enough to allow the formation of organised clusters of mutants and wildtypes through the evolutionary dynamics. Indeed, for simulations started on connected graphs a minimum in the fixation probability as a function of the flow speed is discernible for the **Db** process (thick green line in Fig. 3.5), and we also notice a shallow maximum for the **Bd** and **bD** processes (thick red and purple lines, respectively). The fragmentation from an initially connected network increases the fixation probability for birth-death processes and decreases it for death-birth processes. Movement of the population, and the resulting mixing between evolutionary events counteracts this amplification or suppression, driving fixation probabilities to their fast-flow limits. The balance of these two effects leads to the extrema in Fig. 3.5.

Square lattice

Regular lattices are particularly convenient for the study of fixation probabilities. The nodes are distributed equidistantly in space, and they all have the same number of neighbours. This means that analytical results can be obtained in the absence of flows. For example, the isothermal theorem [28] applies; the fixation probabilities of the global birth-death and death-processes are the same as those for complete graphs; only small deviations from ϕ_{CG} are expected for local-selection processes [5].

In order to relate the success of mutants in populations advected by flows to these benchmark results, we show the outcome of simulations in which individuals are initially placed on the nodes of a regular lattice in Fig. 3.7. Broadly, three different regimes can be distinguished:

Quasi-isothermal regime. On the left-hand side of Fig. 3.7 (slow flows) fixation probabilities for all processes are approximately the same as on complete graphs. This is to be expected; in the limit of slow flows the evolutionary process concludes before the lattice structure is modified. The interaction network remains regular and, in line

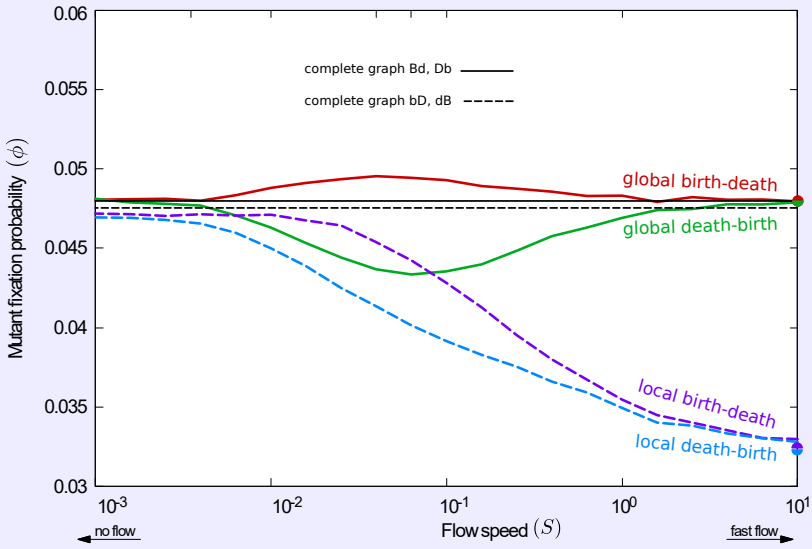

Figure 3.7: Fixation probability at different flow speeds for simulations started from a square lattice. For the global death-birth process a minimum of fixation probability is found at intermediate flow speeds; conversely, the global birth-death process shows a maximum. For the local processes no extrema are found; instead varying the flow speed interpolates monotonously between the behaviour on fixed lattices and the limit of fast flows.

with the isothermal theorem, the fixation probability for global processes (continuous lines) is the one known from complete graphs; results for local processes (dashed lines) only differ slightly from ϕ_{CG}.

With the periodic parallel shear flow, this agreement extends to slow, but non-vanishing flows. As described in Sec. 3.2, during the first half of each period the flow moves the particles only vertically, with velocities dependent on their horizontal position. This means that some elements of the initial lattice remain intact; for example initial 'columns' of individuals (those with the same horizontal coordinate) move jointly. There is then only limited variation in the degree of the nodes in the network, and the interaction graph remains nearly regular. If fixation or extinction occurs before the flow disrupts this quasi-isothermal structure, the predictions of the isothermal theorem remain a good approximation. The flow speed above which this is no longer the case can be estimated from a comparison of the the time until the lattice structure is disrupted and the time-to-fixation; see Sec. 3.5 for further details.

Intermediate regime. At intermediate flow speeds the fixation probability for the **Bd** process exhibits a maximum; a minimum is found for the **Db** process. These

features can be related to the amplification or suppression effects on heterogeneous graphs, discussed in the previous sections. For intermediate flow speeds, the individuals' motion is fast enough to distort the initial lattice structure before the evolutionary process concludes. On the other hand the flow is also sufficiently slow so that evolution has time to organise in clusters on the heterogeneous interaction network. Effectively evolution takes place on a slowly moving heterogeneous graph. This heterogeneity, in conjunction with the clustering of species, leads to amplification of selection for birth-death processes and suppression for death-birth processes. When selection is local this merely accelerates or delays the approach to the behaviour on complete graphs. When selection is global, however, the minimum (for **Db**) and maximum (for **Bd**) are generated. A rough estimate for the flow speed at which the extrema are seen can be obtained by comparing the time-to-fixation of the mutant species with the network renewal time; details can be found in Sec. 3.5.

Fast flow. In this regime the positions of individuals in space at each evolutionary event are essentially random, and the set of neighbours of any one particle is uncorrelated from an evolutionary event to the next one. The population is then 'well-stirred', and the analytical predictions from ref. [56] apply.

3.4 Discussion

We studied evolutionary dynamics in populations immersed in flows. In computer simulations, we measured the effect that the speed of the motion has on the success of an invading mutant, and found that different evolutionary processes show distinct responses of the fixation probability to the flow speed. Our results highlight the importance of including motion in the modelling of evolutionary dynamics. Just as population structure can generate amplification or suppression of selection, we find that the flow can act against or in favour of mutant invasion. While the models we study are stylised, we can identify general emerging principles. For instance, for the majority of evolutionary processes we observe a decrease in fixation probability when populations are in motion. This observation could be useful, for example, in industries where mutations are detrimental for the desired product but beneficial to the mutant, such as in microalgae, bacteria, fungi and yeast, relevant for the production of biodiesel [72–75].

Another example are the features we found to dominate fixation probability in the limits of very slow or very fast flows. If populations are mostly static in an experiment, our results indicate that whether selection acts locally or globally is a more important factor than the order of birth and death events. If an experiment involves populations in motion, on the other hand, careful consideration has to be given whether to use a birth-death or a death-birth process as a model, and it is less important in what step of evolutionary events competition takes place.

We hypothesise that the characteristic responses to flow may be used as an aid for choosing the most adequate update mechanism to model a given biological system. Despite the fact that direct measurements of the success of a specific mutation are not necessarily easy to perform, there is experimental evidence of differences in fixation probabilities in static and in stirred populations [7–9]. In these studies, cultures of *E. coli* were grown in a continuously stirred liquid medium, on Petri dishes, mixed every 24 hours, and on static Petri dishes. The structure and cluster formation of the cultures were found to have different dynamics under the different mixing conditions. The authors of ref. [9], for example, find that the ability to adapt, as measured by reproduction rates, is greater in the continuously-stirred case than in the case of only occasional mixing. This suggests a lower fixation probability in the slowly moving medium. Comparing this with our results, we speculate that a **Db** process might best describe this biological system.

It is appropriate to briefly comment on the limitations of our study. For example, we focused on the periodic parallel shear flow in our simulations. However, we note that most features of the amplification or suppression of selection are not due to particulars of the flow field. Instead they arise from the mixing of the population and the heterogeneity of the interaction network. Both of these features can be expected in most real flows, and we believe that the essence of our findings is relevant beyond the exemplar of the shear flow. This is supported by observations in our earlier work [56], in which we obtained analytic results for limit of fast flows and demonstrated that these predictions are independent of many details of the flow field. Our study is also limited to frequency-independent selection; natural extensions would include more complex fitness functions to better model the experimental situation in ref. [8], where frequency-dependent fitness was identified for completely static conditions. We

are aware that our simulations are for relatively small populations; this is due to computational costs associated with numerical experiments on a larger scale. Further work may also be necessary to relax assumption of a fixed population size. This may be useful to explore the effects of demographic stochasticity. On the other hand, dilution techniques or resource-limited environments can be used in experiments to keep the population approximately constant without significantly modifying the mutants' chances of success [76].

Recent advances in technology make direct measurements of the fixation probability of a specific mutation feasible [77]. We believe that this, together with computational studies of different evolutionary models in varying conditions, can open up promising routes to more informed choices of evolutionary mechanics for systems in evolutionary biology.

Acknowledgements

FHA thanks Consejo Nacional de Ciencia y Tecnología (CONACyT, Mexico) for support. VPM acknowledges financial support by CRETUS strategic partnership (ED431E2018/01), co-funded by the ERDF (EU). We would also like to thank Joseph W. Baron for his helpful comments.

Author contributions statement

FHA carried out the simulations and analytical calculations. All authors contributed to designing the research, to analysing the data and to writing the paper.

Additional information

We declare no competing interests.

3.5 Appendix A: Identification of relevant timescales for simulations started from regular lattices

In Sec. 3.3.2 of the main text we discuss the behaviour of the population when the initial condition is a regular lattice. We identify three different regimes: fast flows, intermediate flow speeds, and the quasi-isothermal regime. Here we discuss how these regimes can be identified from the simulations, and show how the time scales for the network renewal and quasi-isothermal regimes can be obtained. Simulations in this section were all initialized from a square lattice. The flow is the periodic parallel shear flow, with parameters as given in the main text.

3.5.1 End of quasi-isothermal regime

Fig. 3.8 shows the average number of components in the interaction graph, the average size of each component, and the average degree in the network as a function of time.

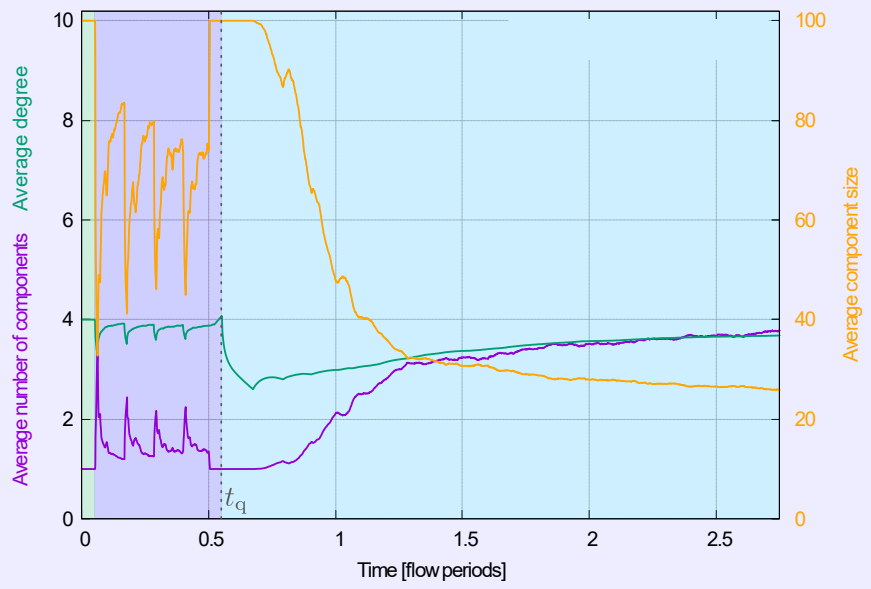

Figure 3.8: Component formation as flow destroys initial lattice configuration. The average number of components (purple) and the average degree (green) are plotted on the left axis; the average component size (orange) is plotted on the right axis. The three phases of the motion described in Sec. 3.5.1 of the Supplementary Information are shaded in different colours. The grey dotted line at t_q marks the end of the phase in which the graph is quasi-isothermal.

We observe three different phases:

(i) At first, there is a very short interval ($t \lesssim 0.05$), in which there is only one component of size N. The lattice interaction graph is still intact.

(ii) Next, for $0.05 \lesssim t \lesssim 0.55$ we see an oscillating number of components; this corresponds to a period in which movement is only vertical (for the most part). Links between individuals with the same horizontal coordinate, i.e., within a 'column' of the original lattice, are not modified. The interaction graph is nearly regular.

(iii) Following this, we see a sharp decline of the average degree. The network cannot be considered isothermal any more, as fragmentation into heterogeneous separate components has begun. All measured quantities approach their stationary asymptotic values (the figure shows an average over multiple runs). Initial positions are washed out and the individuals take random positions in space.

We refer to the two initial stages (i) and (ii) as the '*quasi-isothermal*' period. If fixation (or extinction) is reached in most runs during this initial period, we expect fixation probabilities close to the one on the complete graph. For the model parameters in our simulations, phase (ii) ends at $t_{\mathrm{q}} \approx 0.55$, shortly after the first half period of the flow ($T/2 = 0.5$). This is marked with a dotted grey line in Fig. 3.8. We note that the notion of the quasi-isothermal regime relies on the conservation of elements of the regular lattice; this may not be the case in other flows, for example if the motion of particles is not strictly vertical or horizontal. However, regardless of the type of flow, a critical flow speed can be found, below which the evolutionary process concludes before the lattice structure is significantly modified. Therefore, distinction of the regimes remains broadly valid.

3.5.2 Network renewal time

The time needed for neighbourhoods of individuals to lose correlation defines the *renewal* time, t_{r}. To measure this we have looked at the persistence of links in the network. As in ref. [56], we consider the probability that two nodes, connected at time t_0, are still connected at time $t_0 + t$; we write q_1 for this probability. Similarly we also measure the probability that two individuals who are not connected at t_0, are neighbours at time $t_0 + t$; we denote this probability by q_0. In the stationary state (i.e.

for large t_0), the time, t, at which $q_0 \approx q_1$ is a good estimate for the time it takes for the network to be 'renewed'. Results are shown in Fig. 3.9. For the parameters used throughout this paper, we estimate the renewal time as $t_\mathrm{r} \approx 6.4$; this is the first time, t, for which both q_0 and q_1 are within 0.1% of their asymptotic value, q. Recalling that the flow period is $T = 1$, this indicates that the set of neighbours of any one individual in the population is uncorrelated from the set of neighbours of the same individual approximately six and half periods earlier.

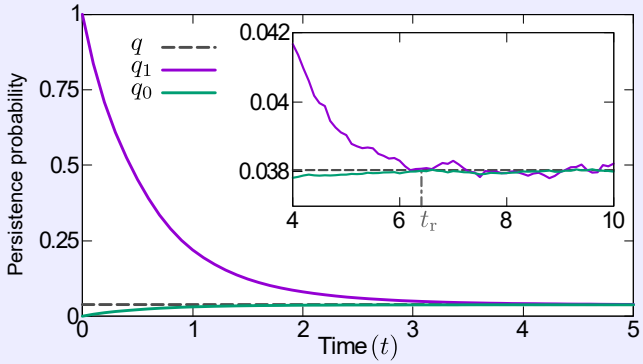

Figure 3.9: Network-renewal time measured from the persistence of links. Continuous lines show the probability that two nodes, connected (purple) or disconnected (green) at t_0 are still connected/disconnected at time $t_0 + t$. The dashed grey line shows the asymptotic value; the time needed for both probabilities (q_1 and q_0) to reach this value is the time it takes to renew the network. Both quantities are within 0.1% of their asymptotic value for the first time at $t_r \approx 6.4$, marked by a vertical dash-dotted grey line in the inset.

3.5.3 Conversion into characteristic flow speeds

The times t_q and t_r can be used to obtain estimates of the characteristic flow speeds separating the different regimes of dynamics described in the main text. These estimates are obtained by comparing t_q and t_r to the time-to-fixation for different flow speeds, S.

This is shown in Fig. 3.10, where we plot the the time, t_1, required for a single mutant to reach fixation. Data is shown as a function of S. The network renewal time t_r is marked with a dash-dotted line on the vertical axis of the main panel, and t_q is marked with a dotted line on the vertical axis of the inset. The flow speeds for which $t_1 = t_\mathrm{q}$ and $t_1 = t_\mathrm{r}$ define flow speeds S_q and S_r, respectively. Due to differences in the mean fixation times, we note that the estimates for S_q and S_r vary between the

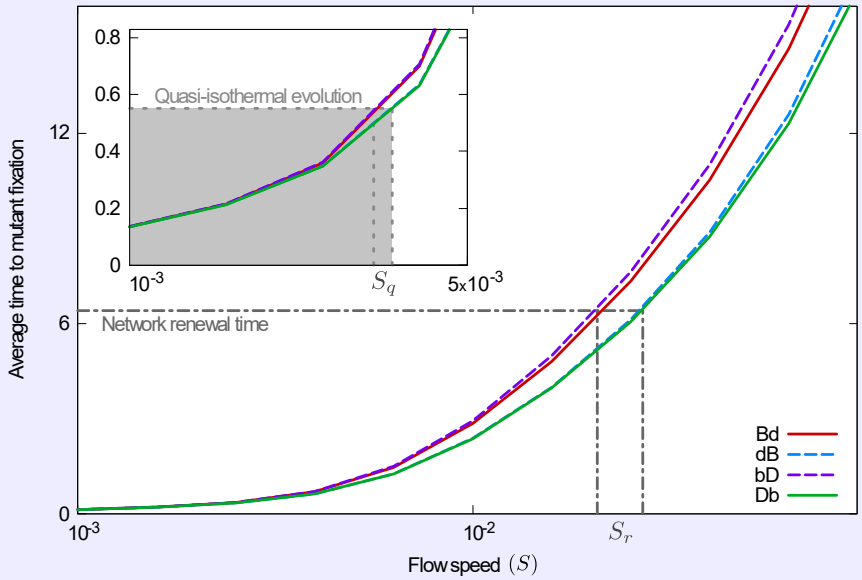

Figure 3.10: Identification of time scales and flow speeds for the different evolutionary regimes. The time to mutant fixation is plotted for the different evolutionary processes as a function of S. The flow speed at which the quasi-isothermal regime ends (S_q) is identified as the speed at which the mean time to fixation coincides with the time needed to significantly disrupt the interaction network, obtained in Fig. 3.8. Similarly, S_r is the flow speed at which the mean fixation time agrees with the network renewal time, obtained in Fig. 3.9.

different evolutionary update rules.

These flow speeds are shown in the context of the fixation probability at different flow speeds in Fig. 3.11. As expected, the S_{q} (grey dotted lines) marks the end of the quasi-isothermal regime. For flow speeds $S < S_{\mathrm{q}}$ the mean time to fixation is shorter than the time t_q it takes the flow to significantly disrupt the initial lattice. This is the quasi-isothermal regime. For $S > S_q$ fixation is usually reached when the lattice has been significantly distorted.

The grey dash-dotted lines in Fig. 3.11 correspond to S_{r}. The location of the extrema of the fixation probability for **Bd** and **Db** processes are found at flow speeds of the same order of magnitude as S_r. Similar observations were made for the time-to-consensus in a voter model in [60].

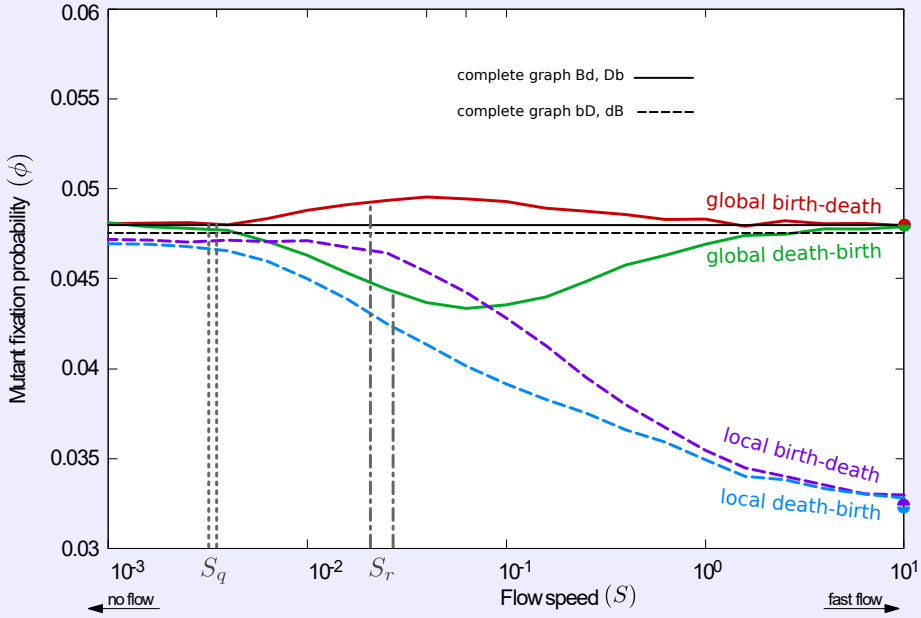

Figure 3.11: Identification of time scales and flow speeds for the different evolutionary regimes. Fixation probability at different flow speeds for simulations started from a square lattice are shown. S_q roughly corresponds to the speed marking the end of the quasi-isothermal regime; S_r is found to be of the same order of magnitude as the speed at the extrema of fixation probability.

3.6 Appendix B: Relevance of the number of active links

The amplification or suppression of selection, observed when comparing the simulations initialized from connected and unrestricted graphs, can be understood using an argument analogous to the one in ref. [68]. The number of active links does not change the probability with which a node is picked in the initial step of an evolutionary event, but it does have an effect on the choice of the second individual.

Wheel graphs are convenient to illustrate this. They consist of a central node (hub), connected to $N-1$ nodes organized in a circle around it (leaves), where N is the total size of the graph. The leaves are only connected to the hub and to their nearest neighbours on the rim of the wheel (see Fig. 3.12 A). If two mutants are placed on a graph of this type, their location affects the number of active links (L_{act}), even though the total population size, the number of mutants and the degree of either mutants or wildtypes in the population remain unchanged. This is shown in Fig. 3.12 B and C.

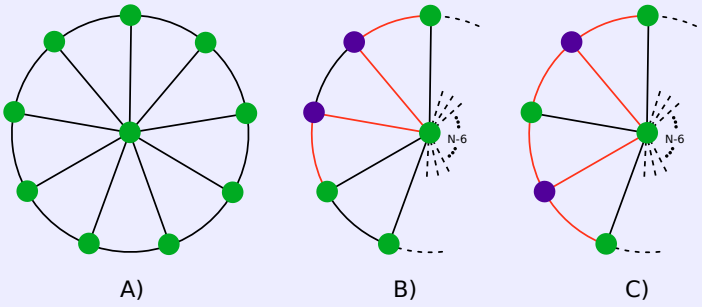

Figure 3.12: Wheel graphs. A) A sample wheel graph of size 10; B) A portion of a wheel graph with two mutants on adjacent leaves, with $L_{\text{act}} = 4$; C) A portion of a wheel graph with two mutants on non-adjacent leaves, with $L_{\text{act}} = 6$. Active links are marked orange. For B and C, $N - 6$ wildtype nodes are not shown.

When the two mutants are neighbours (B), the network has 4 active links. If they are not neighbours (C), $L_{\text{act}} = 6$. To be able to have both settings one needs $N \geq 5$. In the two cases, both mutants have degree 3, and there are $N - 3$ wildtypes with degree 3, and one with degree $N - 1$. The probability that a mutant is replaced by a wildtype, however, is not the same for the two cases.

To see this, we focus on the case of neutral selection. We write $p_{m,w}$ for the probability that, in a single evolutionary event, a mutant is chosen first and a wildtype second. Similarly $p_{w,m}$ is the probability that a wildtype is chosen first and a mutant second. We then look at the ratio $Q = p_{m,w}/p_{w,m}$, to determine which one of these is more likely.

The probability that the individual picked in the first step is a mutant is $p_m = 2/N$; for a wildtype, $p_w = (N-2)/N$. This is the case in both configurations, B and C in Fig. 3.12. For configuration B we then have:

$$p^B_{m,w} = \frac{2}{N}\left[\frac{1}{2}\left(\frac{2}{3} + \frac{2}{3}\right)\right] = \frac{4}{3N},$$
$$p^B_{w,m} = \frac{N-2}{N}\left[\frac{1}{N-2}\left(\frac{2}{N-1} + 2\frac{1}{3}\right)\right] = \frac{2}{N}\frac{N+2}{3(N-1)}.$$

From this we find

$$Q_B = \frac{\frac{4}{3N}}{\frac{2}{N}\frac{N+2}{3(N-1)}} = \frac{2(N-1)}{N+2} \tag{3.1}$$

For configuration C we find

$$p^C_{m,w} = \frac{2}{N}\left[\frac{1}{2}\left(\frac{3}{3}+\frac{3}{3}\right)\right] = \frac{2}{N},$$
$$p^C_{w,m} = \frac{N-2}{N}\left[\frac{1}{N-2}\left(\frac{2}{N-1}+4\frac{1}{3}\right)\right] = \frac{2}{N}\frac{2N+1}{3(N-1)},$$

and hence

$$Q_C = \frac{\frac{2}{N}}{\frac{2}{N}\frac{2N+1}{3(N-1)}} = \frac{3(N-1)}{2N+1} \tag{3.2}$$

Comparing Eqs. (3.1) and (3.2), and assuming $N \geq 5$, we find $Q_B > Q_C$, i.e., the scenario with more active links (C) is more likely to result in events in which a wildtype is picked first and a mutant second. For a death-birth process, this means that mutants are more likely to reproduce, and for a birth-death process that they are more likely to die. This is in line with the results obtained in Fig. 3.5 of the main text.

A further configuration on a the wheel graphs is possible, placing one of the two mutants in the hub, which results in $L_{\text{act}} = N$. A similar analysis leads to $Q = (5N-8)/[N(N-1)]$, which is even smaller than Q_C. We note however that the average degree of mutants and wildtypes in this scenario is different from those in the other two settings.

3.7 Appendix C: Dual selection processes

As mentioned in Sec. 3.2, the most general process of the birth-death or death-birth type is one that includes selection in both steps. In line with ref. [56], we call these 'dual-selection' processes; we label them **BD** and **DB**, respectively.

In this section, we present and discuss the simulation results for fixation probabilities at different flow speeds for both dual-selection processes. These are shown in Fig. 3.13 for all configurations of initial positions studied in the main text: RGGs, CRGGs, and the square lattice.

Naively, one could expect to be able to describe the response of the fixation probabilities to the flow speed in dual-selection processes through a combination of those observed for the corresponding global and local processes. That is, for **BD** one would expect to see similar features as in **Bd** and **bD**, and the behaviour of **DB** could be expected to show elements of that of **Db** and **dB**. For example, both **BD** and **DB** involve local selection, and for fast flows we find that the resulting fixation

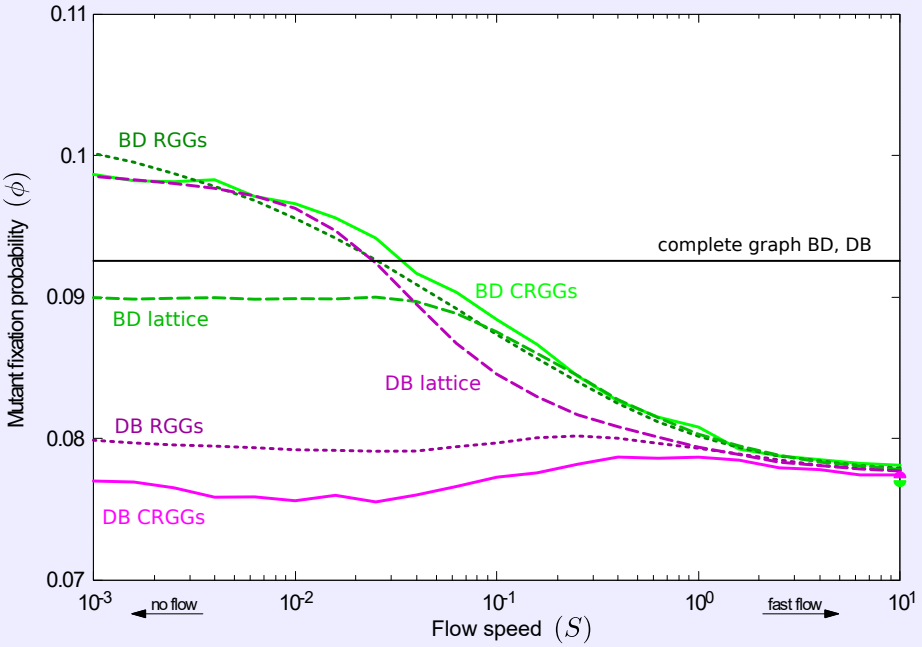

Figure 3.13: Fixation probability at different flow speeds for dual-selection processes. The result for the complete graph is plotted as a reference. Continuous lines correspond to simulations initialized from CRGGs, dotted lines to unrestricted RGGs, and dashed lines to simulations started from a lattice.

probability is lower than that of the complete graph, as is the case for both local processes, **bD** and **dB**.

For slow flows we make the following observations:

Dual-selection birth-death process: For simulations initialized on RGGs and CRGGs, the fixation probability of the **BD** process (dotted and continuous green lines in Fig. 3.13) is above the one on complete graphs, as is the case for both **Bd** and **bD** (see red and purple lines in Fig. 3.5).

If simulations are started from a lattice (dashed green line in Fig. 3.13), the fixation probability of the **BD** process is slightly below ϕ_{CG}; this could also be expected, as the isothermal theorem does not hold due to the presence of local selection; we note that the fixation probability of the **bD** process is below that on a complete graph (see purple dashed line in Fig. 3.7).

Interestingly, at slow flow speeds random initial positions act as an amplifier of selection (compared to the complete graph) for the **BD** process, whereas suppression of selection is observed for lattice initial positions.

Dual-selection death-birth process: The fixation probability of the **DB** process in simulations started on RGGs and CRGGs (dotted and continuous magenta lines in Fig. 3.13) is well below ϕ_{CG}; we note that the mutant's success for both **Db** and **dB** is below that on a complete graph (see green and blue lines in Fig. 3.5), so it is not surprising that the **DB** process shows this feature as well.

However, if simulations are started from a lattice (dashed magenta line in Fig. 3.13), the fixation probability of the **DB** process is above ϕ_{CG}. This is different from both the **Db** or **dB** processes, who both lead to $\phi \leq \phi_{CG}$ (see green and blue lines in Fig. 3.7). This indicates that simple intuition may fail – features present in **Db** and in **dB** processes may be altered when selection acts in both the death and the birth step. This, we believe is an unexpected observation, which could be pursued in future work. In particular it would be interesting to test when exactly such counter-intuitive behaviour is found when combining local and global selection, i.e., for example, for what types of graphs does this occur, and what common features do these graphs have?

We also note that, in contrast to the **BD** process, we find amplification of selection for the **DB** process when starting from regular lattice and slow flow. For random initial positions we find suppressed selection.

Bibliography

[1] Maynard Smith, John (1982), *Evolution and the Theory of Games*, Cambridge University Press, Cambridge, UK.

[2] Ewens, Warren J. (2004), *Mathematical Population Genetics 1: Theoretical Introduction*, Springer, New York, NY.

[3] Nowak, Martin A. (2006a), *Evolutionary Dynamics*, Harvard University Press, Cambridge, Massachusetts.

[4] Zukewich, Joshua et al. (2013), 'Consolidating Birth-Death and Death-Birth Processes in Structured Populations', *PLoS ONE* **8** (1):e54639, DOI: 10.1371/journal.pone.0054639.

[5] Kaveh, Kamran, Natalia L. Komarova and Mohammad Kohandel (2015), 'The duality of spatial death-birth and birth-death processes and limitations of the isothermal theorem', *Royal Society Open Science* **2** (4):140465–140465, DOI: 10.1098/rsos.140465.

[6] Hindersin, Laura and Arne Traulsen (2015), 'Most undirected random graphs are amplifiers of selection for Birth-death dynamics, but suppressors of selection for death-Birth dynamics', *PLOS Computational Biology* **11** (11):e1004437, DOI: 10.1371/journal.pcbi.1004437.

[7] Kerr, Benjamin et al. (2002), 'Local dispersal promotes biodiversity in a real-life game of rock–paper–scissors', *Nature* **418** (6894):171–174, DOI: 10.1038/nature00823.

[8] Habets, Michelle G J L et al. (2006), 'The effect of population structure on the adaptive radiation of microbial populations evolving in spatially structured environments', *Ecology Letters* **9** (9):1041–1048, DOI: 10.1111/j.1461-0248.2006.00955.x.

[9] Perfeito, Lilia et al. (2008), 'The effect of spatial structure on adaptation in Escherichia coli', *Biology Letters* **4** (1):57–59, DOI: 10.1098/rsbl.2007.0481.

[10] Nowak, Martin A. and Robert M. May (1992), 'Evolutionary games and spatial chaos', *Nature* **359** (6398):826–829, DOI: 10.1038/359826a0.

[11] Ebel, Holger and Stefan Bornholdt (2002), 'Coevolutionary games on networks', *Physical Review E* **66** (5):056118, DOI: 10.1103/PhysRevE.66.056118.

[12] Nowak, Martin A. (2006b), 'Five rules for the evolution of cooperation', *Science* **314** (5805):1560–1563, DOI: 10.1126/science.1133755.

[13] Santos, Francisco C., Jorge M. Pacheco and Tom Lenaerts (2006), 'Evolutionary dynamics of social dilemmas in structured heterogeneous populations', *Proceedings of the National Academy of Sciences* **103** (9):3490–3494, DOI: 10.1073/pnas.0508201103.

[14] Ohtsuki, Hisashi et al. (2006), 'A simple rule for the evolution of cooperation on graphs and social networks', *Nature* **441** (7092):502–505, DOI: 10.1038/nature04605.

[15] Nowak, Martin A., Corina E. Tarnita and Tibor Antal (2010), 'Evolutionary dynamics in structured populations', *Philosophical Transactions of the Royal Society B: Biological Sciences* **365** (1537):19–30, DOI: 10.1098/rstb.2009.0215.

[16] Szabó, György and Gábor Fáth (2007), 'Evolutionary games on graphs', *Physics Reports* **446** (4-6):97–216, DOI: 10.1016/j.physrep.2007.04.004.

[17] Gross, Thilo and Bernd Blasius (2008), 'Adaptive coevolutionary networks: A review', *Journal of the Royal Society Interface* **5** (20):259–271, DOI: 10.1098/rsif.2007.1229.

[18] Poncela, Julia et al. (2009), 'Evolutionary game dynamics in a growing structured population', *New Journal of Physics* **11** (8):083031, DOI: 10.1088/1367-2630/11/8/083031.

[19] Masuda, Naoki and Hisashi Ohtsuki (2009), 'Evolutionary dynamics and fixation probabilities in directed networks', *New Journal of Physics* **11** (3):033012, DOI: 10.1088/1367-2630/11/3/033012.

[20] Broom, Mark, Jan Rychtář and B. T. Stadler (2011), 'Evolutionary Dynamics on Graphs - the Effect of Graph Structure and Initial Placement on Mutant Spread', *Journal of Statistical Theory and Practice* **5** (3):369–381, DOI: 10.1080/15598608.2011.10412035.

[21] Perc, Matjaž and Attila Szolnoki (2012), 'Self-organization of punishment in structured populations', *New Journal of Physics* **14** (4):043013, DOI: 10.1088/1367-2630/14/4/043013.

[22] Wang, Ruiqi (2013), 'Noise, Intrinsic and Extrinsic', *Encyclopedia of Systems Biology*, ed. by Werner Dubitzky et al., Springer New York, New York, NY, p. 1527, DOI: 10.1007/978-1-4419-9863-7_353.

[23] Perc, Matjaž et al. (2013), 'Evolutionary dynamics of group interactions on structured populations: a review', *Journal of The Royal Society Interface* **10** (80):20120997–20120997, DOI: 10.1098/rsif.2012.0997.

[24] Hindersin, Laura and Arne Traulsen (2014), 'Counterintuitive properties of the fixation time in network-structured populations', *Journal of The Royal Society Interface* **11** (99):20140606–20140606, DOI: 10.1098/rsif.2014.0606.

[25] Jiang, Chunxiao, Yan Chen and K. J. Ray Liu (2014), 'Evolutionary Dynamics of Information Diffusion Over Social Networks', *IEEE Transactions on Signal Processing* **62** (17):4573–4586, DOI: 10.1109/TSP.2014.2339799.

[26] Allen, Benjamin et al. (2017), 'Evolutionary dynamics on any population structure', *Nature* **544** (7649):227–230, DOI: 10.1038/nature21723.

[27] Pavlogiannis, Andreas et al. (2018), 'Construction of arbitrarily strong amplifiers of natural selection using evolutionary graph theory', *Communications Biology* **1** (1):71, DOI: 10.1038/s42003-018-0078-7.

[28] Lieberman, Erez, Christoph Hauert and Martin A. Nowak (2005), 'Evolutionary dynamics on graphs', *Nature* **433** (7023):312–316, DOI: 10.1038/nature03204.

[29] Shakarian, Paulo, Patrick Roos and Anthony Johnson (2012), 'A review of evolutionary graph theory with applications to game theory', *BioSystems* **107** (2):66–80, DOI: 10.1016/j.biosystems.2011.09.006.

[30] Broom, Mark and Jan Rychtar (2008), 'An analysis of the fixation probability of a mutant on special classes of non-directed graphs', *Proceedings of the Royal Society A: Mathematical, Physical and Engineering Sciences* **464** (2098):2609–2627, DOI: 10.1098/rspa.2008.0058.

[31] Broom, Mark, J. Rychtář and B. Stadler (2009), 'Evolutionary dynamics on small-order graphs', *Journal of Interdisciplinary Mathematics* **12** (2):129–140, DOI: 10.1080/09720502.2009.10700618.

[32] Houchmandzadeh, Bahram and Marcel Vallade (2011a), 'The fixation probability of a beneficial mutation in a geographically structured population', *New Journal of Physics* **13** (7):073020, DOI: 10.1088/1367-2630/13/7/073020.

[33] Pattni, Karan et al. (2015), 'Evolutionary graph theory revisited: when is an evolutionary process equivalent to the Moran process?', *Proceedings of the Royal Society A: Mathematical, Physical and Engineering Science* **471** (2182):20150334, DOI: 10.1098/rspa.2015.0334.

[34] Lushi, Enkeleida, Hugo Wioland and Raymond E. Goldstein (2014), 'Fluid flows created by swimming bacteria drive self-organization in confined suspensions', *Proceedings of the National Academy of Sciences* **111** (27):9733–9738, DOI: 10.1073/pnas.1405698111.

[35] Lapin, Alexei, Joachim Schmid and Matthias Reuss (2006), 'Modeling the dynamics of E. coli populations in the three-dimensional turbulent field of a stirred-tank bioreactor - A structured-segregated approach', *Chemical Engineering Science* **61** (14):4783–4797, DOI: 10.1016/j.ces.2006.03.003.

[36] Nagylaki, Thomas (1980), 'The strong-migration limit in geographically structured populations', *Journal of Mathematical Biology* **9** (2):101–114, DOI: 10.1007/BF00275916.

[37] McPeek, Mark A. and Robert D. Holt (1992), 'The Evolution of Dispersal in Spatially and Temporally Varying Environments', *The American Naturalist* **140** (6):1010–1027, DOI: 10.1086/285453.

[38] Hill, M. Forrest, Alan Hastings and Louis W. Botsford (2002), 'The Effects of Small Dispersal Rates on Extinction Times in Structured Metapopulation Models', *The American Naturalist* **160** (3):389–402, DOI: 10.1086/341526.

[39] Casagrandi, Renato and Marino Gatto (2006), 'The intermediate dispersal principle in spatially explicit metapopulations', *Journal of Theoretical Biology* **239** (1):22–32, DOI: 10.1016/j.jtbi.2005.07.009.

[40] Houchmandzadeh, Bahram and Marcel Vallade (2011b), 'The fixation probability of a beneficial mutation in a geographically structured population', *New Journal of Physics* **13** (7):073020, DOI: 10.1088/1367-2630/13/7/073020.

[41] Thalhauser, Craig J. et al. (2010), 'Selection in spatial stochastic models of cancer: Migration as a key modulator of fitness', *Biology Direct* **5** (1):21, DOI: 10.1186/1745-6150-5-21.

[42] Krieger, Madison S., Alex McAvoy and Martin A. Nowak (2017), 'Effects of motion in structured populations', *Journal of The Royal Society Interface* **14** (135):20170509, DOI: 10.1098/rsif.2017.0509.

[43] Zimmermann, Martín G., Víctor M. Eguíluz and Maxi San Miguel (2004), 'Coevolution of dynamical states and interactions in dynamic networks', *Physical Review E* **69** (6):065102, DOI: 10.1103/PhysRevE.69.065102.

[44] Zimmermann, Martín G. and Víctor M. Eguíluz (2005), 'Cooperation, social networks, and the emergence of leadership in a prisoner's dilemma with adaptive local interactions', *Physical Review E* **72** (5):056118, DOI: 10.1103/PhysRevE.72.056118.

[45] Gross, Thilo, Carlos J. Dommar D'Lima and Bernd Blasius (2006), 'Epidemic Dynamics on an Adaptive Network', *Physical Review Letters* **96** (20):208701, DOI: 10.1103/PhysRevLett.96.208701.

[46] Ehrhardt, George C. M. A., Matteo Marsili and Fernando Vega-Redondo (2006), 'Phenomenological models of socioeconomic network dynamics', *Physical Review E* **74** (3):036106, DOI: 10.1103/PhysRevE.74.036106.

[47] Pacheco, Jorge M., Arne Traulsen and Martin A. Nowak (2006), 'Coevolution of Strategy and Structure in Complex Networks with Dynamical Linking', *Physical Review Letters* **97** (25):258103, DOI: 10.1103/PhysRevLett.97.258103.

[48] Károlyi, György, Zoltán Neufeld and István Scheuring (2005), 'Rock-scissors-paper game in a chaotic flow: The effect of dispersion on the cyclic competition of microorganisms', *Journal of Theoretical Biology* **236** (1):12–20, DOI: 10.1016/j.jtbi.2005.02.012.

[49] Perlekar, Prasad et al. (2011), 'Particle algorithms for population dynamics in flows', *Journal of Physics: Conference Series* **333** (1):012013, DOI: 10.1088/1742-6596/333/1/012013.

[50] Pigolotti, Simone et al. (2012), 'Population Genetics in Compressible Flows', *Physical Review Letters* **108** (12):128102, DOI: 10.1103/PhysRevLett.108.128102.

[51] Benzi, Roberto et al. (2012), 'Population dynamics in compressible flows', *The European Physical Journal Special Topics* **204** (1):57–73, DOI: 10.1140/epjst/e2012-01552-0.

[52] Pigolotti, Simone et al. (2013), 'Growth, competition and cooperation in spatial population genetics', *Theoretical Population Biology* **84** (1):72–86, DOI: 10.1016/j.tpb.2012.12.002.

[53] Pigolotti, Simone and Roberto Benzi (2014), 'Selective Advantage of Diffusing Faster', *Physical Review Letters* **112** (18):188102, DOI: 10.1103/PhysRevLett.112.188102.

[54] Plummer, Abigail et al. (2019), 'Fixation probabilities in weakly compressible fluid flows', *Proceedings of the National Academy of Sciences* **116** (2):373–378, DOI: 10.1073/pnas.1812829116.

[55] Minors, Kevin, Tim Rogers and Christian A. Yates (2018), 'Noise-driven bias in the non-local voter model', *EPL (Europhysics Letters)* **122** (1):10004, DOI: 10.1209/0295-5075/122/10004.

[56] Herrerías-Azcué, Francisco, Vicente Pérez-Muñuzuri and Tobias Galla (2018), 'Stirring does not make populations well mixed', *Scientific Reports* **8** (1):4068, DOI: 10.1038/s41598-018-22062-w.

[57] Ottino, Julio M. (1989), *The kinematics of mixing: stretching, chaos, and transport*, Cambridge University Press, Cambridge, UK.

[58] Neufeld, Zoltán and Emilio Hernández-García (2010), *Chemical and biological processes in fluid flows: a dynamical systems approach*, Imperial College Press, London, UK.

[59] Pérez-Muñuzuri, Vicente and Guillermo Fernández-García (2007), 'Mixing efficiency in an excitable medium with chaotic shear flow', *Physical Review E* **75** (4):046209, DOI: 10.1103/PhysRevE.75.046209.

[60] Galla, Tobias and Vicente Pérez-Muñuzuri (2017), 'Time scales and species coexistence in chaotic flows', *EPL (Europhysics Letters)* **117** (6):68001, DOI: 10.1209/0295-5075/117/68001.

[61] Young, William R., Anthony J. Roberts and Gordan R. Stuhne (2001), 'Reproductive pair correlations and the clustering of organisms', *Nature* **412** (6844):328–331, DOI: 10.1038/35085561.

[62] Sandulescu, Mathias et al. (2007), 'Plankton blooms in vortices: the role of biological and hydrodynamic timescales', *Nonlinear Processes in Geophysics* **14** (4):443–454, DOI: 10.5194/npg-14-443-2007.

[63] Neufeld, Zoltán, Peter H. Haynes and Tamás Tél (2002), 'Chaotic mixing induced transitions in reaction–diffusion systems', *Chaos: An Interdisciplinary Journal of Nonlinear Science* **12** (2):426–438, DOI: 10.1063/1.1476949.

[64] Gilbert, Edgar N. (1961), 'Random Plane Networks', *Journal of the Society for Industrial and Applied Mathematics* **9** (4):533–543, DOI: 10.1137/0109045.

[65] Hindersin, Laura et al. (2016), 'Exact numerical calculation of fixation probability and time on graphs', *Biosystems* **150**:87–91, DOI: 10.1016/j.biosystems.2016.08.010.

[66] Giakkoupis, George (2016), 'Amplifiers and Suppressors of Selection for the Moran Process on Undirected Graphs', *arXiv preprint*, arXiv: 1611.01585.

[67] Adlam, Ben, Krishnendu Chatterjee and Martin A. Nowak (2015), 'Amplifiers of selection', *Proceedings of the Royal Society A: Mathematical, Physical and Engineering Science* **471** (2181):20150114, DOI: 10.1098/rspa.2015.0114.

[68] Antal, Tibor, Sidney Redner and Vishal Sood (2006), 'Evolutionary Dynamics on Degree-Heterogeneous Graphs', *Physical Review Letters* **96** (18):188104, DOI: 10.1103/PhysRevLett.96.188104.

[69] Sood, Vishal, Tibor Antal and Sidney Redner (2008), 'Voter models on heterogeneous networks', *Physical Review E* **77** (4):041121, DOI: 10.1103/PhysRevE.77.041121.

[70] Maciejewski, Wes (2014), 'Reproductive value in graph-structured populations', *Journal of Theoretical Biology* **340**:285–293, DOI: 10.1016/j.jtbi.2013.09.032.

[71] Tan, Shaolin and Jinhu Lü (2015), 'Characterizing the effect of population heterogeneity on evolutionary dynamics on complex networks', *Scientific Reports* **4** (1):5034, DOI: 10.1038/srep05034.

[72] Ma, Fangrui and Milford A. Hanna (1999), 'Biodiesel production: a review', *Bioresource Technology* **70** (1):1–15, DOI: 10.1016/S0960-8524(99)00025-5.

[73] Chisti, Yusuf (2007), 'Biodiesel from microalgae', *Biotechnology Advances* **25** (3):294–306, DOI: 10.1016/j.biotechadv.2007.02.001.

[74] Jeon, Dong Jin and Sung Ho Yeom (2010), 'Two-step bioprocess employing whole cell and enzyme for economical biodiesel production', *Korean Journal of Chemical Engineering* **27** (5):1555–1559, DOI: 10.1007/s11814-010-0263-y.

[75] Meng, Xin et al. (2009), 'Biodiesel production from oleaginous microorganisms', *Renewable Energy* **34** (1):1–5, DOI: 10.1016/j.renene.2008.04.014.

[76] Wahl, Lindi M., Philip J Gerrish and Ivan Saika-Voivod (2002), 'Evaluating the impact of population bottlenecks in experimental evolution.', *Genetics* **162** (2):961–71.

[77] Patwa, Zaheerabbas and Lindi M. Wahl (2008), 'The fixation probability of beneficial mutations', *Journal of The Royal Society Interface* **5** (28):1279–1289, DOI: 10.1098/rsif.2008.0248.

Chapter 4

The effects of heterogeneity on stochastic cycles in epidemics

Preface

The contents of this chapter constitute a manuscript published by Scientific Reports[1]. The manuscript was authored by Francisco Herrerías-Azcué[2], and Tobias Galla[2].

F.H.A.'s contributions include the inception of the project, performing all calculations and analysis, coding simulations, producing the data for all figures, finalising all figures, and writing all sections of the paper alongside T.G.

[1] F. Herrerías-Azcué and T. Galla, (2017), "The effects of heterogeneity on stochastic cycles in epidemics", *Scientific Reports* **7**(1):13008, doi:10.1038/s41598-017-12606-x.

[2] Theoretical Physics, School of Physics and Astronomy, The University of Manchester, Manchester, M13 9PL, United Kingdom.

Abstract

Models of biological processes are often subject to different sources of noise. Developing an understanding of the combined effects of different types of uncertainty is an open challenge. In this paper, we study a variant of the susceptible-infective-recovered model of epidemic spread, which combines both agent-to-agent heterogeneity and intrinsic noise. We focus on epidemic cycles, driven by the stochasticity of infection and recovery events, and study in detail how heterogeneity in susceptibilities and propensities to pass on the disease affects these quasi-cycles. While the system can only be described by a large hierarchical set of equations in the transient regime, we derive a reduced closed set of equations for population-level quantities in the stationary regime. We analytically obtain the spectra of quasi-cycles in the linear-noise approximation. We find that the characteristic frequency of these cycles is typically determined by population averages of susceptibilities and infectivities, but that their amplitude depends on higher-order moments of the heterogeneity. We also investigate the synchronisation properties and phase lag between different groups of susceptible and infected individuals.

4.1 Introduction

It is now widely recognised that noise and uncertainty play an important role in modelling biological systems. Traditional approaches to modelling phenomena in biology[1] are often based on deterministic ordinary or partial differential equations, and do not aim to describe stochasticity. In order to capture epistemic uncertainty, static or dynamic noise variables are introduced in more modern mathematical biology. This randomness reflects the lack of detailed knowledge about phenomena at finer scales than described by the model at hand; any modelling approach necessarily operates at a set scale (e.g. cell, individual, or population), and does not capture in detail the processes at smaller scales. These are 'emulated' through effective randomness. Different types of such noise are frequently found in models of biological phenomena, including intrinsic demographic noise, extrinsic stochasticity, parameter uncertainty or heterogeneity between different types of interacting entities [2, 3]. Some of these random

variables are static and do not evolve in time, others are described by dynamic time-dependent noise. Intrinsic noise, due to the stochastic dynamics of a system has lately been the focus of many studies (see for example [4–6]). Extrinsic or parametric noise, due to variations, heterogeneity or uncertainties in the parameters or the environment surrounding the process, has received similar attention (e.g. [7–9]). To be able to adequately describe biological systems, however, it may be necessary to account for both these uncertainties which contribute to the noisy dynamics.

In the modelling of epidemics this is of particular importance. The infection process, driven by serendipitous contacts, is inherently stochastic, and heterogeneity in susceptibility to a disease or infectiousness of different individuals are known to exist and play a role in viral spread. Genetic differences that result in heterogeneous susceptibilities to a disease have been suggested to play an important role [10, 11], and variation in viral reproduction from host to host have been observed in [12]. Behavioural, structural or contact differences between individuals are inevitable, but we focus our study on the former type of heterogeneity. However, the better part of the existing work focusing on heterogeneity of this type, does not explicitly seek to capture demographic noise. Instead one often assumes infinite populations and deterministic dynamics. This approach is often taken outside epidemics as well. Much existing work studies *individual* sources of uncertainty, heterogeneity and noise in isolation, but not their interacting together. A notable exception is the modelling of gene regulatory networks, in which the interaction of intrinsic and extrinsic noise is actively studied, see e.g. [13–15].

The effects of intrinsic noise have been recognised in recent years. In models with demographic processes, for example, intrinsic stochasticity has been seen to lead to sustained quasi-cycles [16–19] in parameter regimes in which a deterministic model would converge to a stable fixed point. These quasi-cycles have been identified not only in models of epidemic spread, but also in other instances of population dynamics, including in genetic circuits, evolutionary systems and in game theory [20–23]. Heterogeneity has been and is being considered in epidemics as well. Age structure is studied for example in [24, 25], seasonally changing infection rates in [26, 27], variation in infectivity and/or susceptibility are addressed in [28–32], spatial structure has been approached in [33–36], and epidemics on static and dynamic networks are studied

in [7, 37–41]. Heterogeneity has been found to generate outbreaks that propagate hierarchically [38, 42], grow faster than in homogeneous populations [39], and have a lower total number of infected individuals [43, 44].

Much of this work, whether describing a well-mixed population, a compartmented or structured one, is based on variants of the celebrated susceptible-infective-recovered (SIR) model. They can be described either by deterministic differential equations, or as a stochastic process involving a population of discrete individuals. In the former approach the population is effectively assumed to be infinite, so that the timing of stochastic infection, recovery or birth-death events 'averages' out, and smooth laws for the time evolution of the population are obtained. The latter approach explicitly captures the intrinsic randomness of infection, recovery and demographics. The population is taken to be finite, and its state discrete. The model evolves through discrete events (e.g. infections). In the simplest case this defines a Markovian random process, which often can be analysed further mathematically, at least to a good approximation. Starting from the master equation in a well-mixed population a set of stochastic differential equations can be derived in the limit of large, but finite populations [45]. These can then be studied further within the 'linear-noise approximation' (LNA) [46]. The mathematics are tractable and the corresponding theory is now well established. While remarkably powerful, this approach so far has mostly been used for well-mixed populations. The linear-noise approximation has also been applied to networked systems with contact heterogeneity (see e.g. [19, 47]), but progress is then much harder and often relies on further moment-closure approximations.

The aim of our work is to introduce agent-to-agent heterogeneity into the SIR dynamics in a finite well-mixed population. This provides a middle ground between homogeneous well-mixed models and an explicitly networked population. At the same time, we maintain tractability and are able to characterise stochastic effects in finite populations via the linear-noise approximation. This allows us to systematically investigate the combination of parameter heterogeneity and demographic noise. We divide the population of agents into K different groups of susceptible individuals, where members of different groups have different susceptibilities. Similarly, in our model there are M classes of infective individuals, with each class representing a different propensity to pass on the disease. This follows the lines of [32], but we explicitly focus

on the combination of heterogeneity and intrinsic noise. Intrinsic stochasticity had not been included in [32].

Our paper is organised as follows: In Sec. 4.2 we describe our model in detail. As a baseline we then construct the deterministic rate equations in Sec. 4.3. They describe the deterministic dynamics in the limit of infinite populations, and are required to carry out the LNA. The most natural deterministic description will generally involve $K + M$ coupled non-linear equations (one for each subclass in the population). We discuss when and how these can be reduced to a smaller set of equations for aggregate quantities. In Sec. 4.4 we perform then the linear-noise approximation and use this approximation to characterise the fluctuations about deterministic fixed points. In particular we set up the theory to obtain the spectra of noise-driven quasi-cycles. Using this theory we then present our main results in Sec. 4.5, where we investigate in detail how the heterogeneity in the population affects the properties of stochastic outbreaks of the disease. Finally, in Sec. 4.6 we summarize our findings.

4.2 Model

We use an extension of the standard SIR model [48], in a population of fixed size N. Broadly, each individual can be of one of three types, susceptible (S), infective (I) or recovered (R). The spreading of the disease is described by infection events. These occur either through contact of a susceptible with an infective individual, as described below, or through spontaneous infection. Individuals recover at rate ρ, and they die at rate κ. The death rate is assumed to be independent of the disease status of an individual. To keep the number of individuals in the population constant, any death event is immediately followed by a birth of a new susceptible individual. This is of course an assumption, valid for large enough populations so that fluctuations in the overall size can be neglected. The assumption is mainly made for simplicity and is not uncommon (see e.g. [16, 49, 50]).

We introduce heterogeneity by dividing the groups of susceptibles and infectives into subclasses. We will write S_i and I_a for these, with $i = 1, \ldots, K$ and $a = 1, \ldots, M$. Individuals in subgroup S_i have susceptibility χ_i to the disease, and infectives in class I_a have infectiousness β_a, which describes the propensity of the infective to pass on the

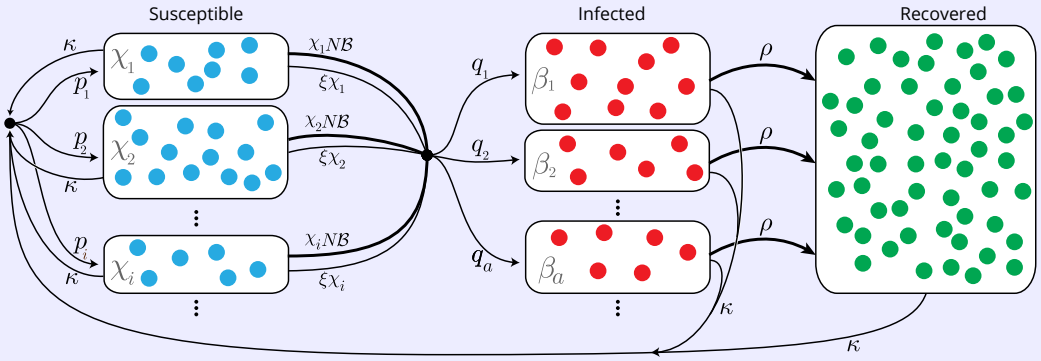

Figure 4.1: SIR model with heterogeneous susceptibility and infectivity. The diagram illustrates the different processes described by the model. New (susceptible) individuals are born at a rate κ, and they are assigned a susceptibility of χ_i with probability p_i. Susceptible individuals transition to an infected state either by spontaneous infection or by contact with any of the infected classes. The former process occurs with rate $\xi\chi_i$, if the susceptible is of type S_i. Conact infection occurs at a rate $\chi_i N\mathcal{B}$, where $N\mathcal{B}$ is the total infective power of the population (see Eq. (4.3)). Once infected, the individual is assigned an infectiousness β_a with probability q_a. All infected individuals recover at the same rate ρ. At any stage, individuals die with a rate κ. To keep the total population N constant, deceased individuals are immediately replaced by a new susceptible individual.

disease to susceptible individuals. We write n_i for the number of individuals of type S_i, and m_a for the number of individuals in class I_a.

The dynamics are illustrated in Fig. 4.1, and can be summarised in the following reaction scheme:

$$\begin{aligned}
\text{Spontaneous infection:} \quad & S_i \xrightarrow{\xi\chi_i q_a} I_a \\
\text{Infection by contact:} \quad & S_i + I_a \xrightarrow{\beta_a \chi_i q_b} I_a + I_b \\
\text{Recovery:} \quad & I_a \xrightarrow{\rho} R \\
\text{Birth/Death:} \quad & S_j \xrightarrow{p_i \kappa} S_i \\
& I_a \xrightarrow{p_i \kappa} S_i \\
& R \xrightarrow{p_i \kappa} S_i,
\end{aligned} \tag{4.1}$$

where $\{p_i\}$ and $\{q_a\}$ represent the probabilities of being assigned a susceptibility χ_i or infectiousness β_a at birth or upon infection, respectively. The first of these reactions describes spontaneous infection, converting an individual in class S_i into an individual of type I_a. The per-capita rate of events of this type is $\xi\chi_i q_a$, where ξ is an overall inverse time scale for spontaneous infection, χ_i is the susceptibility of S_i to the disease,

and q_a is the probability that the newly infected individual is in class I_a. Similarly, the second reaction describes infection of an individual of type S_i upon contact with an individual of type I_a. The newly infected individual is in class I_b. Events of this particular type occur with a rate proportional to β_a (the propensity of I_a to spread the disease), to χ_i (the susceptibility of S_i) and to q_b. The third reaction describes recovery, and the final three reactions are birth/death events. The newly born individual is assumed to be randomly placed into one of the classes S_i ($i = 1, \ldots, K$), occurring with respective probability p_i. We note that our model does not describe potential correlations between the susceptibility of an individual and its infectivity after they become infected; our focus is on heterogeneity of susceptibility due to physiological factors, and not primarily due to contact patterns. Extensions to include correlations can however be constructed among similar lines.

The model defines a continuous-time Markov process, and can be simulated straightforwardly using for example the celebrated Gillespie algorithm [51]. The starting point for the analytical study of the model is the master equation. Our analysis below will be based on approximating the solution to this master equation by performing a system-size expansion [46] and linear-noise approximation, leading to a stochastic differential equation describing the dynamics in the limit of large, but finite population size. In order to do this it is useful to first introduce

$$\overline{\chi} = \sum_i p_i \chi_i, \qquad \text{and} \qquad \mathfrak{X} = \frac{1}{N} \sum_i \chi_i n_i. \tag{4.2}$$

The quantity $\overline{\chi}$ is the mean susceptibility of a newly born individual, whereas $N\mathfrak{X}$ describes the aggregate susceptibility of the population. Similarly we define

$$\overline{\beta} = \sum_a q_a \beta_a \qquad \text{and} \qquad \mathcal{B} = \frac{1}{N} \sum_a \beta_a m_a, \tag{4.3}$$

where $\overline{\beta}$ represents the mean infectivity of a newly infected individual, and $N\mathcal{B}$ the total 'infective power' in the population. We note that $\overline{\chi}$ and $\overline{\beta}$ are fixed in time, and are properties of the distributions $\{p_i, \chi_i\}$ and $\{q_a, \beta_i\}$. The quantities $\mathfrak{X}$ and $\mathcal{B}$, on the other hand, are time-dependent and evolve as the composition of the population changes.

4.3 Deterministic analysis

4.3.1 Dynamics

In the limit of an infinite population the dynamics can be described by deterministic equations for the quantities $x_i = \lim_{N\to\infty} n_i/N$, $y_a = \lim_{N\to\infty} m_a/N$. They are given by

$$\begin{aligned} \dot{x}_i &= \kappa p_i - \kappa x_i - \xi\chi_i x_i - \chi_i x_i \mathcal{B}, \\ \dot{y}_a &= \xi q_a \mathfrak{X} + q_a \mathfrak{X}\mathcal{B} - \rho y_a - \kappa y_a. \end{aligned} \tag{4.4}$$

These ordinary differential equations can be derived either by using direct mass-action kinetics, or from the lowest-order expressions in an expansion of the master equation in the inverse system size [46].

Ultimately we will mostly be interested in aggregate quantities, i.e. the total density of susceptibles or infectives in the population, irrespective of what subclass they belong to. We therefore introduce

$$S = \sum_i x_i \qquad \text{and} \qquad I = \sum_a y_a. \tag{4.5}$$

From Eqs. (4.4) we find

$$\begin{aligned} \dot{S} &= \kappa - \kappa S - \xi\mathfrak{X} - \mathcal{B}\mathfrak{X}, \\ \dot{I} &= \xi\mathfrak{X} + \mathfrak{X}\mathcal{B} - \rho I - \kappa I. \end{aligned} \tag{4.6}$$

This system is not closed due to the presence of $\mathfrak{X}$ and $\mathcal{B}$ on the right-hand side. These quantities in turn evolve in time according to

$$\begin{aligned} \dot{\mathfrak{X}} &= \kappa\overline{\chi} - \kappa\mathfrak{X} - (\xi + \mathcal{B})\sum_i \chi_i^2 x_i, \\ \dot{\mathcal{B}} &= \xi\mathfrak{X}\overline{\beta} + \overline{\beta}\mathfrak{X}\mathcal{B} - (\rho + \kappa)\mathcal{B}, \end{aligned} \tag{4.7}$$

which again does not close the set of equations, due to the presence of the term $\mathfrak{X}_2(t) \equiv \sum_i \chi_i^2 x_i(t)$. Modulo normalisation and recalling that the $\{x_i\}$ are time-dependent, this object is recognised as the second moment of the distribution of susceptibilities among the group of susceptibles *at time t*. It cannot be determined from Eqs. (4.6) and (4.7) alone. Instead we find

$$\dot{\mathfrak{X}}_n = \kappa\overline{\chi^n} - \kappa\mathfrak{X}_n - (\xi + \mathcal{B})\mathfrak{X}_{n+1}, \tag{4.8}$$

where we have introduced $\overline{\chi^n} = \sum_i p_i \chi_i^n$ and $\mathfrak{X}_n = \sum_i x_i \chi_i^n$. This indicates that the deterministic dynamics at the aggregate level is described by an infinite hierarchy of equations. This set of equations does not close in the transient regime. However, as we will see next, closure can be achieved assuming the system settles down to a fixed point in the long run.

4.3.2 Fixed point

We proceed by a brief analysis of the fixed points of the deterministic dynamics. We will label these by a star. They can be obtained by setting $\dot{x}_i = 0$ and $\dot{y}_a = 0$ in Eqs. (4.4), leading to

$$\begin{aligned} x_i^\star &= \frac{\kappa p_i}{\kappa + (\xi + \mathcal{B}^\star)\,\chi_i}, \\ y_a^\star &= \frac{(\xi + \mathcal{B}^\star)\,\mathfrak{X}^\star q_a}{\rho + \kappa}. \end{aligned} \tag{4.9}$$

Similarly, we find the fixed points of the aggregate quantities S, I, $\mathfrak{X}$ and $\mathcal{B}$ from Eqs. (4.6,4.7). After re-arranging and using Eqs. (4.9) we arrive at

$$\begin{aligned} S^\star &= 1 - \frac{(\rho+\kappa)}{\kappa}\frac{\mathcal{B}^\star}{\overline{\beta}}, \\ I^\star &= \frac{\mathcal{B}^\star}{\overline{\beta}}, \\ \mathfrak{X}^\star &= \frac{(\rho+\kappa)}{(\xi+\mathcal{B}^\star)}\frac{\mathcal{B}^\star}{\overline{\beta}}, \\ \mathcal{B}^\star &= \frac{\overline{\beta}\kappa}{(\rho+\kappa)} \sum_i \left(\frac{\chi_i p_i}{\frac{\kappa}{\xi+\mathcal{B}^\star} + \chi_i} \right). \end{aligned} \tag{4.10}$$

which is a closed set of equations, for a given set of parameters $\{p_i, \chi_i, q_a, \beta_a\}$.

We highlight that while the transient dynamics of the system described in terms of the four macroscopic variables S, I, $\mathfrak{X}$ and $\mathcal{B}$ generates an infinite hierarchy of equations, potential fixed points can be uniquely described by a closed set of equations, assuming that the distribution of susceptibilities at birth and of the propensity of newly infected individuals to pass on the disease are known. In other words, the fixed point can be obtained in terms of the model parameters $\{q_a, \beta_a\}$ and $\{p_i, \chi_i\}$. While we cannot provide an analytical proof that the deterministic system will always converge to a fixed point, we note that, for the range of parameter used, we have not detected a single case in which numerically integrating Eqs. (4.4) did not lead to a fixed point. In

this context it is useful to point out that, in a homogeneous model, any combination of susceptibility and infectivity within the range of parameters used here would lead to a basic reproductive number above unity. For such models it is known that stable fixed points are eventually reached [52].

4.4 Linear-noise approximation

We now proceed to analyse the effects of stochasticity in the model, with a particular focus on the interaction between heterogeneity of individuals in the population and the noise induced by the demographics of the finite system.

We illustrate these effects in Fig. 4.2, and show an example of both the deterministic time-evolution of the system (thick continuous lines) and a realization of an individual-based simulation (thin dashed lines); the latter illustrates the intrinsic stochasticity of the process. Even after the deterministic model has reached a fixed point, the individual-based model shows sustained oscillations around it. These oscillations arise from a combination of complex eigenvalues of the underlying deterministic dynamics and the presence of intrinsic noise coming from the Poissonian jump process of the master equation. We will focus our attention on these stochasticity-driven periodic outbreaks in the remainder of this article, and build on the mathematical analysis via the linear-noise approximation [20]. In particular we will study how the heterogeneity in the population affects the properties of these cycles.

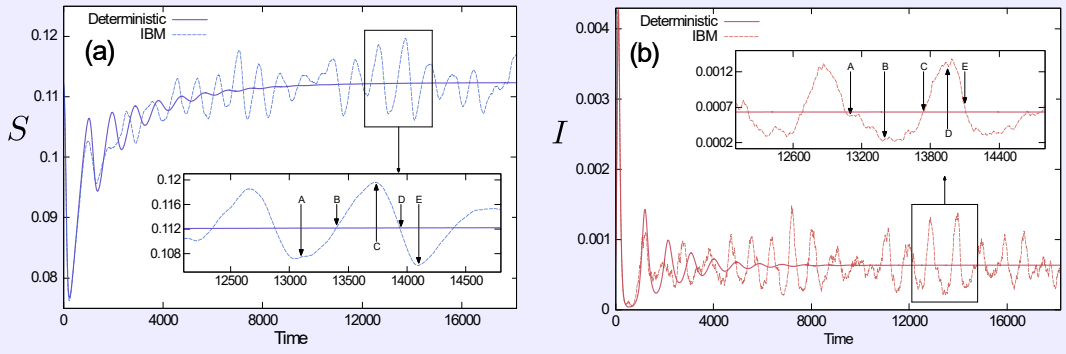

Figure 4.2: Population dynamics. Time series of the population density of total susceptible (panel **(a)**) and total infected individuals (panel **(b)**). Noise-sustained oscillations are clearly seen. The insets show a zoom in on the cycles. Labels $A, B, \ldots, E$ are for later purposes (see below).

4.4.1 Stochastic Dynamics

In order to carry out an analysis of the stochastic dynamics, we write $n_i/N = x_i + \tilde{x}_i/\sqrt{N}$, and $m_a/N = y_a + \tilde{y}_a/\sqrt{N}$, where $x_i(t)$ and $y_a(t)$ are the solutions of the deterministic equations (4.4) and the quantities with a tilde describe the stochastic fluctuations about the deterministic trajectory. The above ansatz reflects the anticipation that these fluctuatons will have a relative magnitude of order $N^{-1/2}$. We then carry out an expansion in the inverse system size up to and including sub-leading order [46]. In the fixed point regime of the deterministic dynamics we then arrive at

$$\begin{aligned}
\dot{\tilde{x}}_i &= -\kappa\tilde{x}_i - (\xi + \mathcal{B}^\star)\,\chi_i\tilde{x}_i - \chi_i x_i^\star\tilde{\mathcal{B}} + \eta_i, \\
\dot{\tilde{y}}_a &= q_a\left(\xi\tilde{\mathfrak{X}} + \tilde{\mathfrak{X}}\mathcal{B}^\star + \mathfrak{X}^\star\tilde{\mathcal{B}}\right) - (\rho+\kappa)\,\tilde{y}_a + \nu_a.
\end{aligned} \tag{4.11}$$

The linear-noise approximation also applies during transients. All objects on the right-hand side of Eqs. (4.11) then become time dependent. Since we ultimately focus on the oscillations about deterministic fixed point, we have not made this more explicit. The $\{\eta_i\}$ and $\{\nu_a\}$ are Gaussian white noise variables, with variance and co-variance (across components) as described in more detail in Section 4.7. Writing $\tilde{S} = \sum_i \tilde{x}_i$ and $\tilde{I} = \sum_a \tilde{y}_a$ we find the following dynamics of fluctuations at the aggregate level,

$$\begin{aligned}
\dot{\tilde{S}} &= -\kappa\tilde{S} - (\xi + \mathcal{B}^\star)\,\tilde{\mathfrak{X}} - \mathfrak{X}^\star\tilde{\mathcal{B}} + \sum_i \eta_i, \\
\dot{\tilde{I}} &= (\xi + \mathcal{B}^\star)\,\tilde{\mathfrak{X}} + \mathfrak{X}^\star\tilde{\mathcal{B}} - (\rho+\kappa)\tilde{I} + \sum_a \nu_a, \\
\dot{\tilde{\mathfrak{X}}} &= -\kappa\tilde{\mathfrak{X}} - \mathfrak{X}_2^\star\tilde{\mathcal{B}} - (\xi + \mathcal{B}^\star)\sum_i \chi_i^2\tilde{x}_i + \sum_i \chi_i\eta_i, \\
\dot{\tilde{\mathcal{B}}} &= (\xi + \mathcal{B}^\star)\,\overline{\beta}\tilde{\mathfrak{X}} + \overline{\beta}\mathfrak{X}^\star\tilde{\mathcal{B}} - (\rho+\kappa)\,\tilde{\mathcal{B}} + \sum_a \beta_a\nu_a.
\end{aligned} \tag{4.12}$$

As in the deterministic analysis, this set of equations is not closed. It describes the dynamics of fluctuations about the deterministic fixed point, but makes no assumption of stationarity of the fluctuations (for example correlation functions need not be time translation invariant). The lack of closure is due to the term $\sum_i \chi_i^2\tilde{x}_i$ in the equation for $\dot{\tilde{\mathfrak{X}}}$. However, as in Section 4.3.2, we will show below that a closed set of equations in the stationary state (of fluctuations) can be derived.

4.4.2 Fluctuation around the deterministic fixed point

We here show that although Eqs. (4.12) are not closed, we can explore noise-induced oscillations around the deterministic fixed point. To this end we introduce the Fourier transforms (with respect to time) of the variables $\tilde{x}_i$ and $\tilde{y}_a$. We will denote these by $\widehat{x}_i$ and $\widehat{y}_a$. From the Langevin equations (4.11) we find, after re-arranging,

$$\begin{aligned}\widehat{x}_i &= \frac{-\chi_i x_i^\star \widehat{\mathcal{B}} + \widehat{\eta}_i}{i\omega + \kappa + (\xi + \mathcal{B}^\star)\,\chi_i},\\ \widehat{y}_a &= \frac{\left[(\xi + \mathcal{B}^\star)\,\widehat{\mathfrak{X}} + \mathfrak{X}^\star \widehat{\mathcal{B}}\right] q_a + \widehat{\nu}_a}{i\omega + \rho + \kappa}.\end{aligned} \tag{4.13}$$

The noise variables $\{\eta_i\}$ and $\{\nu_a\}$ are uncorrelated in time, and their variance and correlation across components can be expressed in terms of known quantities (see Eqs. (4.24) in Section 4.7). The variable ω is the conjugate of time under Fourier transform. Similarly, we find the following for the relevant aggregate quantities,

$$\begin{aligned}\widehat{S} &= \frac{1}{i\omega + \kappa}\left[-\frac{i\omega + D}{\overline{\beta}}\widehat{\mathcal{B}} + \frac{1}{\overline{\beta}}\sum_a \beta_a \widehat{\nu}_a + \sum_i \widehat{\eta}_i\right],\\ \widehat{I} &= \frac{1}{i\omega + D}\left[\frac{i\omega + D}{\overline{\beta}}\widehat{\mathcal{B}} - \frac{1}{\overline{\beta}}\sum_a \beta_a \widehat{\nu}_a + \sum_a \widehat{\nu}_a\right],\\ \widehat{\mathfrak{X}} &= \frac{1}{\overline{\beta}C}\left[(i\omega + E)\,\widehat{\mathcal{B}} - \sum_a \beta_a \widehat{\nu}_a\right],\\ \widehat{\mathcal{B}} &= \frac{\overline{\beta}C\sum_i \frac{\chi_i \widehat{\eta}_i}{i\omega + A_i} + \sum_a \beta_a \widehat{\nu}_a}{i\omega + E + \overline{\beta}C\kappa\sum_i \frac{\chi_i^2 p_i}{A_i(i\omega + A_i)}},\end{aligned} \tag{4.14}$$

where, for simplicity, we have introduced the notation

$$\begin{aligned}A_i &= \kappa + (\xi + \mathcal{B}^\star)\,\chi_i,\\ C &= \xi + \mathcal{B}^\star,\\ D &= \rho + \kappa,\\ E &= \rho + \kappa - \overline{\beta}\mathfrak{X}^\star.\end{aligned} \tag{4.15}$$

Eqs. (4.14) constitute a closed set of equations for the Fourier transforms of the aggregate fluctuations $\tilde{S}, \tilde{I}, \tilde{\mathfrak{X}}$ and $\tilde{\mathcal{B}}$ in the stationary state. We thus make an observation similar to that in Section 4.3: although we cannot describe the evolution of fluctuations in the transient regime, we can derive a closed description of the statistics of fluctuations about deterministic fixed points within the linear-noise approximation.

4.4.3 Power Spectral Density

Eqs. (4.14) can be used describe the periodic cycles shown in Fig. 4.2; we will now proceed to analyse these in more detail. Specifically we will use the above results to compute the power spectral density (PSD) of fluctuations. This allows us to identify the characteristic frequency of noise-driven epidemic cycles, and to infer information about their amplitude.

The (average) power spectral density of a time series, $z(t)$, generated from the stochastic individual-based model is given by $\mathcal{P}_z(\omega) = \langle |\hat{z}(\omega)|^2 \rangle$, where $\langle \cdots \rangle$ stands for an average over realizations of the stochastic dynamics. The PSD can be computed analytically for all individual signals x_i, y_a, and for the aggregate variables S, I, $\mathfrak{X}$ and $\mathcal{B}$. The resulting expressions are lengthy; for completeness we provide them in Section 4.8. As an illustration we here show the PSD of $\mathcal{B}$,

$$\begin{aligned}\mathcal{P}_{\mathcal{B}}(\omega) =& \frac{2\mathfrak{X}^\star C}{|g|^2}\left(\overline{\beta^2} - \frac{\overline{\beta}^2 C\kappa}{D}\sum_i \frac{\chi_i p_i A_i}{\omega^2 + A_i^2}\right) \\ & - \frac{\left(\overline{\beta} C\kappa\right)^2}{|g|^2}\left[\sum_{i,j}\frac{p_i p_j \chi_i \chi_j (A_i + A_j)(\omega^2 + A_i A_j)}{A_i A_j (\omega^2 + A_i^2)(\omega^2 + A_j^2)}\right], \end{aligned} \tag{4.16}$$

with

$$|g|^2 = \left[E + \overline{\beta} C\kappa \sum_i \frac{\chi_i^2 p_i}{\omega^2 + A_i^2}\right]^2 + \omega^2 \left[1 - \overline{\beta} C\kappa \sum_i \frac{\chi_i^2 p_i}{A_i\,(\omega^2 + A_i^2)}\right]^2 . \tag{4.17}$$

As detailed in Section 4.8, the power spectra of S, I and $\mathfrak{X}$ can be expressed in terms of that of $\mathcal{B}$; many of the characteristics of the spectra of S, I and $\mathfrak{X}$ are shared with those of $\mathcal{B}$, or directly related to it. We note that the RHS of Eq. (4.16) is proportional to $1/|g|^2$, and the same is the case for the spectral densities of $\mathfrak{X}, S$ and I (see Eqs. (4.31) in Section 4.8); as a result, some of the key properties of the power spectra are determined by the behaviour of $|g|^2$, as discussed in more detail below.

4.4.4 Test Against Simulations

To illustrate the model and test our analytical results, we sampled possible heterogeneous populations. Specifically, the simulations shown in Fig. 4.3 are for populations with five susceptible and three infected subclasses. For each example, the probabilities $\{p_i\}$ and $\{q_a\}$ were drawn at random from a flat distribution over the simplexes $\sum_i p_i = 1$

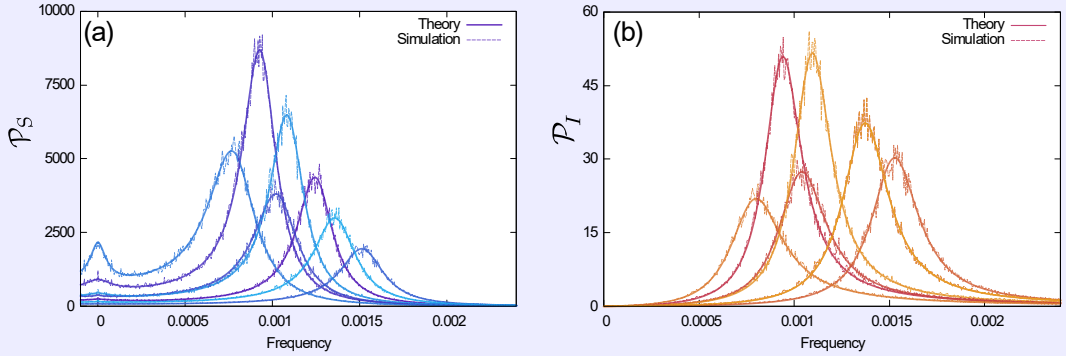

Figure 4.3: Power spectral densities of the fluctuations of **(a)** Susceptible and **(b)** Infected population for seven different examples of the model, generated as explained in more detail in the text. In all cases theory and simulations agree.

and $\sum_a q_a = 1$. Susceptibilities and infectivities were assigned randomly in the intervals $0.5 \leq \chi_i \leq 2.5$ and $0.3 \leq \beta_a \leq 1.3$. Simulations are for $N = 10^6$, and the rates for recovery, birth/death and immigration were set at $\rho = 0.07$, $\kappa = 5.5 \times 10^{-5}$ and $\xi = 5 \times 10^{-6}$ respectively. The rates β_a, ρ, κ and ξ have units of days^{-1}, whereas χ_i is dimensionless. The chosen rates are representative of childhood diseases such as whooping cough, measles, rubella or chickenpox [53]. The resulting PSDs are shown in Fig. 4.3. The continuous thick lines show the analytical result, and dashed lines are obtained from simulations, as an average over realizations of the individual-based model. As can be seen from the figure, the predictions of Eqs. (S10) precisely match the results from simulations. In all figures, axes labelled 'frequency' show $f = \omega/2\pi$, and have units of days^{-1}.

It is interesting to note that the power spectral density can remain non-zero at $\omega = 0$. A more detailed analysis reveals that its value is finite (i.e. not diverging); there is no evidence of e.g. a delta-peak at $\omega = 0$. This indicates that the area under the overall correlation function of fluctuations is non-zero, but finite, and there is no discernible shift of the overall stationary equilibrium (such a shift would result in a diverging contribution to the power spectrum at $\omega = 0$).

4.5 Consequences of Heterogeneity

Having established an analytical description of quasi-cycles, we now use this theory to identify which properties of the distribution of p_i, χ_i, q_a and β_a are most relevant for

the characteristics of stochastic quasi-cycles in heterogeneous populations. Specifically, we study how heterogeneity in the population affects the dominant frequency of quasi-cycles, their amplitude and the sharpness of the spectra. We will then also discuss if and how the different subgroups synchronise during the epidemic cycles.

4.5.1 Dominant Cycle Frequency

Numerical inspection of the different terms in the analytical solution of the PSDs suggests that the dominating element is the factor $1/|g|^2$, as briefly indicated in Sec. 4.4.3. The frequency for which $|g|^2$ reaches its minimum roughly corresponds to the dominant cycle frequency, ω_d, in the PSDs. The minimum of $|g|^2$ can be found by differentiation of the expression in Eq. (4.17). Assuming that $C\chi_i \gg \kappa$ we further approximate the location of this minimum. This assumption is valid if infection processes occur on a time scale which is much shorter than the life expectancy of an individual. Further, we assume that $\omega \gg A_i$, i.e. that a susceptible individual typically lives through several epidemic events before it becomes infected. Both approximations are intuitively plausible for childhood diseases, known to show periodic outbreaks [53]. Making these assumptions we find that the frequency for which $|g|^2$ is minimal can be approximated as

$$\omega_d \approx \sqrt{\kappa\overline{\chi}\overline{\beta}}. \tag{4.18}$$

This implies that the characteristic frequency is determined (mostly) by the mean susceptibility at birth and the mean infectivity at infection ($\overline{\chi}$ and $\overline{\beta}$) and the capacity of replenishment of the susceptible pool (κ).

The validity of our approach is confirmed in Fig. 4.4(a), where we test the approximation against simulations for a wide set of parameters. A perhaps more intuitive representation of our result can be found in Fig. 4.4(b), where we show the power spectra of several sample populations, each with different distributions of $\{p_i, \chi_i, q_a, \beta_a\}$, but all with the same first moments $\overline{\chi}$ and $\overline{\beta}$. As seen in the figure, this produces spectra of different amplitudes but with the same characteristic frequency. For comparison we include the homogeneous case $K = M = 1$.

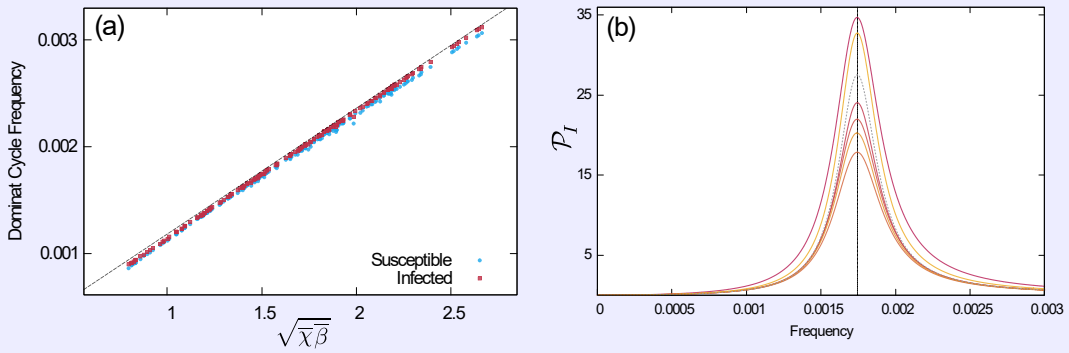

Figure 4.4: Verification of approximation (4.18) for the dominating frequency of cycles. **(a)** Frequency $f = \omega/2\pi$ at the maximum of the PSD, determined from Eqs. (S10) as a function of $\sqrt{\overline{\chi}\overline{\beta}}$, for fixed κ. The black dashed line corresponds to Eq. (4.18). Markers are from 200 different populations, each with 5 susceptible and 3 infected subgroups, and with random choices of $\{p_i, \chi_i, q_a, \beta_a\}$. The values of χ_i and β_a were chosen from the interval 1.7 ± 1.6999995; q_a and p_i from a flat distribution. This resulted in values of $\overline{\chi}$ and $\overline{\beta}$ in the range 0.3 to 3.3, and for $\overline{\chi^2}$ and $\overline{\beta^2}$ in the range 0.1 to 10. **(b)** PSD of the total infected population of different random distributions of $\{p_i, \chi_i, q_a, \beta_a\}$, with equal values for $\overline{\chi}$ and $\overline{\beta}$, but different values of $\overline{\chi^2}$ and $\overline{\beta^2}$. As a consequence of Eqs. (4.18) and (4.19), the characteristic frequency is the same for all such samples, but the height of the peak in the PSD varies considerably (the amplitude of the oscillations changes with the square root of the amplitude of the power spectra). The dashed grey line correspond to the homogeneous model, i.e. $K = M = 1$. The vertical dotted line is a visual aid.

4.5.2 Amplitude of Stochastic Cycles

While we have found above that the dominant frequency of stochastic cycles is largely determined by the first moments $\overline{\chi}$ and $\overline{\beta}$, the results shown in Fig. 4.4(b) demonstrate that this is not the case for the amplitude of the spectra at the dominant frequency. To investigate this further we evaluate the analytic expressions for the PSDs in Eqs. (S10) at the approximation of ω_d in Eq. (4.18). Making the same assumptions as in Section 4.5.1, we find that the height of the peak in the power spectra can be approximated as

$$\mathcal{P}_I(\omega_d) \approx \frac{2(\rho+\kappa)}{\left[\frac{(\rho+\kappa)\xi}{\mathcal{B}^\star} + \frac{\mathcal{B}^\star\overline{\chi^2}}{\overline{\chi}}\right]^2}\frac{\overline{\beta^2}}{\overline{\beta}^3},$$
$$\mathcal{P}_S(\omega_d) \approx \frac{(\rho+\kappa)^2}{\kappa\overline{\chi}\overline{\beta}}\mathcal{P}_I(\omega_d). \tag{4.19}$$

We note the presence of the second moments $\overline{\chi^2}$ and $\overline{\beta^2}$, unlike in Eq. (4.18). This indicates that the spread of susceptibilities and infectivities is relevant to the size of the fluctuations about the endemic equilibrium. We note that the case $K = M = 1$ in Fig.

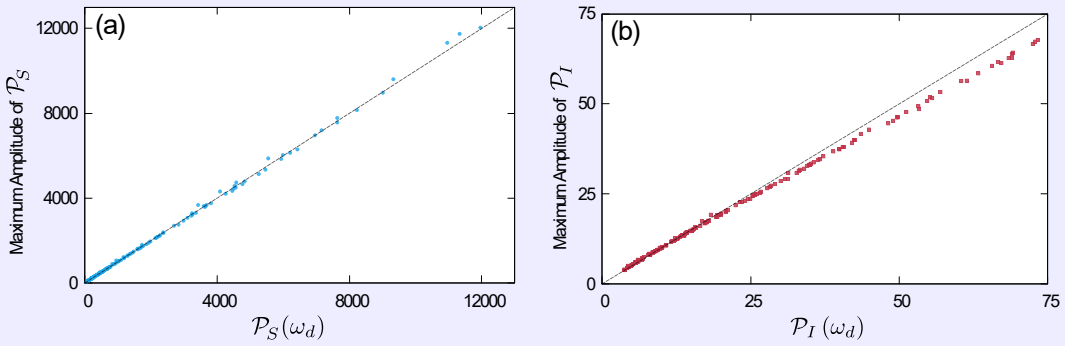

Figure 4.5: Verification of approximation (4.19) for the peak-height of the spectral densities. Horizontal axes show the prediction of Eqs. (4.19) for susceptibles **(a)**, and infectives **(b)**. On the vertical axis we show the height at the peak of the spectra, as determined numerically from Eqs. (4.31) in Section 4.8. Black dashed lines are the diagonal ('$y = x$'), and markers represent the populations described in Fig. 4.4.

4.4 (b) is special, as it leads to zero variance of the disorder by construction. We have experimented with the number of groups, K and M, and to a good approximation we find that the number of groups only affects the height and location of the peak in the spectrum through the mean and variance of the distributions of β and χ.

In Fig. 4.5 we plot results from the approximation in Eqs. (4.19) against the maximum amplitude of spectra obtained numerically from the full expression (within the LNA), see Eqs. (4.31) in Section 4.8. The data confirms that the approximation is valid for a wide range of parameters. While we find slight deviations at large amplitudes in the case of the infectives, the approximation is very robust for the susceptible population.

4.5.3 Sharpness of the Spectra

We now turn to the sharpness of the peak in the PSDs. The sharper the peak, the closer the stochastic outbreaks are to perfect cyclic behaviour. Conversely, cyclic behaviour is less distinct if the peak in the spectrum is shallow. This has been described before as the 'coherence' of the spectra [16]. As we will investigate a different notion of coherence in Sec. 4.5.4 and in order to avoid confusion, we will refer to the concentration of power near the peak of the spectrum as 'sharpness'.

Following [16], we define the sharpness as the relative spectral power accumulated

in an interval around the peak,

$$\mathbb{S} = \frac{\int_{\omega_d-\Delta\omega}^{\omega_d+\Delta\omega} \mathcal{P}(\omega)\, d\omega}{\int_{-\infty}^{+\infty} \mathcal{P}(\omega)\, d\omega}. \tag{4.20}$$

We compute the sharpness numerically, using the expressions in Eqs. (S10). In order to evaluate the denominator in Eq. (4.20) we integrate up to an upper cutoff of $\omega_{max} = \pi/100$ days^{-1}. In the numerator we use $\Delta\omega = 0.05\,\omega_{max}$. The choice of $\Delta\omega$ can be illustrated using Fig. 4.4(b), where the sharpness $\mathbb{S}$ of the peak roughly corresponds to the fraction of total power concentrated in the interval between frequencies of 0.0015 and 0.002 days^{-1}.

In Fig. 4.6 we show the sharpness of spectra for 200 random populations (as described in Fig 4.4). It is clear from the figure that there is a trend of increasing sharpness as the product of the mean susceptibility and infectivity at birth approaches unity (in the dimensions used here). The spread of the markers on the vertical axis indicates that there are significant effects of heterogeneity. It proves difficult, though, to find a functional dependence on higher moments of the distributions of susceptibilities and/or infectivities which would further collapse the data. While we do not show this data here in detail, we have also experimented with heterogeneity drawn from several distributions (e.g. flat, normal, Gamma). Results suggest that – to a good approximation – the functional shape of the spectra is determined by $\overline{\beta}, \overline{\chi}, \overline{\beta^2}$ and $\overline{\chi^2}$, i.e. by the first two moments of the heterogeneity. Higher-order features do

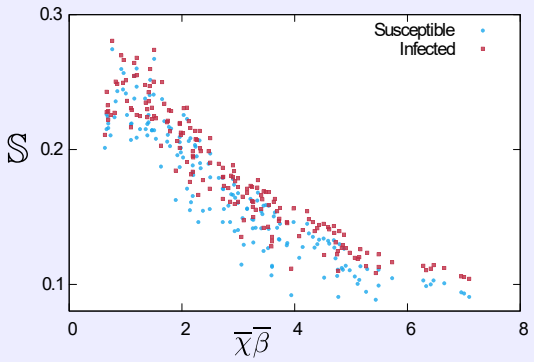

Figure 4.6: Sharpness of the power spectra as a function of the product of the mean susceptibilities and infectivities at birth/infection. Data is for the populations described in Fig. 4.4

not seem to play an important role. We have also tested the stronger property of full collapse upon re-scaling by peak height and location of peak, i.e. whether there is a scaling property of the type $\mathcal{P}(\omega) = P_{\max} \times f(\omega/\omega_d)$. This appears not to be the case.

4.5.4 Synchronization between Subgroups

We have established so far that introducing heterogeneity leads to significant changes in the quasi-cycles of the aggregate numbers of susceptible and infective individuals. However, we have not yet said much about the dynamics of the individual subgroups. In Fig. 4.7 we show the same example of sustained oscillations as in the inset of Fig. 4.2, but instead of the total susceptible and infected population we now highlight the time evolution of each of the subgroups.

In the upper two panels, (a) and (b), we show time series of the number of individuals in each subgroup normalised by the total population size. More specifically, we show susceptible subclasses (n_i/N) in panel (a), and infective subclasses (m_a/N) in panel (b). For each of these, stochastic oscillations can be observed. These cycles are pronounced for the case of the infective subgroups, panel (b), and more shallow for

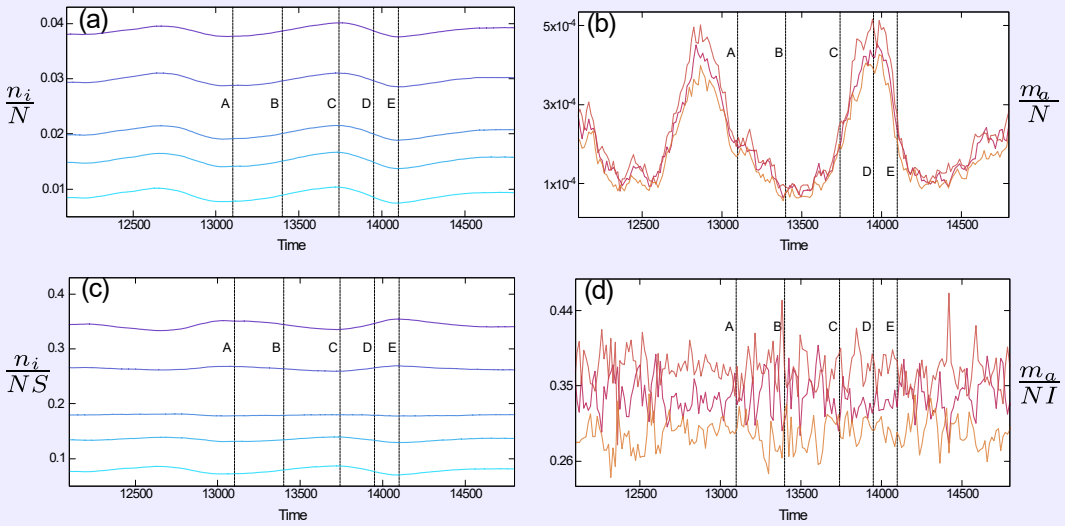

Figure 4.7: Stochastic cycles in subgroups of susceptibles and infectives. We show the same simulation run as in Fig. 4.2, but now split up into the different subgroups. Panels **(a)** and **(b)** show the number of individuals in each susceptible and infective subgroup normalised by the total population (N). In panels **(c)** and **(d)**, we show the number of individuals in each subgroup divided by the total number of susceptible or infected individuals, respectively (NS and NI). Lines labelled A to E refer to points in the cycles of the aggregate variables S, I shown in Fig. 4.2.

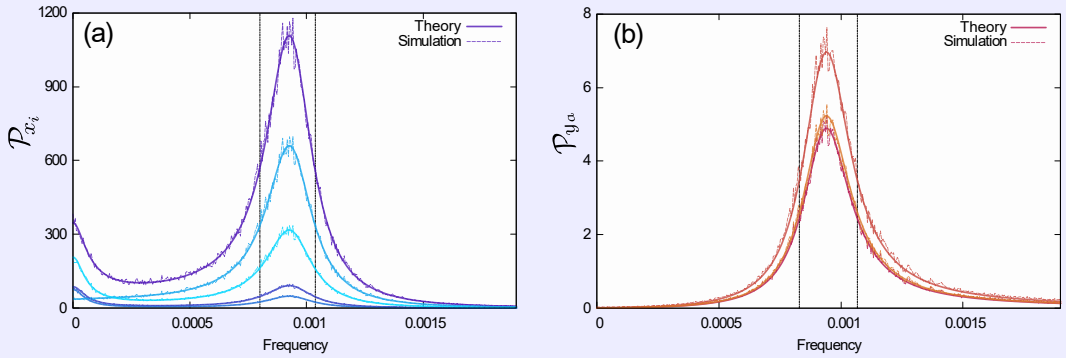

Figure 4.8: Power spectra of fluctuations for different subclasses of susceptibles and infectives. We use the same sample of the model parameters $\{\chi_i, p_i, \beta_a, q_a\}$ as in Fig. 4.3. Simulations are averaged over multiple realizations of the stochastic dynamics, at fixed model parameters. The vertical dotted lines are for later purposes and mark the locations at which the power spectra take values approximately equal to half the maximum amplitude.

the susceptibles, panel (a). This is to be expected, given that the total number of susceptibles is more than an order of magnitude larger than those of the infectives (see also Fig. 4.2). From Fig. 4.7 (a) and (b) it is clear that all subgroups undergo cycling of roughly the same frequency. This is confirmed by the power spectra in Fig. 4.8.

We note that these statements rely on expressing number of individuals in each class as a fraction of the total population, and not relative to the time-dependent total number of susceptibles or infectives respectively. We contrast the above with a representation in which we express the occupancy in each infective subgroup as a fraction of the infectives only, and similarly for the susceptibles. To this end we replot the simulation run shown in Fig. 4.7 (a) and (b), but now in terms of $n_i/(NS)$ and $m_a/(NI)$, respectively. The quantities $NS = \sum_j n_j$ and $NI = \sum_b m_b$ are the total number susceptible and infective individuals respectively, and they are time-dependent themselves. Results are shown in Fig. 4.7(c) and (d). Although the overall number of infectives, NI, undergoes the noise-driven cycles shown in Fig. 4.2, we find no discernible structure within the group of infectives; the time series $m_a/(NI)$ in Fig. 4.7(d) are essentially flat noisy lines. This is what one would expect, since the allocation to each subgroup, I_a, of infectives is random when an individual is newly infected, and the recovery rate is the same for all infective subgroups.

A more complex behaviour can be seen within the group of susceptibles. This group

as a whole undergoes stochastic cycles (see Fig. 4.2), but an interesting structure is observed within the group of susceptibles as well. The time series $n_i/(NS)$ in Fig. 4.7(c) show cyclic behaviour, and – to a good approximation – any pair of these time series is either in phase with each other, or they have a phase difference of $\pm\pi$. To explore the phase lag between the different time series we use the so-called complex coherence function [54]. This technique relies on computing the cross-spectrum $\left\langle \widehat{x}_i(\omega)\widehat{x}_j^*(\omega)\right\rangle$ between time series $x_i(t)$ and $x_j(t)$. The phase lag is then obtained as

$$\mathcal{L}_{x_i x_j}(\omega) = \tan^{-1}\frac{\mathrm{Im}\left\langle \widehat{x}_i(\omega)\widehat{x}_j^*(\omega)\right\rangle}{\mathrm{Re}\left\langle \widehat{x}_i(\omega)\widehat{x}_j^*(\omega)\right\rangle}. \tag{4.21}$$

We stress that the subscript * denotes complex conjugation, and is not to be confused with *, used earlier to indicate fixed points of the deterministic dynamics. Eq. (4.21) returns a phase lag for each spectral component, ω. Details can be found in Section 4.9.

The phase lag between the different groups of susceptible individuals is shown in Fig. 4.9. The data in panel (a) corresponds to Fig. 4.7 (a). More precisely, in Fig. 4.9 (a) we pick the time series n_1/N as a reference, and show the phase lag of all subgroups n_i/N with respect to this reference time series. We find that the phase lag for frequencies around the dominant frequency in the power spectra is small, consistent with Fig. 4.7 (a); all time series n_i/N oscillate (roughly) in phase with each other. In Fig. 4.9 (b) we repeat this procedure, but now taking the time series $n_i/(NS)$ as an input, corresponding to Fig. 4.7 (c). One then finds a rather different picture; the

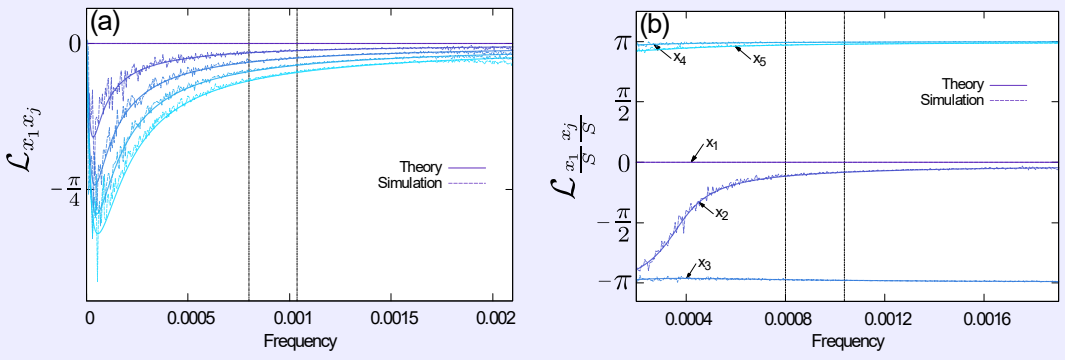

Figure 4.9: Phase-lag of time series between different subgroups of susceptibles. Data is for the same setup as in Fig. 4.7. We show the phase-lag between subgroups i and reference subgroup 1. Panel **(a)** depicts the case in which time series are normalized with respect to the total population, N; in panel **(b)** input time series are normalized with respect to the total number of susceptibles NS. As in Fig. 4.8, the vertical dotted lines mark the half-width of the peaks in the corresponding power spectra.

phase lag around the dominant frequency takes values either near zero, or close to $\pm\pi$. This indicates that the different classes of susceptible individuals fall into two groups. The time series in either group are in phase with each other, and in anti-phase with those in the respective other group. A closer inspection shows that these two groups are formed by the time series i with $x_i^\star < S^\star/K$ and with $x_i^\star > S^\star/K$ respectively. This behaviour in turn can be understood intuitively by revisiting Eqs. (4.9). Assuming $\kappa \ll (\xi + \mathcal{B}^\star)\chi_i$ for all i (a valid approximation for the cases analysed here), we find $x_i^\star \propto 1/\chi_i$, indicating that the more susceptible classes are less populated at the deterministic fixed point than the less susceptible ones. During the increasing leg of a stochastic cycle, we expect the number of newly infected individuals among class i to be proportional to $x_i^\star\chi_i$, suggesting that all susceptible classes are depleted in equal absolute numbers. This in turn means that subclasses with $x_i^\star > S^\star/K$ will represent an even larger fraction of the susceptible population as the total susceptible population decreases, while the subclasses with $x_i^\star < S^\star/K$ will represent a smaller fraction. This is what is observed in Fig. 4.7 (c).

4.6 Conclusions

In summary, we have explored the SIR model in finite populations, including demographic processes and allowed for agent-to-agent heterogeneity in both the susceptibility to a disease and the capacity to spread the disease. This system combines the effects of intrinsic demographic stochasticity (due to random infection, recovery and birth-death events), with quenched heterogeneity. The focus of our paper is to characterise the interplay between these two types of stochasticity, and to investigate how the heterogeneity between individuals affects quasi-cycles driven by intrinsic noise. Our analysis relies on the system-size expansion, which allows us to compute the properties of these cycles analytically in the linear-noise approximation.

Our principal results can be summarised as follows: (i) In the deterministic limit of infinite populations no closed set of equations for macroscopic quantities can be found in the transient regime. Fixed points for aggregate quantities of this deterministic dynamics can however be fully determined from a set of closed equations for the total susceptible ($S^\star$) and infected ($I^\star$) population, and weighted averages of the

susceptibility ($\mathfrak{X}^\star$) and infectivity ($\mathcal{B}^\star$). (ii) Similarly, the Langevin equations in the linear-noise approximation do not close easily at the aggregate level, but a closed set of equations for the spectra of fluctuations in $S, I, \mathfrak{X}$ and $\mathcal{B}$ about the deterministic fixed point can be found in the stationary state. These can be used to analytically describe the stochastic oscillations about the fixed point. (iii) Within reasonable assumptions, the characteristic frequency of the noise-driven oscillations is determined mostly by the mean susceptibility and infectivity at birth or infection ($\overline{\chi}$ and $\overline{\beta}$). However, the amplitude of the oscillations and the sharpness of peaks in the power spectra will generally depend on the higher moments of the distribution of susceptibilities and infectivities, in particular also on the agent-to-agent heterogeneity. (iv) Finally, the number of individuals in the different subclasses of infectives and susceptibles undergo stochastic cycles as well. If expressed in relation to the total population, these time series are synchronised and in phase. Normalized against the time-dependent total number of infectives, however, the different infective subclasses show no discernible oscillatory behaviour. Using a similar normalization within the susceptible population, we find that different subclasses are syncronized and either in phase with each other or have a phase difference of $\pm\pi$. These results are confirmed analytically. Regardless of the normalization, we find that the periodic outbreaks do not follow a hierarchical infection process, and all subgroups have similar absolute depletion/increase in absolute numbers. This is in contrast to what has been reported in single outbreak studies [38, 42]. However, it is important to note that in this existing work the outbreak is tracked in an initial transient period. Our results are valid after this period, at a deterministic fixed point, where the susceptible population is distributed in inverse proportion to their susceptibility (as explained above); this is a scenario different to the one studied in [38, 42].

We think our results can be relevant for future work in several ways. First, our work contributes to the ongoing discussion about when and how a model with heterogeneity can be replaced or approximated by a homogeneous model. In previous studies, heterogeneous models were compared to homogeneous models with susceptibility equivalent to the arithmetic [55] or harmonic mean [44] of the susceptibilities in the different groups. More recently, the focus has been placed on equivalent basic reproduction numbers (R_0) [56]. In the heterogeneous model this requires estimating R_0 based on, for example,

the outbreak size, and therefore the comparison is not straightforward. Here we have shown that all models within the class we have looked at and with equal values of $\overline{\chi}\overline{\beta}$ generate periodic outbreaks with the same dominating frequency. This characteristic frequency can be used to define a unique homogeneous model to which models of varying degrees of heterogeneity can be compared. Furthermore, the dependence of the spectra of oscillations on both the first and higher moments of the distribution of heterogeneity might provide an avenue towards estimating how heterogeneous a population is from the observation of epidemic cycles. Finally, the formalism we have developed is versatile and can be applied to study quasi-cycles in other areas in which heterogeneity might be relevant, for example in predator-prey dynamics or evolution [20, 22, 57–60]. Our findings indicate that the frequency of quasi-cycles can, to a good approximation, be obtained from the first moment of the distribution of heterogeneous agent properties, but that their amplitude depends on higher moments of the disorder. We expect similar behaviour in other heterogeneous systems with noise-driven cycles.

4.7 Appendix A: Linear-noise approximation

Carrying out the system-size expansion for the model with heterogeneity is tedious, but straightforward and follows the lines of [46]. The final outcome is the linear-noise approximation in Eqs. (4.11). The variables η_i and ν_a, represent Gaussian noise, with no correlation in time, but with potential correlation between the different noise variables at equal time. These noise variables can be decomposed as

$$\begin{aligned}\eta_i &= -\sum_a u_{ia} - \sum_{ab} v_{iab} - \sum_{k\neq i} x_{ik} + \sum_{k\neq i} x_{ki} + \sum_a y_{ai} + z_i,\\ \nu_a &= \sum_i u_{ia} + \sum_{ib} v_{iba} - w_a - \sum_i y_{ai},\end{aligned} \tag{4.22}$$

where, broadly speaking, each term on the right-hand side represents one possible type of event in the microscopic model. For example, u_{ia} relates to spontaneous infection of a susceptible individual of type S_i, resulting in a newly infective of type I_a. Similarly,

v_{iab} represents an event in which an individual of type S_i is infected by an individual of type I_a, and the newly infected is of type I_b. The variable w_a relates to a recovery event of an individual of type I_a, death of susceptible S_i and simultaneous birth of susceptible S_k is reflected by x_{ik}; death of an individual of type I_a and simultaenous birth of susceptible S_i is described by y_{ai}, and finally death of a recovered individual and simultaneous birth of susceptible S_i, by z_i. The signs on the right-hand-side in Eqs. (4.22) reflect the fact that each of these events may either increase or reduce the number of individuals of type S_i and I_a, respectively.

Each of the noise variables on the right-hand-side of Eqs. (4.22) are uncorrelated in time, and they have no cross-correlations. Within the LNA their variances are set by the corresponding reaction rates at the deterministic fixed point, i.e. we have

$$\begin{aligned}
\langle u_{ia}(t)u_{ia}(t')\rangle &= \xi\chi_i q_a x_i^\star \delta(t-t'),\\
\langle v_{iab}(t)v_{iab}(t')\rangle &= \beta_a\chi_i q_b x_i^\star I_a^\star \delta(t-t'),\\
\langle w_a(t)w_a(t')\rangle &= \rho I_a^\star \delta(t-t'),\\
\langle x_{ik}(t)x_{ik}(t')\rangle &= p_k\kappa x_i^\star \delta(t-t'),\\
\langle y_{ai}(t)y_{ai}(t')\rangle &= p_i\kappa I_a^\star \delta(t-t'),\\
\langle z_i(t)z_i(t')\rangle &= (1-S^\star-I^\star)\, p_i\kappa\delta(t-t').
\end{aligned} \tag{4.23}$$

Using the shorthand introduced in Eqs. (15), we then find

$$\begin{aligned}
\langle \eta_i(t)\eta_j(t')\rangle &= -\kappa^2\left(\frac{1}{A_i}+\frac{1}{A_j}\right)p_ip_j\delta(t-t'),\ \text{for } i\neq j,\\
\langle \eta_i(t)\eta_i(t')\rangle &= 2\kappa\left(1-\frac{\kappa p_i}{A_i}\right)p_i\delta(t-t'),\\
\langle \nu_a(t)\nu_b(t')\rangle &= 0,\ \text{for } a\neq b\\
\langle \nu_a(t)\nu_a(t')\rangle &= 2C\mathfrak{X}^\star q_a\delta(t-t'),\\
\langle \eta_i(t)\nu_a(t')\rangle &= -\kappa C\left(\frac{\chi_i}{A_i}+\frac{\mathfrak{X}^\star}{D}\right)p_iq_a\delta(t-t'),
\end{aligned} \tag{4.24}$$

which are needed for the computation of the PSDs.

4.8 Appendix B: Calculation of power spectra

We start from the result in Eqs. (4.14) in Section 4.4.2:

$$\begin{aligned}
\widehat{S}(\omega) &= \frac{1}{i\omega+\kappa}\left[-\frac{i\omega+D}{\overline{\beta}}\widehat{\mathcal{B}} + \frac{1}{\overline{\beta}}\sum_a \beta_a\widehat{\nu}_a + \sum_i \widehat{\eta}_i\right], \\
\widehat{I}(\omega) &= \frac{1}{i\omega+D}\left[\frac{i\omega+D}{\overline{\beta}}\widehat{\mathcal{B}} - \frac{1}{\overline{\beta}}\sum_a \beta_a\widehat{\nu}_a + \sum_a \widehat{\nu}_a\right], \\
\widehat{\mathfrak{X}}(\omega) &= \frac{1}{\overline{\beta}C}\left[(i\omega+E)\,\widehat{\mathcal{B}} - \sum_a \beta_a\widehat{\nu}_a\right], \\
\widehat{\mathcal{B}}(\omega) &= \frac{\overline{\beta}C\sum_i \frac{\chi_i\widehat{\eta}_i}{i\omega+A_i} + \sum_a \beta_a\widehat{\nu}_a}{i\omega+E+\overline{\beta}C\kappa\sum_i \frac{\chi_i^2 p_i}{A_i(i\omega+A_i)}}.
\end{aligned} \tag{4.25}$$

As an illustration let us now compute the power spectrum of $\widehat{\mathcal{B}}$. To keep equations manageable, we define

$$\begin{aligned}
f_i(\omega) &= \overline{\beta}C\frac{\chi_i}{(i\omega+A_i)}, \\
g(\omega) &= (i\omega+E) + \overline{\beta}C\kappa\sum_i \frac{\chi_i^2 p_i}{A_i\,(i\omega+A_i)},
\end{aligned} \tag{4.26}$$

and so we write the Fourier transform of $\tilde{\mathcal{B}}$ as

$$\widehat{\mathcal{B}}(\omega) = \frac{\sum_i f_i\widehat{\eta}_i + \sum_a \beta_a\widehat{\nu}_a}{g}, \tag{4.27}$$

where f_i, β_a, $\widehat{\eta}_i$ and $\widehat{\nu}_a$ are all functions of ω. We then find

$$\begin{aligned}
\mathcal{P}_{\mathcal{B}}(\omega) &= \left\langle\left(\frac{\sum_i f_i\widehat{\eta}_i + \sum_a \beta_a\widehat{\nu}_a}{g}\right)\left(\frac{\sum_i f_i^*\widehat{\eta}_i + \sum_a \beta_a\widehat{\nu}_a}{g^*}\right)\right\rangle \\
&= \frac{1}{|g|^2}\left(\sum_{i,j} f_i f_j^*\langle\widehat{\eta}_i\widehat{\eta}_j\rangle + \sum_{i,b} f_i\beta_b\langle\widehat{\eta}_i\widehat{\nu}_b\rangle + \sum_{a,j} f_j^*\beta_a\langle\widehat{\eta}_j\widehat{\nu}_a\rangle + \sum_{a,b}\beta_a\beta_b\langle\widehat{\nu}_a\widehat{\nu}_b\rangle\right) \\
&= \frac{1}{|g|^2}\left(\sum_i f_i f_i^*\langle\widehat{\eta}_i\widehat{\eta}_i\rangle + \sum_i\sum_{j\neq i} f_i f_j^*\langle\widehat{\eta}_i\widehat{\eta}_j\rangle\right. \\
&\qquad\left. + \sum_{i,b}(f_i+f_i^*)\beta_b\langle\widehat{\eta}_i\widehat{\nu}_b\rangle + \sum_a \beta_a^2\langle\widehat{\nu}_a\widehat{\nu}_a\rangle\right).
\end{aligned} \tag{4.28}$$

The notation $*$ denotes complex conjugation. Substituting the noise correlators from Eqs. (4.24),

$$\begin{aligned}
\mathcal{P}_{\mathcal{B}}(\omega) =& \frac{1}{|g|^2}\left(2\kappa\sum_i f_i f_i^* p_i - \kappa^2\sum_{i,j} f_i f_j^*\left(\frac{1}{A_i}+\frac{1}{A_j}\right)p_i p_j\right. \\
&\left. -\overline{\beta}\kappa C\sum_i (f_i+f_i^*)\left(\frac{\chi_i}{A_i}+\frac{\phi^\star}{D}\right)p_i + 2\overline{\beta^2}C\phi^\star\right),
\end{aligned} \tag{4.29}$$

and, using Eq. (4.27), we find

$$\mathcal{P}_{\mathcal{B}}(\omega) = \frac{2\phi^\star C}{|g|^2}\left(\overline{\beta^2} - \frac{\overline{\beta}^2 C\kappa}{D}\sum_i \frac{\chi_i p_i A_i}{\omega^2+A_i^2}\right) - \frac{\left(\overline{\beta}C\kappa\right)^2}{|g|^2}\sum_{i,j}\frac{\chi_i p_i \chi_j p_j\left(A_i+A_j\right)\left(\omega^2+A_iA_j\right)}{A_iA_j(\omega^2+A_i^2)(\omega^2+A_j^2)}, \tag{4.30}$$

which is the PSD of $\mathcal{B}$, as also reported in Eq. (4.16) in the main text.

Following the same process, we can compute the PSD for the remaining quantities, $\mathfrak{X}$, I and S. We do not report all details, but only the final results

$$\begin{aligned}\mathcal{P}_{\mathfrak{X}}(\omega) = {}& \frac{1}{\overline{\beta}^2 C}\left[2\overline{\beta^2}\mathfrak{X}^\star + \left(\omega^2+E^2\right)\left(\frac{\mathcal{P}_{\mathcal{B}}}{C} - \frac{4\overline{\beta^2}\mathfrak{X}^\star}{|g|^2}\right)\right] \\ & + \frac{2\kappa}{\overline{\beta}|g|^2}\sum_i \frac{\chi_i^2 p_i}{A_i\left(\omega^2+A_i^2\right)}\left[2\mathfrak{X}^\star\overline{\beta^2}\left(\omega^2 - EA_i\right) + \overline{\beta}A_i\left(\frac{A_i\mathfrak{X}^\star}{D\chi_i}+1\right)\left(\omega^2+E^2\right)\right] \\ & + \frac{2\overline{\beta}C\kappa^2}{|g|^2}\sum_{i,j}\frac{\chi_i^2 p_i \chi_j^2 p_j\left[E\left(\omega^2+A_iA_j\right)+\omega^2\left(A_j-A_i\right)\right]}{A_iA_j\left(\omega^2+A_i^2\right)\left(\omega^2+A_j^2\right)}\left(\frac{A_i\mathfrak{X}^\star}{D\chi_i}+1\right),\end{aligned}$$

$$\begin{aligned}\mathcal{P}_I(\omega) = {}& \frac{\mathcal{P}_{\mathcal{B}}}{\overline{\beta}^2} + \frac{4C\mathfrak{X}^\star\left(\overline{\beta}^2 - \overline{\beta^2}\right)\left(DE+\omega^2\right)}{|g|^2\overline{\beta}^2\left(\omega^2+D^2\right)} \\ & + \frac{4\kappa C^2\mathfrak{X}^\star\left(\overline{\beta}^2-\overline{\beta^2}\right)}{\left(|g|^2\right)\left(\omega^2+D^2\right)\left(\overline{\beta}\right)}\sum_i\frac{\chi_i^2 p_i\left(DA_i-\omega^2\right)}{A_i\left(\omega^2+A_i^2\right)},\end{aligned}$$

$$\begin{aligned}\mathcal{P}_S(\omega) = {}& \frac{1}{\omega^2+\kappa^2}\left[\left(\frac{\omega^2+D^2}{\overline{\beta}^2}\right)\mathcal{P}_{\mathcal{B}} + 2\kappa\left(1-\kappa\sum_i\frac{p_i}{A_i}\right) - C\kappa\left(\frac{\mathfrak{X}^\star}{D}+\sum_i\frac{\chi_i p_i}{A_i}\right)\right] \\ & + \frac{2C}{|g|^2\left(\omega^2+\kappa^2\right)}\left[-\frac{2\mathfrak{X}^\star\overline{\beta^2}}{\overline{\beta}^2} + \kappa\left(\frac{\mathfrak{X}^\star}{D}+\sum_i\frac{\chi_i p_i}{A_i}\right)\right] \\ & \qquad \left[DE+\omega^2 - \frac{|g|^2}{2} + \overline{\beta}C\kappa\sum_j\frac{\chi_j^2 p_j\left(DA_j-\omega^2\right)}{A_j\left(\omega^2+A_j^2\right)}\right] \\ & + \frac{2C\kappa}{|g|^2\left(\omega^2+\kappa^2\right)}\sum_i\frac{\chi_i p_i}{A_i\left(\omega^2+A_i^2\right)}\left[C\left(\frac{A_i\mathfrak{X}^\star}{D}+\chi_i\right) - 2A_i\right. \\ & \qquad \left.+\kappa\left(1+A_i\sum_k\frac{p_k}{A_k}\right)\right]\left\{A_iDE + \omega^2\left(A_i+E-D\right)\right. \\ & \qquad \left.+\overline{\beta}C\kappa\sum_j\frac{\chi_j^2 p_j\left[D\left(A_iA_j+\omega^2\right)+\omega^2\left(A_j-A_i\right)\right]}{A_j\left(\omega^2+A_j^2\right)}\right\}.\end{aligned} \tag{4.31}$$

The power spectra of fluctuations for the individual subgroups of infectives and susceptibles are found as

$$\begin{aligned}\mathcal{P}_{x_i}(\omega) =& \frac{1}{\omega^2+A_i^2}\left[\left(\frac{\kappa\chi_i p_i}{A_i}\right)^2 \mathcal{P}_{\mathcal{B}} + 2\kappa\left(1-\frac{\kappa p_i}{A_i}\right)p_i\right] \\ &+ \frac{2\overline{\beta}C\kappa^2\chi_i p_i^2}{|g|^2 A_i\left(\omega^2+A_i^2\right)}\left(E+\sum_k \frac{\overline{\beta}C\kappa\chi_k^2 p_k}{\omega^2+A_k^2}\right) \\ &\qquad \left[\frac{\mathfrak{X}^\star}{D}+\frac{\chi_i\left(\omega^2-A_i^2\right)}{A_i\left(\omega^2+A_i^2\right)}+\frac{\kappa}{A_i}\sum_j \frac{\chi_j p_j\left(A_i+A_j\right)}{\omega^2+A_j^2}\right] \\ &+ \frac{2\overline{\beta}C\kappa^2\chi_i p_i^2\omega^2}{|g|^2 A_i\left(\omega^2+A_i^2\right)}\left(1-\sum_k \frac{\overline{\beta}C\kappa\chi_k^2 p_k}{A_k\left(\omega^2+A_k^2\right)}\right) \\ &\qquad \left[\frac{2\chi_i}{\omega^2+A_i^2}-\frac{\kappa}{A_i}\sum_j \frac{\chi_j p_j\left(A_i+A_j\right)}{A_j\left(\omega^2+A_j^2\right)}\right], \end{aligned} \tag{4.32}$$

$$\mathcal{P}_{y_a}(\omega) = q_a^2\mathcal{P}_I + \frac{2C\mathfrak{X}^\star q_a\left(1-q_a\right)}{\omega^2+D^2}. \tag{4.33}$$

4.9 Appendix C: Phase Lag

In order to explore the the phase lag we use the so-called complex coherence function, $\mathcal{CCF}_{ij}$, between subgroups i and j, defined as

$$\mathcal{CCF}_{ij}(\omega) = \frac{\left\langle \widehat{x}_i\widehat{x}_j^*\right\rangle}{\sqrt{\left\langle \widehat{x}_i\widehat{x}_i^*\right\rangle\left\langle \widehat{x}_j\widehat{x}_j^*\right\rangle}} = \frac{\mathcal{P}_{x_ix_j}}{\sqrt{\mathcal{P}_{x_i}\mathcal{P}_{x_j}}}, \tag{4.34}$$

where $\widehat{x}_i$ and $\mathcal{P}$ are functions of ω.

For $i \neq j$ this is in general a complex-valued function (of ω). The argument of $\mathcal{CCF}_{ij}$, given by

$$\mathfrak{L}_{x_ix_j}(\omega) = \tan^{-1}\frac{\text{Im }\mathcal{CCF}_{ij}(\omega)}{\text{Re }\mathcal{CCF}_{ij}(\omega)} = \tan^{-1}\frac{\text{Im }\mathcal{P}_{x_ix_j}(\omega)}{\text{Re }\mathcal{P}_{x_ix_j}(\omega)}, \tag{4.35}$$

is known as the phase spectrum; it describes the phase-lag between the time series $x_i(t)$ and $x_j(t)$ [61].

The cross spectra of the population in the susceptible classes normalized with respect to the total population ($x_i = n_i/N$) is given by

$$\mathcal{P}_{x_ix_j}(\omega) = \left\langle \widehat{x}_i\widehat{x}_j^*\right\rangle = \left\langle\left(\frac{-\chi_i x_i^\star\widehat{\mathcal{B}}+\widehat{\eta}_i}{i\omega+A_i}\right)\left(\frac{-\chi_j x_j^\star\widehat{\mathcal{B}}^*+\widehat{\eta}_j}{-i\omega+A_j}\right)\right\rangle. \tag{4.36}$$

This can be written as

$$\mathcal{P}_{x_i x_j}(\omega) = \frac{(\omega^2 + A_i A_j)\,\mathcal{W}_{ij} - \omega\,(A_i - A_j)\,\mathcal{U}_{ij}}{(\omega^2 + A_i^2)\left(\omega^2 + A_j^2\right)} + i\,\frac{(\omega^2 + A_i A_j)\,\mathcal{U}_{ij} + \omega\,(A_i - A_j)\,\mathcal{W}_{ij}}{(\omega^2 + A_i^2)\left(\omega^2 + A_j^2\right)}, \tag{4.37}$$

where we introduced the notation

$$\begin{aligned}\mathcal{U}_{ij}(\omega) &= \chi_j x_j^\star \mathrm{Im}\left\langle \widehat{\eta}_i \widehat{\mathcal{B}} \right\rangle - \chi_i x_i^\star \mathrm{Im}\left\langle \widehat{\eta}_j \widehat{\mathcal{B}} \right\rangle, \\ \mathcal{W}_{ij}(\omega) &= \left(\chi_i \chi_j x_i^\star x_j^\star\right)\mathcal{P}_{\mathcal{B}} + \langle \widehat{\eta}_i \widehat{\eta}_j \rangle - \chi_j x_j^\star \mathrm{Re}\left\langle \widehat{\eta}_i \widehat{\mathcal{B}} \right\rangle - \chi_i x_i^\star \mathrm{Re}\left\langle \widehat{\eta}_j \widehat{\mathcal{B}} \right\rangle.\end{aligned} \tag{4.38}$$

From these we obtain the phase lag as

$$\mathfrak{L}_{x_i x_j}(\omega) = \tan^{-1}\,\frac{\omega\,(A_i - A_j)\,\mathcal{W}_{ij} + (\omega^2 + A_i A_j)\,\mathcal{U}_{ij}}{(\omega^2 + A_i A_j)\,\mathcal{W}_{ij} - \omega\,(A_i - A_j)\,\mathcal{U}_{ij}}, \tag{4.39}$$

which yields the theoretical lines in Fig. 4.9a.

To explore the phase lag between the susceptible subgroups when normalized by the total susceptible population ($x_i' = n_i/NS$), we first need to compute the cross-spectra of the renormalized signals $\mathcal{P}_{x_i' x_j'}(\omega)$. As in Section 4.4.1, we start from the ansatz

$$\frac{n_i}{NS} = x_i' + \frac{1}{\sqrt{N}}\tilde{x}_i'. \tag{4.40}$$

We then have

$$\frac{n_i}{NS} = \frac{n_i/N}{S} = \frac{x_i + \frac{1}{\sqrt{N}}\tilde{x}_i}{S + \frac{1}{\sqrt{N}}\tilde{S}} \equiv x_i' + \frac{1}{\sqrt{N}}\tilde{x}_i', \tag{4.41}$$

and so (after expanding in $1/\sqrt{N}$)

$$\tilde{x}_i' = \frac{S^\star\,\tilde{x}_i - x_i^\star\,\tilde{S}}{(S^\star)^2}. \tag{4.42}$$

In Fourier space this turns into

$$\widehat{x}_i' = \frac{S^\star\,\widehat{x}_i - x_i^\star\,\widehat{S}}{(S^\star)^2}. \tag{4.43}$$

For the cross spectra we then find

$$\mathcal{P}_{x_i' x_j'}(\omega) = \left\langle \widehat{x}_i' \widehat{x}_j'^{*} \right\rangle = \left\langle \frac{\left(S^\star \widehat{x}_i - x_i^\star \widehat{S}\right)\left(S^\star \widehat{x}_j^* - x_j^\star\,\widehat{S}^*\right)}{(S^\star)^4} \right\rangle, \tag{4.44}$$

which can be rewritten as

$$\mathcal{P}_{x_i' x_j'}(\omega) = \frac{1}{(S^\star)^3}\left(S^\star \mathrm{Re}\left[\mathcal{P}_{x_i x_j}\right] + \frac{\kappa^2 p_i p_j}{S^\star A_i A_j}\mathcal{P}_S - \frac{Y_{ij\,R} + Y_{ji\,R}}{\overline{\beta}\,(\omega^2 + \kappa^2)}\right) + \frac{i}{(S^\star)^3}\left(S^\star \mathrm{Im}\left[\mathcal{P}_{x_i x_j}\right] - \frac{Y_{ij\,I} - Y_{ji\,I}}{\overline{\beta}\,(\omega^2 + \kappa^2)}\right). \tag{4.45}$$

We have introduced the notation $Y_{ij\,R} = \mathrm{Re}\left[Y_{ij}\right]$ and $Y_{ij\,I} = \mathrm{Im}\left[Y_{ij}\right]$ with

$$\begin{aligned} Y_{ij}(\omega) =& \frac{\left(\omega^2 + i\omega\left(\kappa - A_j\right) + \kappa A_j\right)\kappa p_i}{\left(\omega^2 + A_j^2\right)A_i}\left\{\frac{\kappa\chi_j p_j}{A_j}\left(D\mathcal{P}_{\mathcal{B}} - \sum_a \beta_a \mathrm{Re}\left\langle\widehat{\nu}_a\widehat{\mathcal{B}}\right\rangle\right.\right. \\ & \left. -\overline{\beta}\sum_k \mathrm{Re}\left\langle\widehat{\eta_k}\widehat{\mathcal{B}}\right\rangle\right)\omega\mathrm{Im}\left\langle\widehat{\eta}_j\widehat{\mathcal{B}}\right\rangle - D\mathrm{Re}\left\langle\widehat{\eta}_j\widehat{\mathcal{B}}\right\rangle \\ & \left.\left. -\kappa\overline{\beta}p_j\left[C\left(\frac{\chi_j}{A_j} + \frac{\mathfrak{X}^\star}{D}\right) - 2 + \frac{\kappa}{A_j} + \kappa\sum_k\left(\frac{p_k}{A_k}\right)\right]\right\} \\ & + i\frac{\left[\omega^2 + i\omega\left(\kappa - A_j\right) + \kappa A_j\right]\kappa p_i}{\left(\omega^2 + A_j^2\right)A_i} \\ & \left[\frac{\kappa\chi_j p_j}{A_j}\left(\omega\mathcal{P}_{\mathcal{B}} + \sum_a \beta_a \mathrm{Im}\left\langle\widehat{\nu}_a\widehat{\mathcal{B}}\right\rangle + \overline{\beta}\sum_k \mathrm{Im}\left\langle\widehat{\eta_k}\widehat{\mathcal{B}}\right\rangle\right)\right. \\ & \left. -\omega\mathrm{Re}\left\langle\widehat{\eta}_j\widehat{\mathcal{B}}\right\rangle - D\,\mathrm{Im}\left\langle\widehat{\eta}_j\widehat{\mathcal{B}}\right\rangle\right]. \end{aligned} \tag{4.46}$$

From these, we can find the phase-lag as

$$\mathfrak{L}_{x_i' x_j'}(\omega) = \tan^{-1}\ \frac{S^\star \mathrm{Im}\left[\mathcal{P}_{x_i x_j}\right] - \frac{Y_{ij\,I} - Y_{ji\,I}}{\overline{\beta}(\omega^2+\kappa^2)}}{S^\star \mathrm{Re}\left[\mathcal{P}_{x_i x_j}\right] + \frac{\kappa^2 p_i p_j}{S^\star A_i A_j}\mathcal{P}_S - \frac{Y_{ij\,R} + Y_{ji\,R}}{\overline{\beta}(\omega^2+\kappa^2)}}. \tag{4.47}$$

This expression was used to obtain the analytical predictions shown in Fig. 4.9b.

4.10 Appendix D: Table of Symbols

		Meaning	Defined in Eqs.
Symbols	N	Total population size.	
	K	Number of susceptible subgroups.	
	M	Number of infective subgroups.	
	S_i	Susceptible subgroup i.	
	I_a	Infective subgroup a.	
	n_i	Number of individuals of type S_i.	
	m_a	Number of individuals in class I_a.	
	p_i	Probability of being assigned a susceptibility χ_i at birth.	
	q_a	Probability of being assigned an infectiousness β_a upon infection.	
	χ_i	Susceptibility of subgroup i.	
	β_a	Infectiousness of subgroup a.	
	ρ	Recovery rate.	
	κ	Death/birth rate.	
	ξ	Spontaneous infection rate.	
	$\overline{\chi}$	Mean susceptibility at birth.	(2)
	$\mathfrak{X}$	Aggregate susceptibility of the population.	(2)
	$\overline{\beta}$	Mean infectiousness upon infection.	(3)
	$\mathcal{B}$	Total 'infective power' in the population.	(3)
	x_i	Fraction of susceptible individuals in subgroup i in the limit of infinite system size.	
	y_a	Fraction of infected individuals in subgroup a in the limit of infinite system size.	
	S	Total density of susceptible individuals in the population.	(5)
	I	Total density of infective individuals in the population.	(5)
	$\mathfrak{X}_n$	Nth moment of the aggregate susceptibility.	
	$\overline{\chi^n}$	Nth moment of susceptibilities at birth.	
	A_i, C, D, E	Notation introduced to simplify equations.	(15)
	$\mathcal{P}_z$	Power spectral density of z.	(16)
	g	Notation introduced to simplify equations.	(17)
	ω_d	Dominant cycle frequency.	(18)
	$\overline{\beta^2}$	Second moment of the infectiousness assigned upon infection.	(19)
	$\mathbb{S}$	Sharpness of the PSD.	(20)
	$\mathcal{L}_{z_1 z_2}$	Phase lag between signals z_1 and z_2.	(21)

		Meaning	Defined in Eqs.
Accents	$\overline{\chi}$	Expected value at birth or upon infection.	(2), (3)
	$\dot{x}$	Deterministic evolution (time derivative).	(4), (6), (7)
	$x^\star$	Deterministic fixed point.	(9), (10)
	$\tilde{x}$	Stochastic fluctuations about the deterministic fixed point.	(11), (12)
	$\widehat{x}$	Fourier transform with respect to time.	(13), (14)
	x^*	Complex conjugate.	

Bibliography

[1] Murray, James D. (2002), *Mathematical biology*, 3rd ed., vol. 17, Interdisciplinary Applied Mathematics, Springer-Verlag, Berlin Heidelberg, DOI: 10.1007/b98868.

[2] Wilkinson, Darren J. (2011), *Stochastic Modelling for Systems Biology*, 2nd ed., CRC Press, Boca Raton.

[3] Goel, Narendra S. and Nira Richter-Dyn (1974), *Stochastic Models in Biology*, Academic Press, New York, NY.

[4] Andersson, Håkan and Tom Britton (2000), *Stochastic epidemic models and their statistical analysis*, vol. 151, Lecture Notes in Statistics, Springer New York, New York, NY, DOI: 10.1007/978-1-4612-1158-7.

[5] Elowitz, Michael B. (2002), 'Stochastic gene expression in a single cell', *Science* **297** (5584):1183–1186, DOI: 10.1126/science.1070919.

[6] Paulsson, Johan (2004), 'Summing up the noise in gene networks.', *Nature* **427** (6973):415–8, DOI: 10.1038/nature02257.

[7] Moreno, Yamir, Romualdo Pastor-Satorras and Alessandro Vespignani (2002), 'Epidemic outbreaks in complex heterogeneous networks', *The European Physical Journal B* **26** (4):521–529, DOI: 10.1007/s10051-002-8996-y.

[8] Raj, Arjun and Alexander van Oudenaarden (2008), 'Nature, nurture, or chance: Stochastic gene expression and its consequences', *Cell* **135** (2):216–226, DOI: 10.1016/j.cell.2008.09.050.

[9] Lafuerza, Luis F. and Raúl Toral (2013), 'On the effect of heterogeneity in stochastic interacting-particle systems', *Scientific Reports* **3** (1):1189, DOI: 10.1038/srep01189.

[10] Bauch, Chris T. et al. (2005), 'Dynamically Modeling SARS and Other Newly Emerging Respiratory Illnesses', *Epidemiology* **16** (6):791–801, DOI: 10.1097/01.ede.0000181633.80269.4c.

[11] Smith, David L. et al. (2005), 'The entomological inoculation rate and Plasmodium falciparum infection in African children', *Nature* **438** (7067):492–495, DOI: 10.1038/nature04024.

[12] Heldt, Frank S. et al. (2015), 'Single-cell analysis and stochastic modelling unveil large cell-to-cell variability in influenza A virus infection', *Nature Communications* **6**:8938, DOI: 10.1038/ncomms9938.

[13] Scott, Matthew, Brian Ingalls and Mads Kærn (2006), 'Estimations of intrinsic and extrinsic noise in models of nonlinear genetic networks', *Chaos: An Interdisciplinary Journal of Nonlinear Science* **16** (2):026107, DOI: 10.1063/1.2211787.

[14] Swain, Peter S., Michael B. Elowitz and Eric D. Siggia (2002), 'Intrinsic and extrinsic contributions to stochasticity in gene expression', *Proceedings of the National Academy of Sciences* **99** (20):12795–12800, DOI: 10.1073/pnas.162041399.

[15] Hilfinger, Andreas and Johan Paulsson (2011), 'Separating intrinsic from extrinsic fluctuations in dynamic biological systems', *Proceedings of the National Academy of Sciences* **108** (29):12167–12172, DOI: 10.1073/pnas.1018832108.

[16] Alonso, David, Alan J. McKane and Mercedes Pascual (2007), 'Stochastic amplification in epidemics', *Journal of The Royal Society Interface* **4** (14):575–582, DOI: 10.1098/rsif.2006.0192.

[17] Olsen, Lars F. and William M. Schaffer (1990), 'Chaos versus noisy periodicity: alternative hypotheses for childhood epidemics', *Science* **249** (4968):499–504, DOI: 10.1126/science.2382131.

[18] Black, Andrew J. et al. (2009), 'Stochastic fluctuations in the susceptible-infective-recovered model with distributed infectious periods', *Physical Review E* **80** (2):021922, DOI: 10.1103/PhysRevE.80.021922.

[19] Rozhnova, Ganna and Ana Nunes (2009a), 'Fluctuations and oscillations in a simple epidemic model', *Physical Review E* **79** (4):041922, DOI: 10.1103/PhysRevE.79.041922.

[20] McKane, Alan J. and Timothy J. Newman (2005), 'Predator-prey cycles from resonant amplification of demographic stochasticity', *Physical Review Letters* **94** (21):1–4, DOI: 10.1103/PhysRevLett.94.218102.

[21] Bjørnstad, Ottar N. and Bryan T. Grenfell (2001), 'Noisy clockwork: time series analysis of population fluctuations in animals.', *Science* **293** (5530):638–643, DOI: 10.1126/science.1062226.

[22] Bladon, Alex J., Tobias Galla and Alan J. McKane (2010), 'Evolutionary dynamics, intrinsic noise, and cycles of cooperation', *Physical Review E* **81** (6):1–14, DOI: 10.1103/PhysRevE.81.066122.

[23] Samoilov, Michael, Sergey Plyasunov and Adam P. Arkin (2005), 'Stochastic amplification and signaling in enzymatic futile cycles through noise-induced bistability with oscillations', *Proceedings of the National Academy of Sciences* **102** (7):2310–2315, DOI: 10.1073/pnas.0406841102.

[24] Bolker, Benjamin M. and Bryan T. Grenfell (1993), 'Chaos and biological complexity in measles dynamics', *Proceedings of the Royal Society B: Biological Sciences* **251** (1330):75–81, DOI: 10.1098/rspb.1993.0011.

[25] Schenzle, Dieter (1984), 'An age-structured model of pre- and post-vaccination measles transmission', *Mathematical Medicine and Biology* **1** (2):169–191, DOI: 10.1093/imammb/1.2.169.

[26] Earn, David J. D. et al. (2000), 'A simple model for complex dynamical transitions in epidemics', *Science* **287** (5453):667–670, DOI: 10.1126/science.287.5453.667.

[27] Stone, Lewi, Ronen Olinky and Amit Huppert (2007), 'Seasonal dynamics of recurrent epidemics', *Nature* **446** (7135):533–536, DOI: 10.1038/nature05638.

[28] Diekmann, Odo, Johan A. P. Heesterbeek and Johan A. J. Metz (1990), 'On the definition and the computation of the basic reproduction ratio R 0 in models for infectious diseases

in heterogeneous populations', *Journal of Mathematical Biology* **28** (4):365–382, DOI: 10.1007/BF00178324.

[29] Hethcote, Herbert W. and James W. Van Ark (1987), 'Epidemiological models for heterogeneous populations: proportionate mixing, parameter estimation, and immunization programs', *Mathematical Biosciences* **84** (1):85–118, DOI: 10.1016/0025-5564(87)90044-7.

[30] Nold, Annett (1980), 'Heterogeneity in disease-transmission modeling', *Mathematical Biosciences* **52** (3-4):227–240, DOI: 10.1016/0025-5564(80)90069-3.

[31] Hickson, Roslyn I. and Mick G. Roberts (2014), 'How population heterogeneity in susceptibility and infectivity influences epidemic dynamics', *Journal of Theoretical Biology* **350**:70–80, DOI: 10.1016/j.jtbi.2014.01.014.

[32] Novozhilov, Artem S. (2012), 'Epidemiological models with parametric heterogeneity: Deterministic theory for closed populations', *Mathematical Modelling of Natural Phenomena* **7** (3):147–167, DOI: 10.1051/mmnp/20127310.

[33] Keeling, Matthew J. (1999), 'The effects of local spatial structure on epidemiological invasions', *Proceedings of the Royal Society B: Biological Sciences* **266** (1421):859–867, DOI: 10.1098/rspb.1999.0716.

[34] Rohani, Pejman (1999), 'Opposite patterns of synchrony in sympatric disease metapopulations', *Science* **286** (5441):968–971, DOI: 10.1126/science.286.5441.968.

[35] Hagenaars, Thomas J., Christl A. Donnelly and Neil M. Ferguson (2004), 'Spatial heterogeneity and the persistence of infectious diseases', *Journal of Theoretical Biology* **229** (3):349–359, DOI: 10.1016/j.jtbi.2004.04.002.

[36] Yu, Jiajia, Daqing Jiang and Ningzhong Shi (2009), 'Global stability of two-group SIR model with random perturbation', *Journal of Mathematical Analysis and Applications* **360** (1):235–244, DOI: 10.1016/j.jmaa.2009.06.050.

[37] Colizza, Vittoria et al. (2006), 'The role of the airline transportation network in the prediction and predictability of global epidemics', *Proceedings of the National Academy of Sciences* **103** (7):2015–2020, DOI: 10.1073/pnas.0510525103.

[38] Barthélemy, Marc et al. (2004), 'Velocity and hierarchical spread of epidemic outbreaks in scale-free networks', *Physical Review Letters* **92** (17):178701–1, DOI: 10.1103/PhysRevLett.92.178701.

[39] Keeling, Matthew J. (2005), 'The implications of network structure for epidemic dynamics', *Theoretical Population Biology* **67** (1):1–8, DOI: 10.1016/j.tpb.2004.08.002.

[40] Hufnagel, Lars, Dirk Brockmann and Theo Geisel (2004), 'Forecast and control of epidemics in a globalized world', *Proceedings of the National Academy of Sciences* **101** (42):15124–15129, DOI: 10.1073/pnas.0308344101.

[41] Holme, Petter (2015), 'Information content of contact-pattern representations and predictability of epidemic outbreaks', *Scientific Reports* **5** (1):14462, DOI: 10.1038/srep14462.

[42] Barthélemy, Marc et al. (2005), 'Dynamical patterns of epidemic outbreaks in complex heterogeneous networks', *Journal of Theoretical Biology* **235** (2):275–288, DOI: 10.1016/j.jtbi.2005.01.011.

[43] Boylan, Ross D. (1991), 'A note on epidemics in heterogeneous populations', *Mathematical Biosciences* **105** (1):133–137, DOI: 10.1016/0025-5564(91)90052-K.

[44] Andersson, Håkan and Tom Britton (1998), 'Heterogeneity in epidemic models and its effect on the spread of infection', *Journal of Applied Probability* **35** (3):651–661, DOI: 10.1239/jap/1032265213.

[45] Gardiner, Crispin W. (2003), *Handbook of stochastic methods*, 3rd ed., Springer, Berlin Heidelberg.

[46] Kampen, Nico G. van (1992), *Stochastic processes in physics and chemistry*, 3rd ed., Elsevier, Amsterdam.

[47] Rozhnova, Ganna and Ana Nunes (2009b), 'Cluster approximations for infection dynamics on random networks', *Physical Review E* **80** (5):051915, DOI: 10.1103/PhysRevE.80.051915.

[48] Kermack, William O. and Anderson G. McKendrick (1927), 'A contribution to the mathematical theory of epidemics', *Proceedings of the Royal Society A: Mathematical, Physical and Engineering Sciences* **115** (772):700–721, DOI: 10.1098/rspa.1927.0118.

[49] Britton, Tom and Philip D. O'Neill (2002), 'Bayesian Inference for Stochastic Epidemics in Populations with Random Social Structure', *Scandinavian Journal of Statistics* **29** (3):375–390, DOI: 10.1111/1467-9469.00296.

[50] Shulgin, Boris, Lewi Stone and Zvia Agur (1998), 'Pulse vaccination strategy in the SIR epidemic model.', *Bulletin of mathematical biology* **60** (6):1123–1148, DOI: 10.1016/S0092-8240(98)90005-2.

[51] Gillespie, Daniel T. (1977), 'Exact stochastic simulation of coupled chemical reactions', *The Journal of Physical Chemistry* **81** (25):2340–2361, DOI: 10.1021/j100540a008.

[52] Keeling, Matthew J. and Pejman Rohani (2008), *Modeling Infectious Diseases in Humans and Animals*, Princeton University Press, Princeton, NJ.

[53] Anderson, Roy M. and Robert M. May (1992), *Infectious diseases of humans: Dynamics and control*, Oxford University Press, Oxford.

[54] Stoica, Petre and Randolph Moses (2004), *Spectral analysis of signals*, Pearson Prentice Hall, Upper Saddle River.

[55] Ball, Frank (1985), 'Deterministic and stochastic epidemics with several kinds of susceptibles', *Advances in Applied Probability* **17** (1):1, DOI: 10.2307/1427049.

[56] Yates, Andrew, Rustom Antia and Roland R. Regoes (2006), 'How do pathogen evolution and host heterogeneity interact in disease emergence?', *Proceedings of the Royal Society B: Biological Sciences* **273** (1605):3075–3083, DOI: 10.1098/rspb.2006.3681.

[57] Butler, Thomas and Nigel Goldenfeld (2009), 'Robust ecological pattern formation induced by demographic noise', *Physical Review E* **80** (3):030902, DOI: 10.1103/PhysRevE.80.030902.

[58] Black, Andrew J. and Alan J. McKane (2012), 'Stochastic formulation of ecological models and their applications', *Trends in Ecology & Evolution* **27** (6):337–345, DOI: 10.1016/j.tree.2012.01.014.

[59] Cremer, Jonas, Tobias Reichenbach and Erwin Frey (2008), 'Anomalous finite-size effects in the Battle of the Sexes', *The European Physical Journal B* **63** (3):373–380, DOI: 10.1140/epjb/e2008-00036-x.

[60] Mobilia, Mauro (2010), 'Oscillatory dynamics in rock–paper–scissors games with mutations', *Journal of Theoretical Biology* **264** (1):1–10, DOI: 10.1016/j.jtbi.2010.01.008.

[61] Rozhnova, Ganna, Ana Nunes and Alan J. McKane (2012), 'Phase lag in epidemics on a network of cities', *Physical Review E* **85** (5), DOI: 10.1103/PhysRevE.85.051912.

Chapter 5

Consensus and diversity in multi-state noisy voter models

Preface

The contents of this chapter constitute a manuscript submitted to Physical Review E, also available in ArXiv[1]. The manuscript was authored by Francisco Herrerías-Azcué[2] and Tobias Galla[2].

F.H.A.'s contributions include the inception of the project, performing all calculations and analysis, coding simulations, producing the data for all figures, finalising all figures, and writing all sections of the paper alongside T.G.

We note that the recent MPhys Reports by Miguel Borrero Ridaura and Babik Dobel-Ober (2018, at the University of Manchester) contain preliminary work that inspired the model used here. All parts of this chapter are original work by F.H.A and T.G.. In particular, we develop techniques to characterize the multi-state noisy voter model analytically.

[1] F. Herrerías-Azcué and T. Galla, (2019), "Consensus and diversity in multi-state noisy voter models", *arXiv preprint*:1903.09198.

[2] Theoretical Physics, School of Physics and Astronomy, The University of Manchester, Manchester, M13 9PL, United Kingdom.

Abstract

We study a variant of the voter model with multiple opinions; individuals can imitate each other and also change their opinion randomly in mutation events. We focus on the case of a population with all-to-all interaction. A noise-driven transition between regimes with multi-modal and unimodal stationary distributions is observed. In the former, the population is mostly in consensus states; in the latter opinions are mixed. We derive an effective death-birth process, describing the dynamics from the perspective of one of the opinions, and use it to analytically compute marginals of the stationary distribution. These calculations are exact for models with homogeneous imitation and mutation rates, and an approximation if rates are heterogeneous. Our approach can be used to characterize the noise-driven transition and to obtain mean switching times between consensus states.

5.1 Introduction

The Voter Model (VM) was initially introduced as a model for spatial conflict [1, 2]. In its most basic variant, the model describes a population of voters with pairwise interactions. Each individual can be in one of two states. In an interaction, one individual copies the state of another. If the population is finite, this process continues until all individuals have reached the same state; no further dynamics are then possible.

This model has been studied in the context of different applications. For example, variants of the VM have been used to describe autocatalytic reactions [3], herding in financial markets [4], opinion dynamics [5], and the evolution of language [5, 6]. In the context of biological evolution, the VM is closely related to the Moran process with neutral selection [7]. In each of these applications the states an individual can take represent different properties. They can be opinions on a given issue, trading behaviors in a model of a financial market, or different species in a biological context.

Although the models used in these applications share common characteristics, different research communities have focused on different aspects of the VM and its applications. For the purpose of opinion dynamics, for example, one may be interested in whether or not a population of agents reaches consensus and, if they do, how long

this takes. In economics one may ask how copying of trading behaviour leads to herding, and in the context of linguistics one might be interested in understanding how features of languages spread and organise in space [8]. Applications of the VM include the use to model actual elections [9].

The VM is also of interest from a point of view of statistical mechanics. The model is similar to spin models in traditional statistical physics, except that it is defined dynamically and not through an energy function. As such, the VM has become one of the most studied models of non-equilibrium statistical physics. The two-state VM in two dimensions has been shown to exhibit logarithmic coarsening [10]. This is in contrast for example with Glauber dynamics for the Ising model, in which coarsening is driven by surface tension and growth laws are algebraic. Multi-state voter models, on the other hand, can show algebraic coarsening [11]. The traditional VM presents an interesting class of dynamics, with two absorbing states and $\mathbb{Z}_2$-symmetry. It has been shown to define its own universality class [10, 12], and field theories have been devised to study its critical point [13]. A further aspect attracting attention in the physics community has been the coupled dynamics of the voter model and interaction networks between agents. Such co-evolutionary processes have, been shown to lead to fragmentation transitions [14, 15], enriching the number and nature of the absorbing states of the VM.

One interesting variant in the class of voter dynamics is the so-called 'noisy voter model' [7]. The terminology might at first sound surprising – the process of opinion changes through interaction in the original VM is already stochastic. However, it allows for absorbing states, in which no further dynamics can occur.

What is meant by the term 'noisy' in this context is that, in addition to the interaction with other individuals, random changes of opinion can occur; they do not require interaction with another agent, and are sometimes also described as 'mutations'. These random changes drive the system away from consensus; there are no absorbing states.

As a consequence, two effects compete in the noisy voter model: a drive towards consensus through interaction, and spontaneous opinion changes promoting coexistence. This leads to a transition between a regime in which the system is mostly ordered (i.e., all agents are of the same opinion), and another regime in which both opinions are

represented in the system. This phenomenon is known as 'noise-induced bistability' and has been investigated in the context of autocatalytic reactions, surface-reaction models, decision making of insects, and biochemical reactions [16–22]. Recently, transitions of this type have also been studied in noisy voter models on complex networks [23–25].

Most of the existing work on models of this type focuses on the case in which individuals can take two different states; the transition is then between a phase in which the stationary distribution of individuals is unimodal and another in which it is bimodal; hence the term 'noise-induced bistability'.

The aim of the present work is to generalise the model to the case of multiple opinion states. In the absence of mutation there are then multiple absorbing states. As we demonstrate, the inclusion of spontaneous state changes leads to noise-induced multi-stability. We investigate this numerically and analytically. To do this, we compute marginals of the stationary distribution of the model, as well as switching times between the different consensus states. Our analysis focuses on the case of a 'mean-field' geometry, that is, a population in which all pairs of individuals can interact at all times.

The remainder of the paper is organized as follows. In Sec. 5.2 we define the model and introduce the general notation. In Sec. 5.3 we derive an effective master equation for the dynamics of a single species and use it to describe marginals of the stationary distribution of the multi-species model; closed-form analytical expressions are obtained. This approach is exact if all species have the same imitation and mutation rates, and an approximation otherwise. We also estimate switching times between different consensus states. Sec. 5.4 focuses on the model with homogeneous imitation and mutation rates. We obtain analytical predictions for its phase diagram and test these predictions against simulations. In Sec. 5.5 we carry out a similar analysis for a multi-state model with heterogeneous rates. Sec. 5.6 contains a discussion of our results and an outlook on future work.

5.2 Definition of the model and noise-induced multi-stability

5.2.1 Model definition and notation

We consider a population of N individuals; each can be of one of m types ($m \in \mathbb{N}$). In the context of social dynamics these would represent different opinions; in evolutionary biology they may stand for different species. Our aim is not to study a specific application, but the general structure that emerges from multi-state noisy voter models; we will therefore use the terms opinions, species and types interchangeably.

The population is unstructured, that is, any individual can interact with any other member of the population at all times. We write n_i for the number of individuals of species i, where $i \in \{1, \dots, m\}$; these variables vary as the population evolves. At each time the state of the system is fully specified by the vector $\mathbf{n} = (n_1, \dots, n_m)$. The size of the population is constant, i.e., we have $\sum_{i=1}^{m} n_i = N$ at all times; the state space is a simplex in m-dimensions.

The dynamics of the model are defined by the following imitation and mutation reactions:

$$\begin{aligned} X_i + X_j &\xrightarrow{r_{ji}} 2X_i \\ X_j &\xrightarrow{\epsilon_{ji}} X_i. \end{aligned} \tag{5.1}$$

The notation X_i represents an individual of species i, and the first reaction describes the process in which an individual of opinion j imitates an individual of opinion i. We write r_{ji} for the corresponding imitation rate; the exact interpretation of these coefficients will be made more precise below in Eq. (5.3). In the context of evolutionary dynamics reactions of this type represent a death-birth event: an individual of type j dies, and is replaced by the offspring of an individual of species i. This offspring is also of type i. To keep the model general, we allow this rate to depend on both species involved, j and i.

The second reaction in Eq. (5.1) describes spontaneous changes of opinion, i.e., an individual of type j turns into an individual of type i. The rate with which this process occurs is ε_{ji}, where we again include possible dependence on j and i. In the context of population dynamics it may be more realistic to incorporate mutation in

the reproduction events; that is, one could consider models in which the offspring of an individual does not necessarily belong to the same species as the parent. The effect of both ways of introducing random state changes is similar though: they allow departure from states in which the entire population is made up of individuals of one single species. We will refer to instances of the second process in Eq. (5.1) as 'mutation events'.

The dynamics are defined in continuous time, and can be described by the master equation

$$\partial_t P(\mathbf{n}, t) = \sum_{i=1}^{m} \sum_{j=1}^{m} \left(\mathcal{E}_i^{-1} \mathcal{E}_j - 1 \right) \left[T_{j \to i}(\mathbf{n}) P(\mathbf{n}, t) \right], \tag{5.2}$$

where $P(\mathbf{n}, t)$ is the probability of finding the population in state $\mathbf{n}$ at time t. We have written $\mathcal{E}_i$ for the creation operator for individuals of species i; it is defined by its action $\mathcal{E}_i f(n_1, \ldots, n_i, \ldots, n_m) = f(n_1, \ldots, n_i + 1, \ldots, n_m)$ on functions $f(\mathbf{n})$ of the state of the population. The quantity $T_{j \to i}(\mathbf{n})$ is the rate with which individuals of type j are converted into individuals of type i if the system is currently in state $\mathbf{n}$; these rates are given by

$$T_{j \to i}(\mathbf{n}) = r_{ji} \frac{n_i n_j}{N} + \epsilon_{ji} n_j. \tag{5.3}$$

We note that this is the overall rate for such events in the population, and not a per capita rate. As it is common practice, the scaling with the population size, N, is such that $T_{j \to i} = \mathcal{O}(N)$. This ensures that $\mathcal{O}(N)$ events occur per unit time; in other words, time is measured in generations, rather than individual events.

Among the states of the population there are states of complete consensus, in the language of opinion dynamics. This is the case when $n_i = N$ for one opinion i, and $n_j = 0$ for all $j \neq i$. In the context of evolutionary dynamics these are monomorphic states; one species has taken over the entire population. These consensus states are not absorbing when mutation rates ε_{ji} are non-zero. As we will discuss next, it is the interplay between imitation, mutation and the associated intrinsic noise that generates the interesting behaviour of the model.

5.2.2 Noise-induced multistability

Simulations of the model can be carried out efficiently using the standard Gillespie algorithm [26, 27]. Different types of outcomes are illustrated in Fig. 5.1. We show the

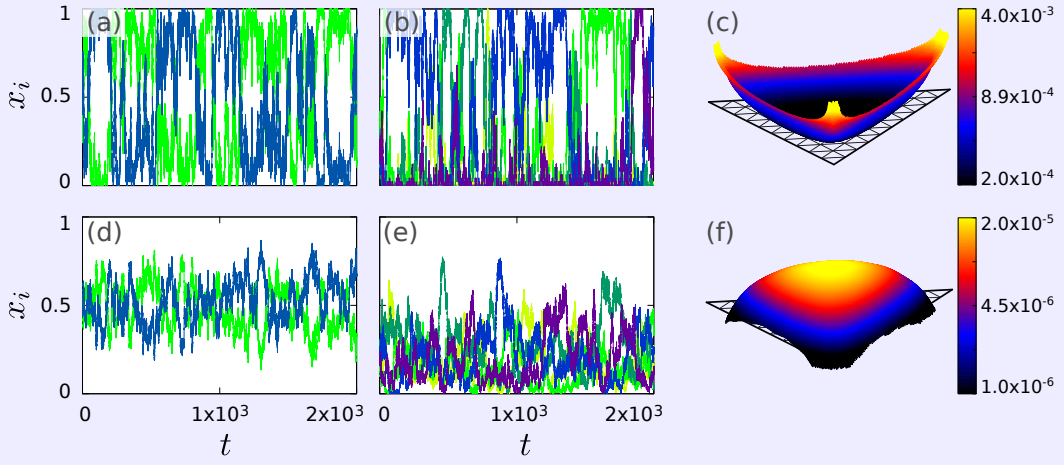

Figure 5.1: Sample trajectories and stationary distribution. Panels (a), (b), (d) and (e) show single realizations of the model dynamics; the distributions in panels (c) and (f) are from an average over many realizations. Panels (a) and (d) are for $m = 2$; (b) and (e) for $m = 5$; (c) and (f) for $m = 3$. The upper panels (a)–(c) are for a population size of $N = 50$; the system is frequently in states of full consensus. In the lower panels (d)–(f) $N = 500$, and diversity of opinions is observed; states of consensus are rarely visited. The imitation and mutation rates are uniform across species; we use $r = 1$ and $\varepsilon = 10^{-2}/(m-1)$.

time evolution of the fraction of individuals in each species, $x_i = n_i/N$, in individual simulations of models with $m = 2$ and $m = 5$ species. In panels (a)–(c) the population is of size $N = 50$, and the population is seen to visit states of complete consensus relatively frequently. These are not permanent; instead, the population switches between different consensus states. In panels (d)–(f) the population size is $N = 500$. Consensus may occasionally be reached, but other than that the system is mostly found in states of diversity, where different opinions are represented at fluctuating frequencies. Panels (c) and (f) show the multi-modal and unimodal stationary distributions for a model with $m = 3$.

5.3 Reduction to effective single-opinion dynamics

We proceed to characterise the multi-state noisy VM analytically. To do this, we first derive an effective death-birth process for the individuals of a particular species. We then study the shape of the stationary distribution resulting from these effective dynamics. We also use the single-species dynamics to obtain information about typical switching times between consensus states.

5.3.1 Effective single-species master equation

We focus on a particular species i and the dynamics of the number of individuals n_i of this species. Events in the population dynamics convert individuals of one species into individuals of another. Many of these events will not involve species i, and are therefore not relevant for the effective dynamics of species i. In the following, we only consider events which either increase or decrease n_i.

The overall rate with which individuals are converted to species i is

$$T_i^+(\mathbf{n}) \equiv \sum_{j\neq i} T_{j\to i}(\mathbf{n}), \tag{5.4}$$

where $T_{j\to i}(\mathbf{n})$ is the conversion rate from j to i, as defined in Eq. (5.3). Similarly, the rate with which individuals of species i are converted into any other type is

$$T_i^-(\mathbf{n}) \equiv \sum_{j\neq i} T_{i\to j}(\mathbf{n}). \tag{5.5}$$

We note that these rates are in general not specified by n_i alone; instead they depend on the entire state vector $\mathbf{n}$. The rates in Eqs. (5.4) and (5.5) by themselves, therefore, do not describe a well-defined stochastic process for species i.

Inserting the definitions from Eq. (5.3) into the expressions in Eqs. (5.4) and (5.5), one finds

$$\begin{aligned} T_i^+(\mathbf{n}) &= \sum_{j\neq i}\left(r_{ji}\frac{n_i n_j}{N} + \varepsilon_{ji} n_j\right), \\ T_i^-(\mathbf{n}) &= \sum_{j\neq i}\left(r_{ij}\frac{n_i n_j}{N} + \varepsilon_{ij} n_i\right). \end{aligned} \tag{5.6}$$

Our analysis in following sections is based on the assumption that we can formulate a closed death-birth process for species i, with birth and death rates $T_i^{\pm}(n_i)$, dependent only on n_i. As we will describe below, an exact description of this form can be obtained for the case of homogeneous rates across opinions (see Sec. 5.4). If the imitation or mutation rates are heterogeneous this approach constitutes an approximation (see Sec. 5.5).

5.3.2 Stationary distribution for individual opinions

At long times the m-species distribution $P(\mathbf{n}, t)$ becomes time-independent; we write $P_{\rm st}(\mathbf{n})$ for the stationary distribution. In principle, this stationary distribution can be

obtained from the linear set of equations for $P_{\rm st}$, obtained by setting the right-hand side of the master equation (5.2) to zero. In practice, it is very difficult to evaluate this analytically. However, as we will describe next, we can obtain the marginal distributions $P_i(n_i) = \sum_{\mathbf{n}_{-i}} P_{\rm st}(\mathbf{n})$ in some cases; the notation $\sum_{\mathbf{n}_{-i}} \dots$ in this expression indicates a sum over all variables $n_1, \dots, n_m$, except n_i.

We assume that we can formulate a closed death-birth process for species i, with birth and death rates $T_i^{\pm}(n_i)$. The stationary distribution of this process, is then the marginal P_i, and it is given by

$$P_i(n_i) = \frac{\prod_{k=1}^{n_i} \frac{T_i^+(k-1)}{T_i^-(k)}}{1 + \sum_{k=1}^{N} \prod_{\ell=1}^{k} \frac{T_i^+(\ell-1)}{T_i^-(\ell)}}. \tag{5.7}$$

This expression for the marginal stationary distribution can be obtained by standard methods from the backward master equation (see for example [28, 29]). We will test these predictions against simulations for the homogeneous and heterogeneous noisy voter models in Sections 5.4 and 5.5. In the figures and in Appendix 5.7 we express the marginals of the stationary distribution in terms of $x_i = n_i/N$; we then use the notation $\mathcal{P}_i(x_i)$.

5.3.3 Noise-induced transition

As discussed above, noisy voter models show a transition between parameter ranges with unimodal and multi-modal stationary distributions. This transition is noise induced, and occurs as the system size is varied. As a consequence, it is useful to identify a critical population size N_c which separates the two types of outcomes. In the case of only two species ($m = 2$) this is particularly straightforward, as there exists a population size for which the stationary distribution becomes flat. This population size has been used to define the transition point in refs. [20, 21]; see also [23].

In the multi-state case ($m > 2$) the situation is more complicated; the marginal distributions for the $\{x_i\}$ do not assume a flat shape for any population size, as we will discuss below. In order to characterise the transition, we therefore consider the shape of the distribution $P_i(n_i)$ at the left and right boundaries of phase space, i.e., near $n_i = 0$ and $n_i = N$, respectively. Specifically we find the population sizes N_L and N_R for which $P_i(0) = P_i(1)$ and $P_i(N-1) = P_i(N)$, respectively. These can be used

to separate the unimodal and multi-modal regimes. We will discuss this in more detail for the homogeneous and heterogeneous multi-state models in Secs. 5.4 and 5.5.

5.3.4 Switching times between states of consensus

The system is said to have reached consensus on opinion i if $n_i = N$, implying $n_j = 0$ for all $j \neq i$. We refer to this as consensus state i. If the population is not in a consensus state, then at least two of the n_j are non-zero, i.e., several opinions are represented in the population; we call these situations mixed states. As shown in Fig. 5.1, the system can transition between consensus states, with intermediate periods in mixed states. We will refer to this as 'switching' between consensus states, and we proceed to calculate the typical time between such switches.

In order to define switching times, we first introduce the concept of an 'arrival' at a consensus state. We say that an arrival at consensus state i occurs at time t if the system transitions from a mixed state into consensus state i at time t, *and* if the last consensus state the population visited before t was not i. This is illustrated in Fig. 5.2.

We define the mean switching time τ as the average time that elapses between two subsequent arrivals. By definition, these arrivals are at two different consensus states. This is again illustrated in Fig. 5.2. The quantity τ^{-1} is the mean number of arrivals per unit time.

In order to compute τ, we generalized the procedure used in ref. [21]. First, we consider the mean time it takes a single species j to reach state $n_j = N$ starting from

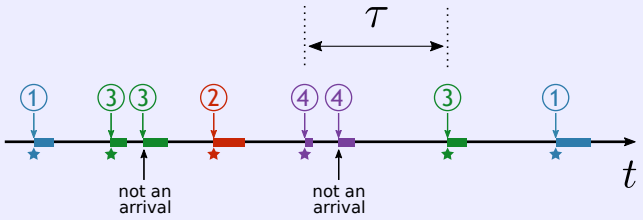

Figure 5.2: Illustration of the concepts of arrival and switching time. We show the time line of a model with $m \geq 4$ opinion states. Times at which the system reaches a consensus state are marked above the time axis by circled numbers. Times during which the system resides at a consensus state are indicated as filled bars on the time axis. Between these times the population is in mixed states. Arrivals at a new consensus state, as defined in the text, are marked by stars below the time axis. The switching time τ is the mean time between subsequent arrivals at new consensus states.

$n_j = 0$; we denote this time by $t_j^{0\to N}$. This is a standard hitting-time problem, and we find [29, 30]

$$t_j^{0\to N} = \sum_{k=0}^{N-1} \sum_{\ell=0}^{k} \frac{1}{T_j^+(\ell)} \prod_{\ell'=\ell+1}^{k} \frac{T_j^-(\ell')}{T_j^+(\ell')}. \tag{5.8}$$

To proceed, we now assume that the population is currently in consensus state i. The mean time it takes any of the species $j \neq i$ to reach the state $n_j = N$ is then given by $t_j^{0\to N}$. This expression is exact, provided closed-form processes can be formulated for the individual species.

To be able to describe the switching time of the multi-state model, we now treat the processes for each of the species $j \neq i$ as independent. We associate each process with a 'clock', and say that the clock for species j 'ticks' when $n_j = N$. We assume that the rate with which this happens is constant in time for each process, and given by $1/t_j^{0\to N}$. This is an approximation. First, due to the coupling of the different species, the processes for the different types j are in general not independent. Second, the distribution of waiting times until state $n_j = N$ is reached is not exponential for one-step Markov processes of the type above; instead, the hitting time can be written as the sum of multiple exponential random variables [31, 32].

Proceeding nevertheless with this approximation, the total rate for any of the clocks $j \neq i$ to tick (i.e., any species $j \neq i$ to take over the population) is given by $\sum_{j\neq i}(t_j^{0\to N})^{-1}$. As a consequence, we find the mean waiting time until any of the consensus states $j \neq i$ is reached as

$$\tau_i = \frac{1}{\sum_{j\neq i}(t_j^{0\to N})^{-1}}. \tag{5.9}$$

This approximates the average time for the system to reach any consensus state $j \neq i$, if it is currently in consensus state i.

The mean time between two subsequent arrivals can then be written as

$$\tau = \sum_{i=1}^{m} p_i \tau_i, \tag{5.10}$$

where p_i denotes the proportion of the number of arrivals at consensus state i among the total number of arrivals. In other words, of all arrivals the system makes, a fraction p_i occurs at consensus state i. Evidently, one has $\sum_{i=1}^{m} p_i = 1$.

We now proceed to estimate the coefficients p_i. To do this, we first consider the typical time between two arrivals at the same consensus state i. This can be

approximated as

$$\overset{\leftrightarrow}{\tau}_i \equiv \tau_i + t_i^{0\to N}. \tag{5.11}$$

This expression can be understood by first assuming that the population is in consensus state i. The term τ_i in Eq. (5.11) is the mean time that elapses until the system reaches any of the other consensus states, $j \neq i$. At that point there will be no individuals of type i ($n_i = 0$). The second term, $t_i^{0\to N}$, is the average time required to reach consensus state i again.

The quantity p_i in turn is proportional to the number of arrivals at i per unit time, given by $(\overset{\leftrightarrow}{\tau}_i)^{-1}$. With appropriate normalization, we find

$$p_i = \frac{(\overset{\leftrightarrow}{\tau}_i)^{-1}}{\sum_{j=1}^{m}(\overset{\leftrightarrow}{\tau}_j)^{-1}}. \tag{5.12}$$

To summarise, the overall switching time is obtained as

$$\tau = \sum_i \left\{ \frac{(\overset{\leftrightarrow}{\tau}_i)^{-1}}{\left[\sum_j (\overset{\leftrightarrow}{\tau}_j)^{-1}\right]\left[\sum_{j\neq i}(t_j^{0\to N})^{-1}\right]} \right\}, \tag{5.13}$$

using the expressions in Eqs. (5.8), (5.9), and (5.11).

5.4 Homogeneous model

We first consider the fully homogeneous set-up. If the rates are homogeneous across species, i.e., if $r_{ij} \equiv r$ and $\varepsilon_{ij} \equiv \varepsilon$, the expressions in Eq. (5.6) reduce to

$$\begin{aligned} T_i^+(n_i) =& \frac{n_i(N-n_i)}{N} r + (N-n_i)\varepsilon, \\ T_i^-(n_i) =& \frac{n_i(N-n_i)}{N} r + \varepsilon(m-1)n_i. \end{aligned} \tag{5.14}$$

In particular, the $T_i^{\pm}$ are now fully specified by n_i alone. Species i undergoes a well-defined death-birth process with rates given by Eq. (5.14). All species $j \neq i$, can be lumped together into one 'other species' and there are $N - n_i$ individuals of this other species. We note that no approximations have been made in deriving this result. As far as the marginal process for any particular species i is concerned, the dynamics effectively reduces to a two-species process, for which analytical descriptions are available (see e.g. [28]). We will use these tools to calculate stationary distributions for individual species, as well as switching times between consensus states.

5.4.1 Marginals of the stationary distribution

For uniform rates, the marginal probability distributions $P_i(n_i)$ are identical across species and can be obtained by using the rates from Eqs. (5.14) in Eq. (5.7). These closed-form expressions can be evaluated numerically.

Results can be found in Fig. 5.3. In panel (a) we show the case of $m = 2$ species, already discussed in refs. [20, 21]. This is shown mainly for comparison.

Given that $n_2 = N - n_1$, the model with two species is, by construction, described by a single death-birth process. As seen in the figure, simulation results and theory are in agreement. For $N > N_c$ the resulting distribution is unimodal; for $N < N_c$ a bimodal shape is observed. At the critical population size $N = N_c$ the distribution is flat; this transition point is $N_c = r/\varepsilon$ [20, 21]. The stationary distribution is symmetric about $x = 1/2$ for all N.

In panel (b) of Fig. 5.3 we show the model with $m = 5$ opinion states. Again, simulations and theoretical predictions are in agreement. As in the case of two states, a transition from a unimodal to a bimodal marginal distribution is observed as the population size is decreased. Bimodality in the marginal single-species distributions indicates multi-modality in the state space of all m species, as illustrated in Fig. 5.1(c) for $m = 3$. In contrast with the two-species case, the marginal distributions for the abundances of individual species never becomes flat in Fig. 5.3(b). We also note that the marginal distributions do not exhibit any particular symmetry, despite the fact

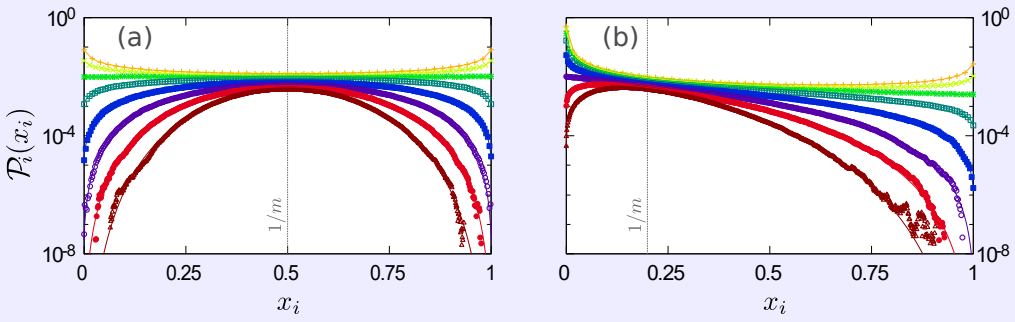

Figure 5.3: Stationary distribution of the model with homogeneous rates across species. Panel (a) is for $m = 2$; panel (b) shows the marginal distribution for single species for the model with $m = 5$. The different curves are for different population sizes in the range $N = 50$ (top) to $N = 900$ (bottom). Markers are from simulations; lines show the analytical predicitions from the theory described in the text. Remaining model parameters are $r = 1$, and $\epsilon = 10^{-2}/(m-1)$.

that the imitation and mutation rates are homogeneous across species.

5.4.2 Phase diagram

As mentioned in Sec. 5.3.3, we use the population sizes at which $P_i(0) = P_i(1)$ or $P_i(N-1) = P_i(N)$ to characterise the transition between the unimodal and multimodal regimes. The condition for the left edge, $P_i(0) = P_i(1)$, translates into $T_i^+(0) = T_i^-(1)$; using Eqs. (5.14) one finds the physical solution

$$N_L = \frac{[1+\widetilde{\varepsilon}_{\text{tot}}] + \sqrt{[1+\widetilde{\varepsilon}_{\text{tot}}]^2 - 4\widetilde{\varepsilon}}}{2\widetilde{\varepsilon}}, \tag{5.15}$$

where we have written $\widetilde{\varepsilon}_{\text{tot}} = (m-1)\varepsilon/r$, and $\widetilde{\varepsilon} = \varepsilon/r$.

Similarly, requiring $P_i(N-1) = P_i(N)$ at the right edge yields $T_i^+(N-1) = T^-(N)$, from which we obtain

$$N_R = \frac{[1+\widetilde{\varepsilon}] + \sqrt{[1+\widetilde{\varepsilon}]^2 - 4\widetilde{\varepsilon}_{\text{tot}}}}{2\widetilde{\varepsilon}_{\text{tot}}}. \tag{5.16}$$

For $m = 2$ this reduces to the result in refs. [20, 21], i.e., $N_L = N_R = r/\varepsilon$.

The resulting expressions for N_L and N_R only depend on the relative mutation rate ε/r. This is due to the fact that, up to a re-scaling of time, the reaction rates in Eq. (5.14) only depend on the ratio of ε and r. We also note that Eqs. (5.15) and (5.16) are symmetric with respect to exchanging $\widetilde{\varepsilon}$ and $\widetilde{\varepsilon}_{\text{tot}}$. This is a consequence of the same symmetry in the pairs $\{T^+(0), T^-(N)\}$ and $\{T^-(1), T^+(N-1)\}$. We also notice that $N_L \approx \widetilde{\varepsilon}^{-1}$ and $N_R \approx (\widetilde{\varepsilon}_{\text{tot}})^{-1}$ when $\varepsilon/r \ll 1$.

The phase diagram resulting from Eqs. (5.15) and (5.16) is depicted in Fig. 5.4. We use $r = 1$ in both panels. In panel (a) we show the population sizes N_R and N_L as a function of the number of species, m, at a fixed mutation rate ε. The upper solid line indicates N_L and the lower solid line is N_R. Results from simulations are shown as markers; as seen in the figure, theoretical predictions are in agreement with simulations.

We note that, in Fig. 5.4(a), N_L is nearly flat as a function of the number of species m. This is in line with the behaviour of $N_L \approx r/\varepsilon$ for small mutation rates, and can be further understood as follows. The shape of the stationary state distribution near $n_i = 0$ is largely determined by the frequency of mutation events that generate new individuals of type i. This mutation rate is given by $N\varepsilon$; if $n_i = 0$, each of the

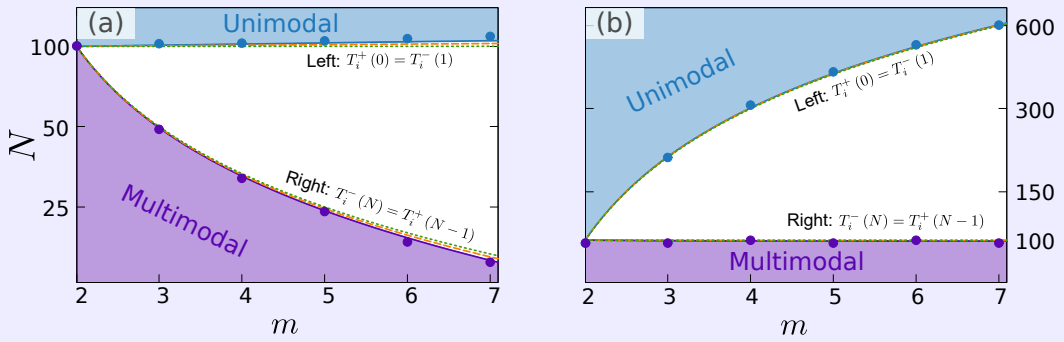

Figure 5.4: Phase diagram for the model with homogeneous rates. The critical system size is plotted as a function of the number of strategies. The continuous blue line is N_L as calculated from Eq. (5.15), and the purple continuous line shows N_R as obtained from Eq. (5.16). The remaining lines are from a diffusion approximation to the model, as discussed in Appendix 5.7. Markers show results from simulations. Mutation rates are $\varepsilon = 10^{-2}$ in panel (a), and $\varepsilon = 10^{-2}/(m-1)$ in panel (b). We set $r = 1$ in both panels.

N individuals in the population mutate into i with rate ε [see Eq. (5.14)]. This is the case independently of the number of species m. Therefore, we expect N_L to be approximately independent of m, as seen in Fig. 5.4(a).

Near $n_i = N$, however, the shape of the distribution is determined by the rate with which individuals of type i mutate into any other species. If $n_i = N$, each of the N individuals mutates into any one of the species $j \neq i$ with rate ε; the total rate of mutation events out of species i is then $N\varepsilon(m-1)$ [see again Eq. (5.14)]. For fixed ε, this total rate increases as either N or $m-1$ are increased. Therefore, we expect N_R to be a decreasing function of m, which is confirmed in the phase diagram in Fig. 5.4(a). This is again consistent with the behaviour $N_R \approx r/[(m-1)\varepsilon]$ for small mutation rates.

In panel (b) of Fig. 5.4 we show the phase diagram for the choice $\varepsilon = 10^{-2}/(m-1)$, i.e., for a fixed value of $\widetilde{\varepsilon}_{\text{tot}} = 10^{-2}$. Recalling that an individual of any species undergoes mutations to any of the other $m-1$ species with rate ε, the *total* mutation rate for any individual is constant with this choice, irrespective of the number of species m. The model shows the same three phases as in Fig. 5.4(a), but the shape of the phase lines changes. We now find that N_L is nearly independent of m, whereas N_R is a decreasing function of m. This is consistent with the interpretation given above. The shape of the distribution near the left edge is largely determined by $T_i^+(0) = 10^{-2}N/(m-1)$. An increased value of m now requires a larger value of N to keep this rate constant.

The shape of the distribution on the right edge is governed by $T_i^-(N) = 10^{-2}N$; this quantity is now independent of the number of species, m.

Similar to [21], our approach so far has not involved any continuous approximation of the discrete state space of the population. The analysis of ref. [20], on the other hand, is based on a diffusion approximation to the dynamics of the two-state noisy voter model. We have extended this approach to the multi-state case. The dashed and dotted lines in both panels of Fig. 5.4 are the predictions for N_L and N_R obtained from the diffusion approximation. The mathematical details are discussed in the Appendix.

The shape of $P_i(n_i)$ in the different regimes of Fig. 5.4 can be summarised as follows [see also Fig. 5.3(b)]: For large populations ($N > N_L$) the single-species distribution is unimodal (light blue shading in Fig. 5.4), taking its maximum strictly in the interior of the interval $0 < n_i < N$. For intermediate sizes ($N_R < N < N_L$, unshaded) the distribution function is monotonously decreasing in n_i, taking its maximum value at $n_i = 0$. Finally, for small populations ($N < N_R$) the distribution for n_i is multi-modal (dark purple shading), with maxima at $n_i = 0$ and $n_i = N$.

5.4.3 Switching times

In the homogeneous case, the times $t_j^{0\to N}$ in Eq. (5.8) are uniform across species; we write $t^{0\to N}$ for their common value. As a consequence, we find $\tau_i = t^{0\to N}/(m-1)$ in Eq. (5.9), and therefore the mean switching time is also given by

$$\tau = \frac{t^{0\to N}}{m-1}. \tag{5.17}$$

Theoretical predictions and results from simulations are compared in Fig. 5.5. We show data for different choices of the number of species m; as before we use $r = 1$. To allow a better comparison, we plot the switching time as a function of $\widetilde{\varepsilon}_{\text{tot}} = (m-1)\varepsilon$. This ensures that the total mutation rate any one species experiences is comparable across the different values of m.

The diagram indicates that the switching time becomes smallest at intermediate values of the mutation rate. This can be understood as follows. For small mutation rates, the population will reside at consensus states for relatively long times; escape from these states occurs through mutation. These long sojourn times at the consensus state mean that the switching time, i.e., the typical time between arrivals, will also be

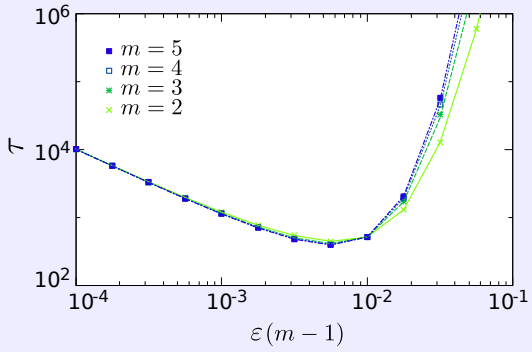

Figure 5.5: Switching times in the model with homogeneous imitation and mutation rates. The figure shows the switching time τ between consensus states for different choices of the number of species m. Lines are from Eq. (5.17), markers show simulation results. In all cases $N = 100$ and $r = 1$.

large. On the other hand, for large mutation rates the population spends most of its time in the interior of phase space. This leads to long periods in which the population does not visit any of the consensus states. As a consequence, the switching time will also be large. The shortest switching times are thus seen in the intermediate range of mutation rates, when neither of these effects dominate.

5.5 Heterogeneous model

We now turn to instances of the model in which the imitation and mutation rates are not homogeneous across species. We limit the discussion to examples in which $r_{ji} = r_j$ and $\varepsilon_{ji} = \varepsilon_j$. The approach we develop can be extended to cover more general cases; we briefly comment on this in Appendix 5.8.

The quantity r_j describes the rate with which members of species j imitate any other species, and ε_j is the rate with which individuals of type j spontaneously change to any other type. In the context of opinion dynamics, large values of r_j and ε_j thus describe beliefs that are only weakly held. If r_j and ε_j are low, on the other hand, then j describes a strong view.

5.5.1 Analytical approximation

With the above choice of reaction rates, the transition rates $T_i^{\pm}$ in Eq. (5.6) can be written as

$$\begin{aligned} T_i^+(\mathbf{n}) &= \frac{n_i(N-n_i)}{N} \langle r \rangle_{-i}(\mathbf{n}) + (N-n_i) \langle \varepsilon \rangle_{-i}(\mathbf{n}), \\ T_i^-(\mathbf{n}) &= \frac{n_i(N-n_i)}{N} r_i + \varepsilon_i n_i, \end{aligned} \tag{5.18}$$

where

$$\langle r\rangle_{-i}(\mathbf{n}) = \frac{1}{N-n_i}\sum_{j\neq i} n_j r_j, \tag{5.19}$$

and similarly for $\langle\varepsilon\rangle_{-i}(\mathbf{n})$. These quantities are weighted averages over the imitation and mutation rates of all species other than i; $\langle r\rangle_{-i}$ for example represents the mean rate with which opinion i is imitated by any other species. We note that $\langle r\rangle_{-i}(\mathbf{n})$ and $\langle\varepsilon\rangle_{-i}(\mathbf{n})$ depend on the variables n_j $(j\neq i)$, i.e., on the entire state of the population. As a consequence, no closed process can be formulated for individual species for the heterogeneous model.

We therefore resort to an approximation. We replace all $\{n_j\}$ with $\{Nx_j^*\}$ in Eq. (5.19); x_j^* represents the proportion of individuals of species j at the fixed point of the deterministic rate equations, i.e., the dynamics in the limit of infinite populations. These can be obtained from a Kramers–Moyal expansion of the master equation (5.2), as detailed in Appendix 5.7. We then define

$$r_{-i}^* \equiv \frac{1}{1-x_i^*}\sum_{j\neq i} x_j^* r_j, \tag{5.20}$$

and similarly for ε_{-i}^*. Our approximation consists in replacing the stochastic quantities $\langle r\rangle_{-i}(\mathbf{n})$ and $\langle\varepsilon\rangle_{-i}(\mathbf{n})$ with r_{-i}^* and ε_{-i}^*, respectively, in Eq. (5.18). In this way we find an approximate, but closed, effective process for species i. This can then be used to obtain marginals of the stationary distribution and switching times, following the procedure described in Sections 5.3.2 and 5.3.4.

5.5.2 Marginals of the stationary distribution

In order to test the accuracy of the approximations described above, we consider an example with $m=5$ species. We choose the imitation rates as $r_j = r[1-\delta+(j-1)\frac{2\delta}{m-1}]$, for $j=1,\ldots,m$, and similarly $\varepsilon_j = \varepsilon[1-\delta+(j-1)\frac{2\delta}{m-1}]$ for the mutation rates. The coefficients ε and r represent the mean rates (across species) and are model parameters. This choice indicates that the rates $\{r_j\}$ and $\{\varepsilon_j\}$ are equally spaced in the intervals $[(1-\delta)r,(1+\delta)r]$ and $[(1-\delta)\varepsilon,(1+\delta)\varepsilon]$, respectively. The parameter δ therefore describes the relative spread of these rates, and quantifies the degree of heterogeneity. We note that species $j=1$ has the lowest rates ε_j and r_j among all species (it represents a strong opinion), and species $j=m$ the highest (it describes a weak opinion). We

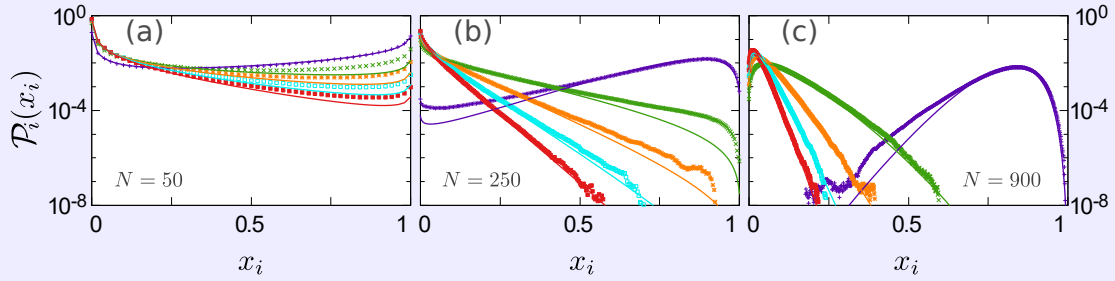

Figure 5.6: Marginals of the stationary distribution for the heterogeneous multi-state noisy voter model. We show the distributions $\mathcal{P}_i(x_i)$ for the different individual species in a model with $m = 5$ for different population sizes, as indicated in the figure. Markers represent simulation results; lines are evaluations of Eq. (5.7), using the rates in Eq. (5.18) with the approximation in Eq. (5.20). The choice of mutation and imitation rates is as described in the text (see Sec. 5.5.2), using $r = 1$, $(m-1)\varepsilon = 10^{-2}$, and $\delta = 0.05$.

restrict our analysis to relatively small values of δ; this avoids situations in which the population spends most of its time in one single consensus state (the one of the strongest opinion). In such cases, it is difficult to measure stationary distributions and switching times in simulations.

The marginals of the resulting stationary distribution are shown in Fig. 5.6. In panel (a) the population is relatively small ($N = 50$), panel (b) shows an intermediate case ($N = 250$), and in panel (c) $N = 900$. As the population size is increased, the marginal distributions change shape. Each marginal is bimodal for very small populations [panel (a)]; in particular, the slope of each curve is negative near $n_i = 0$, and positive near $n_i = N$. For larger populations the gradient near $n_i = N$ changes sign when a critical size, $N_{R,i}$, is reached [panel (b)], similar to what was found in the homogeneous model. Notably though the population size at which this happens can differ across the species, as indicated by the subscript i in $N_{R,i}$. If the population size is larger still, the gradient of the marginal distribution near $n_i = 0$ will also change sign [panel (c)]; this occurs at population sizes $N_{L,i}$, which can again vary across the different species. Mathematically, $N_{L,i}$ and $N_{R,i}$ can be defined using conditions similar to those in Sec. 5.4.2; $N_{L,i}$ is the population size for which $T_i^+(0) = T_i^-(1)$, and $N_{R,i}$ is defined as the population size for which $T_i^+(N-1) = T_i^-(N)$.

5.5.3 Phase diagram

In Fig. 5.6(a) the population size is such that $N < N_{R,i}$ for all i, so that all marginals have bimodal shape. In panel (b) we have $N_{R,i} < N < N_{L,i}$ for all i, and in panel (c) the population is sufficiently large so that $N > N_{L,i}$ for all i.

The resulting phase diagram for the model with heterogeneous rates is shown in Fig. 5.7. It exhibits the three different phases outlined above. For a given value of the mean mutation rate, the marginal distributions for all species are unimodal if $N > N_{L,i}$ for all i. On the other hand, if $N < N_{R,i}$ for all i then all marginals are bimodal. It is useful to define $N_L^{\min} \equiv \min_i N_{L,i}$, and $N_L^{\max} \equiv \max_i N_{L,i}$, and similarly for $N_R^{\min}$ and $N_R^{\max}$. We also define $N_L^{\hom}$ and $N_R^{\hom}$ as the corresponding quantities for the homogeneous model, with $r_i \equiv r, \varepsilon_i \equiv \varepsilon$ for all i [see Eqs. (5.15) and (5.16)].

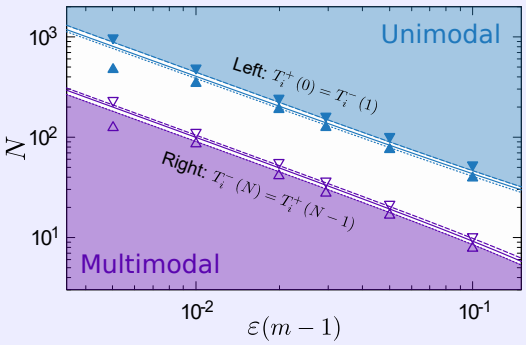

Figure 5.7: Phase diagram of the model with $m = 5$ species and heterogeneous rates. Upper and lower dashed lines show $N_L^{\max}$ and $N_R^{\max}$, respectively; upper and lower dotted lines are $N_L^{\min}$ and $N_R^{\min}$. Solid lines are $N_L^{\hom}$ and $N_R^{\hom}$ (see text for definitions). Markers are from simulations (with $\blacktriangledown, \blacktriangle, \triangledown, \triangle$ showing $N_L^{\max}, N_L^{\min}, N_R^{\max}, N_R^{\min}$, respectively). Mutation and imitation rates for each species are chosen as described in the text (see Sec. 5.5.2).

In Fig. 5.7, we plot these quantities for different choices of m. The white unshaded region shows population sizes for which $N_R^{\min} < N < N_L^{\max}$. Simulation results for $N_R^{\min}$, $N_R^{\max}$, $N_L^{\min}$, and $N_L^{\max}$ are also shown, and confirm the theoretical predictions.

5.5.4 Switching times

In Fig. 5.8 we demonstrate the accuracy of the analytical approximation in Eq. (5.13) for the switching times in the model with heterogeneous rates. Panel (a) shows the times $t_i^{0\to N}$ for the different species i in the model with $m = 5$. Imitation and mutation

rates were chosen as described in Sec. 5.5.2. As seen in the figure, the overall agreement is reasonable, although not quantitatively accurate. This is not surprising, as the approximation of Eq. (5.20) is a relatively severe intervention. Nevertheless, the approximation accurately predicts the qualitative shape of $t_i^{0\to N}$ as a function of the mutation rate, as well as the ordering across species. We note that the different curves in panel (a) show species $i = 1, \ldots, 5$ from bottom to top. This is in-line with intuition: individuals who are of opinion $i = 5$ are easily convinced of other opinions and are likely to change their views spontaneously. It is therefore difficult for this opinion to spread in the population; as a consequence $t_5^{0\to N}$ is large. Individuals who are of opinion $i = 1$, on the other hand, do not easily change to any other opinion; this leads to a relatively small time $t_1^{0\to N}$.

In Fig. 5.8(b) we show the resulting switching time τ for the model with heterogeneous rates. Results are reported for models with different numbers of species, m, and as a function of $(m-1)\varepsilon$ as in previous figures. In each case the switching time shows a minimum as a function of the mean mutation rate, as in the homogenous model.

It is interesting to note that the switching time is found to decrease at a fixed mutation rate $(m-1)\varepsilon$ when the number of species increases. To understand this, we observe that the spacing between rates for different species is proportional to $\delta/(m-1)$;

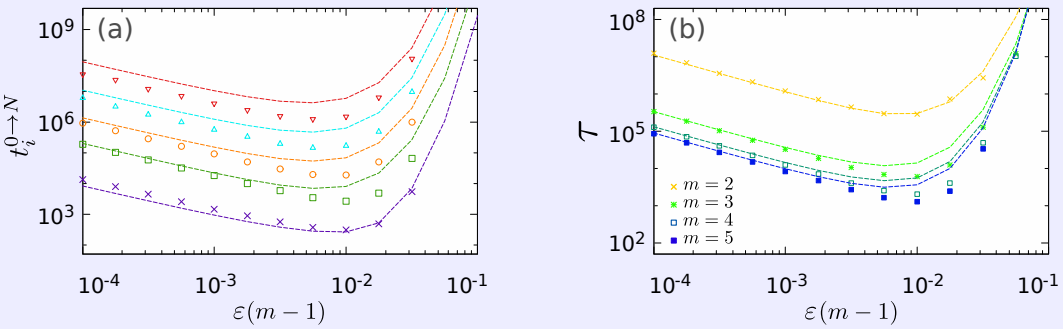

Figure 5.8: Switching times in the noisy voter model with heterogeneous rates. Panel (a) shows the quantities $t_i^{0\to N}$ for the different species $i = 1, \ldots, 5$ (bottom to top) in the model with $m = 5$. Panel (b) shows the resulting switching time τ for models with $m = 2, 3, 4, 5$ species, from top to bottom. Lines are from the analytical approximation [Eq. (5.13) with the rates as approximated in Eq. (5.20)]; markers are from simulations. In all cases, $N = 100$, $\delta = 0.05$; imitation and mutation rates are distributed as described in Sec. 5.5.2, using $r = 1$ and ε as indicated on the horizontal axis.

see the definitions at the beginning of Sec. 5.5.2. At fixed δ species $i = 1$ is thus the strongest opinion by a large margin when m is small. In the extreme case there are only two opinions; one is a very strong view and the other very weak in comparison. The population visits consensus on the stronger opinion frequently, and remains there for relatively long times. This leads to long switching times. When there are more species available (larger values of m) and δ is kept fixed, the opinion spectrum becomes more finely spaced and the advantage of the most strongly held view is reduced. This leads to a reduction in switching times.

A similar effect occurs when the parameter δ is varied keeping all other model parameters fixed. This parameter controls the spread of the rates r_j and ε_j. We find in simulations that switching times increase with increasing spread δ. This is again due to an increased advantage of the most strongly held opinion.

5.6 Summary and discussion

We have introduced a multi-state noisy voter model and studied its behaviour in a population with all-to-all interaction. It can be seen as a stylised model of imitation and mutation processes in opinion dynamics or evolution, for example. The model shows a noise-driven transition between a state of diversity for large populations and a mostly ordered state in small populations. In the diverse state multiple opinions (or species) are present in the population at most times, and the resulting stationary distribution is unimodal, with a peak in the interior of state space. The ordered regime occurs for small population sizes; the system is frequently found in consensus states, in which all individuals are of the same type. Switches between these consensus states are possible, as the dynamics do not permit absorbing states for non-zero mutation rates.

The transition between the two types of behaviour is a consequence of the balance of mutation effects, driving the system towards mixed states, and intrinsic noise due to the discreteness of the population. Similar to what was reported in ref. [20] for the model with two states, this noise is strongest in the interior of phase space, and drives the system away from mixed states. The overall amplitude of this noise scales as $N^{-1/2}$; as a consequence consensus states are more likely in small populations, when the noise is strong.

While this general behavior is well-known in the two-species noisy voter model, our analysis focuses on the case of multiple species, and specifically includes models with heterogeneity in the properties of the different species. We find that the transition persists, and we devise a method with which to calculate marginals of the multi-species stationary distribution. Our approach is based on formulating a reduced stochastic process for single species. This reduction is exact if imitation and mutation rates are homogeneous across species; in the heterogeneous model it is an approximation. We use the effective processes for individual species to obtain analytical results for marginals of the stationary distribution of the model. This allows us to identify the population sizes N_L and N_R, which characterise the transition from a unimodal to a multi-modal stationary distribution. The effective dynamics for single species can also be used to approximate the typical switching times between different consensus states.

There are some limitations to our work. The most severe restriction is that, in its present form, the approach requires all-to-all interaction; this simplifies the analysis greatly. It is an obvious challenge to extend the results we have obtained to multi-state noisy voter models on lattices and more complex graphs. For example, it would be interesting to see if and how our ideas can be combined with pair-approximation methods used recently for noisy voter models in [25]. A further limitation of our approach consists in its inability to capture correlations between species. The method focuses on the marginal dynamics of individual species, and so by construction correlations are not part of the analysis. In order to include these, one next step may be to consider the effective dynamics of pairs of species, while lumping together the remaining species. This would generate an effective three-species model; it is not immediately clear how to proceed with the analytical calculation of joint distributions or switching times. However, progress might be possible in the homogeneous case and exploiting symmetries, similar for example to what has been done in the context of cyclic dynamics in [33, 34].

Despite these limitations, we believe our work can contribute to future research in several ways. For example, the method of decoupling multi-species dynamics into several effective single-species processes is likely to be applicable more widely. This includes other models of opinion dynamics and language evolution. In many of these instances evolution is ‘neutral’, i.e., no species has an intrinsic advantage over any other. In such homogeneous models, an approach based on effective single-species

processes can be expected to produce accurate results. On the other hand, there are also situations in which heterogeneity is relevant, including evolutionary processes in biology. The method we have put forward can then be useful as an approximation.

Acknowledgements

FHA thanks Consejo Nacional de Ciencia y Tecnología (CONACyT, Mexico) for support.

5.7 Appendix A: Diffusion approximation

Insight into the model can be gained by approximating the discrete degrees of freedom by continuous variables, and the stochasticity in the dynamics as Gaussian noise. This is based on an expansion in the inverse size of the population, known as the diffusion approximation in mathematical biology [35]. In this Appendix we briefly summarise the outcome of this approximation for the multi-state noisy voter model.

5.7.1 Kramers–Moyal expansion and stochastic differential equation

Formally, the approximation results in a set of coupled stochastic differential equations (SDEs) for the variables $x_i = n_i/N$. These can be obtained by carrying out a Kramers–Moyal expansion of the master equation (5.2) in the limit of large, but finite population sizes N. Alternatively, these SDEs can also be written down using Kurtz' theorem [36], or Gillespie's derivation of the chemical Langevin equation for reaction systems [37].

For the multi-state noisy VM, as defined by Eqs. (5.2) and (5.3), one obtains

$$\dot{x}_i = f_i(\mathbf{x}) + \frac{1}{\sqrt{N}}\xi_i(t), \tag{5.21}$$

where the $\{\xi_i(t)\}$ are zero-average Gaussian noise variables, and where

$$f_i(\mathbf{x}) = \sum_j [\mathcal{T}_{j\to i}(\mathbf{x}) - \mathcal{T}_{i\to j}(\mathbf{x})]. \tag{5.22}$$

We have introduced the notation $\mathcal{T}_{j\to i}(\mathbf{x}) \equiv T_{j\to i}(N\mathbf{x})/N$. The $f_i(\mathbf{x})$ are commonly referred to as 'deterministic drift' [38]. They describe the flow of the dynamics in the limit of infinite populations, $N \to \infty$. In this limit intrinsic stochasticity reduces to zero, due to the pre-factor $N^{-1/2}$ in Eq. (5.21). The noise variables $\xi_i(t)$ are uncorrelated in time, but correlated across components. Writing

$$\langle \xi_i(t)\xi_j(t')\rangle = B_{ij}(\mathbf{x})\delta(t-t'), \tag{5.23}$$

one has, for example based on Kurtz' theorem [36],

$$B_{ij}(\mathbf{x}) = \begin{cases} \sum_{k\neq i} [\mathcal{T}_{i\to k}(\mathbf{x}) + \mathcal{T}_{k\to i}(\mathbf{x})] & \text{if } i = j \\ \\ -[\mathcal{T}_{j\to i}(\mathbf{x}) + \mathcal{T}_{i\to j}(\mathbf{x})] & \text{if } i \neq j \end{cases}. \tag{5.24}$$

See also [39] for further details in a different context. We note that $\sum_j B_{ij} = 0$ for all i, reflecting the fact that the total number of individuals in the population is constant.

In explicit form, one finds the drift terms for the multi-state noisy VM as follows,

$$f_i(\mathbf{x}) = \sum_{j\neq i} \left[x_i x_j (r_{ij} - r_{ji}) + \varepsilon_{ji} x_j - \varepsilon_{ij} x_i\right], \tag{5.25}$$

and the correlation matrix (across components) for the variables $\xi_i(t)$ has entries

$$B_{ij}(\mathbf{x}) = -x_i x_j \left(r_{ij} + r_{ji}\right) - \varepsilon_{ij} x_i - \varepsilon_{ji} x_j, \tag{5.26}$$

for $i \neq j$, and

$$B_{ii}(\mathbf{x}) = -\sum_{j\neq i} B_{ij}(\mathbf{x}). \tag{5.27}$$

These results are valid both in the case of homogeneous and heterogeneous imitation and mutation rates across species.

5.7.2 Homogeneous rates

We now focus on individual species in the model with homogeneous rates. The Fokker-Planck equation governing the marginal distribution for species i is given by

$$\begin{aligned} \frac{\partial \mathcal{P}_i(x_i)}{\partial t} =& -\frac{\partial}{\partial x_i}\left[f_i(x_i)\mathcal{P}_i(x_i)\right] \\ &+ \frac{1}{2N}\frac{\partial^2}{\partial x_i^2}\left[B_{ii}(x_i)\mathcal{P}_i(x_i)\right], \end{aligned} \tag{5.28}$$

where $f_i(x_i)$ and $B_{ii}(x_i)$ are found to depend only on x_i in the homogeneous model. This reduction is similar to the one observed for the transition rates $T_i^{\pm}$ in Sec. 5.4. We note that Eq. (5.28) can be obtained from a direct Kramers–Moyal expansion of the master equation describing the death-birth process for species i, with rates as in Eq. (5.14).

In explicit form we have

$$f_i(x_i) = \varepsilon(1 - m x_i), \tag{5.29}$$

and

$$B_{ii}(x_i) = \left[\varepsilon(m-2) + 2r(1-x_i)\right] x_i + \varepsilon. \tag{5.30}$$

In the homogeneous model these are the same for all species.

The stationary solution of Eq. (5.28) is found as

$$\mathcal{P}_i(x_i) = C_i \exp\left[\int_0^{x_i} dy\, \frac{2f_i(y) - N^{-1}B'_{ii}(y)}{B_{ii}(y)}\right], \tag{5.31}$$

where $B'_{ii}(y)$ is the derivative of $B_{ii}(y)$ with respect to y, and where C_i is a constant ensuring normalisation.

We note that the derivative of the marginal stationary distribution with respect to x_i is given by

$$\mathcal{P}'_i(x_i) = C_i \left[2f_i(x_i) - N^{-1}B'_{ii}(x_i)\right] / B_{ii}(x_i). \tag{5.32}$$

The conditions used to define N_L and N_R translate into $\mathcal{P}'_i(0) = 0$ and $\mathcal{P}'_i(1) = 0$, respectively. We therefore find

$$N_L = \frac{B'_{ii}(0)}{2f_i(0)}, \quad N_R = \frac{B'_{ii}(1)}{2f_i(1)}, \tag{5.33}$$

within the diffusion approximation.

From Eq. (5.33) one then obtains

$$\begin{aligned} N_L &= \frac{2 + (m-2)\varepsilon/r}{2\varepsilon/r}, \\ N_R &= \frac{2 - (m-2)\varepsilon/r}{2(m-1)\varepsilon/r}. \end{aligned} \tag{5.34}$$

Results from Eqs. (5.34) are shown as dashed lines in Fig. 5.4.

In the limit of small mutation rates, $\varepsilon \ll r$, we find

$$N_L \approx \frac{r}{\varepsilon}, \; N_R \approx \frac{r}{(m-1)\varepsilon}. \tag{5.35}$$

This reproduces the asymptotic behaviour of N_L and N_R in Eqs. (5.15) and (5.16).

The results given in this section are for the case of homogeneous rates; one can then formulate a closed Fokker-Planck equation for the marginal distribution of single species [Eq. (5.28)]. If the imitation and mutation rates vary across species, this is no longer possible in exact form. However, an approximate closed Fokker-Planck equation can be formulated for $\mathcal{P}_i$, following the principles of Sec. 5.5.1. The approximation consists of replacing x_j, $j \neq i$, with the fixed point values x_j^* of the deterministic dynamics for infinite populations. The analog of Eqs. (5.33) can then be obtained following the steps described above.

5.7.3 Further criterion to characterise the transition

In this section we briefly discuss a further method to identify the transition between the regimes with unimodal and multi-modal stationary distributions. This is motivated by the procedure used in [20]. We restrict the discussion to models with homogeneous imitation and mutation rates across species.

The solution in Eq. (5.31) can be written in two equivalent forms,

$$\mathcal{P}(x) = \frac{D\left[A \pm q(x)\right]^{\mp 2\gamma\alpha}}{B(x)^{1-\gamma(1\pm\alpha)}}, \tag{5.36}$$

where we have dropped the index i for simplicity, and where

$$\begin{aligned} A =& \sqrt{\left(\frac{\varepsilon}{r}\frac{m-2}{2}+1\right)^2 + 2\frac{\varepsilon}{r}}, \\ q(x) =& 2x - \left(\frac{\varepsilon}{r}\frac{m-2}{2}+1\right), \\ \alpha =& \frac{\left(\frac{\varepsilon}{r}+\frac{2}{m}\right)\left(\frac{m-2}{2}\right)}{A}, \\ \gamma =& N\frac{m}{2}\frac{\varepsilon}{r}. \end{aligned} \tag{5.37}$$

The constant D in Eq. (5.36) ensures normalisation. We stress that both forms of $\mathcal{P}$ in Eq. (5.36) describe the same mathematical expression. The purpose of giving both representations will become clear below. We also note that the only dependence of $\mathcal{P}(x)$ on N is in γ, and the only dependence on x is in $q(x)$ and $B(x)$.

In ref. [20] a similar form of the stationary distribution is obtained for the model with two species; our result reduces to this known case when $m = 2$. We note that the dependence on x in the numerator of Eq. (5.36) vanishes for $m = 2$, as $\alpha = 0$ in

this case. In ref. [20] the phase transition for the two-species model was identified as the population size N for which the stationary distribution is flat; for $m = 2$, this is equivalent to setting the exponent of $B(x)$ in Eq. (5.36) to zero, leading to $\gamma = 1$, i.e., $N_c = r/\varepsilon$.

We propose a similar criterion to characterise the transition for the multi-state model: we find the population size at which the exponent $1-\gamma(1\pm\alpha)$ in the denominator of Eq. (5.36) vanishes, notwithstanding the fact that a residual dependence on x remains through $q(x)$.

Proceeding on this basis, we use

$$\gamma\,(1 \pm \alpha) - 1 = 0 \tag{5.38}$$

to characterise the population size associated with the transition between the unimodal and multi-modal regimes. We note that solving Eq. (5.38) for N leads to two different solutions, one for each choice of the sign in front of α. We label these as $N_\pm$, and find

$$N_- = \frac{2r}{m\varepsilon}\frac{1}{1-\alpha}, \quad N_+ = \frac{2r}{m\varepsilon}\frac{1}{1+\alpha}, \tag{5.39}$$

which for $\varepsilon/r \ll 1$ simplifies to

$$N_- \approx \frac{r}{\varepsilon}, \quad N_+ \approx \frac{r}{\varepsilon}\frac{1}{m-1}. \tag{5.40}$$

To see this note that $A \approx 1$, and $\alpha \approx \frac{m-2}{m}$ in this limit. Eqs. (5.40) reproduce the asymptotic behaviour of the expressions for N_L and N_R in Eqs. (5.34) for $\varepsilon/r \ll 1$. Results from Eqs. (5.39) are shown as dotted lines in Fig. 5.4.

5.8 Appendix B: General heterogeneous model

We briefly address the model with general heterogeneous imitation and mutation rates, r_{ij} and ε_{ij}.

Using the transition rates in Eq. (5.3), the effective birth and death rates for species i in Eq. (5.6) can be written as

$$\begin{aligned} T_i^+(\mathbf{n}) =& \frac{n_i(N-n_i)}{N}\rho_i(\mathbf{n}) + (N-n_i)\mu_i(\mathbf{n}), \\ T_i^-(\mathbf{n}) =& \frac{n_i(N-n_i)}{N}\lambda_i(\mathbf{n}) + n_i(m-1)\nu_i, \end{aligned} \tag{5.41}$$

where

$$\begin{aligned} \rho_i(\mathbf{n}) =& \frac{1}{N-n_i}\sum_{j\neq i} n_j r_{ji}, \\ \mu_i(\mathbf{n}) =& \frac{1}{N-n_i}\sum_{j\neq i} n_j \varepsilon_{ji}, \\ \lambda_i(\mathbf{n}) =& \frac{1}{N-n_i}\sum_{j\neq i} n_j r_{ij}, \\ \nu_i =& \frac{1}{m-1}\sum_{j\neq i} \varepsilon_{ij}. \end{aligned} \tag{5.42}$$

The averages $\rho_i(\mathbf{n})$, $\mu_i(\mathbf{n})$ and $\lambda_i(\mathbf{n})$ are similar to those in Eq. (5.19). The only complication is a second index of the object which is being averaged. The object ν_i is a uniform average of ε_{ij} over all species $j \neq i$, and not dependent on the state $\mathbf{n}$ of the population.

As in the main text, one can proceed by replacing n_i/N with the values x_i^* at the deterministic fixed point. This approximation results in closed definitions for death-birth processes for individual species i. These can then be analysed following the same steps as in Sections 5.3.2 and 5.3.4.

Bibliography

[1] Clifford, Peter and Aidan Sudbury (1973), 'A model for spatial conflict', *Biometrika* **60** (3):581–588, DOI: 10.1093/biomet/60.3.581.

[2] Liggett, Thomas M. (1985), *Interacting Particle Systems*, vol. 276, Grundlehren der mathematischen Wissenschaften, Springer-Verlag, New York, NY, DOI: 10.1007/978-1-4613-8542-4.

[3] Frachebourg, L. and Pavel L. Krapivsky (1996), 'Exact results for kinetics of catalytic reactions', *Physical Review E* **53** (4):R3009–R3012, DOI: 10.1103/PhysRevE.53.R3009.

[4] Kirman, Alan (1993), 'Ants, Rationality, and Recruitment', *The Quarterly Journal of Economics* **108** (1):137–156, DOI: 10.2307/2118498.

[5] Castellano, Claudio, Santo Fortunato and Vittorio Loreto (2009), 'Statistical physics of social dynamics', *Reviews of Modern Physics* **81** (2):591–646, DOI: 10.1103/RevModPhys.81.591.

[6] Castelló, Xavier, Víctor M. Eguíluz and Maxi San Miguel (2006), 'Ordering dynamics with two non-excluding options: bilingualism in language competition', *New Journal of Physics* **8** (12):308–308, DOI: 10.1088/1367-2630/8/12/308.

[7] Granovsky, Boris L. and Neal Madras (1995), 'The noisy voter model', *Stochastic Processes and their Applications* **55** (1):23–43, DOI: 10.1016/0304-4149(94)00035-R.

[8] Kauhanen, Henri et al. (2018), 'Geospatial distributions reflect rates of evolution of features of language', *arXiv preprint*, arXiv: 1801.09637.

[9] Fernández-Gracia, Juan et al. (2014), 'Is the Voter Model a Model for Voters?', *Physical Review Letters* **112** (15):158701, DOI: 10.1103/PhysRevLett.112.158701.

[10] Dornic, Ivan et al. (2001), 'Critical Coarsening without Surface Tension: The Universality Class of the Voter Model', *Physical Review Letters* **87** (4):045701, DOI: 10.1103/PhysRevLett.87.045701.

[11] Dall'Asta, Luca and Tobias Galla (2008), 'Algebraic coarsening in voter models with intermediate states', *Journal of Physics A: Mathematical and Theoretical* **41** (43):435003, DOI: 10.1088/1751-8113/41/43/435003.

[12] Al Hammal, Omar et al. (2005), 'Langevin Description of Critical Phenomena with Two Symmetric Absorbing States', *Physical Review Letters* **94** (23):230601, DOI: 10.1103/PhysRevLett.94.230601.

[13] Dornic, Ivan, Hugues Chaté and Miguel A. Muñoz (2005), 'Integration of Langevin Equations with Multiplicative Noise and the Viability of Field Theories for Absorbing Phase Transitions', *Physical Review Letters* **94** (10):100601, DOI: 10.1103/PhysRevLett.94.100601.

[14] Holme, Petter and Mark E. J. Newman (2006), 'Nonequilibrium phase transition in the coevolution of networks and opinions', *Physical Review E* **74** (5):056108, DOI: 10.1103/PhysRevE.74.056108.

[15] Vazquez, Federico, Víctor M. Eguíluz and Maxi San Miguel (2008), 'Generic Absorbing Transition in Coevolution Dynamics', *Physical Review Letters* **100** (10):108702, DOI: 10.1103/PhysRevLett.100.108702.

[16] Fichthorn, Kristen, Erdogan Gulari and Robert Ziff (1989), 'Noise-induced bistability in a Monte Carlo surface-reaction model', *Physical Review Letters* **63** (14):1527–1530, DOI: 10.1103/PhysRevLett.63.1527.

[17] Togashi, Yuichi and Kunihiko Kaneko (2001), 'Transitions Induced by the Discreteness of Molecules in a Small Autocatalytic System', *Physical Review Letters* **86** (11):2459–2462, DOI: 10.1103/PhysRevLett.86.2459.

[18] Ohkubo, Jun, Nadav Shnerb and David A. Kessler (2008), 'Transition Phenomena Induced by Internal Noise and Quasi-Absorbing State', *Journal of the Physical Society of Japan* **77** (4):044002, DOI: 10.1143/JPSJ.77.044002.

[19] Biancalani, Tommaso, Tim Rogers and Alan J. McKane (2012), 'Noise-induced metastability in biochemical networks', *Physical Review E* **86** (1):010106, DOI: 10.1103/PhysRevE.86.010106.

[20] Biancalani, Tommaso, Louise Dyson and Alan J. McKane (2014), 'Noise-Induced Bistable States and Their Mean Switching Time in Foraging Colonies', *Physical Review Letters* **112** (3):038101, DOI: 10.1103/PhysRevLett.112.038101.

[21] Houchmandzadeh, Bahram and Marcel Vallade (2015), 'Exact results for a noise-induced bistable system', *Physical Review E* **91** (2):022115, DOI: 10.1103/PhysRevE.91.022115.

[22] Saito, Yohei et al. (2016), 'Discreteness-induced transitions in multibody reaction systems', *Physical Review E* **94** (2):022140, DOI: 10.1103/PhysRevE.94.022140.

[23] Carro, Adrián, Raúl Toral and Maxi San Miguel (2016), 'The noisy voter model on complex networks', *Scientific Reports* **6** (1):24775, DOI: 10.1038/srep24775.

[24] Peralta, Antonio F. et al. (2018a), 'Analytical and numerical study of the non-linear noisy voter model on complex networks', *Chaos: An Interdisciplinary Journal of Nonlinear Science* **28** (7):075516, DOI: 10.1063/1.5030112.

[25] — (2018b), 'Stochastic pair approximation treatment of the noisy voter model', *New Journal of Physics* **20** (10):103045, DOI: 10.1088/1367-2630/aae7f5.

[26] Gillespie, Daniel T. (1976), 'A general method for numerically simulating the stochastic time evolution of coupled chemical reactions', *Journal of Computational Physics* **22** (4):403–434, DOI: 10.1016/0021-9991(76)90041-3.

[27] — (1977), 'Exact stochastic simulation of coupled chemical reactions', *The Journal of Physical Chemistry* **81** (25):2340–2361, DOI: 10.1021/j100540a008.

[28] Ewens, Warren J. (2004), *Mathematical Population Genetics 1: Theoretical Introduction*, Springer, New York, NY.

[29] Traulsen, Arne and Christoph Hauert (2009), 'Stochastic evolutionary game dynamics', *Reviews of nonlinear dynamics and complexity*, ed. by Heinz Georg Schuster, vol. II, Wiley-VCH, Weinheim, p. 25–61, DOI: 10.1002/9783527628001.

[30] Norris, James R. (1998), *Markov Chains*, Cambridge University Press, Cambridge, UK.

[31] Karlin, Samuel and James McGregor (1959), 'Coincidence properties of birth and death processes', *Pacific Journal of Mathematics* **9** (4):1109–1140.

[32] Keilson, Julian (1979), *Markov Chain Models — Rarity and Exponentiality*, vol. 28, Applied Mathematical Sciences, Springer-Verlag, New York, NY, DOI: 10.1007/978-1-4612-6200-8.

[33] Cremer, Jonas, Tobias Reichenbach and Erwin Frey (2008), 'Anomalous finite-size effects in the Battle of the Sexes', *The European Physical Journal B* **63** (3):373–380, DOI: 10.1140/epjb/e2008-00036-x.

[34] Mobilia, Mauro (2010), 'Oscillatory dynamics in rock–paper–scissors games with mutations', *Journal of Theoretical Biology* **264** (1):1–10, DOI: 10.1016/j.jtbi.2010.01.008.

[35] Hartl, Daniel L. and Andrew G. Clark (2007), *Principles of Population Genetics*, 4th ed., Sinauer Associates, Sunderland, MA.

[36] Kurtz, Thomas G. (1978), 'Strong approximation theorems for density dependent Markov chains', *Stochastic Processes and their Applications* **6** (3):223–240, DOI: 10.1016/0304-4149(78)90020-0.

[37] Gillespie, Daniel T. (2000), 'The chemical Langevin equation', *Journal of Chemical Physics* **113** (1):297–306, DOI: 10.1063/1.481811.

[38] Risken, Hannes (1996), *The Fokker-Planck Equation*, 2nd ed., Springer-Verlag, Berlin Heidelberg, DOI: 10.1007/978-3-642-61544-3.

[39] Bladon, Alex J., Tobias Galla and Alan J. McKane (2010), 'Evolutionary dynamics, intrinsic noise, and cycles of cooperation', *Physical Review E* **81** (6):1–14, DOI: 10.1103/PhysRevE.81.066122.

Chapter 6

Conclusions

This thesis has been concerned with studying stochastic processes, which describe the time evolution of dynamics which are fundamentally *noisy*. We view this noise not as a nuisance that prevents our understanding of the 'true' dynamics underneath, but as the source of relevant and interesting phenomena. This perspective has proven useful in many areas of research, and has opened a window to a better understanding of the environment and society we live in.

Throughout the thesis, we have been interested in the interplay between *extrinsic* and *intrinsic* noise. All our models consider systems composed of discrete individuals which interact with one another. Due to their discrete nature, the dynamics of these systems have intrinsic noise. Additionally, we focused on studying models which include either motion or agent-to-agent heterogeneity; we have treated these characteristics as sources of extrinsic noise.

In this chapter, we briefly summarise our findings on how heterogeneity and motion influence the dynamics of models which are intrinsically noisy. Then, we outline areas of opportunity to expand our work. These include expansions to the specific models studied in the intermediate chapters and also prospects to combine the results obtained across them. Finally, we conclude by remarking on the significance and applicability of our findings with a broader view.

6.1 Summary of results

The models studied in this thesis can be divided into two classes: those which include motion, and those with heterogeneous populations. We here recapitulate the key findings in these two categories.

6.1.1 Motion

Chapters 2 and 3 considered the evolutionary dynamics of mobile populations. In both chapters we implemented motion by immersing the population in a flow, which 'stirs' individuals in space. We considered structured populations, where the contact network is generated by connecting individuals within a given interaction radius from each other. We obtained and compared results for different evolutionary processes, which occur in two steps: reproduction, and death. The order in which these steps take place differentiates birth-death and death-birth mechanisms. Whether individuals compete in the first or second step distinguishes between global and local selection. Combining the results from both chapters, we can confidently assert that:

Well-stirred is not well-mixed. In the literature, the term 'well-mixed' is often used to refer to populations in which interactions can occur between any pair of individuals [1–3]. We find, however, that the term is misleading, as it suggests that all-to-all interaction dynamics would be recovered if the population is sufficiently stirred. In Chapter 2 we showed that this is not the case. The analytical expression obtained for the limit of fast flows evidences that the interaction radius of individuals, which determines how well connected to the rest of the population they are, is a much more important factor than the actual 'mixing'.

Motion amplifies or suppresses selection at different flow speeds. We found that the speed with which individuals move, relative to the rate of evolutionary events, can lead to different effects on the fixation probability of an invading mutant: with slow flows, selection is amplified for birth-death processes, whereas it is suppressed for death-birth processes[1]; for fast flows, local selection leads to suppressed natural selection, and global selection recovers the complete-graph result.

[1] Amplification of selection implies that the chances of success of an advantageous mutant are larger than on a complete-interaction graph, while the fixation probability of a disadvantageous mutant are smaller. Suppression of selection describes the opposite effect.

The order of birth and death events is paramount at intermediate flow speeds. The movement of the individuals makes the interaction network dynamic; it gets fragmented and reconnected in a different way. In these conditions, species more easily segregate, and clusters of a single type are formed. This reduces the number of interaction paths, which ultimately results in the order of death and birth of individuals being crucial to the evolutionary process.

Motion can help identify the underlying evolutionary mechanism. As shown in Chapter 3, by studying how the speed of the flow changes the probability with which a mutant successfully invades a population, one could identify the underlying evolutionary mechanism.

On the whole, the movement of individuals substantially modifies the evolutionary dynamics, for which we consider its inclusion in models essential; traditional static models are inadequate for studying mobile populations. Furthermore, since we provide analytical expressions to describe these systems, the incorporation of this type of motion is made readily available for future use.

6.1.2 Heterogeneity

Chapters 4 and 5 addressed heterogeneity between individuals in the population. The models in each of the two chapters differed in a few key aspects. For instance, the population sizes considered in Chapter 5 are generally small, which makes the effects of intrinsic noise dominant; the system then spends most of the time far from the deterministic fixed point. In Chapter 4, on the other hand, we focused on large populations; due to this, the system dynamics were localised around the fixed point. Consequently, in the two chapters we studied two disparate phenomena. In the noisy voter model (Chapter 5), a transition between uni-modal and multi-modal stationary probability distributions is the focus. In the epidemics model (Chapter 4), we concentrate on characterising the stochastic quasi-cycles around the fixed point.

Although the models in the two chapters were constructed with different objectives in mind, in both cases heterogeneity was modelled in a similar way, i.e., by setting up an arbitrary number of compartments to which individuals belong. In Chapter 4, the susceptible and infected groups were divided into sub-groups, which account for

different susceptibilities and infectiousness of individuals. In Chapter 5, we studied a noisy voter model with multiple types, which can represent different species or opinions.

Using a large number of compartments can potentially make the models less amenable to analytic solution. The method with which we approached this complication was similar in both models. We studied the dynamics of each system through the aggregate of its components and obtained information about the original model via the marginalised description. This reduced the dimensionality of the problem, and analytical progress could be made. In Chapter 5, for example, this meant focusing on one of the 'opinions', and consider the rest of the population as part of 'the other' group. In Chapter 4, on the other hand, we described the dynamics through the total number of infected or susceptible individuals, instead of each of the sub-groups. With this technique, we found that:

The frequency of stochastic quasi-cycles is well approximated by the mean of the heterogeneous parameters. Analytical expressions to characterises the frequency of oscillations around the fixed point were obtained in Chapter 4; these depend only on the first moment of the heterogeneous parameters across sub-groups, which are time independent — they depend only on the probabilities with which susceptibilities are assigned at birth, or infectiousness upon contagion.

Marginal descriptions of heterogeneous models are a valuable tool. In both chapters we aggregated the multiple compartments in the system into larger groups. We made use of weighted averages to construct *effective* models that emulated the original dynamics.

In Chapter 5, these weighted averages were used to 'homogenize' the aggregated types that conform 'the other' opinion; weights were assigned according to the fixed points of the corresponding mean-field dynamics. With this approximation, closed analytical expressions were obtained to describe the state probability distribution at long times, as well as the critical system size in which the transition between ordered and mixed states occurs.

In Chapter 4, susceptible sub-groups were lumped into a macroscopic group, and similarly for infected individuals. Also, a 'total infective power' and 'aggregate susceptibility' were defined, with weights corresponding to the population densities in each sub-group. These two quantities permitted analytical progress, and were necessary to obtain the

power spectral densities of the oscillations around the fixed point. They also featured on the analytical expression obtained to approximate the amplitude of the outbreaks.

Heterogeneity has non-trivial effects on the macroscopic dynamics. We found, for example, that the amplitude of the stochastic cycles in Chapter 4 depends non-trivially on higher moments of the distribution of susceptibilities and infectiousness. The amplitude of the cycles determines the size of outbreaks. Therefore, the model dynamics are impossible to reproduce if heterogeneity is not carefully considered.
In the noisy voter model presented in Chapter 5 we found that the nature of the noise-induced phase transition changes when more than two types are permitted, for instance. Instead of a single critical system size that divides the unimodal and bimodal regimes of the stationary distribution, as found in the two-state model, at least two critical points are needed to characterize the transition in the multi-state model. One is determined by the slope of the marginal stationary distributions at the right edge of state-space, i.e., by the dynamics near states of consensus. The other is defined on the left edge of state-space, and is characterized by the dynamics near states of extinction.

Overall, we find that the multiplicity of the states and the heterogeneity among them have a significant impact on the macroscopic model dynamics. The tools and methods presented in Chapters 4 and 5 facilitate the inclusion and analysis of heterogeneity, and are applicable in a wider context.

6.2 Outlook

The research presented in this thesis provides ample opportunities to branch out. In this section, we provide examples of direction in which further work could continue. We divide these examples in two: those which arise if certain assumptions of the presented models are relaxed, and those in which the results of both motion *and* heterogeneity may become relevant.

6.2.1 Extending the models

The models studied throughout this thesis are intentionally minimalistic. Therefore, there are many possible extensions to our models that could increase the applicability of our results.

For example, in all our models we assume a *fixed population size*. This assumption is made for mathematical convinience, but it does not capture the fluctuating populations observed in nature. Varying population sizes could be important in the models described in Chapters 2 and 3; applicability of the results in these chapters to biological settings would be more straightforward with this extension. Although it is possible to devise laboratory settings in which the population remains approximately constant [4], a more realistic model would assume births and deaths of individuals at separate rates. Models of this type have been shown to signifficantly affect evolutionary dynamics, and the demographic stochasticity in them can even lead to the extinction of both species in the population [5].

Another potential extension to our models is the inclusion of *frequency dependent fitnesses*. In Chapters 2 and 3 we assume that when individuals compete to reproduce (or to not die) they have an inherent fitness, which is independent of their opponents or surroundings; this is known as *frequency independent fitnesses*. This approximation could limit the extent with which our results can be used in a wider context. In game theoretical scenarios, for example, the fitness of individuals is, in general, dependent on the interaction partners of each individual. This takes into account that 'strategies' are not equally successful in all circumstances. In the context of cooperation games, defectors are much fitter when surrounded by cooperators than when among other defectors [6]. Frequency dependent fitness has been reported in biological settings [7–9], and so its inclusion is a natural next step of our work.

Further opportunities for augmentation to the models studied in this thesis include the study of *ranked* multi-state noisy voter models. In ranked models the transition between types is sequential; that is, type 2 can only change into type 1 or 3, but not 5, for example. The contents of Chapter 5 are restricted to the simplest case, in which imitation across opinions or strategies is performed independently of the 'distance' between them. However, this may not reflect important features of certain phenomena, such as opinion formation or the evolution of language, where changes tend to occur gradually. The phase transition observed in the multi-state noisy voter model is still found in ranked models, but the behaviour of the system can change significantly (see Fig. 6.1). Since transition between strategies needs to be sequential, intermediate types are more often occupied than extremal opinions. This is a substantial change to

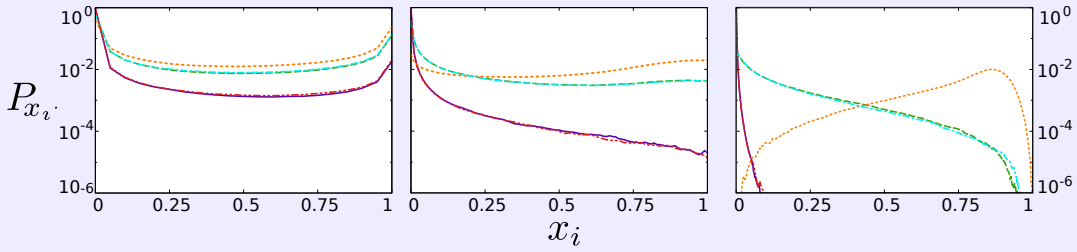

Figure 6.1: Stationary probability distribution for each opinion in a multi-state ranked noisy voter model. Sample stationary distributions of a ranked noisy voter model are shown. In the model, 5 opinions are possible. Individuals only transition from and to 'neighbouring' opinions $i \pm 1$. Each line shows the probability with which the system is found in a state in which Nx_i individuals are of opinion i. From left to right, the panels correspond to simulations with $N = 20$, 100 and 500. A noise induced transition is observed. However, the dynamics of the system are clearly different. The central species (orange), contains a higher proportion of the population. The model is symmetric, so that the species contiguous to the central one (green and blue) are equally abundant to each other, but more so than the extremal opinions (red and purple). In all panels, the mutation rate is $\varepsilon = 0.01$ for all species, and the imitation rate is set to $r = 1$.

the model dynamics, which should be interesting to study in more detail and has the potential to be widely applicable.

Of similar importance would be to consider *structured* populations in the multi-state noisy voter model. In Chapter 5 we consider a complete interaction graph; this makes our mathematical description possible and provides an interesting first insight into the dynamics of the model. As we have remarked on this thesis, however, population structure can modify the dynamics. In two-species noisy voter models it has been found to lead to a larger critical system syze [10].

The model of epidemics stuided in Chapter 4 also provides opportunities for extension. One could consider models with *correlation* between the susceptibility and infectiousness of individuals, for example. Neglecting such correlations facilitated a mathematically tractable model, but decreases its universality. The lack of correlation is justified for the study of, for example, varying pathogen resistance [11], where individuals become infected with different rates, due to their distinct resistances. Once infected, however, these differences need not determine their ability to spread the disease. On the other hand, neglecting correlations is inadequate to simulate heterogeneity that arises from a contact network. In this case, the better connected nodes are more likely to get infected and more likely to spread the disease.

Also, *vaccination* was not included in the epidemics model in Chapter 4. Although this extension to the model would be minor, interesting questions could be answered, such as how heterogeneity affects herd-immunity[2].

6.2.2 Combining motion and heterogeneity

The previous section focused on extensions to the particular models presented in this thesis. We have addressed motion and heterogeneity independently in order to distinguish their effects. However, potential lines of research for which our work may be relevant also include cases in which both noise sources are present. Motion and agent-to-agent heterogeneity are ubiquitous in nature, and so occasions to explore them in conjunction abound. For example, heterogeneous interaction radii of individuals in moving populations have been explored in ref. [12], and populations with different diffusion speeds in ref. [13].

There are many other yet unexplored areas of research that combine the two noise sources. For instance, one could study the effect of motion on the periodicity of outbreaks of a disease. We found in Chapters 2 and 3 that the movement of individuals produces changes in both fixation probabilities and fixation times. It is reasonable to expect that motion affects the spread of a pathogen [14] and so the frequency of the stochastic cycles would be modified too. Furthermore, we observed that at some speeds of motion clustering of species is promoted. This is likely to also be the case for disease spreading, where heterogeneity between individuals in the population may play a more prominent role. Therefore, both the frequency and amplitude of the stochastic cycles may be changed.

However, it is important to stress that the evolutionary processes described in Chapters 2 and 3 are different to the epidemics model in Chapter 4 in various aspects. For instance, in the model of epidemics individuals transition from the susceptible to the infected stage mostly through 'contact' between members of each group, whereas the reverse only happens when infected individuals die, i.e., without the need of an interaction. In the evolutionary processes studied in Chapters 2 and 3, on the other hand, the system *always* evolves through pairwise interactions.

[2]In epidemics, herd-immunity is the term used to describe a population that, although partly composed of susceptible individuals, is highly unlikely to be invaded by a pathogen, due to the number of recovered (or vaccinated) individuals in the population.

6.3 Closing remarks

Through the publications reproduced in this work and in the summary above we have discussed the role of intrinsic and extrinsic noise sources in the particular process being described in each chapter. However, the models used throughout the thesis are set up in a way that makes them applicable to a wide variety of phenomena.

Chapter 4 uses an epidemic model, and we found that the characteristic frequency of the stochastic cycles is accurately described by the mean of the heterogeneous parameters. This can be used as a guide in other models with cycles of the same nature, such as ecological processes or theoretical games [15–17].

Chapters 2 and 3 have a wide scope by design, due to the variety of evolutionary update rules that are studied. The results have implications that go further than just biological processes; the set-up is common to game-theoretical models in general, which are used in the analysis and description of social dynamics and financial markets [18, 19], for example.

Finally, noisy voter models, like the one studied in Chapter 5, have proved useful in modelling various physical and social systems, such as opinion dynamics, language evolution, or magnetization. The use of more than two states is often avoided due to the lack of mathematically tractable dynamics, which results in the need to rely on numerical approaches. In the study of flocking dynamics, for example, two-state voter models have been used [20]; however, multi-state models could much more accurately describe changes in the direction of movement, and so our work could be of relevance. Furthermore, the method used to extract information from the heterogeneous system is amenable to application in other models. The underlying technique with which the problem is approached, then, is valuable beyond the model under study.

Motion and agent-to-agent heterogeneity are common characteristics of complex systems. The tools and techniques presented in this thesis can help to describe and understand their impact on model dynamics. Therefore, we hope that the results compiled in this thesis are not only seen as extensions of particular models, but that the underlying methods are used more widely and help to further our understanding of the complex world we live in.

Bibliography

[1] Ohtsuki, Hisashi et al. (2006), 'A simple rule for the evolution of cooperation on graphs and social networks', *Nature* **441** (7092):502–505, DOI: 10.1038/nature04605.

[2] Tarnita, Corina E. et al. (2009), 'Evolutionary dynamics in set structured populations', *Proceedings of the National Academy of Sciences* **106** (21):8601–8604, DOI: 10.1073/pnas.0903019106.

[3] Santos, Francisco C., Jorge M. Pacheco and Tom Lenaerts (2006), 'Evolutionary dynamics of social dilemmas in structured heterogeneous populations', *Proceedings of the National Academy of Sciences* **103** (9):3490–3494, DOI: 10.1073/pnas.0508201103.

[4] Wahl, Lindi M., Philip J Gerrish and Ivan Saika-Voivod (2002), 'Evaluating the impact of population bottlenecks in experimental evolution.', *Genetics* **162** (2):961–71.

[5] Huang, Weini, Christoph Hauert and Arne Traulsen (2015), 'Stochastic game dynamics under demographic fluctuations', *Proceedings of the National Academy of Sciences* **112** (29):9064–9069, DOI: 10.1073/pnas.1418745112.

[6] Nowak, Martin A. (2006), 'Five rules for the evolution of cooperation', *Science* **314** (5805):1560–1563, DOI: 10.1126/science.1133755.

[7] Habets, Michelle G J L et al. (2006), 'The effect of population structure on the adaptive radiation of microbial populations evolving in spatially structured environments', *Ecology Letters* **9** (9):1041–1048, DOI: 10.1111/j.1461-0248.2006.00955.x.

[8] Endler, J. A. and J. J. D. Greenwood (1988), 'Frequency-Dependent Predation, Crypsis and Aposematic Coloration [and Discussion]', *Philosophical Transactions of the Royal Society B: Biological Sciences* **319** (1196):505–523, DOI: 10.1098/rstb.1988.0062.

[9] McCauley, David E. and Marcus T. Brock (1998), 'Frequency-Dependent Fitness in Silene vulgaris, a Gynodioecious Plant', *Evolution* **52** (1):30, DOI: 10.2307/2410917.

[10] Carro, Adrián, Raúl Toral and Maxi San Miguel (2016), 'The noisy voter model on complex networks', *Scientific Reports* **6** (1):24775, DOI: 10.1038/srep24775.

[11] Keeling, Matthew J. (2005), 'The implications of network structure for epidemic dynamics', *Theoretical Population Biology* **67** (1):1–8, DOI: 10.1016/j.tpb.2004.08.002.

[12] Minors, Kevin, Tim Rogers and Christian A. Yates (2018), 'Noise-driven bias in the non-local voter model', *EPL (Europhysics Letters)* **122** (1):10004, DOI: 10.1209/0295-5075/122/10004.

[13] Pigolotti, Simone and Roberto Benzi (2014), 'Selective Advantage of Diffusing Faster', *Physical Review Letters* **112** (18):188102, DOI: 10.1103/PhysRevLett.112.188102.

[14] Colizza, Vittoria et al. (2006), 'The role of the airline transportation network in the prediction and predictability of global epidemics', *Proceedings of the National Academy of Sciences* **103** (7):2015–2020, DOI: 10.1073/pnas.0510525103.

[15] Bladon, Alex J., Tobias Galla and Alan J. McKane (2010), 'Evolutionary dynamics, intrinsic noise, and cycles of cooperation', *Physical Review E* **81** (6):1–14, DOI: 10.1103/PhysRevE.81.066122.

[16] McKane, Alan J. and Timothy J. Newman (2005), 'Predator-prey cycles from resonant amplification of demographic stochasticity', *Physical Review Letters* **94** (21):1–4, DOI: 10.1103/PhysRevLett.94.218102.

[17] Mobilia, Mauro (2010), 'Oscillatory dynamics in rock–paper–scissors games with mutations', *Journal of Theoretical Biology* **264** (1):1–10, DOI: 10.1016/j.jtbi.2010.01.008.

[18] Paul, Wolfgang and Jörg Baschnagel (2013), *Stochastic Processes: From Physics to Finance*, Springer International Publishing.

[19] Diekmann, Andreas and Peter Mitter (1984), *Stochastic Modelling of Social Processes*, Academic Press, London, UK.

[20] Baglietto, Gabriel and Federico Vazquez (2016), 'Flocking dynamics with voter-like interactions: speed-dependent transition and fast polar consensus', *arXiv preprint*, arXiv: 1608.08231.